Family A G protein-coupled receptor ligand interactions: the role of the extracellular region

Author:
Leonar, Erica

Publication Date:
2017

DOI:
https://doi.org/10.26190/unsworks/3143

Family A G protein-coupled receptor ligand interactions: the role of the extracellular region

Erica Leonar

A thesis in fulfilment of the requirements for the degree of

Doctor of Philosophy

School of Medical Sciences

Faculty of Medicine

January 2017

PLEASE TYPE

THE UNIVERSITY OF NEW SOUTH WALES
Thesis/Dissertation Sheet

Surname or Family name: Leonar

First name: Erica Other name/s:

Abbreviation for degree as given in the University calendar: PhD

School: School of Medical Sciences Faculty: Medicine

Title: Family A G protein-coupled receptor ligand interactions: the role of the extracellular region

Abstract 350 words maximum: (PLEASE TYPE)

Increasing interest in the role of the extracellular loops (ECL) in family A G protein-coupled receptor (GPCR) function stems from (i) the discovery that many allosteric modulators of alpha branch receptors interact with the ECL, (ii) predictions that this region forms an initial interaction site for orthosteric ligands, (iii) ECL mutations alter receptor signalling and (iv) the ECL interacts with peptide ligands from the gamma branch receptors. This thesis investigated the role of the ECL and surrounding regions in allosteric and orthosteric ligand interactions across family A GPCRs using the alpha branch beta2 adrenoceptor (b2AR) and the gamma branch complement 5a receptor (C5aR).

THRX100361 and tacrine displayed positive modulation of 3H-dihydroalprenolol (DHA) dissociation from the b2AR but negative modulation of b2AR activation. Using docking and mutagenesis, an allosteric site comprised of residues from ECL2 (F193) and the top of helices 6 (H296) and 7 (K305 and Y308) was identified. Mutation of these residues to alanine reduced the modulatory actions of THRX100361 and tacrine. These mutations also increased the dissociation rate of 3H-DHA. This supports the existence of a metastable binding site on the b2AR as predicted in computational studies and that this region is important in orthosteric and allosteric interactions.

PMX53 is potent inhibitor of the C5aR and has previously been described as a non-competitive antagonist in myeloperoxidase and calcium release assays. Surprisingly, in this study, PMX53 behaved as a competitive antagonist of C5a-mediated Gi activation. This discrepancy suggests that PMX53 has a slow off rate, resulting in hemi-equilibrium conditions in signalling assays with short incubation times and is in fact a competitive antagonist. Supporting this, docking of PMX53 into a homology model suggested interactions with ECL1-2 and helices 2,3,5,6-7 including residues involved in C5a binding. The affinity of PMX53 is 400 fold lower at the mouse compared to human and rat C5aR. Docking and sequence alignment suggested that 2 residues in ECL2 may contribute to this difference. The human to mouse mutation L187V has no effect, while D191N increased PMX53 potency, indicating that ECL2 may play a role in PMX53 binding but does account for the species variation in affinity. Further studies are required to fully understand PMX53 molecular mechanism of action.

The data in this thesis suggest an important role for the ECL2 in family A GPCRs.

Declaration relating to disposition of project thesis/dissertation

I hereby grant to the University of New South Wales or its agents the right to archive and to make available my thesis or dissertation in whole or in part in the University libraries in all forms of media, now or here after known, subject to the provisions of the Copyright Act 1968. I retain all property rights, such as patent rights. I also retain the right to use in future works (such as articles or books) all or part of this thesis or dissertation.

I also authorise University Microfilms to use the 350 word abstract of my thesis in Dissertation Abstracts International (this is applicable to doctoral theses only).

09/03/2017

Signature Witness Signature Date

The University recognises that there may be exceptional circumstances requiring restrictions on copying or conditions on use. Requests for restriction for a period of up to 2 years must be made in writing. Requests for a longer period of restriction may be considered in exceptional circumstances and require the approval of the Dean of Graduate Research.

FOR OFFICE USE ONLY Date of completion of requirements for Award:

Copyright Statement

Signed.....

Date.....09/03/2017.....

Authenticity Statement

‘I certify that the Library deposit digital copy is a direct equivalent of the final officially approved version of my thesis. No emendation of content has occurred and if there are any minor variations in formatting, they are the result of the conversion to digital format.’

Signed.....

Date.....09/03/2017.....

Originality Statement

'I hereby declare that this submission is my own work and to the best of my knowledge it contains no materials previously published or written by another person, or substantial proportions of material which have been accepted for the award of any other degree or diploma at UNSW or any other educational institution, except where due acknowledgement is made in the thesis. Any contribution made to the research by others, with whom I have worked at UNSW or elsewhere, is explicitly acknowledged in the thesis. I also declare that the intellectual content of this thesis is the product of my own work, except to the extent that assistance from others in the project's design and conception or in style, presentation and linguistic expression is acknowledged.'

Signed……

Date 09/03/2017……

Acknowledgements

To my primary supervisor, Dr Angela Finch, thank you for your guidance throughout my candidature and for teaching me the skills to be a good scientist. I would also like to thank you for always encouraging me to achieve my best.

To my co-supervisors, A/Prof Renate Griffith and A/Prof Trent Woodruff, thank you too for your guidance and advice.

To A/Prof Pall Thordarson, thank you for sharing your expertise in peptide synthesis.

To the Finch and Griffith lab members, especially Adrian, Rob, Urmi and Tom, thank you sharing your knowledge with me and for your friendship and encouraging words. To Susan and Brendan, thank you for your kind friendship and for your help in proof-reading this thesis.

To everyone who has helped me along the way, especially Dr Trevor Lewis, Dr Nicole Jones and A/Prof Lu Liu, thank you for your generosity.

To my family and parents in-law, especially my beautiful mother, thank you for your unconditional love and endless support. I will not be where I am today without you.

To my husband and my best friend, Hong, thank you for being there. I would not have made it without your never-ending support and encouragement.

Abstract

Increasing interest in the role of the extracellular loops (ECL) in family A G protein-coupled receptor (GPCR) function stems from (i) the discovery that many allosteric modulators of α branch receptors interact with the ECL, (ii) predictions that this region forms an initial interaction site for orthosteric ligands, (iii) ECL mutations can alter receptor signalling and (iv) the ECL interacts with peptide ligands from the gamma branch receptors. This thesis investigated the role of the ECL and surrounding regions in allosteric and orthosteric ligand interactions across family A GPCRs using the α branch β_2 adrenoceptor (β_2AR) and the gamma branch complement 5a receptor (C5aR) as exemplars of each branch.

At the β_2AR, an M_2/M_3 mAChR antagonist THRX100361 and an $M_1/M_2/M_3$ mAChR allosteric modulator tacrine displayed positive modulation of the dissociation of the orthosteric antagonist [^{3}H]dihydroalprenolol (DHA), increasing its residence time. However, both compounds displayed negative modulation of isoprenaline-mediated receptor activation. Docking of THRX100361 and tacrine identified an allosteric site comprised of residues from the ECL2 and transmembrane helices (TM) 6 and 7, in particular F193^{ECL2}, H296$^{6.58}$, K305$^{7.32}$ and Y305$^{7.35}$. The mutation of these residues to alanine reduced the modulatory actions of THRX100361 and tacrine, suggesting their role in mediating the allosteric effects of these compounds.

The mutation of the residues identified to be involved in an allosteric binding site of the β_2AR to alanine increased the dissociation rate of [^{3}H]DHA from the

β_2AR, suggesting that these residues control the exit of orthosteric ligands from the receptor. This data supports the existence of a metastable binding site on the β_2AR that is located extracellular to the orthosteric site, as predicted in molecular dynamics studies. Taken together, these data suggest that the extracellular region of the β_2AR formed by the ECL2 and TM6 and 7 is important in both the control of orthosteric ligand residence time and the modulatory effects of allosteric ligand.

PMX53 is potent inhibitor of the C5aR and has previously been described as a non-competitive antagonist in myeloperoxidase and calcium release assays. Surprisingly, in this study, PMX53 behaved as a competitive antagonist of C5a-mediated $G_{\alpha i}$ activation. This discrepancy suggests that PMX53 has a long residence time at the C5aR, resulting in hemi-equilibrium conditions in signalling assays with short incubation times and is in fact a competitive antagonist. Supporting this, docking of PMX53 into a homology model based on the chemokine CXCR4 receptor suggested interactions with ECL1-2 and TM2,3,5,6-7 including residues important for the binding of C5a.

The affinity of PMX53 is 400 fold lower at the mouse compared to human and rat C5aR and sequence alignment of the C5aR from these species suggested that residues from the ECL2 may contribute to this observed difference in the affinity of PMX53. Docking of PMX53 into a homology model of the C5aR suggested that high affinity binding of PMX53 at the human C5aR may be due to interactions with $L187^{ECL2}$ and $D191^{ECL2}$. While the human to mouse mutation $L187^{ECL2}V$ has no effect on the potency of PMX53, the mutation $D191^{ECL2}N$ increased its potency, suggesting that the ECL2 plays a role in the binding of PMX53 but does not account for the species variation in affinity.

The data in this thesis suggest an important role for the extracellular region of family A GPCRs in orthosteric and allosteric ligand interactions. The characterisation of the extracellular allosteric binding site of the β_2AR and the interactions of PMX53 at the C5aR will be useful for future design of drugs targeting these receptors.

Conference Abstracts

Finch AM, Campbell AP, **Leonar E**, Chen J, Urmi KF, Noh W-J, Xu K, Wilkins BP, So SS, Griffith R. There and back again: Understanding GPCR ligand binding pathways to design better drugs. Oral presentation at the ASCEPT NZ meeting as part of Queenstown Research Week, Nelson, New Zealand, August 28th – September 2nd, 2016.

Leonar E, Griffith R, Woodruff T, Finch AM. Pharmacological characterisation of PMX53 interactions at the complement 5a receptor. Oral presentation at the Sydney GPCR Research Symposium, Sydney, Australia, March 21st, 2016.

Leonar E, Ngo T, Griffith R, Finch AM. The role of the extracellular vestibule in β_2 adrenoceptor orthosteric and allosteric ligand interactions. Poster presentation at the UNSW Medicinal Chemistry/Drug Discovery Symposium, Sydney, Australia, November 18th, 2015.

Leonar E, Ngo T, Griffith R, Finch AM. The role of the extracellular vestibule in β_2 adrenoceptor orthosteric and allosteric ligand interactions. Poster presentation at the Gordon Research Conference and Gordon Research Seminar on Molecular Pharmacology, Ventura, USA, January 31st – February 6th, 2015.

Leonar E, Ngo T, Griffith R, Finch AM. The role of the extracellular vestibule in β_2 adrenoceptor orthosteric and allosteric ligand interactions. Oral and poster presentation at the ASCEPT-MPGPCR Joint Scientific Meeting, Melbourne, Australia, December 7th – 11th, 2014.

Leonar E, Ngo T, Smith NJ, Finch AM. Amino acids regulating orthosteric ligand dissociation from β_2 adrenoceptors. Molecular Pharmacology of G Protein-Coupled Receptors Meeting, Melbourne, Australia, December 6th – 8th, 2012.

Leonar E, Ngo T, Smith NJ, Finch AM. Amino acids regulating orthosteric ligand dissociation from β_2 adrenoceptors. UNSW Medicinal Chemistry/Drug Discovery Symposium, Sydney, Australia, November 14th, 2012.

Table of Contents

List of Tables

List of Figures

List of Abbreviations

5-HT	5-hydroxytryptamine
Ahx	Amino hexanoic acid
ANOVA	Analysis of variance
AR	Adrenoceptor
BA	β_2 adrenergic agonist
BRET	Bioluminescence resonance energy transfer
BSA	Bovine serum albumin
C5a	Complement 5a
C5aR	Complement 5a receptor
cAMP	Cyclic adenosine monophosphate
CAMYEL	cAMP sensor using YFP-Epac-RLuc
CHO	Chinese hamster ovary
COPD	Chronic obstructive pulmonary disease
COS-1	African green monkey kidney cells
DHA	Dihydroalprenolol
DMEM	Dulbecco's modified eagle medium
DMSO	Dimethyl sulfoxide
ECL	Extracellular loop
EDTA	Ethylenediaminetetraacetic acid
ERK	Extracellular signal-regulated kinase
FBS	Fetal bovine serum
FITC	Fluorescein isothiocyanate
GOLD	Genetic Optimisation for Ligand Docking
GPCR	G protein-coupled receptor
GRK	G protein receptor kinase

HBSS	Hank's balanced salt solution
HEPES	4-(2-hydroxyethyl)-1-piperazineethanesulfonic acid
HPLC	High performance liquid chromatography
IBMX	3-isobutyl-1-methylxanthine
ICL	Intracellular loop
MA	Muscarinic acetylcholine receptor antagonist
MABA	Muscarinic acetylcholine receptor antagonist, β_2 adrenoceptor agonist
mAChR	Muscarinic acetylcholine receptor
MAPK	Mitogen-activated protein kinase
NMR	Nuclear magnetic resonance
PBS	Phosphate buffered saline
PDB	Protein Data Bank
PKA	Protein kinase A
PMN	Polymorphonuclear leukocytes
RLuc	Renilla luciferase
SEM	Standard error of mean
TM	Transmembrane
TRIS	Tris(hydroxymethyl)aminomethane
WT	Wild type
YFP	Yellow fluorescent protein

CHAPTER 1

Introduction

1.1 G protein-coupled receptors

G protein-coupled receptors (GPCRs) form the largest transmembrane receptor superfamily in humans. Over 800 unique GPCRs have been identified in the human genome which are encoded by 1% of all identified genes (Fredriksson *et al.*, 2003; Venter *et al.*, 2001). GPCRs mediate cellular responses to diverse extracellular stimuli, ranging from photons to small molecules, lipids, peptides and proteins (Lagerstrom and Schioth, 2008). Approximately 25% of clinically available therapeutics act on GPCRs (Garland, 2013). However, these drugs only target 7% of GPCRs, mainly the aminergic receptors such as the adrenoceptors, muscarinic and serotonin and dopamine receptors (Garland, 2013). As such, the GPCR superfamily provides opportunities for novel targets in drug discovery programs.

Despite little sequence conservation amongst the different GPCR families, all GPCRs share a common structural feature of seven transmembrane (TM) helices connected by three extracellular (ECL) and three intracellular (ICL) loops with an extracellular N-terminus and an intracellular C-terminus. Most GPCRs signal through coupling to one or more heterotrimeric guanine nucleotide-binding proteins or G proteins, resulting in the modulation of the levels of intracellular messengers such as 3',5'-cyclic adenosine monophosphate (cAMP), inositol

triphosphate (IP_3) and calcium (Akam *et al.*, 2001; Kilts *et al.*, 2000; Lefkowitz *et al.*, 2002; Palmer *et al.*, 1995) (Figure 1.1). However, GPCRs have also been shown to mediate extracellular signals through coupling to non-G protein signalling effectors such as β-arrestins, G protein-coupled receptor kinases, PDZ domain-containing proteins and small GTP-binding proteins (Ahn *et al.*, 2004; Hall *et al.*, 1998; Mitchell *et al.*, 1998; Ruiz-Gómez and Mayor Jr, 1997; Shenoy *et al.*, 2006) (Figure 1.1).

1.1.1 GPCR classification

The most often used classification of GPCRs was developed by Kolakowski (1994), where GPCRs are classified into six families – A to F, based on their sequence homology. This classification includes GPCRs found in humans, animals and plants. Family A is by far the largest family and contains rhodopsin-like GPCRs; family B contains secretin-like receptors; family C contains metabotropic glutamate-like receptors; family D contains pheromone receptors; family E contains the slime mold cAMP receptors while family F contains the frizzled/smoothened receptors. However, the identification of a large number of GPCRs that do not fit in the classification system by Kolakowski (1994) prompted an updated classification. The classification developed by Fredriksson *et al*. (2003) catagorises human GPCRs into Glutamate, Rhodopsin, Adhesion, Frizzled/Taste2 and Secretin (GRAFS) families based on phylogenetic analysis (Figure 1.2). This classification differs from the one developed by Kolakowski in that it separates family B receptors into two families, Secretin and Adhesion. In addition, it also places the Taste2 receptors in the Frizzled receptor family. Unique structural

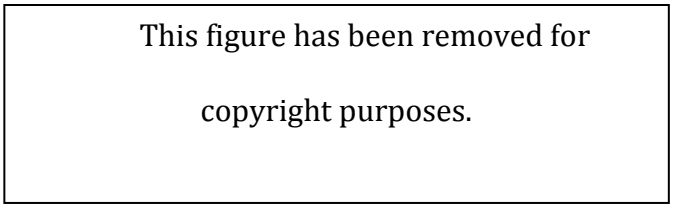

Figure 1.1 A schematic representation of GPCR signalling

G protein-coupled receptors (GPCRs) are transmembrane receptors that couple to G proteins. Activation of GPCRs promotes G protein coupling which leads to signalling events mediated by second messengers such as 3',5'-cyclic adenosine monophosphate (cAMP), inositol triphosphate (IP_3) and calcium ions. GPCRs can also couple to other signalling molecules such as β-arrestins, leading to desensitisation as well as signalling events mediated by proteins such as mitogen-activated protein kinase (MAPK), tyrosine kinase, and E3 ubiquitin ligase. Figure reproduced from (Ghosh *et al.*, 2015).

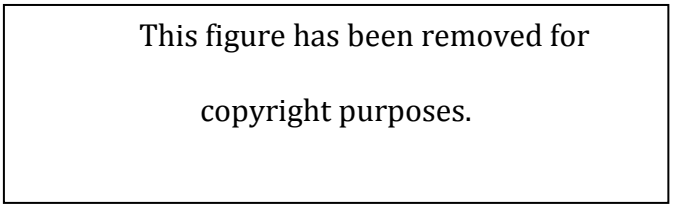

Figure 1.2 Human GPCR phylogenetic tree

Phylogenetic analysis of human GPCRs based on the Glutamate, Rhodopsin, Adhesion, Frizzled/Taste2 and Secretin (GRAFS) system (Fredriksson *et al.*, 2003). The different families are coloured in orange, blue, purple, green and red respectively. The rhodopsin family is further divided into four groups – α, β, γ and δ. The β_2 adrenoceptor and the complement 5a receptor are circled in red. Figure adapted from the GPCR Network (http://gpcr.usc.edu/).

characteristics of the different families are apparent in the GRAFS classification. For example, the glutamate family has a venus fly trap domain on the N-terminal domain; the rhodopsin family has E/DRY and NPXXY motifs within TM3 and 7 and ICL2; the adhesion family has adhesion-like motifs in the N terminus; the frizzled/taste2 family share consensus sequences such as the IFL, SFLL and SXKTL motifs in TM2, 5 and 7 respectively; and the secretin family contains conserved cysteine bridges on the N-terminus of the receptors (Fredriksson *et al.*, 2003). The rhodopsin family corresponds to family A in the classification system developed by Kolakowski (1994). The rhodopsin family is still the largest family with a total of 701 members and is further divided into four groups - α, β, γ and δ (Fredriksson *et al.*, 2003). In this classification system, the biogenic amine receptors are clustered in the α group while the complement receptors are clustered in the γ group (Figure 1.2).

Contrary to previous classifications based on sequence similarity, Lin *et al.* (2013) re-classified GPCRs based on their orthosteric ligand similarity, focusing on family A GPCRs. Analysis of over 146 GPCRs, each with a minimum of 6 ligands, resulted in the re-organisation of these receptors as shown in Figure 1.3 (Lin *et al.*, 2013). An interesting observation that can be made from this study is that the classification of these receptors based on their ligand similarity is strikingly different from the classification based on their sequence homology. For example, despite their close sequence homology to the β adrenoceptors (βARs), the α adrenoceptors (αARs) are pharmacologically more closely related to the 5-hydroxytyptamine (5-HT) or serotonin and the dopamine receptors compared to the βARs (Figure 1.3) (Lin *et al.*, 2013). This method of classification also resulted

This figure has been removed for copyright purposes.

Figure 1.3 Comparisons of family A GPCR classifications

Family A GPCRs are classified according to ligand binding site sequence similarity (A) or ligand similarity (B). Receptors that bind biogenic amines are highlighted in blue, melatonins in gold, lipids in green, peptides in black, purinergics in dark blue, adenosines in light blue, retinal in purple and orphan receptors are highlighted in red. The $\alpha_{1A/1D}$ adrenoceptors, β_2 adrenoceptors, serotonin 5-HT_{1A} and dopamine D_3 receptors are indicated with red arrows while the opioid receptors, complement receptors, chemokine CXCR4 receptor and neurotensin receptors are indicated with blue arrows. Figure adapted from (Lin *et al.*, 2013).

in the reorganisation of peptide-binding receptors such as the opioid receptors, complement receptors, chemokine receptors and neurotensin receptors. In this classification, the complement 3a receptor (C3aR) is placed away from the complement 5a receptor (C5aR). In addition, the neurotensin receptors become close relatives of the C5aR, along with the chemokine CXCR4 receptor and the opioid receptors (Figure 1.3) (Lin *et al.*, 2013).

The classification by Lin *et al*. (2013) reflects the conservation of the orthosteric binding pocket of these receptors and may be useful in the prediction of off-target side effects. For example, naftopidil and tamsulosin are $\alpha_{1A/1D}$AR antagonists used clinically for the treatment of benign prostatic hyperplasia (Andersson and Wyllie, 2003; Sorbi *et al.*, 2009). Both naftopidil and tamsulosin cause ejaculatory disorders which can be attributed to their off-target affinity at the 5-HT_{1A}R and the dopamine D_3 receptors (Andersson and Wyllie, 2003; Sorbi *et al.*, 2009; Yokoyama *et al.*, 2011).

1.1.2 Structures of GPCRs

The first crystal structure of a GPCR to be solved was that of bovine rhodopsin in 2000 (Palczewski *et al.*, 2000). The effort to crystallise GPCRs has proven difficult due to their inherent conformational flexibility (Ghosh *et al.*, 2015). The challenges in obtaining crystal structures of GPCRs include the production of large quantities of recombinant proteins that are stable in detergent, constraining the conformational flexibility of the receptors to yield crystals as well as generating crystals with desirable diffraction properties (Carpenter *et al.*, 2008; Ghosh *et al.*, 2015).

Recent advances in protein crystallography techniques have caused an exponential increase in the number of GPCRs solved over the last five years. As of August 2016, the structures of as many as 30 unique GPCRs can be found on the Protein Data Bank (PDB, http://www.rcsb.org/pdb/). Of these 30 GPCRs, 25 are from the rhodopsin family or family A, with at least one representative structure from the α, β, γ and δ branches. The opioid receptors from the γ branch are the only receptor group with all four subtypes solved (Granier *et al.*, 2012; Manglik *et al.*, 2012; Thompson *et al.*, 2012; Wu *et al.*, 2012).* They are closely followed by the α branch muscarinic acetylcholine receptors (mAChRs) with four out of five subtypes solved (M_1-M_4) (Haga *et al.*, 2012; Kruse *et al.*, 2012; Thal *et al.*, 2016) and the βARs with two out of three subtypes solved (β_1 and β_2) (Cherezov *et al.*, 2007; Warne *et al.*, 2008). Other receptors from the α branch which have been solved include the adenosine A_{2A} receptor (Jaakola *et al.*, 2008), sphingosine-1-phosphate receptor 1 (Hanson *et al.*, 2012), serotonin 5-HT_{1B} and 5-HT_{2B} receptors (Wacker *et al.*, 2013; Wang *et al.*, 2013a), dopamine D_3 receptor (Chien *et al.*, 2010) and histamine H_1 receptor (Shimamura *et al.*, 2011). The remaining eight family A GPCRs with their structures solved are the neurotensin 1 receptor from the β branch (White *et al.*, 2012), the chemokine CXCR1, CXCR4 and CCR5 receptors from the γ branch (Park *et al.*, 2012; Tan *et al.*, 2013; Wu *et al.*, 2010) and the protease-activated PAR1 receptor, purinergic $P2Y_1$ and $P2Y_{12}$ receptors and free fatty acid FFAR1 receptor from the δ branch (Srivastava *et al.*, 2014; Zhang *et al.*, 2012a; Zhang *et al.*, 2015; Zhang *et al.*, 2014). To date, the structures of the corticotropin-releasing hormone receptor 1 and the glucagon receptor from the

* If multiple structures of a receptor are available, only the first structure published is referenced.

secretin family (Hollenstein *et al.*, 2013; Siu *et al.*, 2013), the metabotropic glutamate receptor 1 and 5 from the glutamate family (Dore *et al.*, 2014; Wu *et al.*, 2014) and the smoothened receptor (Wang *et al.*, 2013b) from the frizzled/taste2 family have also been solved, leaving the adhesion family as the only family without a solved structure. Most of the GPCR structures solved so far are in inactive states. However, several GPCRs, such as the β_2AR, μ opioid receptor and M_2 mAChR have been solved in both the active and inactive states, allowing for the determination of the structural basis of GPCR activation (Cherezov *et al.*, 2007; Haga *et al.*, 2012; Huang *et al.*, 2015; Kruse *et al.*, 2013; Manglik *et al.*, 2012; Rasmussen *et al.*, 2011b).

The 30 GPCRs for which structures have been solved represent only 3% of known GPCRs that exist in humans, all of which have a tertiary structure of a seven TM-helix topology. The highest structural variation can be found on the extracellular domain of these receptors. In family A GPCRs, the ECL2 is the most variable structure. Figure 1.4 shows a superimposition of four family A GPCRs – rhodopsin (PDB ID 1F88), β_2AR (PDB ID 2RH1), dopamine D_2 receptor (PDB ID 3PBL) and M_3 mAChR. (PDB ID 4DAJ). There is considerable conservation of the structure of the TM helices where the endogenous ligands and most drugs that target these receptors bind. In contrast, there is a large variation in the structure of the ECL2 of these receptors, which may be exploited by drug discovery programs to improve receptor subtype selectivity and reduce off-target side effects.

Ballesteros and Weinstein took advantage of the conservation of the TM domains of family A GPCRs and developed a numbering system which allows for comparisons of residues across multiple GPCRs (1995). The first number in this

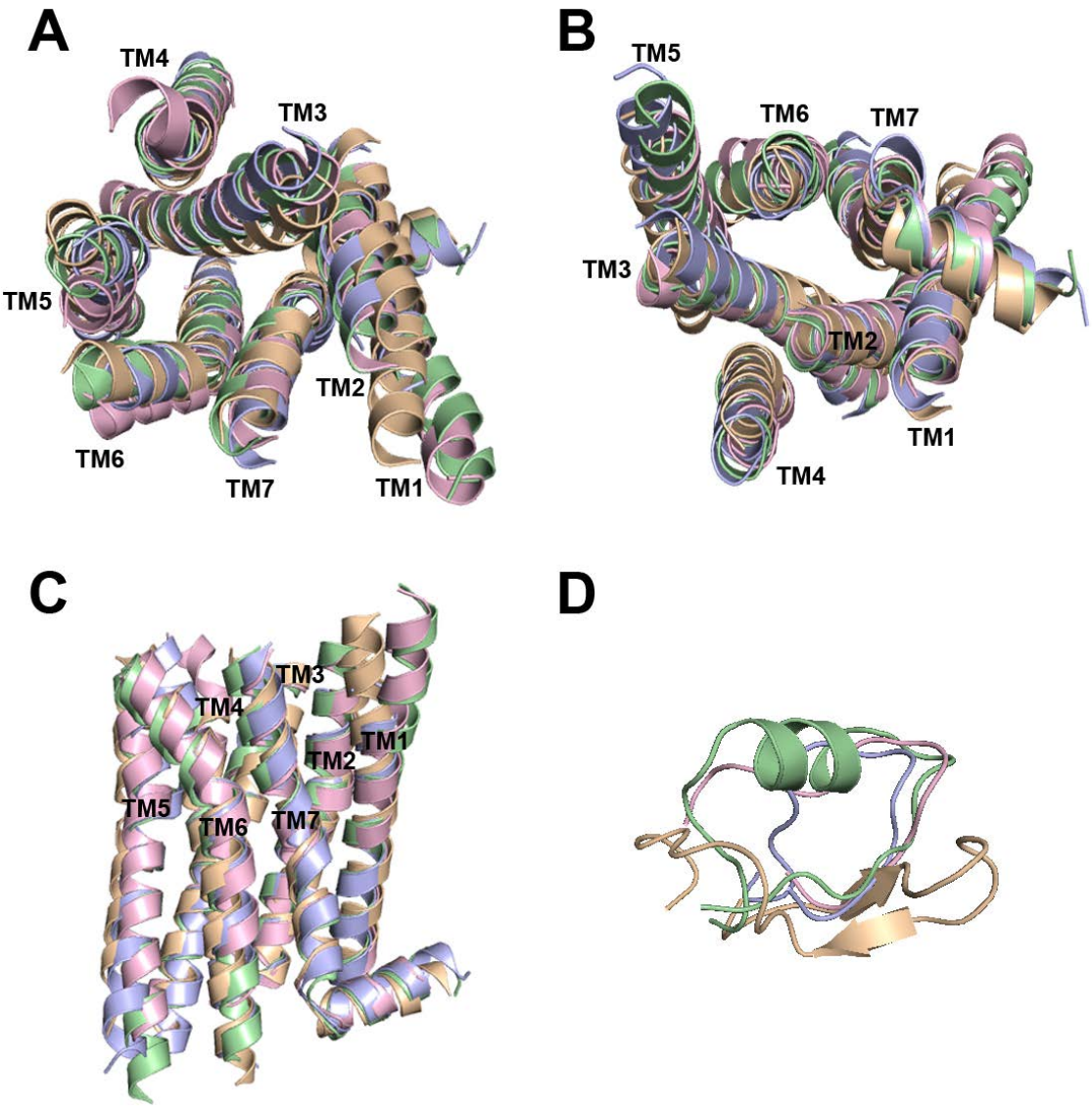

Figure 1.4 Comparisons of the structures of α branch family A GPCRs

The crystal structures of rhodopsin (PDB ID 1F88) in yellow, β_2AR (PDB ID 2RH1) in green, D_2 dopamine receptor (PDB ID 3PBL) in blue and M_3 mAChR (PDB ID 4DAJ) in pink are overlayed. Top down view (A), bottom up view (B), horizontal view (C) and overlay of the ECL2 (D). The loops have been removed in panel A-C to improve clarity. The receptors were aligned by the most conserved residue in each of the seven TM helices and the figures were generated using Pymol.

numbering system represents the helix in which the residue is located, while the second number represents the position of the residue relative to the most conserved residue in the helix. The most conserved residue in each helix is designated as residue .50, while the next N-terminal residue is designated .49 and the next C terminal residue is designated .51. For example, the most conserved residue in helix 1 of family A GPCR is an asparagine (N).† At the human β_2AR, this residue is designated $N^{1.50}$. The residue N-terminal to this conserved $N^{1.50}$ is $G^{1.49}$ and the residue C-terminal to $N^{1.50}$ is $V^{1.51}$. The Ballesteros-Weinstein numbering system is not used for residues on the loop regions due to the large variation in sequence and length. The Ballesteros-Weinstein numbering system will be used throughout this thesis.

1.2 The β_2AR

The endogenous catecholamines adrenaline and noradrenaline mediate their effects on the body through adrenoceptors. Nine distinct adrenoceptors have been cloned in humans, namely α_{1A}, α_{1B}, α_{1D}, α_{2A}, α_{2B}, α_{2C}, β_1, β_2 and β_3 ARs (Bylund, 1988; Cheung *et al.*, 1982; Cotecchia *et al.*, 1988; Emorine *et al.*, 1989; Lands *et al.*, 1967a; Lands *et al.*, 1967b; Lomasney *et al.*, 1991; Murphy and Bylund, 1988; Perez *et al.*, 1991; Petrash and Bylund, 1986; Schwinn *et al.*, 1990). Evidence exists for the presence of another pharmacologically distinct α_1AR, the α_{1L}AR, which has been suggested to be a functional isoform of the interactions between the α_{1A}AR and the cysteine rich epidermal growth factor like domain 1α (CRELD1α) (Nishimune *et al.*, 2010).

† One-letter amino acid codes are used in this thesis.

The β_2AR, like all adrenoceptors, is a member of the α branch of family A GPCRs. The gene for the β_2AR is located on q31-q32 of chromosome 5 and encodes 413 residues with a molecular mass of approximately 46.5 kilodaltons (kD) (Kobilka *et al.*, 1987). The β_2AR is primarily expressed in the lungs (Carstairs *et al.*, 1985; Regard *et al.*, 2008), but is also expressed in other tissues such as the blood vessels, heart, brain, adipose tissue, liver, bladder, uterus, kidneys and skeletal muscle (Blair *et al.*, 1979; Healy *et al.*, 1985; Heitz *et al.*, 1983; Hinkle *et al.*, 2002; Langin *et al.*, 1991; Longhurst and Levendusky, 1999; Simon *et al.*, 2003).

The β_2AR is a target for the treatment of asthma and chronic obstructive pulmonary disease (COPD) (Bateman *et al.*, 2008; Kew *et al.*, 2013; Qaseem *et al.*, 2011). Long-acting β_2AR agonists are used clinically in combination with inhaled corticosteroids or leukotriene receptor antagonists to provide acute symptomatic relief and as preventative treatment (Cazzola and Matera, 2007; Ducharme *et al.*, 2010). However, long term use of β_2AR agonists has been associated with increased exacerbations and mortality rate (Bateman *et al.*, 2008; Chowdhury and Dal Pan, 2010; Crane *et al.*, 1989; Lougheed *et al.*, 2012). In addition, β_2AR agonists often cause tachycardia due to off-target activation of the β_1AR and muscle tremor due to activation of the β_2AR on the skeletal muscle (Larsson and Svedmyr, 1977; Mann *et al.*, 1996). Prolonged use of β_2AR agonists has also been shown to cause tolerance due to receptor desensitisation (Haney and Hancox, 2005; Haney and Hancox, 2007). Therefore, there is a need for improved β_2AR pharmacotherapy, which could potentially be achieved with the use of allosteric modulators. Allosteric modulation of family A GPCRs is described in depth in section 1.4 of this literature review.

1.2.1 Structure of the β_2AR

The first crystal structure of the β_2AR was published in 2007 and is the first structure available of a GPCR that binds diffusible ligands (Cherezov *et al.*, 2007). The β_2AR is one of the best characterised GPCRs, not only pharmacologically but also structurally. As many as 19 distinct structures of the β_2AR have been deposited in the PDB (http://www.rcsb.org/pdb/). In addition, the β_2AR is the only GPCR that has been successfully crystallised with its cognate G protein $G_{\alpha s}$ (Rasmussen *et al.*, 2011a). Together with biophysical data of receptor activation (Altenbach *et al.*, 2008; Dunham and Farrens, 1999; Farrens *et al.*, 1996; Gether *et al.*, 1997; Gether *et al.*, 1995), the structures of active and inactive β_2ARs provide insights into the structural basis of GPCR activation, which will be further discussed in section 1.2.3 of this chapter.

In addition to seven TM helices, the β_2AR also possesses a short 8^{th} helix (Cherezov *et al.*, 2007). This short helix is also present in all other family A GPCRs for which structures have been solved. The ECL2 of the β_2AR adopts an α helix conformation and is displaced away from the TM domain of the receptor (Cherezov *et al.*, 2007). This ECL2 structure is distinct from most other family A GPCRs but is also present in the β_1AR (Warne *et al.*, 2008). The helix structure in the ECL2 of the β_2AR is stabilised by two disulfide bonds, $C106^{3.25}$ – $C191^{ECL2}$ and $C184^{ECL2}$ – $C190^{ECL2}$.‡

1.2.2 Orthosteric ligand binding at the β_2AR

The orthosteric ligand binding site of the β_2AR is located within the TM

‡ Superscript denotes Ballesteros-Weinstein residue numbering system.

domain approximately 11 Å from the extracellular surface of the receptor. Mutagenesis studies suggest that orthosteric ligand binding at the β_2AR involves a charge interaction between the positively charged ammonium moiety of the ligands with D113$^{3.32}$, hydrogen bonds between the meta and para hydroxyl groups with S203$^{5.42}$, S204$^{5.43}$ and S207$^{5.46}$, a π- π interaction between the phenyl rings of the ligands with F289$^{6.51}$ and F290$^{6.52}$ and an interaction between the β-hydroxyl group with N293$^{6.55}$ (Liapakis *et al.*, 2000; Strader *et al.*, 1989a; Strader *et al.*, 1989b; Strader *et al.*, 1989c; Strader *et al.*, 1987; Wieland *et al.*, 1996). These mutagenesis studies are supported by the crystal structure of adrenaline-bound β_2AR (Figure 1.5) (Ring *et al.*, 2013). In this active state crystal structure, adrenaline can be seen to interact with D113$^{3.32}$, V114$^{3.33}$, V117$^{3.36}$, S203$^{5.42}$, F290$^{6.52}$, N293$^{6.55}$ and N312$^{7.39}$ (Figure 1.5).

Analysis of the active and inactive state β_2AR crystal structures reveals subtle structural differences in the orthosteric binding pocket following agonist and antagonist binding. Compared to an inactive structure, agonist binding at the β_2AR caused an inward bulge of TM5 at S207$^{5.46}$ of approximately 2 Å, suggesting a more contracted pocket (Rasmussen *et al.*, 2011b). In the active structure, the agonist BI-167107 made extensive polar interactions with D113$^{3.32}$, S203$^{5.42}$, S207$^{5.46}$, N293$^{6.55}$ and N312$^{7.39}$ (Rasmussen *et al.*, 2011b). In contrast, polar interactions were only observed for D113$^{3.32}$, S203$^{5.42}$ and N312$^{7.39}$ with the inverse agonist carazolol (Rasmussen *et al.*, 2011b). Also in the active state crystal structure, F193^{ECL2} and Y308$^{7.35}$ located at the top of TM7 move closer towards one another to close off the binding pocket from the extracellular space (Rasmussen *et al.*, 2011b). In addition, K305$^{7.32}$ redirects its interaction from D192^{ECL2} to the

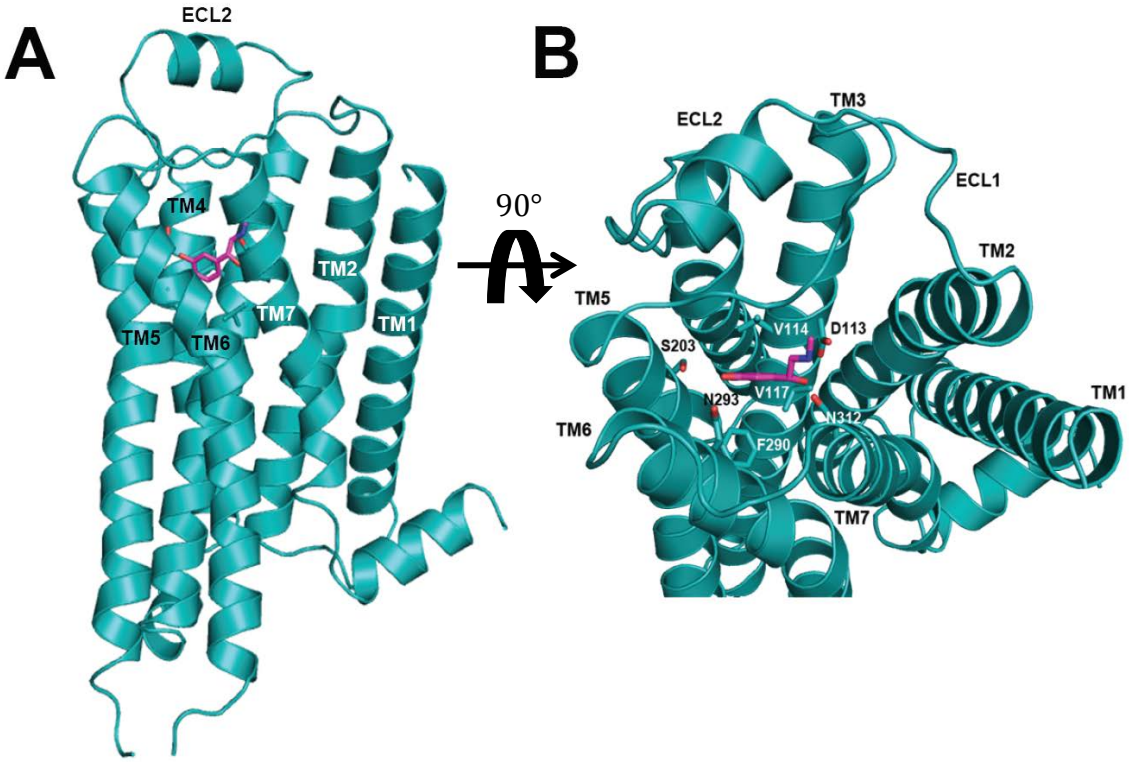

Figure 1.5 Crystal structure of the β_2AR bound to adrenaline

The X-ray crystal structure of human β_2 adrenoceptor (β_2AR) in the presence of adrenaline (PDB ID 4LDO) (Ring *et al.*, 2013). Side view (A), top view (B). The β_2AR and interacting amino acids are shown in teal, while adrenaline is shown in magenta. Oxygen atoms are shown in red and nitrogen atoms are shown in blue. The co-crystallised nanobody Nb6B9 was removed for clarity. Figures were generated using Pymol.

backbone carbonyl group of F193^{ECL2} to stabilise the F193^{ECL2}-Y308$^{7.35}$ "gate" in a closed position (DeVree *et al.*, 2016) (Figure 1.6).

The orthosteric binding site of the β_1AR and β_2AR is highly conserved. This high conservation is reflected in the difficulty in developing selective ligands for these receptors (Baker, 2005; Baker, 2010). Seven out of nine interactions of the inverse agonist carazolol at the β_2AR can be found at the turkey β_1AR (Cherezov *et al.*, 2007; Moukhametzianov *et al.*, 2011). These common interactions include D113$^{3.32}$, V114$^{3.33}$, V117$^{3.36}$, F193^{ECL2}, F290$^{6.52}$, N293$^{6.55}$ and N312$^{7.39}$ (Cherezov *et al.*, 2007; Moukhametzianov *et al.*, 2011). In addition, at the β_1AR, the antagonist cyanopindolol has been shown to also interact with residues corresponding to D113$^{3.32}$, S203$^{5.42}$, S207$^{5.46}$ and N293$^{6.55}$ of the β_2AR (Warne *et al.*, 2008).

1.2.3 Activation of the β_2AR

The β_2AR primarily couples to $G_{\alpha s}$ and its activation leads to increased intracellular 3',5'-cyclic adenosine monophosphate (cAMP) concentrations and protein kinase A (PKA) activation (Figure 1.7) (Hausdorff *et al.*, 1989; Strulovici *et al.*, 1984). PKA activation in bronchial smooth muscle has been shown to promote Ca^{2+}/Na^{+} exchange resulting in decreased intracellular calcium concentrations and increased bronchial smooth muscle relaxation (Giembycz and Raeburn, 1991; Gunst and Stropp, 1988). The activation of β_2AR-mediated $G_{\alpha s}$ signalling results in the initiation of a negative feedback loop which switches the coupling efficiency of the β_2AR from $G_{\alpha s}$ to $G_{\alpha i}$ (Figure 1.7) (Daaka *et al.*, 1997). This switch in coupling efficiency decreases intracellular cAMP concentrations and is mediated by phosphorylation of the receptor by PKA (Daaka *et al.*, 1997). In addition, activation

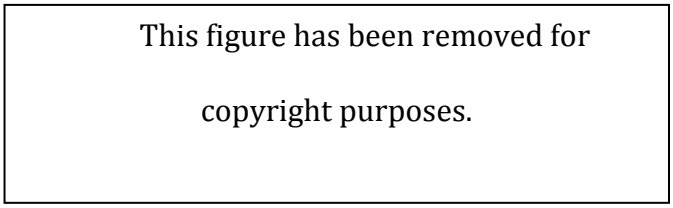

Figure 1.6 Movement of the extracellular residues of the β_2AR following agonist binding

Superimposition of the extracellular residues of the β_2AR in the active (cyan) and inactive (grey) β_2AR crystal structures. Agonist binding at the β_2AR causes extracellular residues F193^{ECL2} and Y308$^{7.53}$ to move closer to each other, resulting in a closed pocket. In addition, K305$^{7.32}$ redirects its interaction from D192^{ECL2} to the carbonyl group of F193^{ECL2} to stabilise the F193^{ECL2}-Y308$^{7.35}$ "gate" in a closed position. Figure adapted from DeVree *et al.* (2016).

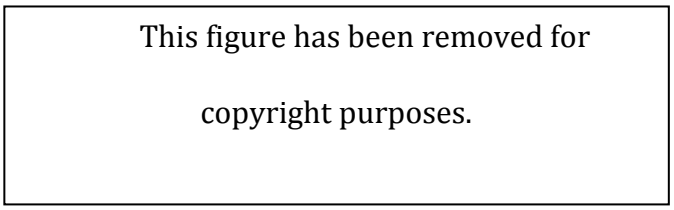

Figure 1.7 β_2AR signalling pathways

The binding of an agonist at the β_2AR promotes $G_{\alpha s}$ coupling to the receptor, which activates adenylate cyclase (AC) resulting in increased intracellular 3',5'-cyclic adenosine monophosphate (cAMP) and activation of protein kinase A (PKA). Activation of PKA switches the coupling efficiency of the β_2AR from $G_{\alpha s}$ to $G_{\alpha i}$, which decreases intracellular cAMP. Phosphorylation of PKA also results in the activation of the mitogen-activated protein kinase (MAPK) signalling pathways. The β_2AR can also activate the MAPK signalling pathways independent of G protein coupling. Phosphorylation of the β_2AR by G protein-coupled receptor kinase (GRK) promotes β-arrestin recruitment. β-arrestin-bound β_2AR internalises and can be recycled or degraded, but can also activate the MAPK signalling pathways. Figure adapted from Padro (2013).

of $G_{\alpha i}$ has been shown to activate the mitogen-activated protein kinase (MAPK) signalling pathway (Daaka *et al.*, 1997).

Termination of $G_{\alpha s}$-mediated β_2AR signalling occurs via the recruitment of β-arrestins, a process which is mediated by G protein-coupled receptor kinases GRK1 and 2 (Benovic *et al.*, 1987; Shenoy *et al.*, 2006). Subsequent binding of β-arrestins to the cytoplasmic domain of the β_2AR results in clathrin-mediated endocytosis and receptor desensitisation (Ahn *et al.*, 2003; Ferguson *et al.*, 1995; Goodman *et al.*, 1996; Lin *et al.*, 1997; Mundell *et al.*, 1999). Later studies have subsequently showed that β-arrestins can also function as signalling proteins. The functional role of β-arrestins is dependent on the subtype of the GRK that phosphorylates the receptor (Shenoy *et al.*, 2006). While phosphorylation of the β_2AR by GRK1 and 2 results in receptor desensitisation, phosphorylation of the β_2AR by GRK5 and 6 have been shown to result in β-arrestin-mediated receptor signalling (Figure 1.7) (Millman *et al.*, 2004; Nobles *et al.*, 2011; Shenoy *et al.*, 2006). β-arrestins have been shown to mediate the activation of the MAPK pathway leading to activation of extracellular-signal regulated kinases 1/2 (ERK 1/2) independent of G protein activity (Nobles *et al.*, 2011; Shenoy *et al.*, 2006). Shenoy *et al.* (2006) showed that while G protein-dependent signalling of the β_2AR was rapid and transient, β-arrestin or G protein-independent signalling occurred at a slower rate and was sustained (Shenoy *et al.*, 2006).

Unlike the subtle structural changes in the orthosteric binding pocket of the β_2AR following agonist binding, receptor activation involves a more dramatic structural rearrangement of the cytoplasmic end of the TM helices (Rasmussen *et al.*, 2011b). In the active state β_2AR crystal structure, the cytoplasmic end of TM5

and 6 moved outwards, while the cytoplasmic end of TM3 and 7 moved inwards (Rasmussen *et al.*, 2011b). The most dramatic movement was observed for TM6, where E268$^{6.30}$ from the E/DRY motif located at the cytoplasmic end of TM6 was displaced 11.4 Å outwards and Y326$^{7.53}$ from the NPXXY motif moved to the space previously occupied by E268$^{6.30}$ in the inactive state (Rasmussen *et al.*, 2011b). The E/DRY motif is highly conserved in family A GPCRs and has been proposed to play a role in receptor activation (Mirzadegan *et al.*, 2003; Valentin-Hansen *et al.*, 2012). R$^{3.50}$ from the E/DRY motif has been observed to form salt bridge interactions with E/D$^{3.49}$ and also with E$^{6.30}$ in many inactive family A GPCR crystal structures and these salt bridge interactions have been proposed to maintain GPCRs in an inactive state (Chien *et al.*, 2010; Okada *et al.*, 2004; Valentin-Hansen *et al.*, 2012). Mutagenesis data showed that the mutation of R131$^{3.50}$ and E268$^{6.30}$ from the NPXXY motif resulted in constitutively active mutant β_2ARs (Valentin-Hansen *et al.*, 2012). In agreement with these data, the salt bridge between D130$^{3.49}$ and R131$^{3.50}$ was broken in the active state β_2AR crystal structure (Rasmussen *et al.*, 2011b). The same structural rearrangement and the breakage of the salt bridge between D130$^{3.49}$ and R131$^{3.50}$ can be observed in the active structure of the μ opioid receptor and the M_2 mAChR, suggesting a conserved mechanism of receptor activation in family A GPCRs (Huang *et al.*, 2015; Kruse *et al.*, 2013).

The β_2AR is the only GPCR that has been successfully crystallised with its cognate intracellular signalling protein $G_{\alpha s}$ (Rasmussen *et al.*, 2011a). In the presence of $G_{\alpha s}$, E268$^{6.30}$ of the E/DRY motif moved outwards by 14 Å, which is 3 Å more than in the active state β_2AR crystal structure obtained in the absence of $G_{\alpha s}$ (Rasmussen *et al.*, 2011a; Rasmussen *et al.*, 2011b), suggesting that G protein

coupling is needed to achieve "full" activation state. The β_2AR interacted with the α5-helix of $G_{\alpha s}$ at the cavity formed by the cytoplasmic end of TM5 and 6 (Rasmussen *et al.*, 2011a). $R131^{3.50}$ of the E/DRY motif was seen to interact with Y391 of the α5-helix and $Y326^{7.53}$ of the NPXXY motif (Rasmussen *et al.*, 2011a). In addition, $T68^{2.39}$ and $D130^{3.49}$ near the cytoplasmic end of the β_2AR interacted with $Y141^{ICL2}$ such that $F139^{ICL2}$ occupied a hydrophobic pocket on the surface of $G_{\alpha s}$, linking it to the β_2AR through the E/DRY motif (Rasmussen *et al.*, 2011a).

1.3 The complement 5a receptor

The C5aR binds endogenous complement 5a (C5a), a potent pro-inflammatory peptide produced in the activation of the complement cascade. There are two subtypes of C5aR, namely C5aR1 (CD88) and C5aR2, also known as C5L2 (GPR77). C5aR1 will be referred to as C5aR throughout this thesis. Both C5aR and C5aR2 belong to the γ branch of family A GPCRs and are close relatives of the chemoattractant receptors, such as the formyl peptide receptors and leukotriene B4 receptors (Fredriksson *et al.*, 2003). The genes for both C5aR and C5aR2 are located on q13.33-13.34 of chromosome 19 (Gerard *et al.*, 1993; Lee *et al.*, 2001). The C5aR is 350 amino acids in length and has a molecular weight of approximately 47 kDa (Boulay *et al.*, 1991), whereas C5aR2 is 337 amino acids in length with a molecular weight of approximately 37 kDa (Ohno *et al.*, 2000).

The C5aR was first discovered on leukocytes such as neutrophils, eosinophils, basophils, monocytes, macrophages and mast cells (Gerard *et al.*, 1989; Kiener *et al.*, 1998; Siciliano *et al.*, 1990). However, it was later discovered that the C5aR is also widely expressed on other cells of the body, including cells of the central

nervous system, blood vessels, kidney, heart and liver (Braun and Davis, 1998; Gasque *et al.*, 1995; Lacy *et al.*, 1995; Laudes *et al.*, 2002; Niederbichler *et al.*, 2006). Increased serum C5a levels have been associated with many inflammatory disorders, such as arthritis, age-related macular degeneration, Alzheimer's disease, inflammatory bowel diseases, systemic lupus erythematosus and sepsis (Ager *et al.*, 2010; Grant *et al.*, 2002; Huber-Lang *et al.*, 2002; Liu *et al.*, 2011; Mahajan *et al.*, 2015; Woodruff *et al.*, 2003; Woodruff *et al.*, 2002). Interestingly, C5a has also been shown to play a role in miscarriage as well as in cerebral malaria (Girardi *et al.*, 2003; Patel *et al.*, 2008). Therefore, the C5aR is an important drug target for a wide range of inflammatory diseases.

1.3.1 C5aR signalling

The C5aR couples to pertussis toxin-sensitive G proteins $G_{i\alpha 2}$ and $G_{i\alpha 3}$ and pertussis toxin insensitive $G_{\alpha 16}$ (Amatruda *et al.*, 1993; Rollins *et al.*, 1991). Activation of the C5aR can lead to intracellular calcium mobilisation and activation of various signalling pathways, such as the phosphatidylinositol-3-kinase (PI3K)/Akt, Ras/B-Raf/MAPK/ERK, phospholipase D, protein kinase C (PKC), p-21 activated kinase and NF-κB pathways (Buhl *et al.*, 1994; Huang *et al.*, 1998; Kastl *et al.*, 2006; Mullmann *et al.*, 1990; Perianayagam *et al.*, 2002; Perianayagam *et al.*, 2004). The C5aR has an anti-apoptotic role in human neutrophils. Activation of the PI3K pathway has been shown to inhibit the activation of pro-apoptotic caspase 9 resulting in delayed apoptosis (Perianayagam *et al.*, 2002; Perianayagam *et al.*, 2004). Activation of phospholipase D has also been shown to regulate neutrophil functions such as phagocytosis and cell degranulation (Gomez-Cambronero *et al.*,

2007). Meanwhile, activation of the Ras/Raf/MAPK/ERK pathway has been shown to increase reactive oxygen species production in macrophages (Torres and Forman, 1999). Activation of the C5aR in neutrophils has been shown to inhibit the NF-κB pathway, while in macrophages C5a activates the NF-κB pathway leading to increased production of chemokines and cytokines (Guo *et al.*, 2004).

1.3.2 The binding of C5a at the C5aR

C5a is a 74-amino acid polypeptide glycosylated at position 64 with a molecular weight of approximately 12 kDa (Fernandez and Hugli, 1978). An NMR structure of human C5a suggests an anti-parallel four-helix core which is stabilised by three disulfide bonds at position C21-C47, C22-C54 and C34-C55 (Figure 1.8A) (Zhang *et al.*, 1997). The C-terminal tail of C5a, residues 69-74, forms a bulky helix which resembles a hook and is connected to the four-helix core via a short loop (Zhang *et al.*, 1997). In the body, C5a is metabolised by removal of its terminal arginine into C5a-desArg by serum and cell surface carboxypeptidases (Bokisch and Muller-Eberhard, 1970).

The C5aR binds C5a with low nanomolar affinity and the affinity of its less potent metabolite C5a-desArg at the C5aR is approximately 10 to 100 fold lower (Finch *et al.*, 1997; Huey and Hugli, 1985; Okinaga *et al.*, 2003; Scola *et al.*, 2007). The C-terminal tail of C5a has been shown to play an important role in receptor activation (Bubeck *et al.*, 1994; Mollison *et al.*, 1989; Toth *et al.*, 1994). A two-site binding mechanism known as the message-address model has been proposed for the binding of C5a at the C5aR where high affinity binding is conferred from the interactions between the acidic residues from the N-terminus of the C5aR with the

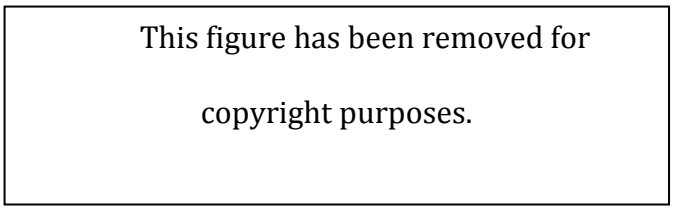

Figure 1.8 C5a and the C5a receptor

(A) An NMR structure of human C5a suggests that C5a adopts a four-helix conformation which is stabilised by three disulfide bonds. The C-terminal tail of C5a is connected to the four-helix core by a short loop. (B) The four-helix core of C5a interacts with the N-terminus and the extracellular loops of the C5aR, while its C-terminal tail interacts with residues within the transmembrane domain of the receptor. Figure reproduced from Ward (2004).

basic residues in the core of C5a (message) and receptor activation is mediated by the interactions between the charged residues at the ECLs and TM helices of the C5aR with the C-terminal tail of C5a (address) (Figure 1.8B) (Boulay *et al.*, 1991; DeMartino *et al.*, 1994; Morgan *et al.*, 1993; Pease *et al.*, 1994).

1.3.2.1 N-terminus binding site

The importance of the N-terminus of the C5aR in the binding of C5a was first demonstrated by Morgan *et al.* (1993) whereby antibodies directed against the N-terminus of the C5aR inhibit the ability of C5a to bind and activate the C5aR. The role of the N-terminus of the C5aR in the binding of C5a was also shown by DeMartino *et al*. (1994) where removal of the first 30 amino acids of the C5aR resulted in a 75 fold decrease in the affinity of C5a. The high affinity binding between C5a and the C5aR has been attributed to the interactions between the positively charged amino acids on the four-helix bundle of C5a and the aspartic acid residues on the N-terminus of the C5aR, as mutations of these residues significantly decreased the ability of C5a to bind to the C5aR (DeMartino *et al.*, 1994; Mery and Boulay, 1994). In addition to these negatively charged residues, sulphated Y11 and Y14 of the C5aR have also been shown to be important for the binding of C5a, as mutation of these residues resulted in a complete loss of C5a binding and a 50% reduction in C5a binding respectively (Farzan *et al.*, 2001).

1.3.2.2 ECL and TM binding site

The presence of additional binding sites at the C5aR was suggested by the

observation that the C-terminal tail of C5a and peptide analogues derived from the C-terminal tail of C5a can bind to and activate the C5aR, although with decreased affinity and potency compared to native C5a (DeMartino *et al.*, 1995; Finch *et al.*, 1997; Kawai *et al.*, 1991). Mutagenesis studies have identified several ECL and TM residues that are important for the binding of C5a at the C5aR.

R206$^{5.42}$ located at the top of TM5 has been suggested as an interacting partner for the R74 of C5a (DeMartino *et al.*, 1995). Using a hexapeptide analogue derived from the C-terminal tail of C5a, DeMartino *et al.* (1995) suggested that the carboxylate group of R74 of C5a interacts with the guanidinium group of R206$^{5.42}$ of the C5aR. The removal or amidation of the C-terminal carboxylate group of the peptide decreased its affinity for the WT C5aR by 40 – 200 fold (DeMartino *et al.*, 1995). However, the mutation R206$^{5.42}$A has little effect on C5a or peptides that terminate in arginine (DeMartino *et al.*, 1995). Interestingly, the R206$^{5.42}$A mutation increased the affinity of peptides which contain a guanidine group but have their carboxyl group deleted, thus suggesting that the carboxyl group of the peptide is important to prevent the loss of binding at the C5aR (DeMartino *et al.*, 1995). The mutation R206$^{5.42}$A resulted in the inability of C5a-desArg to activate the C5aR, but not C5a, suggesting that a direct interaction between R74 of C5a and R206$^{5.42}$ of the C5aR is unlikely (Cain *et al.*, 2001a) and that the interactions of C5a may differ from peptide agonists. In addition, the mutation R206$^{5.42}$H has been shown to completely inactivate a constitutively active mutant C5aR I124$^{3.40}$N/L127$^{3.43}$Q, suggesting that R206$^{5.42}$ plays a role in C5aR activation (Gerber *et al.*, 2001).

R74 of C5a has also been proposed to interact with D282$^{7.35}$ and R175^{ECL2} of the C5aR (Cain *et al.*, 2001a; Cain *et al.*, 2003; Higginbottom *et al.*, 2005). The mutation D282$^{7.35}$A decreased the ability of C5a to activate the C5aR, but not C5a-desArg (Cain *et al.*, 2001a). Similarly, the ability of the mutant C5a R74A to activate the C5aR was decreased by 60 fold compared to native C5a, but only decreased by 2 fold at the D282$^{7.35}$A C5aR mutant (Cain *et al.*, 2001a). In addition, the mutant C5a R74D was inactive at wild type (WT) and D282$^{7.35}$A C5aR, but active at the D282$^{7.35}$R C5aR mutant (Cain *et al.*, 2001a). These data suggest a direct interaction between R74 of C5a and D282$^{7.35}$ of the C5aR. Another possible C5a contact residue is R175^{ECL2} located at the interface between ECL2 and the top of TM4 (Cain *et al.*, 2003; Higginbottom *et al.*, 2005). The mutant C5aRs R175^{ECL2}A and R175^{ECL2}D have a reduced affinity for C5a and C5a-desArg and lost nearly all signalling with C5a and C5a-desArg, suggesting that these mutations may cause a conformational change of the receptor which resulted in the loss of G protein coupling (Cain *et al.*, 2003; Higginbottom *et al.*, 2005). However, the mutant C5aRs R175^{ECL2}A and R175^{ECL2}D can be strongly activated by a mutant form of C5a-desArg (C27R/E32A/Q60R/D69A/Q72L), but not native C5a or C5a-desArg, suggesting that these mutations have not caused a loss in signalling capabilities (Cain *et al.*, 2003). Instead, a specific interaction between R74 of C5a and R175^{ECL2} of the C5aR was lost when R175^{ECL2} was mutated to either an alanine or arginine (Cain *et al.*, 2003). The residue analogous to R175^{ECL2} at the closely related complement 3a receptor (C3aR) has been shown to be involved in the interaction of the C-terminal carboxylate of complement 3a (C3a) (Sun *et al.*, 1999).

K68 of C5a has been proposed to interact with E199$^{5.35}$ at the top of TM5 of the C5aR (Crass *et al.*, 1999; Monk *et al.*, 1995). The mutations E199$^{5.35}$Q and E199$^{5.35}$K reduced the affinity and potency of C5a (Crass *et al.*, 1999; Monk *et al.*, 1995). The reduction in the affinity and potency of C5a at the E199$^{5.35}$K mutant can be reversed by the mutant C5a K68E, suggesting a specific interaction between K_{68} of C5a and E199$^{5.35}$ of the C5aR (Crass *et al.*, 1999). If K68 of C5a interacts with E199$^{5.35}$, C5a and C5a-desArg would be expected to have identical affinity and potency at the E199$^{5.35}$Q mutant. However, the affinity and potency of C5a-desArg was lower at the E199$^{5.35}$Q mutant compared to C5a (Monk *et al.*, 1995). A nine-amino acid peptide agonist lacking the C-terminal arginine could weakly activate the WT receptor, but not the E199$^{5.35}$Q mutant. However, a peptide with a C-terminal arginine and a methionine instead of a lysine residue at position 2 of the peptide had equal potencies at both the WT and E199$^{5.35}$Q mutant C5aRs, suggesting that K68 and not R74 interacts with E199$^{5.35}$, as K68 and R74 were the only positively charged amino acids present on the C-terminal tail of C5a (Monk *et al.*, 1995).

C5a has also been shown to interact with a number of residues located deep within the TM domain of the C5aR. Using site-specific disulfide capture, P113$^{3.29}$, L117$^{3.33}$ and G262$^{6.55}$ have been shown to play a role in the interaction between C5a and the C5aR (Buck *et al.*, 2005). D82$^{2.50}$ has also been shown to be important for C5a-mediated activation of the C5aR, but not for its binding (Kolakowski, 1994; Monk *et al.*, 1994).

The binding of C5a at the C5aR was modelled by Nikiforovich *et al.* (2008) using a homology model based on a crystal structure of rhodopsin with *de novo*

loop generation. The results of this computational study largely agree with available mutagenesis data. In this model, D15, D16 and D21 of C5aR were predicted to interact with K17 of the C5aR, suggesting that the decrease in the affinity of C5a previously observed with the C5aR containing multiple aspartic acid mutation at these positions may be due to a disruption in the conformation of the receptor, rather than loss of specific interactions (Mery and Boulay, 1994; Nikiforovich *et al.*, 2008). Also in this model, D18 of the C5aR was predicted to interact with K19 or K20 of C5a, which is in agreement with the mutagenesis data which showed that the mutations K19A and K20A of C5a decreased its affinity for the C5aR (Bubeck *et al.*, 1994; Toth *et al.*, 1994). Another interaction that was predicted in this model was the interaction of C27 of C5a with region 24-30 of the C5aR, which has been suggested to interact with C5a in a random saturation mutagenesis studies (Hagemann *et al.*, 2008; Hagemann *et al.*, 2006; Nikiforovich *et al.*, 2008). With regards to the interactions of C5a with residues on the ECL loops and TM helices of the C5aR, the model predicted an extensive list of potential interactions such as $L117^{3.33}$, $M120^{3.36}$, $Y121^{3.37}$, $L167^{4.56}$, $F172^{4.61}$, $L187^{ECL2}$, $C188^{ECL2}$, $D191^{ECL2}$, $H194^{ECL2}$, $E199^{5.35}$, $R200^{5.36}$, $A203^{5.39}$, $R206^{5.42}$, $L207^{5.43}$, $L209^{5.45}$, $P214^{5.50}$, $M265^{6.58}$, $L277^{7.30}$ and $K279^{7.32}$ (Nikiforovich *et al.*, 2008), supporting the experimental data for residues such as $L117^{3.33}$ and $E199^{5.35}$ previously shown to interact with C5a in mutagenesis studies (Buck *et al.*, 2005; Crass *et al.*, 1999; Monk *et al.*, 1995).

1.3.3 C5aR2

Like the C5aR, C5aR2 is also expressed in immune and non-immune cells such

as neutrophils, macrophages, immature dendritic cells, adipocytes, skin fibroblasts, spleen, adrenal gland, liver, lung, kidney, brain and heart (Chen *et al.*, 2007; Gao *et al.*, 2005; Kalant *et al.*, 2005; Ohno *et al.*, 2000). C5aR2 shares 38% sequence homology to the C5aR and the same pattern of acidic and hydrophobic residues in the N-terminus, ECL and TM regions as the C5aR, which has been shown to play an important role in the binding of C5a (Ohno *et al.*, 2000; Scola *et al.*, 2007). However, C5aR2 lacks the highly conserved E/DRY motif which is important for G protein-mediated signalling of family A GPCRs. C5aR2 has been shown to lack signalling capabilities as measured in calcium assays, cell degranulation assays and MAPK activation assays (Cain and Monk, 2002; Johswich *et al.*, 2006; Kalant *et al.*, 2003; Mirzadegan *et al.*, 2003; Ohno *et al.*, 2000; Okinaga *et al.*, 2003; Valentin-Hansen *et al.*, 2012). Instead, C5aR2 has DLC in place of E/DRY and C5aR2 with the L132$^{3.50}$R mutation has been shown to couple to $G_{\alpha16}$ in transfected HEK-293T cells and is able to cause a small increase in intracellular calcium levels, suggesting that the lack of E/DRY motif results in the inability of the C5aR2 to couple to G proteins (Okinaga *et al.*, 2003).

The role of C5aR2 in inflammation is currently not well understood. Scola *et al.* (2009) proposed that C5aR2 acts as a recycling decoy receptor which removes active C5a from the plasma, as C5aR2 is constitutively internalised through a clathrin-mediated mechanism, causing C5a and its active metabolite, C5a-desArg, to be degraded in intracellular compartments. Similarly, Bamberg *et al.* (2010) suggested an anti-inflammatory role for C5aR2 as C5aR2 was found to inhibit β-arrestin-mediated C5aR signalling by C5a. However, a pro-inflammatory role for C5aR2 has also been reported in the literature. C5aR2-deficient mice were shown

to have a reduced mortality rate compared to wild type mice following a cecal-ligation and puncture model of sepsis and the C5aR2-deficient mice also had significantly lower plasma concentrations of inflammatory mediators (Rittirsch *et al.*, 2008). The pro-inflammatory role of C5aR2 in sepsis was suggested to be mediated through the inflammatory mediator HMGB1 via the MAPK pathway, despite the lack of the E/DRY motif which is essential for G protein coupling (Rittirsch *et al.*, 2008). C5L2 has been suggested to signal through ERK1/2 and Akt pathways in polymorphonuclear leukocytes (PMNs), as C3a and C5a-mediated activation of these signalling pathways were impaired in the PMNs of C5L2 deficient mice (Chen *et al.*, 2007).

1.3.4 C5aR antagonists

The C5aR is an active target for the treatment of a wide range of inflammatory diseases. There is currently no clinically available C5aR antagonist and the effort to commercialise C5aR antagonists is currently ongoing. One of the reasons for the difficulty in developing a successful small molecule inhibitor of the C5aR may be due to the large peptidic nature of C5a, which may be difficult to antagonise with small molecules. Currently, the only clinically approved therapy targeting the C5a-C5aR axis is eculizumab (Soliris), a monoclonal antibody against C5a used for the treatment of congenital atypical haemolytic-uremic syndrome and paroxysmal nocturnal hemoglobinuria (Hillmen *et al.*, 2006; Legendre *et al.*, 2013).

PMX53 (AcF[OPdChaWR])[§] is one of the most potent cyclic peptidomimetic antagonists of the C5aR (Figure 1.9) (March *et al.*, 2004; Paczkowski *et al.*, 1999). PMX53 was developed from the modification of a partial agonist based on the C-terminal tail of C5a, MeFKPdChaFr (Drapeau *et al.*, 1993). The substitution of phenylalanine to tryptophan at position 5 of the linear hexapeptide resulted in the first antagonist of the C5aR, MeFKPdChaWr (Konteatis *et al.*, 1994). PMX53 was developed by further substitution and cyclisation of the linear peptide antagonist (March *et al.*, 2004; Paczkowski *et al.*, 1999). PMX53 binds to the human C5aR with low nanomolar affinity and despite being developed from the C-terminal tail of C5a, inhibits C5a-mediated receptor activation in an apparently non-competitive manner (Finch *et al.*, 1999; March *et al.*, 2004; Paczkowski *et al.*, 1999). The precise molecular mechanism of PMX53 inhibition has not been investigated.

PMX53 showed promise in many rodent models of inflammatory diseases such as arthritis, sepsis, inflammatory bowel diseases and ischemia-reperfusion injuries (Arumugam *et al.*, 2002; Huber-Lang *et al.*, 2002; Woodruff *et al.*, 2003; Woodruff *et al.*, 2002). PMX53 was licenced to Promics Pty Ltd in 1999 and completed phase Ia and phase Ib/IIa clinical trials in psoriasis and rheumatoid arthritis(Woodruff *et al.*, 2011). While PMX53 was shown to be effective in a rat model of rheumatoid arthritis (Woodruff *et al.*, 2002), it failed to show any efficacy in a cohort of patients suffering from rheumatoid arthritis (Vergunst *et al.*, 2007). It has since been argued that the limited timeframe and study size may have confounded the outcomes of the study (Woodruff *et al.*, 2011). However, PMX53 was efficacious in psoriasis with 9 out of 10 patients in the trial showed improvements (Kohl, 2006).

[§] Peptides are described using one-letter amino acid symbols. L-amino acids are shown in capitals and D-amino acids in small letters. Synthetic amino acids L-ornithine and D-cyclohexylalanine are denoted O and dCha respectively. Ac – acetylated, Me – methylated.

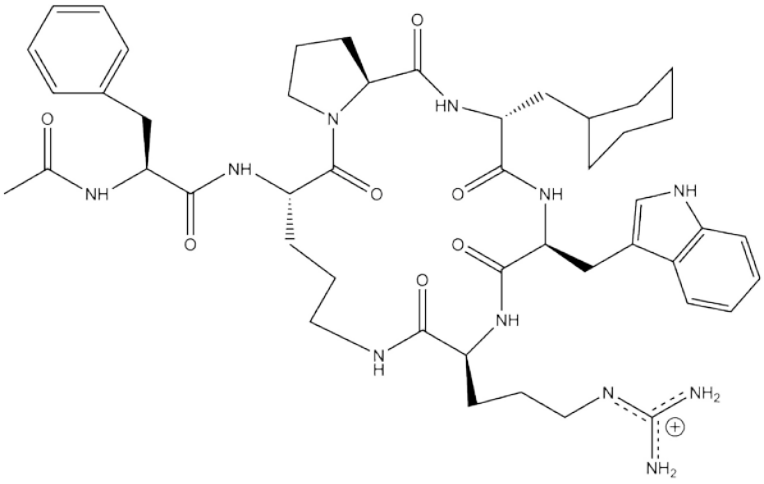

Figure 1.9 Chemical structure of PMX53

The chemical structure of the C5aR cyclic peptidomimetic antagonist PMX53 (AcF[OPdChaWR]).

Further development of PMX53 and its analogue with improved pharmacokinetics profile, PMX205, has not been announced since the lapse of the patent in 2014.

An understanding of the binding site and the molecular mechanism of PMX53 inhibition at the C5aR will be useful in the design of next generation C5aR antagonists. PMX53 exhibits species selectivity in that it binds to human, rat and dog PMNs with high affinity, but with lower affinity to other species such as mouse, sheep, pig, rabbit and guinea pig (Woodruff *et al.*, 2001). The affinity of PMX53 at the human and rat C5aR is 90 nM and 40 nM respectively, whereas its affinity for the mouse C5aR is approximately 400 fold less at 36 μM (Woodruff *et al.*, 2001). Guided by the sequence alignment of these species, residues on the first ECL of the human C5aR, $P103^{ECL1}$ and $G105^{ECL1}$, were identified as possible interaction sites for PMX53 (Cain *et al.*, 2001b). However, the mutation of these residues to the corresponding mouse residues did not alter the affinity of PMX53 at the human C5aR, suggesting that these residues are not involved in the interactions of PMX53 at the human C5aR (Cain *et al.*, 2001b). The binding of PMX53 was recently modelled using a homology model of the C5aR based on a crystal structure of bovine rhodopsin with *de novo* loops generation (Tamamis *et al.*, 2014). In this study, PMX53 was suggested to form strong interactions with $D191^{ECL2}$, $H194^{ECL2}$, $R206^{5.42}$, $Y258^{6.51}$, $L287^{7.31}$ and $D282^{7.35}$ (Tamamis *et al.*, 2014).

1.4 Allosteric modulation of family A GPCRs

In the past decade, there has been increasing interest in targeting the allosteric binding sites of GPCRs in drug design due to the potential advantages that allosteric modulators may offer. Allosteric modulators are defined as ligands that

bind to a site that is topographically distinct from the binding site of the orthosteric ligands (Christopoulos and Kenakin, 2002). Allosteric modulators can exert their effect through conformational changes that are transmitted from the orthosteric to the allosteric site (and vice versa) and/or directly through effector proteins (Christopoulos and Kenakin, 2002). Positive or negative allosteric modulators (PAM/NAMs) may positively or negatively modulate the binding of orthosteric ligands and/or the ability of receptors to activate signalling pathways in the presence of bound orthosteric ligands (Christopoulos *et al.*, 2014). Meanwhile, PAM agonists bind to allosteric sites and directly activate signalling pathways in the absence of bound orthosteric ligands and neutral allosteric ligands bind to receptors without exerting any effect (Christopoulos *et al.*, 2014).

To date, only two allosteric modulators of GPCRs are used clinically. Cinacalcet is the first GPCR allosteric modulator approved by the food and drug administration (FDA) in 2004 (Poon, 2005). Cinacalcet acts on the family C calcium-sensing receptor and is used for the treatment of hyperparathyroidism (Goodman *et al.*, 2000). In the following year, maraviroc which acts on the chemokine C-C receptor type 5, a family A GPCR was approved as a novel treatment for human immunodeficiency virus (HIV)/acquired immune deficiency syndrome (AIDS) (Fatkenheuer *et al.*, 2005).

1.4.1 Advantages of allosteric modulators

Allosteric modulators present potential advantages over orthosteric ligands, such as increased receptor subtype selectivity, which may be difficult to achieve with orthosteric ligands. The potential for increased receptor subtype selectivity

from allosteric ligands may be due to binding to a less conserved site. For example, alcuronium and gallamine are allosteric modulators of the mAChRs with greater potency at the M_2 mAChR compared to M_3 mAChR (Krejci and Tucek, 2001). However, the potency of both modulators at the M_3 mAChR was increased when the ECL3 of the M_3 mAChR were mutated to that of the M_2 mAChR (Krejci and Tucek, 2001), demonstrating that the selectivity of these modulators comes from sequence differences in the ECL3 of these receptors. Increased receptor subtype selectivity may also be achieved through selective cooperativity with the orthosteric binding site of one receptor subtype but not the others. For example, tiochrome is a functionally selective M_4 mAChR allosteric modulator which possesses equal affinity at M_1-M_4 mAChR subtypes (Lazareno *et al.*, 2004).

Allosteric modulators are potentially safer alternatives to orthosteric drugs. A hallmark of receptor allosterism is the saturability of the observed allosteric effects (Christopoulos and Kenakin, 2002). Allosteric ligands with no intrinsic efficacy cannot directly activate the receptor. At saturating concentrations where all of the available allosteric binding sites have been occupied, activation of the receptor is still dependent on the presence of the orthosteric or endogenous ligands, making allosteric modulators safer alternatives. This is exemplified by the benzodiazepines which are clinically used allosteric modulators of the ionotropic γ-aminobutyric acid $(GABA)_A$ receptors and are preferred over directly-acting agonists in the treatment of anxiety and sleep disorders due to their improved safety profile (Mohler *et al.*, 2002).

Another advantage of allosteric modulators is the maintenance of the physiological rhythm of receptor signalling. This cannot be achieved with

orthosteric ligands because orthosteric ligands continuously exert their effects until they are eliminated from the body. Allosteric modulators, on the other hand, can only exert their effects in the presence of endogenous ligands. Allosteric modulators therefore fine-tune endogenous signalling and preserve spatio-temporal control of receptor signalling. A recent pre-clinical study on the family C metabotropic glutamate receptor, $mGluR_5$, demonstrates the importance of spatio-temporal conservation of receptor signalling in treating central nervous system disorders (Rook *et al.*, 2013). Adverse effects such as epileptiform activity and behavioural convulsions in rats caused by the $mGluR_5$ allosteric agonist VU0424465 were not observed with the pure positive allosteric modulator VU0361747 (Rook *et al.*, 2013).

Probe dependence of allosteric modulation may be exploited in drug design. Probe dependence is a phenomenon observed with allosteric modulators, whereby the magnitude and direction of allosteric effects are dependent on bound orthosteric ligands or probes. For example, benzyl quinolone carboxylic acid (BQCA) is an allosteric modulator which can potentiate the effect of M_1 mAChR activation by agonists acetylcholine, carbachol and pilocarpine, but not xanomeline (Canals *et al.*, 2012). Probe dependence may therefore be exploited in the development of allosteric drugs by tethering allosteric modulators to orthosteric ligands which produce desirable cooperativity in the form of bitopic ligands for diseases in which the endogenous agonists are depleted. Probe dependence has implications not only in the detection and characterisation of allosteric modulators *in vitro* but also in physiological settings. For example, many GPCRs can be activated by more than one endogenous agonist and therefore the endogenous

agonists should be use in the screening and characterisation of allosteric modulators (Wootten *et al.*, 2013). However, many of these agonists are not stable and synthetic agonists are commonly used as surrogate ligands, especially in *in viv*o experiments (Suratman *et al.*, 2011). As allosteric modulators display probe dependence, the use of surrogate ligands in pre-clinical development and testing could lead to unexpected modulatory profiles in later stages of the drug development (Suratman *et al.*, 2011).

1.4.2 Endogenous allosteric modulators

Great focus has been given to exogenous synthetic allosteric modulators in the literature due to their potential therapeutic benefits. However, GPCRs can also be modulated by various endogenous ligands, from ions, lipids, amino acids and peptides to G proteins (van der Westhuizen *et al.*, 2015). One of the best characterised allosteric modulations of GPCRs is the positive cooperativity between the orthosteric binding site and the intracellular G protein binding site (Samama *et al.*, 1993; Whorton *et al.*, 2007). The association of G proteins with the β_2AR has been shown to positively modulate agonist binding (Samama *et al.*, 1993; Whorton *et al.*, 2007).

Ions such as Na^+, Zn^{2+} and Mg^{2+} have been shown to modulate ligand binding at GPCRs and subsequent receptor activation. The allosteric effects of Na^+ on orthosteric ligand binding have been documented for many GPCRs, including the adenosine, dopamine, adrenergic and opioid receptors (Gao and Ijzerman, 2000; Horstman *et al.*, 1990; Mahmoud *et al.*, 2010; Neve, 1991). For example, the binding of the agonist quinpirole at the D_2 dopamine receptor is positively

modulated by Na^+, but the binding of the inverse agonist epidepride is negatively modulated by Na^+ (Neve, 1991), suggesting that Na^+ stabilises an active state of the receptor. However, Na^+ has been shown to positively modulates the binding of the orthosteric antagonist [^{3}H]ZM241385 at the A_{2A} adenosine receptor (Liu *et al.*, 2012). Mutagenesis and crystallography data suggest that Na^+ binds allosterically to the highly conserved $D^{2.50}$ at family A GPCRs (Horstman *et al.*, 1990; Liu *et al.*, 2012; Neve, 1991).

Zn^{2+} has been shown to differentially modulate the binding of the agonist isoprenaline and the antagonist [^{3}H]dihydroalprenolol (DHA) at the β_2AR as well as isoprenaline-mediated receptor activation in a complex manner depending on its concentration (Swaminath *et al.*, 2002). In contrast to the binding site of Na^+ which is located within the TM domain, Zn^{2+} has been shown to bind intracellularly to $H269^{ICL3}$ of the β_2AR to exert its allosteric effects (Swaminath *et al.*, 2003).

Agonist binding at both the dopamine D_2 receptor and the β_2AR can also be positively modulated by Mg^{2+} (Sibley and Creese, 1983; Williams *et al.*, 1978). However, Mg^{2+} has also been shown to be important for the function of G proteins (Birnbaumer and Zurita, 2010). Therefore, the positive effects of Mg^{2+} on ligand binding at the dopamine D_2 receptor and the β_2AR may be partially due to allosteric interactions with the G proteins. However, Mg^{2+} has been proposed to allosterically inhibit the action of the allosteric modulator W84 at the M_2 mAChR by binding to a site within the receptor (Burgmer *et al.*, 1998).

1.4.3 Exogenous allosteric modulators

To date, many family A GPCRs have been shown to be susceptible to modulation by synthetic allosteric ligands. These receptors include the adrenergic, muscarinic, adenosine, serotonin, cannabinoid, chemokine, cholecystokinin, dopamine, endothelin, free fatty acid, neurokinin and opioid receptors (Bertini *et al.*, 2004; Burford *et al.*, 2013; Canals *et al.*, 2012; Gao *et al.*, 2008; Gao and Ijzerman, 2000; Ignatowska-Jankowska *et al.*, 2015; Im *et al.*, 2003; Knaus *et al.*, 1991; Kruse *et al.*, 2013; Lane *et al.*, 2014; Leppik *et al.*, 2000; Lin *et al.*, 2012; Steinfeld *et al.*, 2011; Talbodec *et al.*, 2000). Of all family A GPCRs, the mAChRs is the best studied group of receptors with regards to allosteric modulation. Allosteric ligands with various mechanisms of action have been identified for the mAChRs, from PAMs and NAMs to allosteric agonists and neutral allosteric ligands (Chan *et al.*, 2008; Jager *et al.*, 2007; Langmead *et al.*, 2006; Litschig *et al.*, 1999). In addition, bitopic ligands which simultaneously occupy orthosteric and allosteric binding sites on a receptor have been identified for the α_1ARs, β_2AR, mAChRs, D_2 dopamine receptor and adenosine A_1 receptor (Campbell, 2015; Narlawar *et al.*, 2010; Steinfeld *et al.*, 2011; Valant *et al.*, 2008).

THRX198321 or MABA (biphenyl-2-yl-carbamicacid 1-(9-[(R)-2-hydroxy-2-(8-hydroxy-2-oxo-1,2-dihydroquinolin-5-yl)-ethylamino]-nonyl)-piperidin-4-yl ester) is an example of a bitopic orthosteric/allosteric ligand of the mAChRs and the β_2AR (Figure 1.10) (Steinfeld *et al.*, 2011). THRX198321 is the first synthetic allosteric modulator reported for the β_2AR and presents a novel pharmacotherapy at the β_2AR. THRX198321 was developed by Theravance Inc. as a monotherapy of a mAChR antagonist and a β_2AR agonist for the treatment of COPD, as a combination

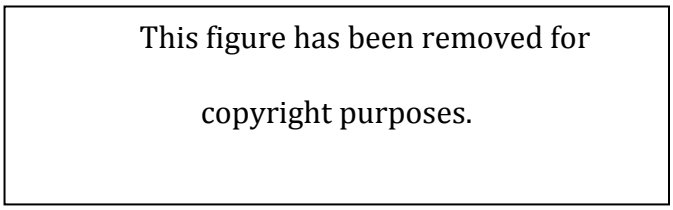

Figure 1.10 Chemical structure of THRX198321 and its proposed binding mode

(A) THRX198321 is a bitopic orthosteric/allosteric ligand of the M_2/M_3 muscarinic acetylcholine receptors (mAChRs) and the β_2 adrenoceptor (β_2AR) which consists of a mAChR antagonist moiety (MA) and a β_2AR agonist moiety (BA) linked together by a nine-carbon polymethylene chain. (B) At the M_2/M_3 mAChRs, the MA moiety of THRX198321 is proposed to bind in the orthosteric site while the BA moiety is proposed to bind to an allosteric site. In contrast, at the β_2AR, the BA moiety binds to the orthosteric site while the MA moiety interacts at an allosteric site. Figure adapted from Steinfeld *et al.* (2011).

β_2AR agonist and $M_2/_3$ antagonist has been shown to improve clinical outcomes in patients suffering from the disease (Aaron *et al.*, 2007; Cazzola *et al.*, 2004; Tashkin *et al.*, 2008; van Noord *et al.*, 2005). THRX198321 is composed of an M_2/M_3 mAChR antagonist moiety (MA or THRX100361) and a β_2AR agonist moiety (BA) linked together by a nine-carbon polymethylene chain, which was shown to be the optimal linker length to confer high binding affinity at the β_2AR and the M_2 and M_3 mAChRs (Steinfeld *et al.*, 2011).

THRX198321 displayed allosteric behaviour by decreasing the dissociation rates of orthosteric antagonists [^{3}H]DHA and [^{3}H]N-methylscopolamine from the β_2AR and the M_3 mAChR respectively (Steinfeld *et al.*, 2011). The proposed binding mode of THRX198321 at both receptors is shown in Figure 1.10. At the M_2/M_3 mAChR, the MA moiety of THRX198321 is proposed to bind to the orthosteric site while the BA moiety interacts at an allosteric site. In contrast, at the β_2AR, the BA moiety is proposed to bind to the orthosteric site while the MA moiety interacts at an allosteric site (Steinfeld *et al.*, 2011). However, this binding mode is unlikely to take place in the dissociation assays as the receptors were pre-equilibrated with the orthosteric antagonists. The allosteric moieties of THRX198321 could still bind to allosteric sites with the orthosteric moiety extending into in the extracellular space, and modulate orthosteric ligand dissociation by steric hindrance or by changing the conformation of the receptors to favour orthosteric ligand binding. However, THRX198321 is a more potent modulator compared to the allosteric moieties MA and BA alone, suggesting that the orthosteric moiety contributes to the modulatory effect of THRX198321. Therefore, alternative mechanisms such as modulatory actions across receptor dimers need to be considered.

An analogue of THRX198321, GSK961081, has recently passed phase I clinical trial for the treatment of COPD (Bateman *et al.*, 2013). GSK961081 was found to be well tolerated and improved lung functions in patients (Bateman *et al.*, 2013). Pure allosteric modulators may not be of high clinical value in asthma attacks where rapid bronchodilation is needed, which could be better achieved with orthosteric agonists. However, bitopic ligands such as THRX198321 which positively modulate the action of its agonist moiety may be useful in asthma attacks where an override of the body's sympathetic tone is needed. In addition, bitopic ligands with increased potency at the β_2AR may be superior to current orthosteric agonists, as lower doses would be needed to achieve the same effects, thereby reducing tolerance and desensitisation.

1.4.4 Allosteric binding site of family A GPCRs

Mutagenesis studies have identified distinct allosteric binding sites at several family A GPCRs. The allosteric binding site of the mAChRs is the best characterised of all family A GPCRs. Most of the allosteric ligands identified for the mAChRs bind to a common allosteric binding site which includes residues from the ECL2 and the top of TM6 and 7, such as E172^{ECL2}, Y177^{ECL2}, N419^{ECL3}, W422$^{7.35}$ and T423$^{7.36}$ (Gnagey *et al.*, 1999; Huang *et al.*, 2005; Jager *et al.*, 2007; Kruse *et al.*, 2012; May *et al.*, 2007; Voigtländer *et al.*, 2003). The M_2 mAChR is the only GPCR that has been crystallised in the presence of both its orthosteric and allosteric ligands (Kruse *et al.*, 2013). The crystal structure of the M_2 mAChR crystallised in the presence of the allosteric modulator LY2119620 confirms the location of the common mAChR allosteric binding site and shows interactions of LY2119620 with Y80$^{2.61}$, E172^{ECL2},

Y177^{ECL2}, N410$^{6.58}$, N419^{ECL3}, W422$^{7.35}$ and Y426$^{7.39}$ (Kruse *et al.*, 2013). There is evidence to support the existence of a second allosteric binding site at the mAChRs. Some allosteric modulators of the mAChRs, termed atypical allosteric modulators, such as amiodarone, indolocarbazole analogues of staurosporine KT5720 and KT5823 and benzimidazole derivatives WIN63577 and WIN51708, have been proposed to bind to a second uncharacterised allosteric site (Lazareno *et al.*, 2002; Lazareno *et al.*, 2000; Stahl *et al.*, 2011).

Tacrine is an allosteric modulator of the mAChRs which has been proposed to simultaneously occupy two distinct allosteric sites at the M_2 mAChR. A mutagenesis study showed that the mutations Y177^{ECL2}Q and T423$^{7.35}$H at the M_2 mAChR decreased the potency of tacrine, suggesting that it interacts at the common allosteric site (Trankle *et al.*, 2005). However, tacrine produced a steep modulatory response curve which is indicative of the presence of multiple binding sites. A tacrine dimer, which consists of two molecules of tacrine linked together using a hexamethylene chain, has increased affinity for the M_2 mAChR and produced a response curve with a Hill slope of unity (Trankle *et al.*, 2005). These data suggest that more than one molecule of tacrine can bind simultaneously to the M_2 mAChR (Trankle *et al.*, 2005). Docking of tacrine into a homology model of the M_2 mAChR suggested that a second molecule of tacrine binds to residues from the N-terminus and ECL1 (Trankle *et al.*, 2005).

Tacrine has also been shown to modulate the dissociation rate of orthosteric antagonist [^{3}H]prazosin at the α_{1A} and α_{1B}-ARs. The docking of tacrine into a homology model of the α_{1A}AR suggested that it binds to residues on the ECL2 and the top of TM2 and 7, making interactions with F86$^{2.64}$, I175^{ECL2}, F308$^{7.35}$ and

F312$^{7.39}$ (Campbell, 2015). The allosteric effect of 9-aminoacridine, a compound highly analogous to tacrine with a phenol ring in place of the saturated six-membered ring, has been shown to be mediated by F86$^{2.64}$ (Campbell, 2015). In addition, the allosteric effect of the bitopic compound C9 bisacridine, which is two 9-aminoacridine molecules joined together by a nine- carbon polymethylene chain, has been shown to be mediated by S83$^{2.61}$ and F86$^{2.64}$ (Campbell, 2015). The allosteric binding site of the α_{1A}AR identified by Campbell (2015) is homologous to the allosteric binding site of the D_2 dopamine receptor. The docking of the bitopic ligand SB269652 to a homology model of the receptor and subsequent mutagenesis studies showed that V91$^{2.61}$ and E95$^{2.65}$ form the allosteric binding site for SB269652 (Lane *et al.*, 2014). The conservation of the allosteric binding site between the dopamine D_2 receptor and the α_{1A}AR indicates a possible conservation of allosteric modulation across closely related family A GPCRs which share similar orthosteric ligands.

An allosteric binding site that is located within the TM domain has been identified for the other α branch family A GPCRs, such as the A_1 and A_3 adenosine receptors (Gao *et al.*, 2003; Kourounakis *et al.*, 2001). The allosteric binding site of these receptors is formed by residues from TM1,2,3,5 and 7 (Gao *et al.*, 2003; Kourounakis *et al.*, 2001).

Although one out of two currently marketed allosteric drugs act on the chemokine receptors from the γ branch of family A GPCRs, the allosteric binding site of these receptors is generally less well understood compared to the α branch family A GPCRs. Mutagenesis studies have identified transmembrane as well as

intracellular binding sites for small molecule allosteric ligands of the chemokine receptors (Andrews *et al.*, 2008; de Kruijf *et al.*, 2011; Salchow *et al.*, 2010).

Diarylurea, thiazolopyrimidine and imidazolopyrimidine compounds are allosteric antagonists of the chemokine CXCR2 receptor (Bradley *et al.*, 2009; de Kruijf *et al.*, 2009). Imidazolopyrimidine compounds were unable to compete with diarylurea and thiazolopyrimidine compounds in competition binding studies, suggesting that these compounds interact at different sites (de Kruijf *et al.*, 2009). In agreement with these binding studies, mutagenesis studies showed that diarylurea compounds such as *N*-(3-(aminosulfonyl)-4-chloro-2-hydroxyphenyl)-*N*'-(2,3-dichlorophenyl) urea and thiazolopyrimidine compounds such as (1*R*)-5-[[(3-chloro-2-fluorophenyl)-methyl]thio]-7-[[2-hydroxy-1-methylethyl]amino]-thiazolo[4,5-*d*]-pyrimidin-2(3H)-one interact with K320 from helix 8 (Nicholls *et al.*, 2008). A further mutagenesis study by Salchow *et al.* (2010) confirmed the involvement of $K320^{helix8}$ and showed that residues on the intracellular domain of TM2 and 3 are also involved in the interactions of other diarylurea compounds at the CXCR2 receptor. In the study, SB265610 were shown to interact with $T83^{2.39}$, $D84^{2.40}$ and $D143^{3.49}$ of the E/DRY motif (Salchow *et al.*, 2010). In addition, Sch527123 which belongs to a different class of allosteric antagonists, also binds to the intracellular region of the CXCR2 receptor, making interactions with $T83^{2.39}$, $D84^{2.40}$, $D143^{3.49}$, $A249^{6.33}$, $Y314^{7.53}$ and $K320^{helix8}$ (Salchow *et al.*, 2010). The interaction of SB265610 and Sch527123 with $D143^{3.49}$ of the E/DRY motif suggests an allosteric mechanism of action which involves inhibition of G protein activity (Salchow *et al.*, 2010). An intracellular allosteric binding site involving the C-terminal domain of the receptor has also been shown for the CCR4 and CCR5

receptors (Andrews *et al.*, 2008). Unlike diarylurea and thiazolopyrimidine compounds, imidazolopyrimidine compounds have been shown to bind within the TM domain of the CXCR2 receptor, making interactions with F130$^{3.36}$, S217$^{5.44}$, F220$^{5.47}$, N268$^{6.52}$ and L271$^{6.55}$ (de Kruijf *et al.*, 2011). These data suggest that allosteric binding sites of family A GPCRs are varied and diverse.

1.5 Binding kinetics at GPCRs

While recent advances in X-ray crystallography expand our knowledge in terms of the key interactions required for the binding of various ligands at many GPCRs, the mechanism of ligand binding cannot be delineated using these static snapshots of receptor-ligand interactions. Instead, molecular dynamics have been used to study the process of GPCR ligand binding and unbinding (Dror *et al.*, 2011; Gonzalez *et al.*, 2011; Guo *et al.*, 2016; Kruse *et al.*, 2012; Plazinska *et al.*, 2015; Sabbadin *et al.*, 2015; Sandal *et al.*, 2015; Thomas *et al.*, 2016; Wang and Duan, 2009). In general, these studies suggest that ligand binding at GPCRs involves the association of the ligand with a metastable binding site which is located above the orthosteric binding site of the receptor, which has been termed the "extracellular vestibule".

Molecular dynamics studies suggest that at the β_2AR, orthosteric ligand binding starts with the association of the ligand with the extracellular vestibule of the receptor, which is formed by residues from the ECL2 and the top of TM6 and 7 (Dror *et al.*, 2011). The transition of the ligand from the extracellular vestibule to the orthosteric pocket is proposed to be facilitated by structural changes at the top of the receptor, whereby F193^{ECL2} and Y308$^{7.35}$ separate to allow the ligand to

traverse the narrow binding pathway into the orthosteric pocket (Dror *et al.*, 2011). Ligand dissociation from the orthosteric pocket of the β_2AR has been proposed to occur through the same pathway (Dror *et al.*, 2011; Gonzalez *et al.*, 2011; Plazinska *et al.*, 2015; Wang and Duan, 2009). However, ligand dissociation has also been observed to occur through the opening between ECL2 and TM5 and 6, albeit less commonly compared to the opening between ECL2 and TM6 and 7 (Gonzalez *et al.*, 2011; Wang and Duan, 2009). Crystallography data suggest that agonist binding at the β_2AR causes F193^{ECL2} and Y308$^{7.35}$ to move closer together, thereby restricting ligand entry and exit from the receptor (Rasmussen *et al.*, 2011b). The involvement of Y308$^{7.35}$ in the kinetics of ligand binding at the β_2AR was recently shown by DeVree *et al.* (2016), where the mutation of Y308$^{7.35}$ to alanine decreased the ability of the nanobody Nb80 to slow the association rate of the orthosteric antagonist [^{3}H]DHA.

A molecular dynamics study suggests that the extracellular binding vestibule of the M_2 and M_3 mAChR corresponds to the common allosteric binding site (Kruse *et al.*, 2013). In agreement with this molecular dynamics study, orthosteric ligands of the M_2 mAChR have been shown to bind weakly at the common allosteric binding site formed by residues from the ECL2 and TM6-7 (Redka *et al.*, 2008). Similarly, molecular dynamics simulation of orthosteric ligand binding at the D_2 and D_3 dopamine receptors also suggest an overlap of the orthosteric binding vestibule with a previously characterised allosteric binding site which is located at the top of TM2 (Lane *et al.*, 2014; Thomas *et al.*, 2016). These data suggest that the extracellular vestibule is important for both orthosteric and allosteric ligand

interactions, and that allosteric ligands may remain at the vestibule because they have low affinities for the orthosteric binding site.

1.5.1 Ligand-receptor residence time

Pharmacological characterisation of GPCR ligands have traditionally been focused on equilibrium-derived parameters, in particular affinity. However, drug-receptor equilibrium is unlikely to occur *in vivo* due to pharmacokinetics parameters such as drug absorption, distribution, metabolism and elimination (Copeland, 2016; Tummino and Copeland, 2008). Instead, ligand-receptor residence time has been proposed as a more appropriate parameter to measure in the characterisation of ligand-receptor interactions, as residence time, or the lifetime of binding of a ligand at a receptor, is more likely to determine the pharmacological activity of a ligand *in vivo* (Copeland *et al.*, 2006; Hothersall *et al.*, 2016; Tummino and Copeland, 2008). Residence time is inversely proportional to the dissociation rate constant of the ligand-receptor complex (Copeland *et al.*, 2006).

Ligand residence time can be exploited to achieve desired therapeutic outcomes and reduce off-target side effects. Depending on the therapeutic context, short or long receptor residence time may be beneficial. For example, it has been inherently difficult to develop mAChR antagonists that preferentially bind to the M_3 over M_2 mAChR for symptomatic relief of bronchoconstriction (Disse *et al.*, 1993). While antagonism of the M_3 mAChR provides bronchodilation, antagonism of the M_2 mAChR causes tachycardia (Disse *et al.*, 1993). The difficulty in developing M_1/M_3 over M_2 selective antagonists was overcome by tiotropium,

which is selective by the nature of its long residence time at the M_1 and M_3 mAChRs compared to the M_2 mAChR (Disse *et al.*, 1993).

Recent studies suggest that residence time, and not affinity, determines the *in vivo* efficacy of many GPCR agonists and antagonists (Casarosa *et al.*, 2009; Guo *et al.*, 2012; Seow *et al.*, 2016; Sykes *et al.*, 2009). For example, a study comparing three M_3 mAChR antagonists as bronchodilatory agents, tiotropium, aclidinium and glycopyrrolate, suggests that the *in vivo* potency of these ligands is directly proportional to their residence time (Casarosa *et al.*, 2009). While the affinity and potency of tiotropium, aclidinium and glycopyrrolate for the M_3 mAChR were similar (pKi (M) = 11.0, 10.7 and 10.0 and pA_2 (M) = 10.4, 9.6 and 9.7 respectively), the residence time of these ligands varied significantly ($t_{1/2}$ (hours) = 27, 11 and 6 respectively) (Casarosa *et al.*, 2009). In this study, equipotent doses of the ligands were administered to anesthetised beagle dogs and the ability of the ligands to antagonise acetylcholine-induced bronchoconstriction was monitored over 24 hours (Casarosa *et al.*, 2009). It was found that the efficacy of tiotropium, aclidinium and glycopyrrolate as bronchodilators were approximately 70%, 45% and 10% respectively at 6 hours and 35%, 21% and 0% at 24 hours (Casarosa *et al.*, 2009). Glycopyrrolate has previously been shown to be effective in providing bronchodilation in mildly asthmatic patients for up to 30 hours (Hansel *et al.*, 2005). However, this broncho-protection was achieved with doses that are at least 200 times higher than the effective doses of tiotropium. Therefore, long-acting antagonists such as tiotropium might be a better alternative compared to glycopyrrolate, as smaller doses can be given to patients to achieve the same clinical outcome (Casarosa *et al.*, 2009).

Similarly, a comparison of three equipotent C5aR antagonists, PMX53, W54011 and JJ47, suggests that the notable *in vivo* efficacy observed with PMX53 may be due to a long residence time (Seow *et al.*, 2016). Using a calcium release assay as a surrogate readout, the residence time of PMX53 at the C5aR was recently estimated to be in excess of 18 hours, while the residence time of W54011 and JJ47 was estimated to be 1.2 and 0.6 hour respectively (Seow *et al.*, 2016). While the plasma concentrations of W54011 and JJ47 peaked at 2 to 3 hours following oral administrations, PMX53 could not be detected in the plasma after oral administrations (Seow *et al.*, 2016). Despite this, the ability of PMX53 to antagonise C5aR agonist-mediated paw swelling in rats was evident 16 hours post antagonist administration, while W54011 and JJ47 were no longer efficacious 2 hours post-administration (Seow *et al.*, 2016), suggesting that residence time is positively correlated with clinical outcome.

Interestingly, increased *in vivo* efficacy as a result of long residence time has been observed not only with antagonists, but also with agonists (Guo *et al.*, 2012; Sykes *et al.*, 2009). A comparison of seven full and partial agonists at the M_3 mAChR suggested that ligand efficacy is directly proportional to residence time and not binding affinity (Sykes *et al.*, 2009). Similarly, a comparison of ten structurally diverse ligands of the adenosine A_{2A} receptor showed that residence time and not affinity is correlated to the functional efficacy of agonists (Guo *et al.*, 2012). In a recent study, superagonism of 7-[(R)-2-((1R,2R)-2-benzyloxycyclo-pentylamino)-1-hydroxyethyl]-4-hydroxybenzothiazol-one, or C27, at the β_2AR has been attributed to its long residence time (Rosethorne *et al.*, 2016).

While prolonged receptor activation by agonists has traditionally been thought to lead to a loss of function due to desensitisation and internalisation (Ahn *et al.*, 2003; Ferguson *et al.*, 1995; Mundell *et al.*, 1999), evidence exists for sustained signalling following continuous agonist exposure from receptor-ligand complexes located at both the cell surface as well as intracellular compartments (Irannejad *et al.*, 2013; Kane *et al.*, 2008; Nishiyama and Hirai, 2015; Unett *et al.*, 2013; Willars *et al.*, 1999). In fact, endosomal signalling has been suggested to correlate with ligand-receptor residence time (Copik *et al.*, 2015; Hothersall *et al.*, 2016; Perez-Aso *et al.*, 2013). In addition to determining the duration of action of a ligand, residence time has been shown to determine signalling outcomes (Klein Herenbrink *et al.*, 2016). D_2 dopamine receptor agonists such as aripiprazole and bifeprunox which display bias towards the ERK1/2 signalling pathway at short incubation time have significantly longer residence time compared to agonists that do not display bias such as dopamine and ropinirole (Klein Herenbrink *et al.*, 2016). In addition, the magnitude and direction of bias of these agonists change over time towards the cAMP pathway, suggesting that residence time plays an important role in the engagement of different signalling molecules (Klein Herenbrink *et al.*, 2016). As such, ligand binding kinetics or residence time is an important parameter to consider in the pharmacological characterisation of GPCR ligands.

1.6 Computer-aided techniques in GPCR research

Computer-aided techniques such as homology modelling and docking are widely used in GPCR research (Carlsson *et al.*, 2011; Diaz *et al.*, 2009; Kolb *et al.*,

2009; Lam *et al.*, 2011; Michielan *et al.*, 2008; Yoshikawa *et al.*, 2013). In the absence of a crystal structure, homology models provide a useful alternative to study potential receptor-ligand interactions. Homology modelling is a method which predicts the structure of a protein based on the observation that evolutionarily related proteins with similar sequences share similar structures (Cavasotto and Phatak, 2009). In general, homology model generation consists of four steps: identification of template protein, sequence alignment between the target and the template protein, homology model generation and model quality assessment (Cavasotto and Phatak, 2009). Factors such as the resolution of the template receptor, the homology or sequence identity between the template and the model receptor, as well as the accuracy of the sequence alignment between the template and the model receptor have been shown to impact the quality of the homology model generated (Davis *et al.*, 2003; Larsson *et al.*, 2008; Yoshikawa *et al.*, 2013). In the case of proteins with low sequence identity (<40%), the use of multiple sequence alignment instead of pairwise alignment has been shown to increase the quality of the homology model (Larsson *et al.*, 2008). MODELLER was used to generate the homology models in this study. MODELLER is one of the most commonly used homology modelling programs which generates models by satisfaction of conformational restraints of side chains on the backbone of the template structure (Šali and Blundell, 1993).

Docking has previously been used to successfully predict ligand binding at GPCRs (Abdul-Ridha *et al.*, 2014; Gerlach *et al.*, 2001; Lane *et al.*, 2014). In this study, Genetic Algorithm for Ligand Docking (GOLD) was used to predict ligand binding at the β_2AR and the C5aR. GOLD is a docking program which uses a genetic

algorithm to generate favourable ligand poses at a specified binding site on a protein (Jones *et al.*, 1995; Jones *et al.*, 1997). To generate poses, "chromosomes" which contains conformational information of the possible protein-ligand interactions are generated. Parent chromosomes are selected and subjected to a genetic algorithm to generate daughter chromosomes. The population of chromosomes are assessed for fitness using the Goldscore scoring system, which is a weighted sum of the intramolecular van der Waals forces, internal torsion of the ligand, van der Waals forces between the ligand and the receptor and H-bond interactions between the ligand and the receptor. Newly generated chromosomes are kept if they are fitter than the least fit chromosome in the pool and a pre-determined number of poses with the highest scores are saved at the conclusion of the algorithm.

1.7 Summary and aims

The extracellular region of family A GPCRs has been shown to be important in ligand binding and receptor function. This thesis examines the role of the extracellular region of family A GPCRs in ligand interactions, using the β_2AR as a representative receptor from the α branch and the C5aR as a representative receptor of the γ branch. The aims of this study are to: (i) characterise the allosteric modulatory effects of THRX100361 and tacrine at the β_2AR and to identify their allosteric binding site, (ii) investigate the role of the allosteric binding site of the β_2AR in orthosteric ligand binding kinetics, and (iii) determine the molecular basis of the non-competitive nature of PMX53 inhibition at the C5aR and to investigate its binding site.

CHAPTER 2

General methods

2.1 Reagents and materials

2.1.1 Mammalian cell culture

High glucose Dulbecco's modified eagle's medium (DMEM), Ham's F12 nutrient mixture, L-glutamine, trypsin, chloroquine diphosphate, diethylaminoethyl-dextran (DEAE-dextran) and dimethyl sulfoxide (DMSO) were purchased from Sigma Aldrich (St. Louis, USA). Foetal bovine serum (FBS) was purchased from Life Technologies (Carlsbad, USA). G418 was purchased from Millipore (Darmstadt, Germany), InvivoGen (San Diego, USA) or Sigma Aldrich (St. Louis, USA). jetPEI was purchased from PolyPlus Transfection (Illkirch, France). COS-1 cells were purchased from ATCC (Virginia, USA). CHO-K1 cells were kindly provided by Dr David Williamson (Centre for Vascular Research, The Lowy Cancer Research Institute, UNSW Australia).

2.1.2 Molecular biology and bacterial cell culture

Ampicillin sodium salt and mutagenic primers were purchased from Sigma Aldrich (St. Louis, USA). DpnI, restriction enzymes EcoRI, HindIII and XbaI, and T4 DNA ligase were purchased from New England Biolabs (Ipswich, USA). Phusion™ DNA polymerase was purchased from Finnzymes (Espoo, Finland). Miniprep and maxiprep kits were purchased from RBC (Banqiao City, Taiwan).

2.1.3 Radioligand binding assays

Bradford's reagent was purchased from BioRad (Hercules, USA). [^{3}H]dihydroalprenolol (DHA) (104.7 Ci/mmol), [^{125}I]human complement 5a (hC5a) (2200 Ci/mmol) and Ultima Gold scintillation cocktail were purchased from Perkin Elmer (Waltham, USA). GF/C glass fibre filters were purchased from Whatman (Maidstone, UK).

2.1.4 cAMP assays

The bioluminescence cAMP sensor pcDNA3L-His-CAMYEL (cAMP sensor using YFP (yellow fluorescent protein)–Epac–RLuc (Renilla luciferase)) plasmid was purchased from ATCC (Virginia, USA). Forskolin, 3-isobutyl-1-methylxanthine (IBMX) and bovine serum albumin (BSA) were purchased from Sigma Aldrich (St. Louis, USA). Coelenterazine-h was purchased from Promega (Wisconsin, USA) or Prolume (Arizona, USA).

2.1.5 Compounds

(±)-Isoprenaline hydrochloride, (*S*)-(-)-propranolol hydrochloride, tacrine hydrochloride, histamine dihydrochloride and recombinant hC5a were purchased from Sigma Aldrich (St. Louis, USA). THRX100361 was supplied by Theravance Bipoharma (San Francisco, USA). PMX53 was kindly provided by A/Prof Trent Woodruff (The University of Queensland, Australia). EP54 and fluorescein isothiocyanate-labelled EP54 with an aminohexanoic acid linker (FITC-ahxEP54)

were synthesised using solid phase peptide synthesis, described in detail in section 6.2.5 and 6.2.8.

2.1.6 Buffers and solutions

The chemicals used in buffers were purchased from Ajax Finechem (Taren Point, Australia). HCl and NaOH were used to adjust the pH of the buffers. The buffer compositions are listed below:

Phosphate-buffered saline (PBS)
137 mM NaCl, 2.7 mM KCl, 10 mM $Na_2HPO_4.KH_2PO_4$, pH 7.4

Luria broth (LB) medium
10 $g.L^{-1}$ tryptone, 5 $g.L^{-1}$ yeast extract, 5 $g.L^{-1}$ NaCl, pH 7.0

Radioligand binding buffer
75 mM tris(hydroxylmethyl)aminomethane (TRIS), pH 7.4

Membrane preparation buffer
20 mM 4-(2-hydroxyethyl)-1-piperazineethanesulfonic acid (HEPES), 10 mM ethylenediaminetetraacetic acid (EDTA), pH 7.4

HEPES-buffered saline (HeBS)
140 mM NaCl, 5 mM KCl, 0.75 mM Na_2HPO_4, 6 mM dextrose, 25 mM HEPES, pH 7.05-7.12

Hank's balanced salt solution (HBSS)
137 mM NaCl, 5.4 mM KCl, 0.3 mM Na2HPO4, 0.4 mM KH2PO4, 4.2 mM NaHCO3, 1.3 mM CaCl2, 0.5 mM MgCl2, 0.6 mM MgSO4, 5.6 mM glucose, pH 7.4

"Homemade" maxiprep buffers

Resuspension buffer (50 mM TRIS, 10 mM EDTA, 100 µg/mL RNase A), lysis buffer (200 mM NaOH, 1% SDS), neutralisation buffer (3 M CH_3COOK), column equilibration buffer (750 mM NaCl, 50 mM 3-(N-Morpholino)propanesulfonic acid, 4-Morpholinepropanesulfonic acid (MOPS), 15% isopropanol, 0.15% Triton X-100), wash buffer (1 M NaCl, 50 mM MOPS, 15% isopropanol), elution buffer (1.25 M NaCl, 50 mM TRIS, 15% isopropanol)

2.2 General methods

2.2.1 Cell culture

COS-1 cells were cultured in high glucose DMEM supplemented with 10% (v/v) heat-inactivated FBS and 4 mM L-glutamine. CHO cells were maintained in Ham's F12 nutrient mix supplemented with 10% (v/v) heat inactivated FBS and 4 mM L-glutamine. All cells were grown at 37°C and 5% CO_2 and maintained using standard cell culture techniques.

2.2.2 Generation of CHO cells stably expressing human β_2ARs

CHO cells were transfected with cDNA of the receptor of interest using the calcium phosphate transfection method (Kingston *et al.*, 2001). A confluent monolayer of cells on a 10 cm dish was split 1:15 one day prior to the transfections. Cells were supplied with 9 mL of fresh Ham's F12 nutrient mix supplemented with 10% FBS and 4 mM of L-glutamine 3 hours before the transfection. DNA used was purified and sterilised by ethanol precipitation. To do

this, 1/10 volume of 3M sodium acetate at pH 5.2 was added to 50 µg of DNA. The DNA solution was vortexed briefly and 2 volumes of ice-cold 100% ethanol were added. The DNA solution was vortexed again and incubated on ice for 30 min. The solution was then centrifuged at 14,000 rpm for 30 min at 4°C. The resulting DNA pellets were washed with 200 µL of ice-cold 70% ethanol and centrifuged at 14,000 rpm for 10 min at 4°C. The supernatant was removed and the DNA pellet was resuspended in 450 µL of milli-Q water. 50 µL of 2.5 M $CaCl_2$ was added to the purified DNA solution. The DNA/$CaCl_2$ solution was then added dropwise to 500 µL of 2X HeBS that was aerated with a pipettor. The mixture was vortexed immediately and incubated for 20 min at room temperature. The DNA mixture was then added dropwise to the cells and the cells were incubated for 4 hours at 37°C and 5% CO_2. At the end of the incubation, DNA mixture was removed from the dish and the cells were incubated with 2 mL of 10% DMSO in PBS for 3 min at room temperature. The DMSO was then diluted with 5 mL of PBS and removed from the dish. 10 mL of fresh Ham's F12 nutrient mix supplemented with 10% FBS and 4 mM of L-glutamine was added to the cells and the cells were allowed to grow for 48 hours at 37°C and 5% CO_2. After 48 hours, the cells were split 1:20 into a 15 cm dish and 600 µg/mL of G418 was added to the media. Single clones were selected using dilution cloning and expanded to generate the stable cell lines which were maintained using 400 µg/mL of G418.

2.2.3 Site-directed mutagenesis

Wild type (WT) receptor cDNA was used as template DNA, unless otherwise stated in the construction of double and triple mutants. Polymerase chain

reactions were performed using Phusion™ high fidelity DNA polymerase according to manufacturer instructions using primers containing the desired mutations, in a total reaction volume of 20 µL. DpnI digests were then performed to remove methylated template DNA. Mutant constructs were then transformed into DH5α *E. coli* cells as previously described (Inoue *et al.*, 1990), isolated by mini preps and sequenced at the Australian Cancer Research Foundation Facility (Darlinghurst, Australia). Confirmed mutant constructs were then transformed into DH5α *E. coli* cells, maxi-prepped and stored in milli-Q water at -20°C. Maxi preps were performed either using commercial maxi prep kits or HCl-regenerated columns and "homemade" buffers as listed in section 2.1.6 (Siddappa *et al.*, 2007).

2.2.4 Transfection for membrane preparations

COS-1 cells were plated at a density of 4 x 10^6 cells on a 15 cm dish one day prior to the transfection. The cells were incubated with a transfection cocktail made up of 0.5 mg/mL of DEAE dextran, 125 nM of chloroquine and 15 µg of DNA in 10 mL of serum free DMEM for 3 hours at 37°C and 5% CO_2. After 3 hours, the transfection cocktail was removed and the cells were incubated with 10% DMSO in PBS for 3 min at room temperature. The DMSO solution was then removed and fully supplemented DMEM was added to the cells. The cells were allowed to grow overnight at 37°C and 5% CO_2. The cells were trypsinised and replated into a fresh 15 cm dish 24 hours post transfection and allowed to grow for another 48 hours.

2.2.5 Membrane preparations

Membranes were harvested from transfected COS-1 cells using a method previously described by Leach *et al*. (2010). Briefly, cells were mechanically scraped from the dishes into cold PBS and centrifuged at 500 x g for 5 min. All subsequent steps were performed at 4°C. The pellet was resuspended in 10 mL of cold 20 mM HEPES/10 mM EDTA buffer at pH 7.4. The cells were then homogenised using a cell disrupter, Ultra-Turrax T25 (IKA Labortechnik), three times for 10 sec each with a 30 sec interval at 13,500 rpm. The lysates were centrifuged at 600 x g for 10 min to remove cellular debris. The supernatant was then collected and centrifuged at 40,000 x g for 1 hour. The resulting cell membranes were resuspended in 75 mM TRIS containing 10% glycerol at pH 7.4 and homogenised using an insulin syringe. The membranes were aliquoted and stored at -80°C. Protein concentration was determined using the Bradford reagent (Sigma Aldrich, St. Louis, USA).

2.2.6 [^{3}H]DHA receptor binding assays

All radioligand binding assays were performed in a total volume of 500 µL of 75 mM TRIS, pH 7.4, at room temperature. Non-specific binding was determined in the presence of 10 µM of propranolol. Reactions were terminated by the addition of cold PBS and vacuum filtration through Whatman GF/C glass fibre filters. Ultima Gold scintillation cocktail was added to dried filters and radioactivity was determined using a scintillation counter (Perkin Elmer TriCarb-2800 TR).

In saturation binding assays, 1-5 µg of COS-1 membranes expressing human β_2AR were incubated with 0.08 to 8 nM of [^{3}H]DHA for 1 hour. In competition

binding assays, membranes were incubated with increasing concentrations of competing unlabelled ligand and 0.5 nM of [^{3}H]DHA for 1 hour. In association kinetics binding assays, reactions were initiated by the addition of 0.5 nM of [^{3}H]DHA to the membranes and incubated for specific durations as indicated. In dissociation kinetics binding assays, membranes were incubated with 0.5 nM of [^{3}H]DHA for 1 hour, following which dissociation was initiated at various time points as indicated by preventing the re-association of [^{3}H]DHA to the receptors using 10 µL of propranolol at a final concentration of 10 µM.

Whole cell binding assays were used to determine the surface receptor expression levels of CHO cells stably transfected with WT and mutant β_2AR. Confluent cells were harvested from plates using 5 mM EDTA in PBS to preserve the integrity of the receptors on the cell surface. Binding assays were performed by incubating 2 x 10^5 cells with a saturating concentration of [^{3}H]DHA (2 nM) for 1 hour.

2.2.7 Transfection for cAMP measurement

A bioluminescence resonance energy transfer (BRET) based cAMP assay was used to measure receptor activation (Jiang *et al.*, 2007). The BRET sensor CAMYEL (cAMP sensor using YFP-Epac-RLuc) was transiently transfected into CHO cells stably expressing human β_2AR using jetPEI according to the manufacturer guidelines. Costar white half-area 96 well plates (Fisher Scientific, USA) were used for the assays.

2.2.7.1 Forward transfection

CHO cells were plated at a density of 10,000 cells per well in 100 µL of media one day before transfection. For each well, 0.1 µg of plasmid DNA in 5 µL of 150 mM NaCl and 0.2 µL of jetPEI in 5 µL of 150 mM NaCl were prepared. The jetPEI solution was added to the DNA solution and incubated for 15 min at room temperature. At the end of the incubation, the DNA/jetPEI mixture was added to 100 µL of Ham's F12 nutrient mix supplemented with 10% FBS and 4 mM of L-glutamine. The medium on the wells was aspirated and replaced with the Ham's F12/DNA/jetPEI mixture. The cells were then returned to the incubator set at 37°C and 5% CO_2. After 24 hours, the medium was changed to fresh Ham's F12 nutrient mix supplemented with 10% FBS and 4 mM of L-glutamine and the cells were allowed to grow for another 24 hours.

2.2.7.2 Reverse transfection

In contrast to the forward transfection method, the reverse transfection method allows the cells to be plated and transfected on the same day. For each well, 0.1 µg of plasmid DNA in 5 µL of 150 mM NaCl and 0.2 µL of jetPEI in 5 µL of 150 mM NaCl were prepared. The jetPEI solution was added to the DNA solution and incubated for 15 min at room temperature. The DNA/jetPEI mixture was then added to 100 µL of complete media containing 20,000 cells. The cells in DNA/jetPEI mixture were then added onto the wells and incubated at 37°C and 5% CO_2. After 24 hours, the medium was changed to fresh Ham's F12 nutrient mix supplemented with 10% FBS and 4 mM of L-glutamine and the cells were allowed to grow for another 24 hours. The transfection efficiency was higher using the forward transfection method compared to the reverse transfection method.

2.2.8 cAMP assay

2.2.8.1 $G_{\alpha s}$-coupled receptors

The ability of isoprenaline to activate the cAMP signalling pathway at the WT and mutant β_2ARs was measured using the BRET CAMYEL assay. The assays were carried out in a total volume of 100 µL. Cells were washed with 40 µL of HBSS and serum starved in 40 µL of HBSS, pH 7.4, for 30 min at 37°C and 5% CO_2. 10 µL of IBMX and coelenterazine-h in HBSS was added at a final concentration of 40 µM and 2 µM respectively and incubated for 5 min at 37°C. To this, 50 µL of increasing concentrations of agonist were then added to stimulate cAMP production. To study the effects of the modulators on cAMP production, the modulators were pre-incubated with the cells for 30 min at 37°C and 5% CO_2. Emission signals of RLuc and YFP were measured sequentially using the BRET1 filter set (475/25 and 535/30 nm) and the BMG FLUOstar Optima plate reader after a 10 or 15 min incubation at 37°C.

2.2.8.2 $G_{\alpha i}$-coupled receptors

The BRET cAMP assay was also used to study C5aR activation. The assays were carried out in a total volume of 100 µL. Cells were washed with 40 µL of HBSS and serum starved in 40 µL of HBSS, pH 7.4, for 30 min at 37°C and 5% CO_2 in the presence of antagonist when being studied. 10 µL of IBMX and coelenterazine-h in HBSS was added to a final concentration of 40 µM and 5 µM respectively and incubated for 5 min at 37°C. 25 µL of increasing concentrations of agonist were added to stimulate cAMP production. This was immediately followed by the addition of 25 µL of forskolin. Emission signals of RLuc and YFP were measured sequentially after a 5 min incubation at 37°C.

2.2.9 Docking

Accelrys Discovery Studio 4.0 (www.accelrys.com) was used as an interface to set up the docking runs and to visualise the docking results. Ligands were constructed using Accelrys Draw 4.1. Where appropriate, small molecule ligands were protonated to create a charged amine at the most basic nitrogen. Ligands were then minimised using the CHARMM force field to convergence using 10,000 steps and a gradient of 0.1 kcal mol^{-1} $Å^{-1}$. The docking program Genetic Optimisation for Ligand Docking (GOLD) was used (Jones *et al.*, 1997). Docking was performed using crystal structures downloaded from the Protein Data Bank (Berman *et al.*, 2000) or homology models. Hydrogen atoms were added to the protein and ligands prior to docking. The binding pocket was determined from the receptor cavities unless otherwise stated. All docking parameters were left at default values except for "Detect Cavity" and "Early Termination" which were set to false. Each docking run generated 100 poses which were then clustered at heavy atoms root mean square deviation of 2Å, unless otherwise stated. The highest scoring pose of the largest cluster was then further analysed

2.2.10 Data analysis

2.2.10.1 Radioligand binding assays

Non-linear regression analyses were performed using GraphPad Prism 6 (San Diego, USA). Data from saturation binding assays were fitted to the one site specific binding equation. Data from competition binding assays were fitted to the one site fit K_i equation. Non-linear regression using one concentration of radioligand was used to determine the association rate constants for [^{3}H]DHA and the dissociation

rate constants of [^{3}H]DHA were determined from non-linear regression using the single exponential decay function. Statistical analyses of kinetics binding data were performed on $\log_{10}$ transformed values to normalise the distribution of the data. Statistical analyses were performed using one-way ANOVA followed by the Dunnett's multiple comparison test or one-sample t-test.

2.2.10.2 cAMP assays

Emission signals from the BRET cAMP assays were plotted as a ratio of emission at 475/535 nm such that an increase in the ratio correlated with an increase in intracellular cAMP, with data normalised to individual assay basal and forskolin values. Statistical analyses were performed using one-way ANOVA followed by the Dunnett's multiple comparison test.

CHAPTER 3

Allosteric modulation of the β_2 adrenoceptors by small molecule ligands

3.1 Introduction

The β_2AR is a major target for the treatment of asthma and COPD. Acute symptomatic relief of asthma and COPD is managed using β_2AR agonists as bronchodilators (Bateman *et al.*, 2008; Lougheed *et al.*, 2012; Qaseem *et al.*, 2011). All clinically used β_2AR agonists exert their effects through binding to the orthosteric site of the receptor (Baker, 2010). Common side effects of β_2AR agonists include tremor due to activation of the β_2AR on skeletal muscles and tachycardia due to activation of the β_1AR on the heart (Larsson and Svedmyr, 1977; Mann *et al.*, 1996). More importantly, prolonged use of β_2AR agonists has been shown to cause tolerance due to receptor desensitisation (Haney and Hancox, 2005; Haney and Hancox, 2007). Some studies have also reported increased mortality rate with long-term β_2AR agonist use (Crane *et al.*, 1989; Nelson *et al.*, 2006). Therefore, alternative treatments that could eliminate the shortcomings of current β_2AR agonists will be clinically useful.

Allosteric modulators are ligands that interact with a site on the receptor that is topographically distinct from the orthosteric site (Christopoulos and Kenakin, 2002). Allosteric modulators offer therapeutic advantages not achievable with orthosteric ligands, one of which is increased receptor subtype selectivity. The orthosteric binding site of the β_2AR is highly homologous to the β_1AR. However,

the ECL2 of these receptors is less conserved. Therefore, a positive allosteric modulator of the β_2AR which binds to the ECL2 could potentially eliminate tachycardia, which is one of the most common off-target side effects associated with current β_2AR agonists (Mann *et al.*, 1996).

THRX198321 or MABA (biphenyl-2-yl-carbamic acid 1-(9-[(R)-2-hydroxy-2-(8-hydroxy-2 - oxo-1,2-dihydro-quinolin-5-yl)-ethylamino]-nonyl)-piperidin-4-yl ester) is a bitopic compound composed of a mAChR antagonist moiety (MA) linked to a β_2AR agonist moiety (BA) through a nine-carbon polymethylene chain (Steinfeld *et al.*, 2011) (Figure 3.1). THRX198321 was developed to allow the delivery of a mAChR antagonist and a β_2AR agonist as a monotherapy for the treatment of COPD (Steinfeld *et al.*, 2011). Further characterisation of the binding of THRX198321 at both mAChRs and the β_2AR suggested that the compound is an allosteric modulator at both receptors (Steinfeld *et al.*, 2011). THRX198321 decreased the dissociation rate of orthosteric antagonists [^{3}H]N-methylscopolamine and [^{3}H]DHA at the mAChRs and the β_2AR respectively (Steinfeld *et al.*, 2011). The allosteric effects observed at the mAChRs have been attributed to the BA moiety while the allosteric effects observed at the β_2AR were attributed to the MA moiety or THRX100361 (Figure 3.1) (Steinfeld *et al.*, 2011). In addition, the BA moiety on its own can also modulate the M_2 and M_3 mAChRs, while the MA moiety alone can modulate the β_2AR, albeit with lower potencies compared to the bitopic parent compound THRX198321 (Steinfeld *et al.*, 2011). A bimodal mode of binding has been proposed for THRX198321, in which the MA moiety binds to the orthosteric site of the mAChRs while the BA moiety binds to an allosteric site (Steinfeld *et al.*, 2011). Similarly, at the β_2AR, the BA moiety binds to the

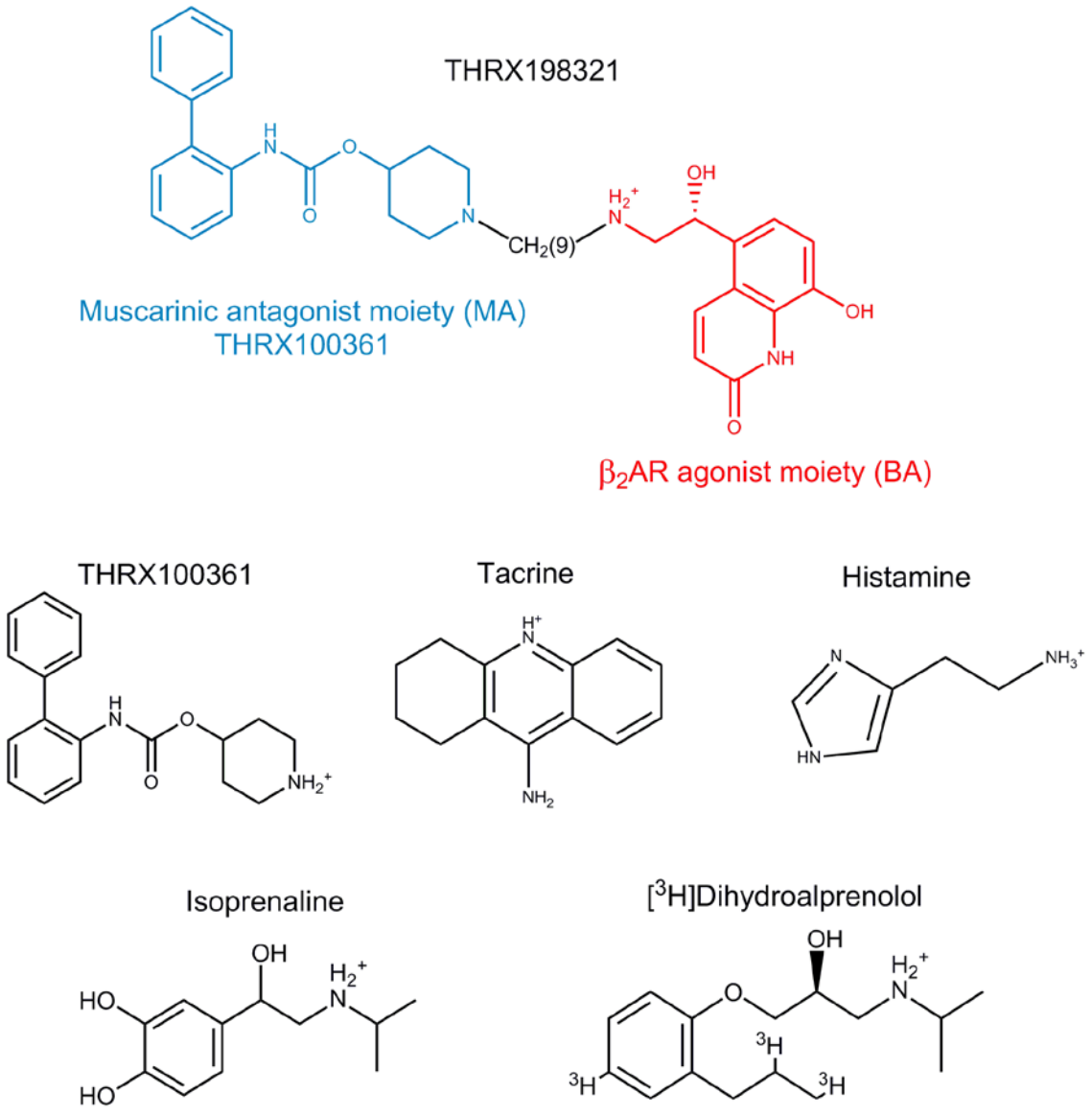

Figure 3.1 Small molecule ligands of the β_2AR

Chemical structures of THRX198321, THRX100361, tacrine and histamine in their protonated form.

orthosteric site while the MA moiety binds to an allosteric site, the location of which has not been identified.

The β_2AR can be modulated by cationic ions such as Zn^{2+} (Swaminath *et al.*, 2002). Zn^{2+} has complex allosteric effects on agonist isoprenaline and antagonist [^{3}H]DHA. Zn^{2+} was shown to increase the affinity of isoprenaline (Swaminath *et al.*, 2002). It also increased isoprenaline-mediated cAMP at low concentrations, but decreased cAMP production at high concentrations (Swaminath *et al.*, 2002). In addition, at high concentrations, Zn^{2+} decreased the binding of [^{3}H]DHA while also decreasing the dissociation rate of [^{3}H]DHA (Swaminath *et al.*, 2002). The allosteric binding site of Zn^{2+} has been determined to be H269 on the ICL3 of the β_2AR (Swaminath *et al.*, 2003). However, it is not likely that THRX100361 binds to this intracellular residue to exert its modulatory effect, as this residue is located at the bottom of TM6.

More recently, two studies have suggested that histamine modulates β_2AR function (Ramos-Jimenez *et al.*, 2007; Soriano-Ursua *et al.*, 2013). Histamine as well as other imidazole-containing compounds such as immepip, clobenpropit and imidazole increased isoprenaline-mediated cAMP production in human prostate cancer cells DU145 (Ramos-Jimenez *et al.*, 2007). Histamine also increased isoprenaline-mediated cAMP production in COS-7 cells (Soriano-Ursua *et al.*, 2013). Both studies suggested that the increase in cAMP was due to allosteric modulation of histamine at the β_2AR, as histamine antagonists were unable to prevent the action of histamine (Ramos-Jimenez *et al.*, 2007; Soriano-Ursua *et al.*, 2013). The location of the allosteric binding site of histamine on the β_2AR has not been determined.

Interestingly, an allosteric ligand which modulates both the mAChRs and the α_1 adrenoceptors (α_1AR) has been identified. Tacrine slows the dissociation rate of antagonist [^{3}H]pirenzepine and [^{3}H]NMS from the M_1, M_2 and M_3 mAChR (Kiefer-Day *et al.*, 1991; Pearce and Potter, 1988; Trankle *et al.*, 2005). However, tacrine has an opposing effect at the α_{1A} and α_{1B}-ARs where it increases the dissociation rate of antagonist [^{3}H]prazosin (Campbell, 2015). Extensive studies into allosteric modulation of mAChRs resulted in the identification of a common allosteric binding site which is formed by residues from the ECL2 and 3, and the top of TM2, 6 and 7 (Gnagey *et al.*, 1999; Huang *et al.*, 2005; Jager *et al.*, 2007; Kruse *et al.*, 2013; May *et al.*, 2007; Voigtländer *et al.*, 2003). Tacrine has been suggested to bind to two allosteric sites on the M_2 mAChR simultaneously, with one molecule binding to the common allosteric site while the other has been predicted to bind between the N-terminus and ECL1 (Trankle *et al.*, 2005). While the allosteric binding site of tacrine at the α_1AR has not been characterised, docking of tacrine into a homology model of the α_{1A}AR suggested that it may bind to the ECL2 and the top of TM2 and 7 (Campbell, 2015).

Given the ability of tacrine to modulate the mAChRs and the α_1ARs, it was hypothesised that tacrine is also an allosteric modulator of the closely related β_2AR. It was also hypothesised that THRX100361, tacrine and histamine modulate the β_2AR by binding to a common or shared extracellular allosteric binding site. To test these hypotheses, the allosteric effects of THRX100361, tacrine and histamine at the β_2AR were characterised using radioligand binding and functional cAMP assays. Docking studies were also carried out to predict the binding site of these ligands at the β_2AR.

3.2 Methods

3.2.1 Experimental protocols

THRX100361, the β_2AR allosteric moiety of the bitopic ligand THRX198321, was supplied by Theravance Biopharma (San Francisco, USA). THRX100361 was made as 200 mM stocks in DMSO, while tacrine and histamine were made as 10 mM stocks in milli-Q water. Isoprenaline was made as 10 mM stocks in 1 mM ascorbic acid for cAMP assays.

The affinity of THRX100361, tacrine and histamine at the WT human β_2AR and their effects on [^{3}H]DHA dissociation were investigated using equilibrium competition and kinetics dissociation binding assays performed with COS-1 cell membranes expressing WT human β_2ARs, as described in section 2.2.6. Binding assays were performed in a total volume of 500 µL of 75 mM TRIS, pH 7.4 at room temperature. In competition assays, membranes were incubated with increasing concentrations of the proposed modulators and 0.5 nM of [^{3}H]DHA for 1 hour. In kinetics dissociation assays, membranes were equilibrated with 0.5 nM of [^{3}H]DHA for 1 hour and re-association of [^{3}H]DHA was prevented using 10 µM of propranolol. Non-specific binding was determined using 10 µM of propranolol.

The effects of the proposed allosteric modulators on receptor activation were investigated using a BRET-based cAMP assay as described in section 2.2.8.1. The BRET sensor CAMYEL was transiently transfected into CHO cells stably expressing WT human β_2ARs as described in 2.2.7.1. On the day of the assay, the cells were pre-incubated with the proposed allosteric modulators for 30 min prior to stimulation with increasing concentrations of isoprenaline to initiate cAMP production. The assays were carried out in 100 µL of HBSS, in the presence of 40

μM of the phosphodiesterase inhibitor IBMX, pH 7.4 at 37°C. cAMP production was measured as emission signals of RLuc and YFP, which were measured sequentially after a 15 min incubation with isoprenaline at 37°C using the BRET1 filter set (475/25 and 535/30 nm).

The active and inactive state human β_2AR crystal structures (PDB ID 3P0G and 3NYA) (Rasmussen *et al.*, 2011b; Wacker *et al.*, 2010) were used in the docking studies as described in section 2.2.9. Dockings were carried out using GOLD through Accelrys Discovery Studio 4.0. The ligands used in docking were protonated as shown in Figure 3.1 and minimised using the CHARMM forcefield prior to docking. Hydrogens were added to the crystal structures and the ligands prior to docking. The binding pockets were defined using $D192^{ECL2}$, $F193^{ECL2}$, $T195^{ECL2}$, $H296^{6.58}$ and $K305^{7.32}$ or from receptor cavities. In the docking with the active state crystal structure, the side chains of $D192^{ECL2}$ and $K305^{7.32}$ were set to flexible, but not in the docking with the inactive state crystal structure. Each docking run generated 100 poses and the poses were clustered at heavy atoms root mean square deviation of 2 Å.

3.2.2 Data analysis

GraphPad Prism 6 was used to plot and analyse the binding and functional data. Competition binding data were fit to one-site fit K_i equation, using K_D values determined from saturation binding assays. Dissociation binding data were fit to a one-site exponential decay. Concentration response curves of THRX100361 and tacrine were generated by plotting K_{obs}/K_{off} and $pEC_{50,diss}$ values were estimated by fitting the data to the log (inhibitor) vs. response (four parameters) equation.

Isoprenaline concentration response curves were fitted to the log (agonist) vs. response (three parameters) equation. Statistical analyses were performed using one-way ANOVA followed by the Dunnett's multiple comparisons test. The kinetics binding data were transformed into $\log_{10}$ values to normalise the distribution of the data. Statistical analyses of the $\log_{10}$ K_{obs}/K_{off} data and the pEC_{50} ratio data were performed using one-sample t-tests which compare the values to the ratio of the control, which has a value of 0.

3.3 Results

THRX100361 and histamine have previously been shown to modulate ligand binding or activation of the β_2AR respectively. In this study, the allosteric effects of THRX100361 on ligand binding and receptor activation were further characterised. As tacrine has been shown to modulate closely related α_1ARs and mAChRs, it was also tested for modulatory effects at the β_2AR. THRX100361, tacrine and histamine were docked into active and inactive crystal structures of the β_2AR to investigate their potential allosteric binding site.

3.3.1 Equilibrium binding assays

Initial characterisation of the proposed β_2AR allosteric modulators THRX100361, tacrine and histamine was done using competition binding assays performed at equilibrium. In these assays, increasing concentrations of THRX100361, tacrine and histamine were competed with radiolabelled orthosteric antagonist [^{3}H]DHA. [^{3}H]DHA bound with normal affinity ranging from 0.11 to 0.18 nM. THRX100361 and tacrine have low apparent affinity for the β_2AR with pK_{iApp} values of 4.2 ± 0.1 and 5.0 ± 0.2 respectively (mean ± SEM, n=3) (Figure 3.2). In contrast, no apparent binding of histamine was detected at the β_2AR (Figure 3.2).

3.3.2 Kinetics dissociation binding assays

Kinetics dissociation binding assays were performed to investigate the ability of THRX100361 and tacrine to modulate the dissociation rate of [^{3}H]DHA. THRX100361 was a poor modulator of [^{3}H]DHA binding. The dissociation rate of

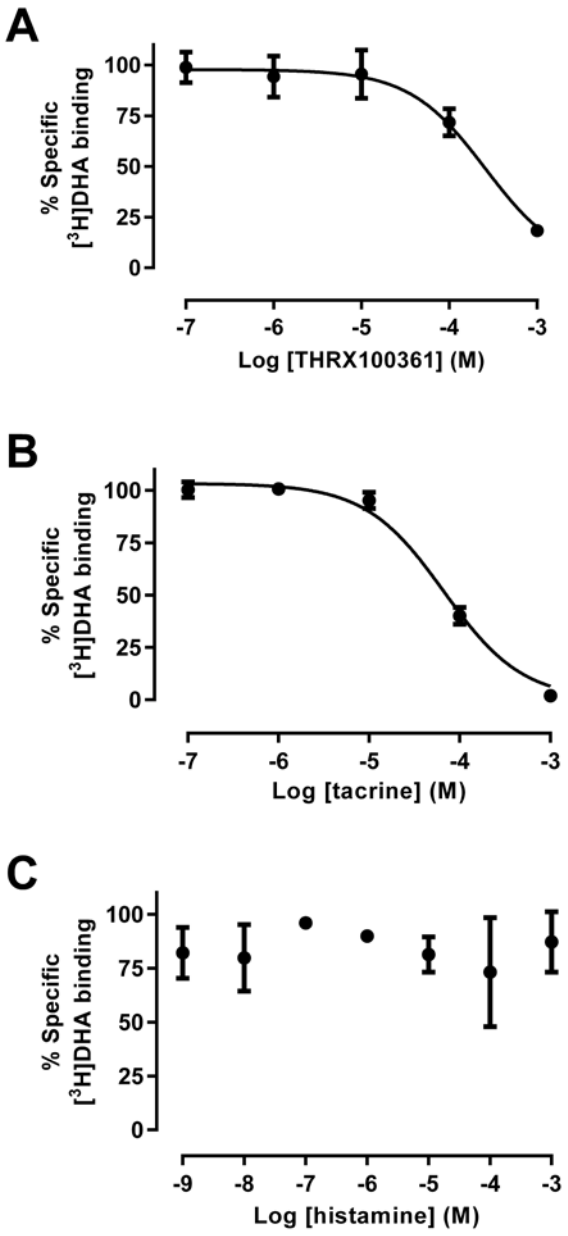

Figure 3.2 Equilibrium binding of proposed allosteric modulators at the WT β2AR

Apparent affinity of THRX100361 (A), tacrine (B) and histamine (C) at WT β2AR was determined using membrane preparations of COS-1 cells expressing WT β2AR incubated with 0.5 nM of [3H]DHA in the presence of increasing concentrations of competing ligand for one hour at room temperature. Curves were fitted to a single site model in GraphPad Prism. Data are presented as the mean ± SEM of 3 independent experiments performed in duplicate.

† *The data in panel A have previously been presented in Leonar (2011).*

[^{3}H]DHA was not changed in the presence of 100 μM and 300 μM of THRX100361. However, the dissociation rate of [^{3}H]DHA was decreased by approximately 2 fold in the presence of 1 mM of THRX100361 ($P < 0.05$) (Table 3.1, Figure 3.3). Higher concentrations of THRX100361 were not tested due to the limited solubility of the compound. Compared to THRX100361, tacrine was a more potent modulator of [^{3}H]DHA binding. The dissociation rate of [^{3}H]DHA was decreased by approximately 3 and 2 fold respectively in the presence of 100 μM and 30 μM of tacrine ($P < 0.05$) (Table 3.1, Figure 3.3).

The ability of THRX100361 and tacrine to slow the dissociation rate of [^{3}H]DHA was plotted as concentration response curves in Figure 3.4. The $pEC_{50,diss}$ value or the negative log of the concentration required to retard [^{3}H]DHA dissociation rate by 50% for THRX100361 was calculated to be 3.2 ± 1.5 (mean ± SEM, n = 3-5). The $pEC_{50,diss}$ value for tacrine could not be determined from the curve, as the top and bottom of the curve were not defined and more concentrations are needed to generate the curve. However, the data suggested that tacrine was a more potent modulator of [^{3}H]DHA dissociation compared to THRX100361. THRX100361 was a less potent modulator of [^{3}H]DHA dissociation in this study compared to the study by Steinfeld *et al*. (2011). At 300 μM and 1 mM, THRX100361 was previously reported to decrease the dissociation rate of [^{3}H]DHA by approximately 40% and 70% respectively (Steinfeld *et al.*, 2011), whereas in this study the rate of [^{3}H]DHA dissociation was only decreased by 20% and 60% respectively. In addition, the concentration-effect of THRX100361 appeared to have reached saturation in the study by Steinfeld *et al.* (2011), but not in this study.

Table 3.1 Dissociation rates of [^{3}H]DHA from the WT β_2AR

Compound		K_{off} (min^{-1})	K_{obs} (min^{-1})	$t_{1/2}$ (min)	K_{obs}/K_{off}	Log_{10} K_{obs}/K_{off}	n
THRX100361†	Control	0.037 ± 0.002		19.2 ± 0.9	1	0	5
	100 µM		0.033 ± 0.003	21.2 ± 1.7	0.96 ± 0.07	-0.02 ± 0.03	3
	300 µM		0.029 ± 0.003	26.3 ± 3.6	0.80 ± 0.11	-0.12 ± 0.07	5
	1 mM		0.015 ± 0.003	52.9 ± 13.3*	0.43 ± 0.08	-0.39 ± 0.09§	4
Tacrine	Control	0.023 ± 0.004		32.7 ± 4.5	1	0	5
	10 µM		0.014 ± 0.001	51.0 ± 2.5	0.67 ± 0.04	-0.18 ± 0.03§	3
	30 µM		0.010 ± 0.001	72.8 ± 6.9*	0.54 ± 0.02	-0.27 ± 0.02§	3
	100 µM		0.007 ± 0.001	105.0 ± 7.5*	0.25 ± 0.04	-0.61 ± 0.07§	3
Histamine	Control	0.024 ± 0.002		29.4 ± 2.4	1	0	3
	100 µM		0.020 ± 0.004	36.7 ± 6.5	0.84 ± 0.13	-0.08 ± 0.07	3
	1 mM		0.021 ± 0.005	37.6 ± 10.1	0.88 ± 0.19	-0.08 ± 0.11	3

K_{off}, dissociation rate of [^{3}H]DHA.

K_{obs}, dissociation rate of [^{3}H]DHA in the presence of an allosteric modulator.

$t_{1/2}$, half-life of [^{3}H]DHA dissociation.

* $P < 0.05$ compared to control by one-way ANOVA with Dunnett's multiple comparison test.

§ $P < 0.05$ compared to control by one-sample t test.

Data are presented as the mean ± SEM of n independent experiments performed in duplicate or triplicate.

† *Data have previously been presented in Leonar (2011).*

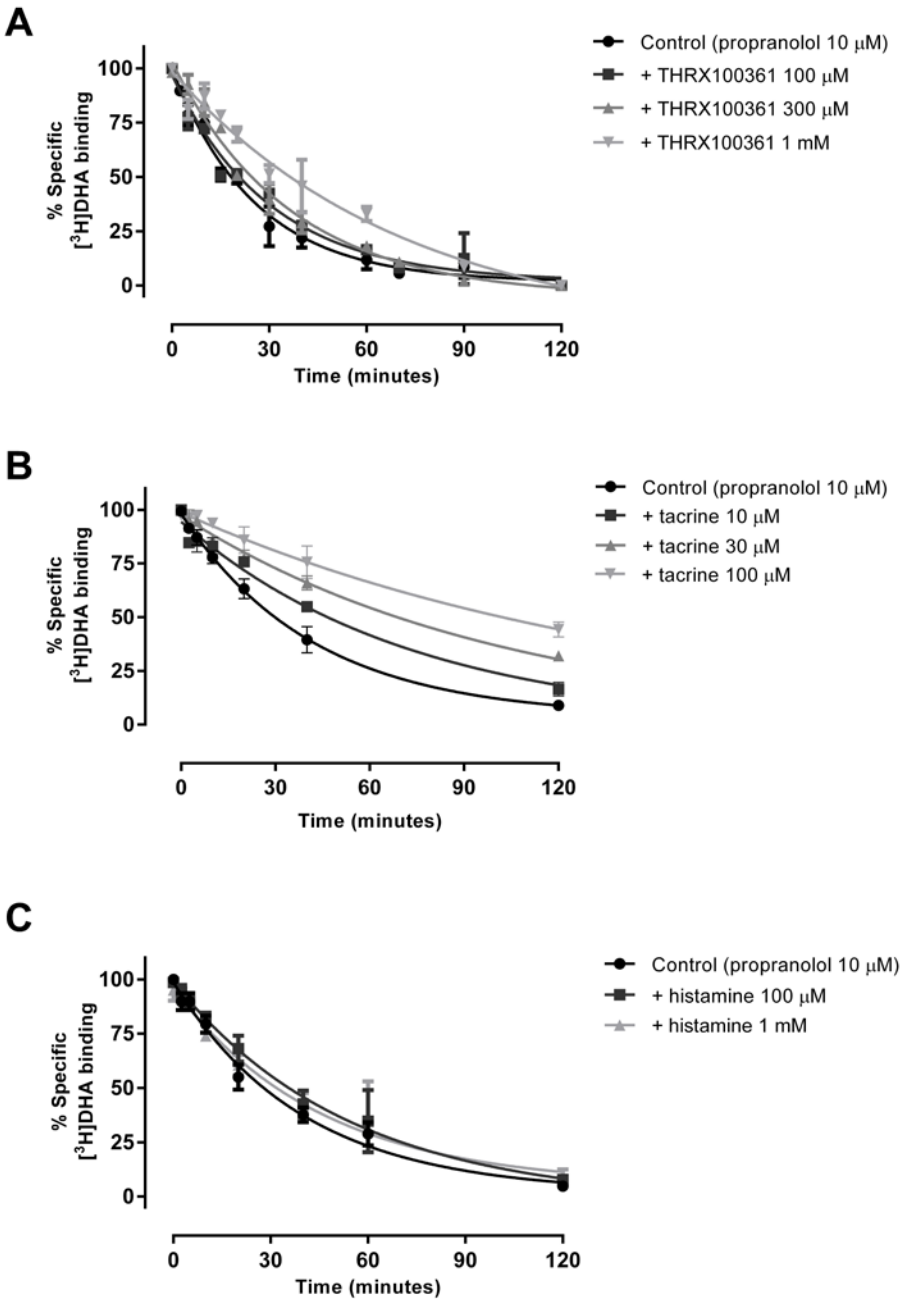

Figure 3.3 Dissociation of [^{3}H]DHA from WT β_2AR

Dissociation of [^{3}H]DHA from WT β_2AR in the absence and presence of THRX100361 (A), tacrine (B) and histamine (C) was determined using membrane preparations of COS-1 cells expressing WT β_2AR pre-incubated with 0.5 nM of [^{3}H]DHA for one hour at room temperature. Subsequent [^{3}H]DHA re-association was inhibited using 10 μM of propranolol in the absence or presence of test compounds at the concentrations shown. Data are presented as the mean ± SEM of 3-5 independent experiments performed in duplicate of triplicate.

† *Data in panel A have previously been presented in Leonar (2011).*

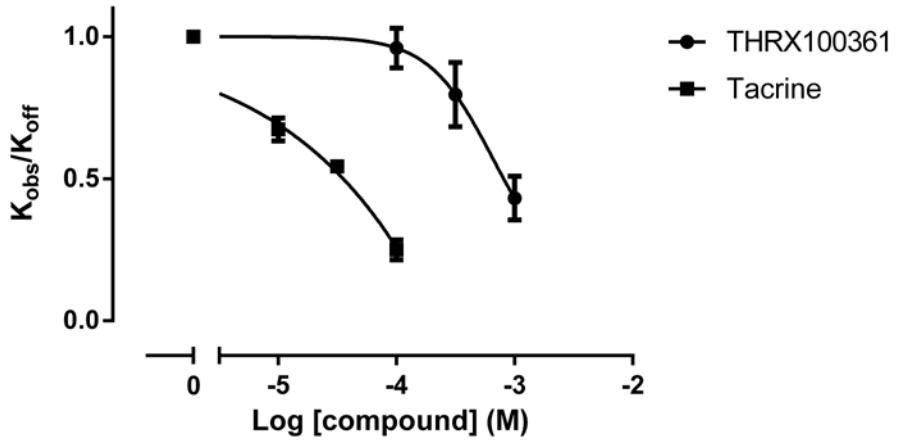

Figure 3.4 The effects of THRX100361 and tacrine on [^{3}H]DHA dissociation

Concentration response curves of allosteric modulators THRX100361 and tacrine on the dissociation rate of [^{3}H]DHA at WT β_2AR. The ability of the modulators to slow [^{3}H]DHA dissociation was expressed as a ratio of [^{3}H]DHA dissociation in the presence (K_{obs}) and absence (K_{off}) of the modulators. Data are presented as the mean ± SEM of 3-5 independent experiments performed in duplicate or triplicate.

Histamine has previously been reported to increase isoprenaline-mediated cAMP production in *in vitro* assays using the mammalian cell line COS-7 and DU145 (Ramos-Jimenez *et al.*, 2007; Soriano-Ursua *et al.*, 2013). In this study, kinetics dissociation binding assays were performed to investigate the effects of histamine on the dissociation rate of [^{3}H]DHA. In contrast to the previously reported effect on agonist signalling, the dissociation rate of the antagonist [^{3}H]DHA was not modulated by 100 μM or 1 mM of histamine ($P > 0.05$) (Table 3.1, Figure 3.3).

3.3.3 cAMP assays

The functional effects of the proposed allosteric modulators on cAMP production were investigated using a BRET-based assay and CHO cells stably transfected with WT β_2AR. Stable CHO cells were generated and used because attempts to optimise cAMP assays using transiently transfected COS-1 cells have been unsuccessful and COS-1 cells are not suitable for stable cell generation. The affinity of isoprenaline at membrane preparations of WT β_2AR from the stable CHO cells and the transient COS cells is not significantly different from one another (pK_i CHO = 6.5 ± 0.1, COS-1 = 6.5 ± 0.1, mean ± SEM, n = 2-3).

Initial analysis of the mean potency of isoprenaline in the absence or presence of the modulators (pEC_{50}) suggested that THRX100361 has no effect on receptor activation (Table 3.2, Figure 3.5). However, analysis of the pEC_{50} ratios which took into account the inter-assay variations observed with this assay showed that 600 μM of THRX100361 significantly reduced the potency of isoprenaline by 4 fold ($P < 0.05$) (Table 3.2). THRX100361 did not show agonist activity at up to 600 μM.

Table 3.2 The effects of THRX100361 and tacrine on isoprenaline-mediated cAMP accumulation at WT β_2AR

Modulator	Concentration (μM)	pEC_{50} (M)	EC_{50} (nM)	pEC_{50} ratio (Δ)	%Potency	E_{max} (%)	n
THRX100361	0 (control)	7.0 ± 0.3	100	0	100	100.8 ± 8.1	10
	300	6.5 ± 0.3	316	0.4 ± 0.3	39.8	64.7 ± 16.0	5
	600	7.1 ± 0.1	79	0.6 ± 0.1*	25.1	84.7 ± 8.1	3
Tacrine	0 (control)	7.1 ± 0.2	79	0	100	95.4 ± 2.8	7
	100	7.0 ± 0.3	100	0.2 ± 0.3	63.1	92.3 ± 1.5	6
	300	6.8 ± 0.2	158	0.4 ± 0.1*	39.8	88.1 ± 7.8	6
	600	6.7 ± 0.2	200	0.6 ± 0.2*	25.1	83.3 ± 5.4	6

pEC_{50}, negative log of the concentration of isoprenaline resulting in 50% of the maximum cAMP production.
pEC_{50} ratio (Δ), pEC_{50} control - pEC_{50} in the presence of the modulator.
% Potency, relative potency of isoprenaline in the presence of the modulator as % control ((antilog –Δ) x 100%).
E_{max}, the maximum amount of cAMP produced from the highest concentration of isoprenaline, expressed as percentage maximum forskolin stimulation.
*$P < 0.05$ compared to control by one-sample t test.
Data are presented as the mean ± SEM of n independent experiments performed in triplicate.

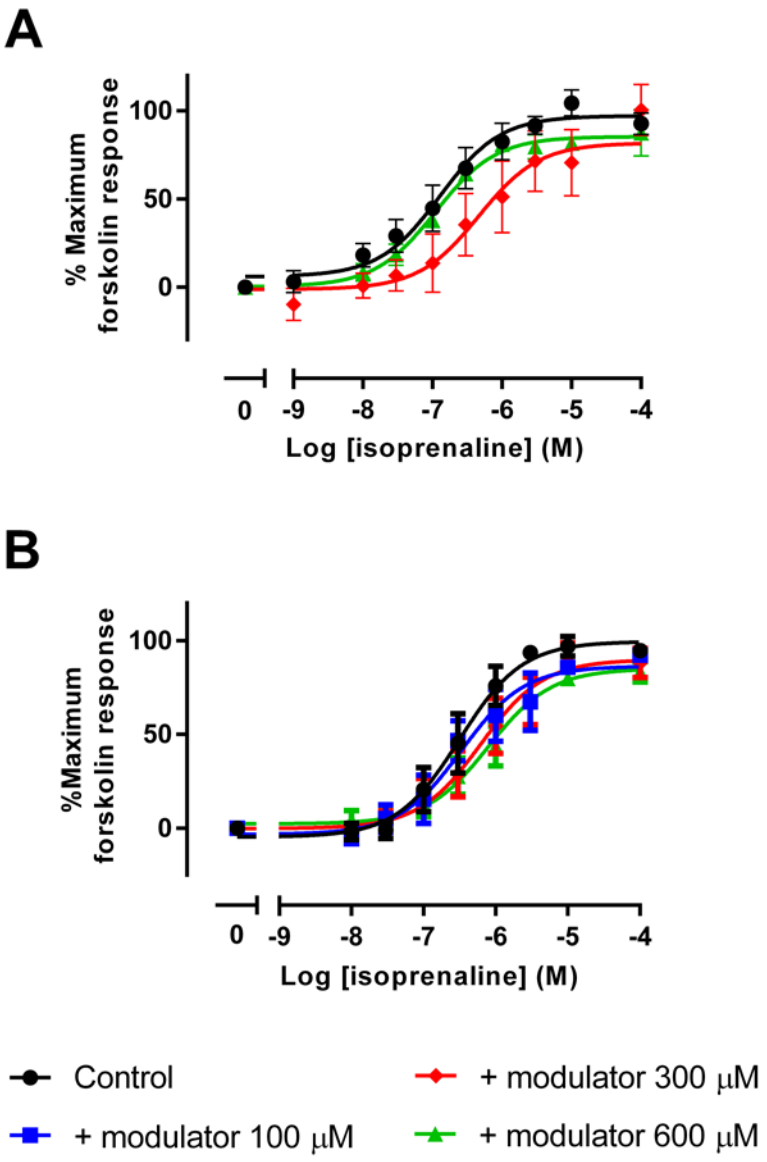

Figure 3.5 The effects of THRX100361 and tacrine on isoprenaline-mediated cAMP accumulation on WT β_2AR

The effects of various concentrations of allosteric modulators THRX100361 (A) and tacrine (B) on isoprenaline-mediated WT β_2AR activation was examined in CHO cells stably expressing WT β_2AR transfected with the BRET cAMP sensor CAMYEL. Cells were pre-incubated with or without the modulators for 30 min and stimulated with increasing concentrations of isoprenaline. cAMP production was measured after a 15 min incubation with isoprenaline in the presence of 40 μM of IBMX. Data are presented as the mean ± SEM of 3-10 independent experiments performed in triplicate using 3 different clones of cells.

THRX100361 was tested at concentrations of 300 μM and 600 μM only, as concentration response curves of isoprenaline could not be obtained in the presence of 1 mM of THRX100361 (0.5% DMSO). At 1 mM, THRX100361 may either be toxic to the cells or interfered with the CAMYEL sensor, as basal response was lowered in the presence of 1 mM of THRX100361. DMSO at 0.5% has no effect on the activation of WT β_2AR by isoprenaline.

In contrast to the observed allosteric effects on [^{3}H]DHA dissociation where tacrine was a more potent modulator compared to THRX100361, tacrine was equipotent to THRX100361 in cAMP assays. At 300 μM and 600 μM, tacrine decreased the potency of isoprenaline by 2.5 and 4 fold respectively (pEC_{50} ratio, $P < 0.05$) (Table 3.2**,** Figure 3.5). Tacrine has no agonist activity in the cAMP assays.

cAMP assays were also performed using histamine to test its modulatory effects on isoprenaline-mediated cAMP production. The data presented in Figure 3.6 were obtained from two independent preliminary experiments. In the first experiment, 10 μM of histamine increased cAMP production in response to 100 μM of isoprenaline by approximately 50% (Figure 3.6A). However, this increase corresponded to the production of cAMP caused by 10 μM of histamine in the absence of isoprenaline (Figure 3.6A). In the second experiment, a lower concentration of isoprenaline (100 nM) and three different concentrations of histamine (1, 10 and 100 μM) were used. In this assay, all three concentrations of histamine tested increased cAMP production in response to 100 nM of isoprenaline (Figure 3.6B). However, similar to the first experiment, histamine by itself also caused an increase in cAMP production (Figure 3.6B).

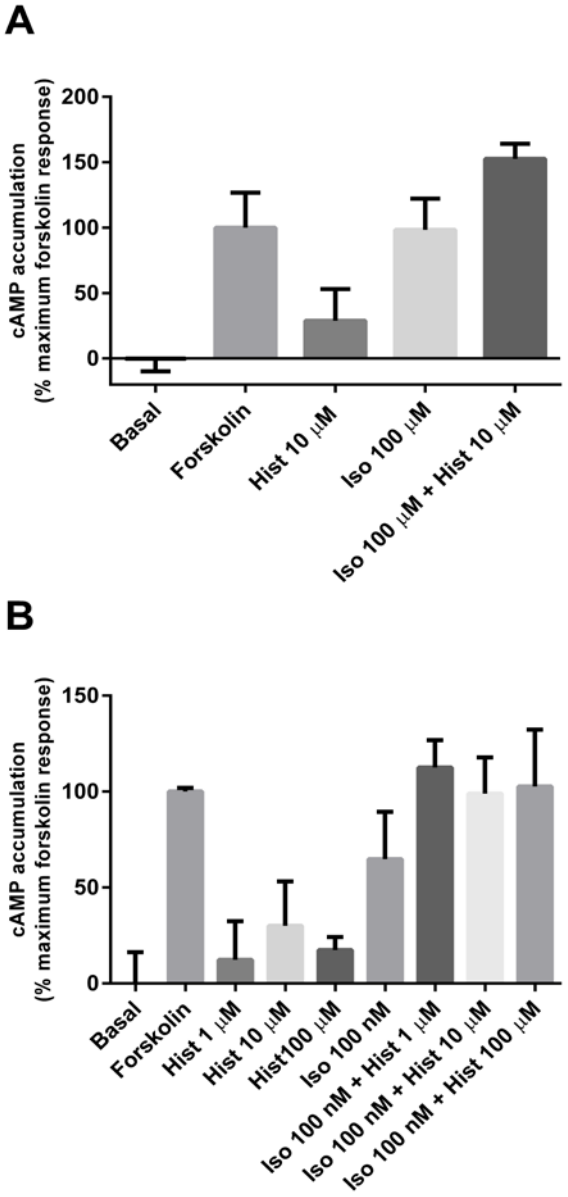

Figure 3.6 The effects of histamine on isoprenaline-mediated cAMP accumulation on WT β_2AR

CHO cells stably expressing WT β_2AR were transfected with the BRET cAMP sensor CAMYEL. cAMP production was measured after a 15 min incubation with either buffer (basal), 10 μM of forskolin, isoprenaline or histamine in the presence of 40 μM of IBMX. To test the effects of histamine on isoprenaline-mediated cAMP production, cells were pre-incubated with histamine and stimulated with isoprenaline. Each panel contains the data (mean ± SEM) obtained from a single experiment.

3.3.4 Docking of the bitopic ligand THRX198321 into an active state β_2AR crystal structure

Docking is commonly used in GPCR research to identify potential ligand binding sites (Gao *et al.*, 2003; Lane *et al.*, 2014; Valant *et al.*, 2008). The bitopic parent compound of THRX100361, THRX198321, is an agonist of the β_2AR (Steinfeld *et al.*, 2011). Therefore, the active state β_2AR crystal structure (PDB ID 3P0G) was used in this docking study. Molecular dynamics studies suggest that the D192^{ECL2}-K305$^{7.32}$ salt bridge breaks and forms multiple times during ligand binding and unbinding (Dror *et al.*, 2011; Wang and Duan, 2009). In addition, an NMR study suggested that this salt bridge interaction is weakened in activated β_2AR (Bokoch *et al.*, 2010). Therefore, the side chains of D192^{ECL2} and K305$^{7.32}$ were set as flexible in subsequent dockings to simulate this event.

To identify the potential allosteric binding site on the β_2AR, the bitopic compound THRX198321 was firstly docked into the active state human β_2AR crystal structure (PDB ID 3P0G). THRX198321 was predicted to interact at two distinct sites at the β_2AR – the agonist moiety bound to the orthosteric site and the allosteric moiety bound to a novel allosteric site. The orthosteric ligand binding site of the β_2AR is well characterised and interactions observed with the β_2AR agonist moiety of THRX198321 serve as method validation. Residues that are critical for orthosteric ligand interactions at the β_2AR as shown in mutagenesis and structural studies include D113$^{3.32}$, S203$^{5.42}$, S204$^{5.43}$, S207$^{5.46}$, F289$^{6.51}$, F290$^{6.52}$ and N293$^{6.55}$ (Liapakis *et al.*, 2000; Ring *et al.*, 2013; Strader *et al.*, 1989b; Strader *et al.*, 1989c; Strader *et al.*, 1987; Wieland *et al.*, 1996).

In 96 out of 100 docking poses, the agonist moiety of THRX198321 interacted with the receptor in the known orthosteric binding pocket while the allosteric moiety extended to interact with residues on the extracellular region of the receptor. The highest scoring pose (pose 1) is shown in Figure 3.7 and the interactions are listed in Table 3.3. In the highest scoring pose, the agonist moiety of THRX198321 made the expected orthosteric interactions with D113$^{3.32}$, S204$^{5.43}$, S207$^{5.46}$, F289$^{6.51}$ and F290$^{6.52}$ while the allosteric moiety interacted with F193^{ECL2}, F194^{ECL2}, T195^{ECL2}, A200$^{5.39}$, H296$^{6.58}$, V297$^{6.59}$, D300$^{6.62}$ and Y308$^{7.35}$.

3.3.5 Docking of THRX100361 into an active state β_2AR crystal structure

Based on the docking of the bitopic ligand THRX198321 which suggested that the allosteric moiety of the ligand bound to the area in the vicinity of the ECL2 and the top of TM5, TM6 and TM7, the residues encompassing this region (D192^{ECL2}, F193^{ECL2}, T195^{ECL2}, H296$^{6.58}$ and K305$^{7.32}$) were selected and used to define the binding site of THRX100361 for initial docking studies. Using this method, the highest scoring pose suggested that THRX100361 interacts with residues from the ECL2 and the top of TM6 and TM7 (Table 3.4**,** Figure 3.8). In this pose, the piperidine ring of THRX100361 interacted with T195^{ECL2} and N293$^{6.55}$, while the phenyl rings of the ligand interacted with H296$^{6.58}$, I303^{ECL3}, K305$^{7.32}$ and Y308$^{7.35}$. The interactions made by THRX100361 in pose 1 are the same as in pose 6, which is the highest scoring pose of the largest cluster. There are two clusters in which THRX100361 bound with slightly different conformations. In poses 8 and 25, as well as other poses belonging to the same clusters, the protonated nitrogen on the piperidine ring interacted with D113$^{3.32}$, a residue critical for orthosteric ligand

Table 3.3 Docking of THRX198361 into the active state human β_2AR crystal structure 3P0G

Docking clusters[a]	Interactions		
| **1** 4 5 11 19 23 27 35 43 48 51 54 64 69 70 76 93 | 2 15 16 17 29 49 50 55 57 60 | 3 10 12 33 36 46 58 84 | 6 14 21 39 42 56 61 63 66 78 82 | 7 20 24 25 30 32 45 65 67 79 85 | 8 87 92 96 | 9 28 37 38 40 47 74 94 | 13 31 73 91 95 | 18 22 | 26 52 59 99 | 34 83 89 | 41 81 | 44 53 77 | 62 | 68 80 98 | 71 90 | 72 | 75 88 | 86 | 97 | 100 |		Pose, Goldscore[b]	1, 64.1
	Orthosteric moiety	H-bond	$D113^{3.32}$, $A200^{5.39}$, $S204^{5.43}$, $S207^{5.46}$, $N312^{7.39}$
		Charge	$D113^{3.32}$
		Hydrophobic	$V114^{3.33}$, $V117^{3.36}$, $F289^{6.51}$, $F290^{6.52}$
	Allosteric moiety	H-bond	$F193^{ECL2}$, $F194^{ECL2}$, $H296^{6.58}$, $T195^{ECL2}$
		Charge	$D300^{6.62}$
		Hydrophobic	$F194^{ECL2}$, $Y308^{7.35}$, $A200^{5.39}$, $V297^{6.59}$

[a] Docking clusters, 100 poses generated from each docking run were clustered at heavy atoms root mean square deviation of 3 Å. The interactions made by THRX198321 in pose 1 is listed in details.

[b] GoldScore, scoring function in GOLD which is a weighted sum of the intramolecular van der Waals forces, internal torsion of the ligand, van der Waals forces between the ligand and the receptor and H-bond interactions between the ligand and the receptor. A positive number indicates favourable interactions.

Superscripts denote Ballesteros-Weinstein residue numbering.

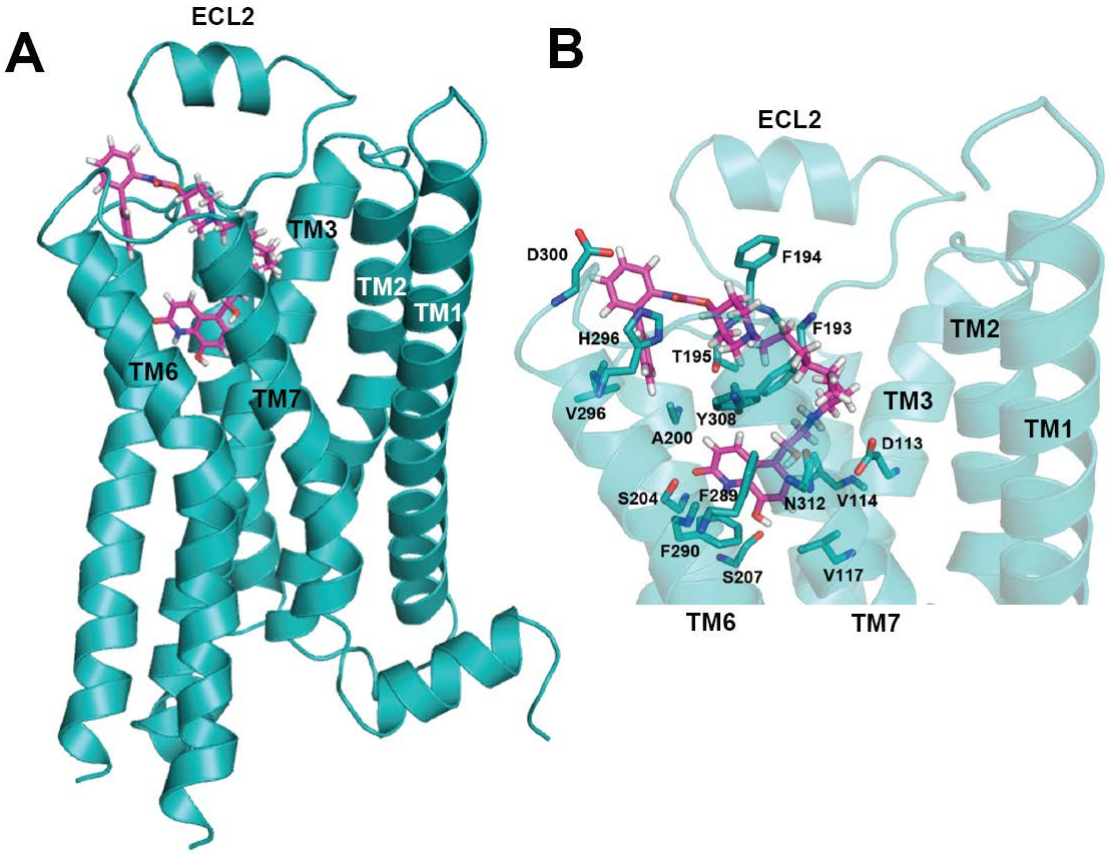

Figure 3.7 Docking of THRX198321 into an active state β_2AR crystal structure
Human β_2AR (PDB ID 3P0G) is shown in teal. THRX198321 is shown as stick and coloured by elements with carbon atoms in magenta, oxygens in red, nitrogens in dark blue and hydrogens in white. (A) The pose shown was the highest scoring pose obtained from a docking run consisting of 100 poses. (B) A close up view of the interactions with TM7 removed for clarity.

Table 3.4 Docking of THRX100361 into the active state human β_2AR crystal structure 3P0G

Binding site defined[a]	Docking clusters[b]	Interactions	
Yes	| **1** 2 4 7 9 11 18 50 64 85 | 3 14 30 37 61 91 | 5 | 6 12 19 20 21 31 34 36 42 46 47 48 49 51 52 53 54 56 57 58 60 63 65 66 67 68 69 70 71 72 73 74 75 76 77 78 79 82 83 84 86 87 88 89 93 94 95 96 97 99 100 | **8** 10 13 15 16 17 22 23 24 26 27 28 29 32 35 38 39 40 41 44 | 25 43 45 55 62 | 33 | 59 | 80 90 92 98 | 81 |	Pose number, Goldscore[c]	1, 59.0 (allosteric[d])
		H-bond	T195^{ECL2†}, N293$^{6.55}$, H296$^{6.58}$, K305$^{7.32}$
		π-charge	K305$^{7.32}$
		Hydrophobic	H296$^{6.58}$, I303^{ECL3}, K305$^{7.32}$, Y308$^{7.35}$
		Pose number, Goldscore	8, 56.3 (orthosteric[e])
		H-bond	D113$^{3.32}$, F193^{ECL2†}, N312$^{7.39}$, Y316$^{7.43}$
		π-charge	D192^{ECL2}, K305$^{7.32}$
		Hydrophobic	K305$^{7.32}$, Y308$^{7.35}$, I309$^{7.36}$
No	| **1** 2 3 4 5 6 8 19 20 21 97 98 | 7 9 10 11 12 13 14 15 16 23 35 | **17** 18 22 24 25 26 27 28 29 30 31 32 33 34 36 37 38 39 40 41 43 44 45 46 47 48 49 50 51 52 53 54 55 56 57 58 59 60 61 62 64 65 66 67 68 69 70 72 73 74 76 77 78 79 80 81 82 83 84 85 86 87 88 90 91 93 94 96 | 42 75 89 92 | 63 71 95 99 | 100 |	Pose number, Goldscore	1, 60.6 (allosteric)
		H-bond	T195^{ECL2†}, N293$^{6.55}$, H296$^{6.58}$, Y308$^{7.35}$
		π-charge	K305$^{7.32}$
		Hydrophobic	F194^{ECL2}, H296$^{6.58}$, I303^{ECL3}, K305$^{7.32}$, Y308$^{7.35}$
		Pose number, Goldscore	17, 56.8 (orthosteric)
		H-bond	N312$^{7.39}$
		Charge	D113$^{3.32}$
		π-charge	K305$^{7.32}$
		Hydrophobic	K305$^{7.32}$, Y308$^{7.35}$, I309$^{7.36}$

[a] Binding site was defined by D192^{ECL2}, F193^{ECL2}, T195^{ECL2}, H296$^{6.58}$ and K305$^{7.32}$.
[b] Docking clusters, 100 poses generated from each docking run were clustered at heavy atoms root mean square deviation of 2Å.
[c] Goldscore, scoring function in GOLD which is a weighted sum of the intramolecular van der Waals forces, internal torsion of the ligand, van der Waals forces between the ligand and the receptor and H-bond interactions between the ligand and the receptor. Large number indicates favourable interactions.
[d] Ligand bind above the orthosteric binding pocket of the β_2AR.
[e] Ligand interacts with the highly conserved D113$^{3.32}$ from the orthosteric pocket of the β_2AR.
[§] Ligand interacts with both the side chain and the carboxyl group of the residue.
[†] Ligand interacts with the backbone atom of the residue.
Superscripts denote Ballesteros-Weinstein residue numbering.

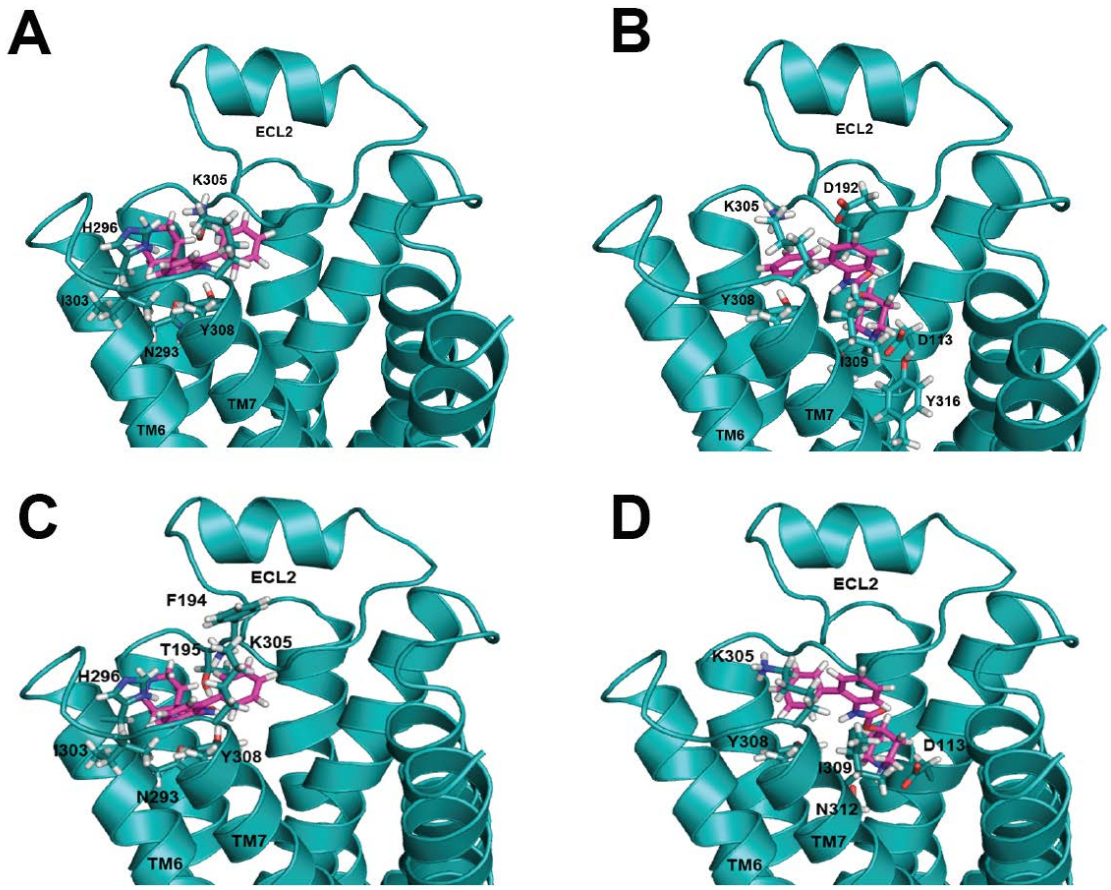

Figure 3.8 Docking of THRX100361 into an active state human β_2AR crystal structure

The human β_2AR (PDB ID 3P0G) is shown in teal. Interacting side chains are shown as sticks coloured by elements with carbon atoms in magenta, oxygens in red, nitrogens in dark blue and hydrogens in white. Each docking run yielded 100 poses. The highest scoring pose of the largest cluster (A) and the first pose where an interaction with $D113^{3.32}$ was found (B) when the binding site was defined using $D192^{ECL2}$, $F193^{ECL2}$, $T195^{ECL2}$, $H296^{6.58}$ and $K305^{7.32}$. The highest scoring pose (C) and the highest scoring pose of the largest cluster (D) when the binding site was not defined.

binding at the β_2AR. More specifically, in poses 8 and 25, the phenyl rings of THRX100361 interacted with K305$^{7.32}$, Y308$^{7.35}$ and I309$^{7.36}$ while the piperidine ring bound deeper into the binding pocket, making an interaction with D113$^{3.32}$ (Table 3.4**,** Figure 3.8).

To further examine the possible binding sites of THRX100361 at the β_2AR, the binding site was expanded to sample a larger area which included the orthosteric binding pocket. In other words, the binding site of THRX100361 was not pre-defined in the docking protocol. In the highest scoring pose, the interactions made were almost identical to the highest scoring pose from when the binding site was defined, except that THRX100361 also interacted with F194^{ECL2} (Table 3.4**,** Figure 3.8). Similar to the previous docking method, THRX100361 was also observed to bind in the orthosteric pocket in a lower scoring pose (pose 17), making interactions with D113$^{3.32}$ and N312$^{7.39}$ in the transmembrane domain as well as with extracellular residues K305$^{7.32}$, Y308$^{7.35}$ and I309$^{7.36}$ (Table 3.4**,** Figure 3.8).

3.3.6 Docking of tacrine and histamine into an active state β_2AR crystal structure

To investigate the role of the residues on the ECLs and the top of the TM helices in the modulatory actions of tacrine, the binding site of tacrine was defined using the same residues as previously used for THRX100361 to exclude binding in the orthosteric pocket. Using this method, tacrine docked into the extracellular region at a similar site where THRX100361 docked (Figure 3.9). In the highest scoring pose, tacrine interacted with D192^{ECL2}, F194^{ECL2}, K305$^{7.32}$, Y308$^{7.35}$ and I309$^{7.36}$ (Table 3.5). Tacrine is a smaller molecule compared to THRX100361 and

Table 3.5 Docking of tacrine and histamine into the active state human β_2AR crystal structure 3P0G

Compound	Docking clusters[a]	Interactions	
Tacrine	| **1** 2 3 4 5 6 7 8 9 10 11 12 13 14 15 16 17 18 19 20 21 22 23 24 25 26 27 28 29 30 31 32 33 34 35 36 37 38 39 40 41 42 43 44 45 46 47 48 49 50 51 52 53 54 55 56 57 58 59 60 61 62 63 64 66 67 68 69 70 71 73 76 77 78 79 80 82 84 86 87 89 91 92 93 94 95 96 98 | 65 72 74 75 81 83 85 88 90 97 99 100 |	Pose number, Goldscore[b] H-bond π-charge Hydrophobic	1, 45.4 D192^{ECL2} K305$^{7.32}$, Y308$^{7.35}$ F194^{ECL2}, K305$^{7.32}$, Y308$^{7.35}$, I309$^{7.36}$
Histamine	| **1** 3 4 5 6 7 8 9 10 11 12 14 15 17 18 19 20 21 23 24 25 26 27 29 31 34 35 36 38 39 40 41 42 43 44 45 46 47 48 49 50 51 54 55 56 58 59 60 61 62 63 64 65 66 67 69 70 72 74 75 76 77 78 79 80 81 82 83 84 86 87 88 89 90 91 93 94 | 2 13 16 22 28 30 32 33 37 52 53 57 71 73 92 95 97 98 99 100 | 68 85 96 |	Pose number, Goldscore H-bond Charge Hydrophobic	1, 50.0 K305$^{7.32}$, Ile303^{ECL3}, F193^{ECL2§} D192^{ECL2} H296$^{6.58}$, K305$^{7.32}$, Y308$^{7.35}$

[a] Docking clusters, 100 poses generated from each docking run were clustered at heavy atoms root mean square deviation of 2Å. The highest scoring pose of the largest cluster is highlighted in bold.

[b] Goldscore, scoring function in GOLD which is a weighted sum of the intramolecular van der Waals forces, internal torsion of the ligand, van der Waals forces between the ligand and the receptor and H-bond interactions between the ligand and the receptor. Large number indicates favourable interactions.

[§] Ligand interacts with the carboxyl group of the residue.

Superscripts denote Ballesteros-Weinstein residue numbering.

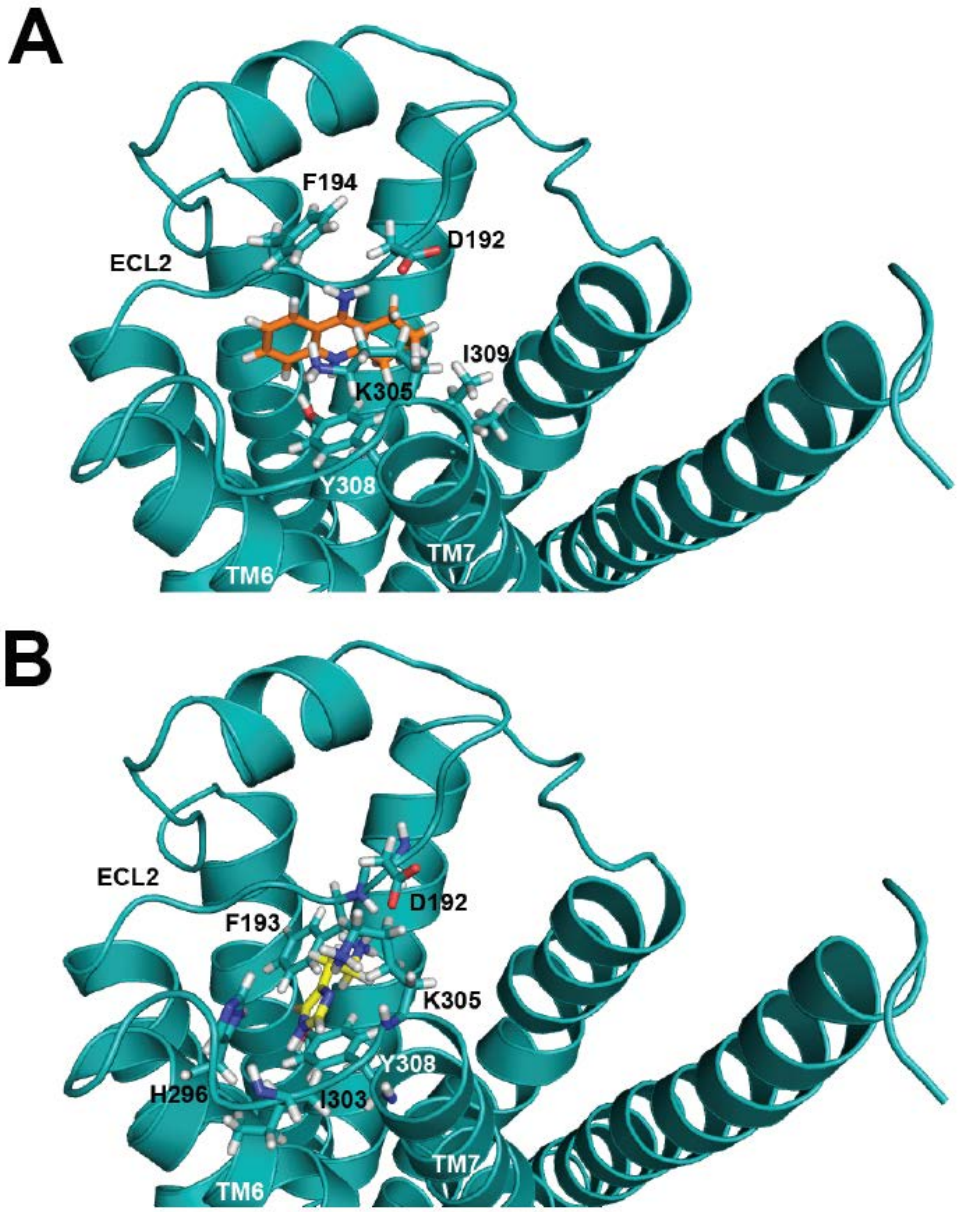

Figure 3.9 Docking of tacrine and histamine into an active state human β_2AR crystal structure

Docking tacrine and histamine into an active state crystal structure of the human β_2AR (PDB ID 3P0G). The human β_2AR is shown in teal. The side chains of the amino acids shown to interact with the ligands are shown as sticks. Tacrine and histamine are shown in a stick representation and coloured by elements with carbon atoms in orange for tacrine and yellow for histamine, oxygens in red, nitrogens in dark blue and hydrogens in white. The pose shown was the highest scoring pose of the largest cluster obtained from a docking run consisting of 100 poses.

unlike THRX100361, it did not interact with residues at the top of TM6. Histamine was also docked using this method. Despite the data in this study which do not support an allosteric mechanism of action for histamine at the β_2AR, it interacted with the same residues as both THRX100361 and tacrine. In the top scoring pose of the largest docking cluster, histamine interacted with D192^{ECL2}, F193^{ECL2}, H296$^{6.58}$, I303^{ECL3}, K305$^{7.32}$ and Y308$^{7.35}$ (Table 3.5**,** Figure 3.9).

Unlike THRX100361, no orthosteric interaction was observed for tacrine when the binding site was expanded to include the orthosteric site. For histamine, only 3 out of 100 poses contained orthosteric interactions when the binding site was not pre-defined. In these poses, histamine interacted with D113$^{3.32}$, N312$^{7.39}$ and Y316$^{7.43}$.

3.3.7 Docking of THRX100361, tacrine and histamine into an inactive state β_2AR crystal structure

Unlike THRX100361 and tacrine, histamine did not modulate the dissociation rate of [^{3}H]DHA (Table 3.1**,** Figure 3.3). However, docking into the active state crystal structure suggested that histamine bound to the same site as THRX100361 and tacrine, making similar interactions (Table 3.5**,** Figure 3.9). To further explore other possible binding modes, the docking of all three ligands was repeated using an inactive structure in the presence of the co-crystallised neutral antagonist alprenolol (PDB ID 3NYA). Docking of THRX100361, tacrine and histamine into the inactive state crystal structure more closely reflects the dissociation kinetics binding assays where the receptor is pre-equilibrated with a neutral antagonist [^{3}H]DHA prior to the addition of the allosteric modulators. In contrast to the

docking method used for the active state structure, the side chains of the D192^{ECL2}-K305$^{7.32}$ salt bridge were not set to flexible, as this salt bridge interaction has been shown in nuclear magnetic resonance (NMR) studies to be strongest in the inactive state (Bokoch *et al.*, 2010).

In the inactive structure, THRX100361 bound at the same region as seen in the docking with the active structure but made slightly different interactions within this site. In the highest scoring pose, the protonated nitrogen of the piperidine ring of THRX100361 interacted with D192^{ECL2}, while the amine interacted with F193^{ECL2}, the carbonyl group with Y308$^{7.35}$ and the phenyl rings with A200$^{5.39}$, H296$^{6.58}$ and Y308$^{7.35}$ (Table 3.6**,** Figure 3.10). Similarly, tacrine also docked in the same site as previously found with the active state crystal structure with slightly different interactions. Interestingly, docking of tacrine into the inactive state crystal structure only produced one cluster at 2 Å. Analysis of the highest scoring pose showed that tacrine interacted with F193^{ECL2}, A200$^{5.39}$, N293$^{6.55}$, H296$^{6.58}$ and Y308$^{7.35}$ (Table 3.6**,** Figure 3.10). Unlike THRX100361 and tacrine, histamine now docked at a completely distinct site compared to the active state β_2AR crystal structure. Analysis of the highest scoring pose showed that histamine bound to the ECL2 making interactions with T110$^{3.29}$, C106$^{3.25}$-C191^{ECL2}, C184^{ECL2}-C190^{ECL2} and Y185^{ECL2} (Figure 3.10**,** Table 3.6).

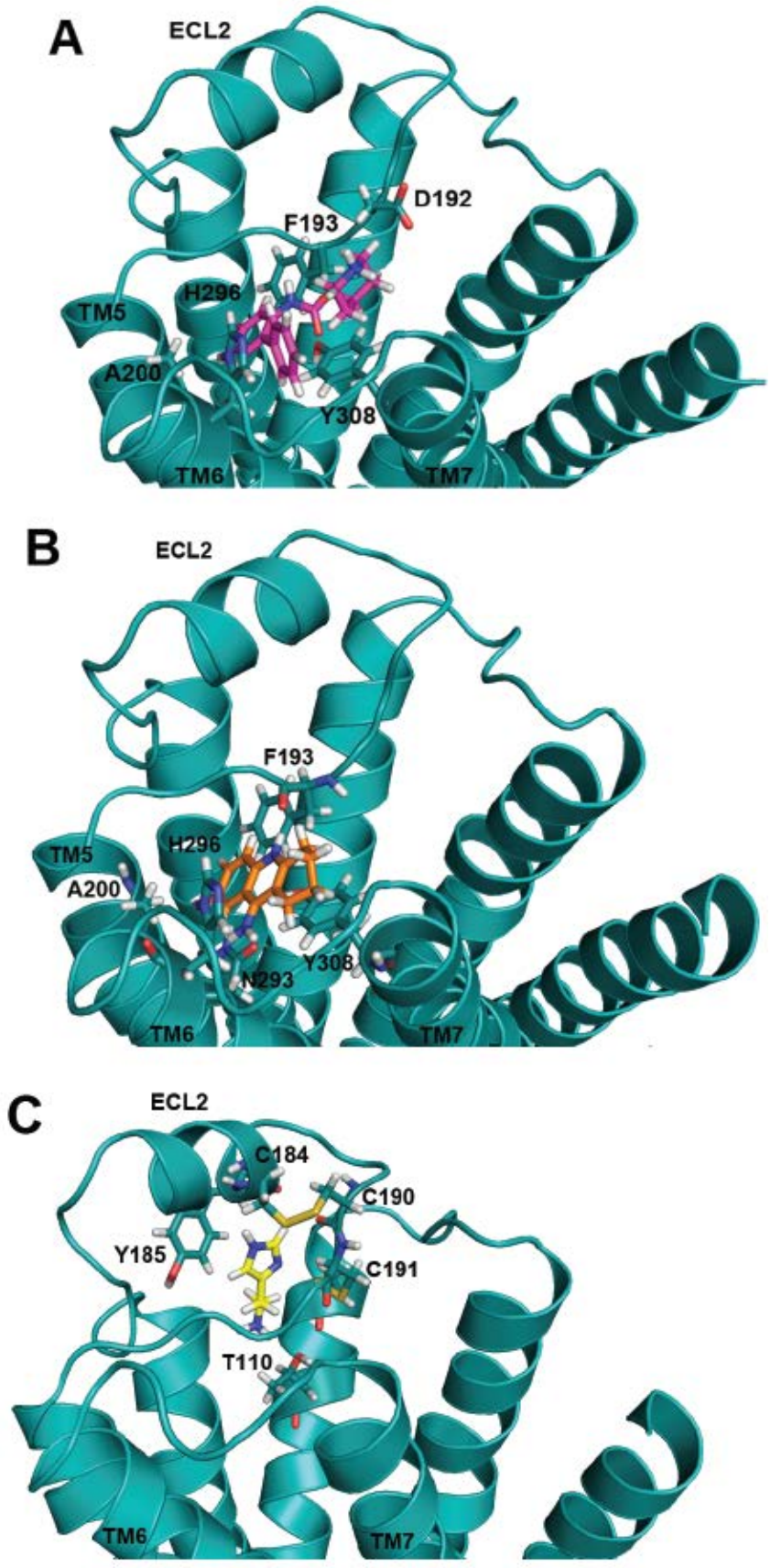
A
ECL2
D192
F193
H296
TM5
A200
Y308
TM6
TM7
B
ECL2
F193
TM5
H296
A200
Y308
N293
TM6
TM7
C
ECL2
C184
C190
Y185
C191
T110
TM6
TM7

Figure 3.10 Docking of allosteric modulators into an inactive state human β_2AR crystal structure

Docking of THRX100361 (A), tacrine (B) and histamine (C) into an inactive state human β_2AR (PDB ID 3NYA). The human β_2AR is shown in teal. Amino acids that were indicated in docking to interact with the ligands are shown as sticks coloured by elements with carbon atoms in teal, oxygens in red, nitrogens in dark blue and hydrogens in white. The pose shown was the highest scoring pose obtained from a docking run consisting of 100 poses. The co-crystallised ligand alprenolol was kept in the binding pocket during the docking but has not been shown in these figures to improve clarity.

Table 3.6 Docking of THRX100361, tacrine and histamine into an inactive human β_2AR crystal structure

Compound	Docking clusters[a]	Interactions	
THRX100631	| **1** 2 3 4 23 48 60 68 | 5 6 8 10 11 12 13 14 15 16 17 18 19 20 21 22 25 26 27 29 30 33 34 35 36 38 39 40 42 43 44 46 47 57 64 67 69 74 76 | 7 52 99 | 9 | 24 28 31 32 37 41 45 49 50 51 53 54 55 56 58 59 61 62 63 65 66 70 71 72 73 75 77 80 81 82 84 87 89 90 91 93 96 100 | 78 79 83 85 86 88 92 94 95 97 98 |	Pose number, Goldscore[b] H-bond Charge Hydrophobic	1, 55.0 F193^{ECL2}§ D192^{ECL2} A200$^{5.39}$, H296$^{6.58}$, Y308$^{7.35}$
Tacrine	| **1** 2 3 4 5 6 7 8 9 10 11 12 13 14 15 16 17 18 19 20 21 22 23 24 25 26 27 28 29 30 31 32 33 34 35 36 37 38 39 40 41 42 43 44 45 46 47 48 49 50 51 52 53 54 55 56 57 58 59 60 61 62 63 64 65 66 67 68 69 70 71 72 73 74 75 76 77 78 79 80 81 82 83 84 85 86 87 88 89 90 91 92 93 94 95 96 97 98 99 100 |	Pose number, Goldscore H-bond π-charge Hydrophobic	1, 47.6 F193^{ECL2}, N293$^{6.55}$ Y308$^{7.35}$ A200$^{5.39}$, H296$^{6.58}$, Y308$^{7.35}$
Histamine	| **1** 2 3 4 5 6 7 8 9 10 11 12 13 15 16 18 19 20 21 22 23 27 28 30 32 33 34 37 38 43 45 46 47 48 51 52 55 56 59 61 62 63 64 65 66 67 68 70 71 73 74 75 79 84 85 86 94 98 99 100 | 14 17 24 25 26 29 31 35 36 39 40 41 42 44 49 50 53 54 57 58 60 69 72 76 77 78 80 81 82 83 87 88 89 91 95 | 90 93 | 92 97 | 96 |	Pose number, Goldscore H-bond Hydrophobic Sulfur	1, 34.6 C184^{ECL2}, C190^{ECL2}, C191^{ECL2}, T110$^{3.29}$ C184^{ECL2}, Y185^{ECL2}, C191^{ECL2} C106$^{3.25}$-C191^{ECL2}, C184^{ECL2}-C190^{ECL2}

[a] Docking clusters, 100 poses generated from each docking run were clustered at root mean square deviation of 2Å. The highest scoring pose is highlighted in bold.

[b] Goldscore, scoring function in GOLD which is a weighted sum of the intramolecular van der Waals forces, internal torsion of the ligand, van der Waals forces between the ligand and the receptor and H-bond interactions between the ligand and the receptor. A positive number indicates favourable interactions.

§ Ligand interacts with the carboxyl group of the residue.

Superscripts denote Ballesteros-Weinstein residue numbering.

3.4 Discussion

Allosteric modulators offer potential therapeutic advantages over orthosteric ligands, such as maintenance of physiological rhythm of receptor signalling, increased safety profile and reduced off-target side effects (Christopoulos and Kenakin, 2002; Gregory *et al.*, 2010; Soudijn *et al.*, 2004). Research efforts focusing on the development of allosteric modulators as therapeutics have resulted in two clinically used allosteric modulators targeting GPCRs from two different families – cinacalcet acts on the calcium-sensing receptor (family C) and is used to treat hyperparathyroidism (Goodman *et al.*, 2000), while maraviroc acts on the C-C chemokine receptor type 5 (family A) and is used to treat AIDS/HIV (Fatkenheuer *et al.*, 2005). Many other allosteric modulators are currently in various stages of development and testing, with a large number of those compounds targeted towards the treatment of neurological and neurodegenerative disorders such as Parkinson's disease and schizophrenia (Salih *et al.*, 2015; Tison *et al.*, 2016).

The data presented in this study shows that THRX100361, an M_2/M_3 mAChR antagonist, can modulate the dissociation rate of orthosteric antagonist [^{3}H]DHA at the β_2AR. THRX100361 was a less potent modulator of [^{3}H]DHA dissociation in this study compared to the study by Steinfeld *et al*. (2011). In contrast to COS-1 cell membrane preparations used in binding assays in this study, Steinfeld *et al.* (2011) used whole HEK293 cells to exclude potential allosteric interactions with the intracellular allosteric residue $H269^{ICL3}$. This difference in experimental setup, while not expected to, appears to have contributed to the discrepancy in the potency of THRX100361 to modulate [^{3}H]DHA binding.

The bitopic parent compound THRX198321 is 5 fold more potent than BA alone in cAMP assays (Steinfeld *et al.*, 2011), in line with the effects observed on [^{3}H]DHA dissociation, suggesting that THRX100361 is a positive modulator of ligand binding. Contrary to these data, THRX100361 caused a 4 fold decrease in the potency of isoprenaline and a modest decrease of its maximum response in cAMP assays. These differential effects may be due to probe dependence. The structure of isoprenaline differs from the BA moiety of THRX198321 in that isoprenaline has a single phenol ring with two hydroxyl groups on one end and a bulky isopropyl group on the other end, which makes it one carbon longer than BA (Figure 3.1). In comparison, BA has a bulky dihydroquinolin-2-one on one end, which is a two ring system, and a less bulky methyl group on the other end (Figure 3.1). Isoprenaline was used in this study because it is a potent full agonist of the β_2AR which is known to bind in the orthosteric pocket of the receptor (Strader *et al.*, 1989b). Probe dependence is a common phenomenon of allosteric modulation whereby the direction and/or magnitude of the observed allosteric effects are dependent upon the orthosteric ligand present in the binding site. For example, benzyl quinolone carboxylic acid (BQCA) is an allosteric modulator of the M_1 mAChR which potentiates the modulatory effects of orthosteric agonists acetylcholine, carbachol and pilocarpine but not xanomeline (Canals *et al.*, 2012). An alternative explanation to negative effects observed with THRX100361 in the cAMP assay is that pre-incubation with THRX100361, providing that THRX100361 binds to an extracellular allosteric site, may block the access of isoprenaline into the orthosteric pocket of the receptor. This could be investigated by measuring the effect of simultaneous addition of THRX100361 and isoprenaline on cAMP production.

This study is the first to show that the β_2AR can also be modulated by tacrine. Although tacrine was more potent than THRX100361 in slowing [^{3}H]DHA dissociation, tacrine was as potent as THRX100361 in modulating isoprenaline-mediated cAMP production. In addition, tacrine was also a more potent modulator of [^{3}H]DHA dissociation compared to isoprenaline-mediated receptor activation. Both THRX100361 and tacrine produced similar allosteric effects at the β_2AR, suggesting that they bind to the same allosteric site. Supporting this, docking of THRX100361 and tacrine into the β_2AR crystal structures predicted that they interact at the same site, at the region between the ECL2 and TM6 and 7. In some docking poses, THRX100361 was also predicted to interact with the orthosteric residue D113$^{3.32}$ while also making interactions with residues on ECL2 and the top of TM7. However, these were not the top ranked poses, suggesting that the extracellular region of the β_2AR may accommodate THRX100361 better than the orthosteric pocket.

The allosteric site predicted for THRX100361 and tacrine at the β_2AR corresponds to the common allosteric site of the mAChRs, which is formed by residues from the ECL2 and the top of TM6 and 7 (Gnagey *et al.*, 1999; Huang *et al.*, 2005; Jager *et al.*, 2007; Kruse *et al.*, 2013; May *et al.*, 2007; Voigtländer *et al.*, 2003). These data suggest that the β_2AR may share the same allosteric site as the mAChRs. The docking of tacrine into a homology model of the α_{1A}AR suggested that it interacts with F86$^{2.64}$, I175^{ECL2}, F308$^{7.35}$ and F312$^{7.39}$ (Campbell, 2015). While F86$^{2.64}$ has been shown to mediate the allosteric effect of 9-aminoacridine, a compound highly analogous to tacrine, the involvement of I175^{ECL2}, F308$^{7.35}$ and F312$^{7.39}$ on allosteric modulation of the α_{1A}AR has not been investigated

(Campbell, 2015). As residues at the ECL2 and the top of TM7 have been shown to mediate the allosteric effects of many small molecule ligands at the mAChRs, including tacrine, their role in allosteric modulation of the α_1ARs and β_2AR should be investigated.

Although histamine has been reported to modulate isoprenaline-mediated cAMP production in DU145 and COS-7 cells through the β_2AR (Ramos-Jimenez *et al.*, 2007; Soriano-Ursua *et al.*, 2013), preliminary experiments in this study did not replicate these results. Unlike the studies by Ramos-Jimenez *et al*. (2007) and Soriano-Ursua *et al*. (2013), an increase in cAMP production can be detected when the cells were stimulated with histamine alone at a concentration equal to or greater than the EC_{50} of histamine for the histamine receptors. However, there is no evidence in the literature which suggests the presence of endogenous histamine receptors in CHO cells, suggesting that histamine may be an agonist of a $G_{\alpha s}$-coupled receptor in the CHO cells. The cAMP assay needs to be repeated in the presence of histamine receptor inhibitors to confirm the allosteric effects of histamine on β_2AR-mediated cAMP production. In this study, histamine has no effect on the dissociation of [^{3}H]DHA. While this was in line with the lack of effect in the functional assay, allosteric modulators have been shown to independently affect orthosteric ligand binding and receptor activation mediated by orthosteric ligands. For example, 7-hydroxyiminocyclopropan[b]-chromen-1a-carboxylic acid ethyl ester (CPCCOEt) is an allosteric modulator of the metabotropic glutamate receptor 1 which modulates glutamate signalling without affecting the binding of glutamate (Litschig *et al.*, 1999). However, results obtained from the docking of histamine into the inactive state β_2AR crystal structure suggest that histamine does

not modulate the dissociation of [^{3}H]DHA because it does not bind to the proposed allosteric binding site – the area surrounding the ECL2 and the top of TM6 and 7.

The β_2AR allosteric binding site predicted in this study has been proposed as a metastable binding site for orthosteric ligands (Dror *et al.*, 2011). Using molecular dynamics, Dror *et al*. (2011) suggested that orthosteric ligands such as alprenolol associate with the extracellular vestibule of the receptor, the area enclosed by ECL2-3 and TM5-7, prior to binding in the orthosteric site. A shared orthosteric/allosteric function for the extracellular region of the receptor has also been proposed for the mAChRs and the D_2 dopamine receptor (Kruse *et al.*, 2012; Thomas *et al.*, 2016). Molecular dynamics used to simulate orthosteric ligand binding at these receptors suggest that the allosteric binding sites of these receptors are located at the extracellular end of their orthosteric ligand binding trajectories and that orthosteric ligands bind transiently to these allosteric sites on the way into and out of the orthosteric pocket (Kruse *et al.*, 2012; Thomas *et al.*, 2016). Taken together, these data suggest that the extracellular region of the β_2AR may be important for both orthosteric and allosteric ligand interactions.

Receptor allosterism has been reported for other small molecule-binding family A GPCRs such as the dopamine receptors, the adenosine receptors and the α_1 adrenoceptors (Campbell, 2015; Gao *et al.*, 2001; Lane *et al.*, 2014). Allosteric binding sites within the transmembrane domain have been identified for the adenosine receptors (Gao *et al.*, 2003; Kourounakis *et al.*, 2001), suggesting that allosteric binding sites at family A GPCRs are not limited to the extracellular region. Unlike the β_2AR and the mAChRs, mutagenesis data suggest that the allosteric binding site of the D_2 dopamine receptor is located at the top of TM2

(Lane *et al.*, 2014), which is also shared by the α_{1A}AR (Campbell, 2015). Although residues from the ECL2 and the top of TM7 of the α_{1A}AR have been predicted in docking studies to interact with tacrine (Campbell, 2015), the contributions of these residues to the allosteric actions of tacrine have not been validated experimentally.

In summary, this study describes the presence of a potential extracellular allosteric binding site at the β_2AR which is solvent accessible and therefore amenable to modulation by synthetic ligands, such as tacrine and THRX100361. This proposed allosteric site is homologous to the well-characterised allosteric site at the mAChRs which may be shared with the α_{1A}AR, suggesting a conservation of allosteric mechanism amongst some members of family A GPCRs. In addition, this proposed allosteric site has also been implicated in computational studies as a metastable binding site for orthosteric ligands, suggesting the importance of the extracellular region of the β_2AR in both orthosteric and allosteric ligand interactions. Mutagenesis studies are needed to confirm the presence of this allosteric site and to investigate the role of these extracellular residues in orthosteric and allosteric ligand interactions.

CHAPTER 4

The role of the extracellular region of the β_2 adrenoceptor in orthosteric ligand binding kinetics

4.1 Introduction

The previous chapter of this thesis described a potential allosteric binding site located at the extracellular region of the β_2AR, which is comprised of residues from the ECL2 and TM6 and 7. This site was identified from the docking of allosteric modulators THRX100361 and tacrine into an active and inactive state β_2AR crystal structures. Interestingly, the same site has been proposed by several computational studies to form the initial transient binding site for orthosteric ligands (Dror *et al.*, 2011; Gonzalez *et al.*, 2011; Plazinska *et al.*, 2015; Wang and Duan, 2009).

Molecular dynamics studies suggest that β_2AR orthosteric ligands transit into and out of the orthosteric binding site along a recognition pathway that includes an intermediate binding site. For example, alprenolol binding at the β_2AR starts with the association of the ligand with hydrophobic amino acids such as F193^{ECL2}, A200$^{5.39}$, H296$^{6.58}$, V297$^{6.59}$ and Y308$^{7.35}$, which form a region on the receptor that has been termed the extracellular vestibule (Dror *et al.*, 2011). This event is followed by a conformational change of the receptor where F193^{ECL2} and Y308$^{7.35}$ separate to allow alprenolol to traverse a narrow pathway before making interactions in the orthosteric pocket, while the D192^{ECL2}-K305$^{7.32}$ salt bridge breaks and forms multiple times during the event (Dror *et al.*, 2011). Similarly,

ligand unbinding simulations suggest that orthosteric ligand dissociation from the β_2AR occurs via the same pathway and orthosteric ligands pause at the intermediate/meta binding site before escaping into the solvent (Gonzalez *et al.*, 2011; Plazinska *et al.*, 2015; Wang and Duan, 2009). Together, these computational studies suggest the mechanism for orthosteric ligand binding at the β_2AR is a multi-step process and that the region above the orthosteric site is instrumental in this process. The role of the residues lining the vestibule and the surrounding area in the kinetics of ligand binding at the β_2AR has not been characterised extensively.

The role of the β_2AR extracellular vestibule and the D192^{ECL2}-K305$^{7.32}$ salt bridge in orthosteric ligand interactions were investigated in this chapter using site-directed mutagenesis, radioligand binding assays and cAMP signalling assays. It was hypothesised that the extracellular vestibule of the β_2AR acts as an energy barrier for orthosteric ligand binding which controls the kinetics of orthosteric ligand binding.

4.2 Methods

4.2.1 Experimental protocols

The following mutations were introduced into WT human β_2AR: D192^{ECL2}A, D192^{ECL2}K/K305$^{7.32}$D, F193^{ECL2}A, F193^{ECL2}I, K505$^{7.32}$A, K305$^{7.32}$D, H296$^{6.58}$A and Y308$^{7.35}$A, using site-directed mutagenesis as described in section 2.2.3. The K305$^{7.32}$D cDNA was used as the template to generate the D192^{ECL2}K/K305$^{7.32}$D double mutant. The primers used to generate these mutant receptors are listed in Table 4.1. Attempts to generate the D192^{ECL2}K mutant were unsuccessful.

Receptor binding assays were performed using 1-5 μg of COS-1 cell membranes containing WT or mutant receptors as described in section 2.2.6. Briefly, binding assays were performed in 500 μL of 75 mM TRIS, pH 7.4 at room temperature. Saturation assays were performed by incubating membranes with 0.08 to 8 nM of [^{3}H]DHA for 1 hour. Competition assays were performed by incubating membranes with 0.5 nM of [^{3}H]DHA and increasing concentrations of competing ligand for 1 hour. Association kinetics assays were performed by adding 0.5 nM of [^{3}H]DHA to membranes and incubated for the duration indicated. Dissociation kinetics assays were performed by incubating membranes with 0.5 nM of [^{3}H]DHA for 1 hour, following which subsequent [^{3}H]DHA re-association was prevented using 10 μM of propranolol at various time points. Non-specific binding was measured in the presence of 10 μM of propranolol.

Isoprenaline-mediated receptor activation was investigated in WT and mutant human β_2AR using CHO cells stably expressing WT or mutant human β_2AR. The relative levels of receptor surface expression on the stable cells were measured

Table 4.1 Human β_2AR mutagenic primers

Mutant	Primers	
D192^{ECL2}A	F	AATGAGACCTGCTGTGCCTTCTTCACGAACCAAGCC
	R	CTTGGTTCGTGAAGAAGGCACAGCAGGTCTCATTGG
D192^{ECL2}K	F	GCCAATGAGACCTGCTGTAAGTTCTTCACGAACCAAGCC
	R	GGCTTGGTTCGTGAAGAACTTACAGCAGGTCTCATTGGC
K305$^{7.32}$A	F	CAGGATAACCTCATCCGTGCGGAAGTTTACATCCTCC
	R	GGAGGATGTAAACTTCCGCACGGATGAGGTTATCCTGG
K305$^{7.32}$D	F	GATCCAGGATAACCTCATCCGTGACGAAGTTTACATCCTCC
	R	GGAGGATGTAAACTTCGTCACGGATGAGGTTATCCTGG
D192^{ECL2}K/K305$^{7.32}$D	F	GCCAATGAGACCTGCTGTAAGTTCTTCACGAACCAAGCC
	R	GGCTTGGTTCGTGAAGAACTTACAGCAGGTCTCATTGGC
F193^{ECL2}A	F	GAGACCTGCTGTGACGCCTTCACGAACCAAGCC
	R	GGCTTGGTTCGTGAAGGCGTCACAGCAGGTCTC
F193^{ECL2}I	F	GAGACCTGCTGTGACATCTTCACGAACCAAGCC
	R	GGCTTGGTTCGTGAAGATGTCACAGCAGGTCTC
Y308$^{7.35}$A	F	CATCCGTAAGGAAGTTGCCATCCTCCTAAATTGGATAGGC
	R	CTATCCAATTTAGGAGGATGGCAACTTCCTTACGGATGAGG
H296$^{6.58}$A	F	CATCGTTAACATTGTGGCTGTGATCCAGGATAACCTCATCCG
	R	GTTATCCTGGATCACAGCCACAATGTTAACGATGAAGAAGGG

F, forward or sense primer.

R, reverse or antisense primer.

The nucleotides of the mutated residues are underlined.

using binding assays as described in section 2.2.6. Isoprenaline-mediated cAMP production was measured using a BRET-based cAMP assay as described in section 2.2.8.1. The BRET sensor CAMYEL was transiently transfected as described in 2.2.7.2. Briefly, the assays were carried out in 100 µL of HBSS, in the presence of 40 µM of the phosphodiesterase inhibitor IBMX, pH 7.4 at 37°C. cAMP production was measured as emission signals of RLuc and YFP, measured sequentially after a 10 min incubation with increasing concentrations of isoprenaline at 37°C, using the BRET1 filter set (475/25 and 535/30 nm).

4.2.2 Data analysis

Nonlinear regression analysis of saturation and competition binding data was performed for one-site binding using GraphPad Prism 6. The affinity of isoproterenol (pK_i) was calculated from the IC_{50} values and the dissociation constant (K_D) of the radioligand, where $K_i=IC_{50}/1+(L/K_D)$ (Cheng and Prusoff, 1973). Non-linear regression using one concentration of radioligand was used to determine the association rate constants for [^{3}H]DHA. The dissociation rate constants of [^{3}H]DHA were determined from non-linear regression using the single exponential decay function. Emission signals from the BRET assays were plotted as a ratio of emission at 475/535 nm such that an increase in the ratio correlates with an increase in intracellular cAMP, with data normalised to individual assay basal and forskolin values. Statistical analyses were performed using one-way ANOVA followed by the Dunnett's comparisons test. Statistical analyses of the kinetics binding data were performed on $\log_{10}$ transformed values to normalise the distribution of the data.

4.3 Results

To investigate the role of the residues identified in Chapter 3 to be involved in allosteric ligand binding and in molecular dynamics stimulation studies to contribute to the β_2AR binding/unbinding pathway (Dror *et al.*, 2011; Gonzalez *et al.*, 2011; Plazinska *et al.*, 2015; Wang and Duan, 2009), D192^{ECL2}, F193^{ECL2}, H296$^{6.58}$, K305$^{7.32}$ and Y308$^{7.35}$ were mutated. The position of these residues on the β_2AR is illustrated in Figure 4.1. There was no significant difference between the expression levels of the WT and the mutant β_2ARs in COS-1 cell membranes (B_{max} (pmol/mg): WT 4.6 ± 0.9, D192^{ECL2}A 7.5 ± 1.6, K305$^{7.32}$A 2.0 ± 0.2, K305$^{7.32}$D 3.5 ± 0.7, D192^{ECL2}K/K305$^{7.32}$D 3.6 ± 0.7, F193^{ECL2}A 1.5 ± 0.2, F193^{ECL2}I 6.0 ± 1.7, Y308$^{7.35}$A 13.2 ± 2.2, H296$^{6.58}$A 17.3 ± 6.9, mean ± SEM, n = 3 – 6, $P > 0.05$). The expression levels of the β_2AR in the stable cell clones used in this study are (sites/cell, min-max): WT 25350-37600, D192^{ECL2}A 12588-22312, K305$^{7.32}$A 2634-32540, K305$^{7.32}$D 4321-24162, D192^{ECL2}K/K305$^{7.32}$D 9832-11084, F193^{ECL2}A 16857-19541, F193^{ECL2}I 10919-25127, Y308$^{7.35}$A 15482-18721, H296$^{6.58}$A 6744-10767. Only the average expression level of the H296$^{6.58}$A mutant is significantly lower compared to WT (mean ± SEM, n = 2-5, $P < 0.05$).

4.3.1 The role of residues proposed to contribute to the binding vestibule in ligand binding kinetics and receptor activation

To examine the role of the hydrophobic residues suggested by molecular dynamics studies to interact with ligands during their transit into and out of the binding pocket (Dror *et al.*, 2011; Gonzalez *et al.*, 2011; Plazinska *et al.*, 2015; Wang and Duan, 2009), H296$^{6.58}$A, Y308$^{7.35}$A and F193^{ECL2}A mutant β_2ARs were

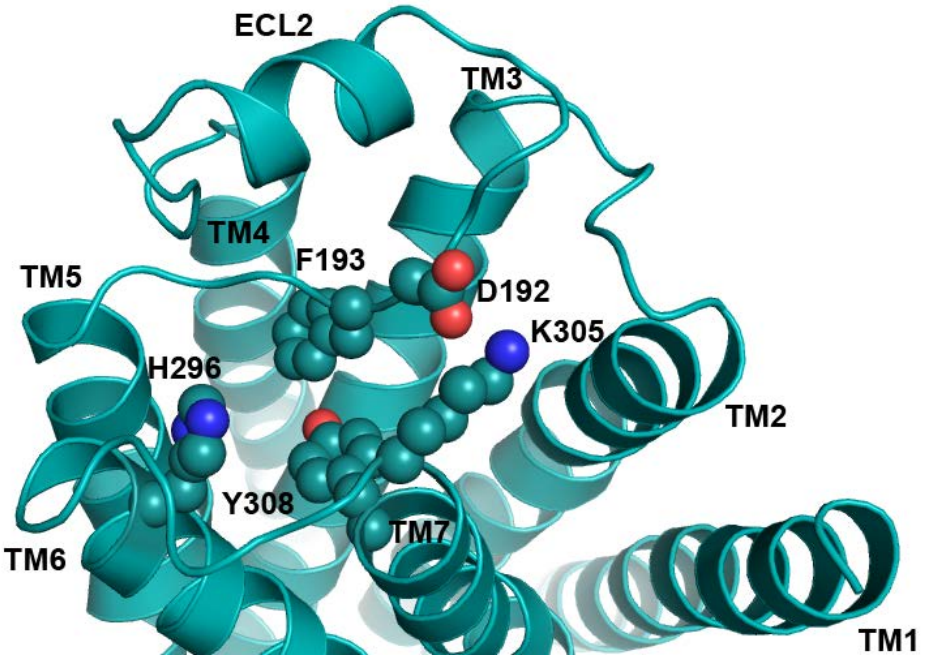

Figure 4.1 Structure of a neutral state β_2AR

The human β_2AR crystal structure crystallised in the presence of the neutral antagonist alprenolol (PDB ID 3NYA) is shown in teal. The extracellular residues F193^{ECL2}, H296$^{6.58}$, Y308$^{7.35}$ as well as D192^{ECL2} and K305$^{7.32}$ which form a salt bridge are shown as spheres with oxygen atoms coloured in red and nitrogen atoms coloured in blue. Alprenolol is removed from the binding pocket for clarity.

constructed. In addition, the F193^{ECL2}I mutant was also constructed to investigate the importance of an aromatic residue at this position in the binding kinetics of orthosteric ligands. Isoleucine was chosen for this substitution because in several crystal structures F193^{ECL2} is directed towards the orthosteric binding pocket and forms a hydrophobic interaction with bound ligands (Cherezov *et al.*, 2007; Ring *et al.*, 2013). As isoleucine is similar in length to phenylalanine and is also hydrophobic, this substitution should allow the residue to participate in this interaction.

The affinity (K_D) of the neutral antagonist [^{3}H]DHA was significantly decreased by approximately 5 fold at the F193^{ECL2}A, F193^{ECL2}I and Y308$^{7.35}$A mutants (P < 0.05) (Table 4.2). The association rate of [^{3}H]DHA for all of the mutations tested (F193^{ECL2}A, F193^{ECL2}I, Y308$^{7.35}$A and H296$^{6.58}$A) was not different to the WT receptor (P > 0.05) (Table 4.2, Figure 4.2). The mutation H296$^{6.58}$A did not significantly affect the affinity or the dissociation rate of [^{3}H]DHA (P > 0.05), while the mutations F193^{ECL2}A and Y308$^{7.35}$A increased the dissociation rate of [^{3}H]DHA from the receptor by 6 and 4 fold respectively (P < 0.05) (Table 4.2**,** Figure 4.2). In contrast to the alanine mutant, the F193^{ECL2}I mutant showed WT [^{3}H]DHA dissociation rate.

Similar to the effects observed with [^{3}H]DHA affinity, the mutations F193^{ECL2}A, F193^{ECL2}I and Y308$^{7.35}$A decreased the affinity of isoprenaline by 8-20 fold (P < 0.05), while the mutation H296$^{6.58}$A decreased the affinity of isoprenaline by 5 fold compared to the WT receptor (P = 0.07) (Table 4.3). Despite the observed decrease

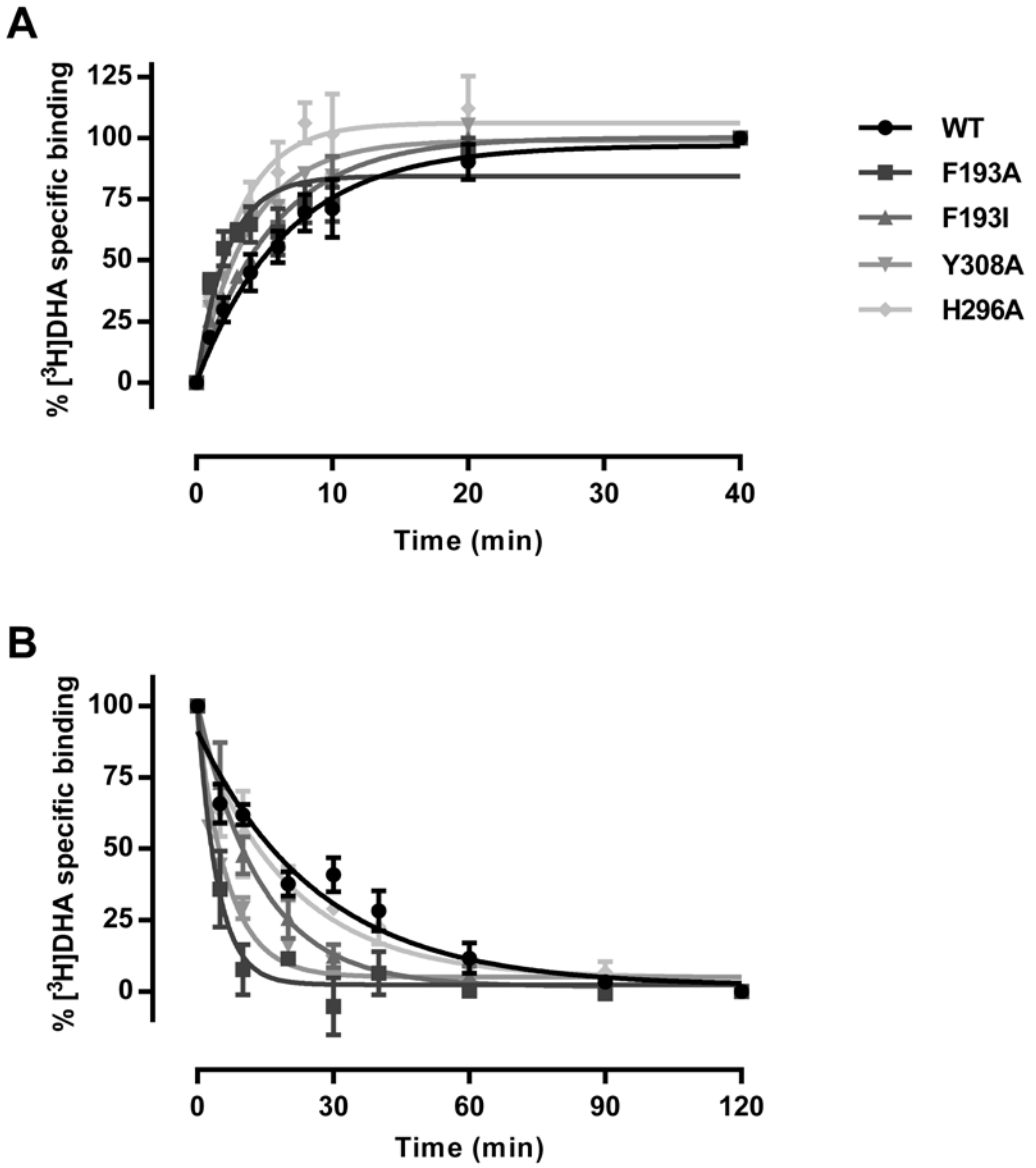

Figure 4.2 The effects of the vestibule mutations on [^{3}H]DHA binding kinetics
Association (A) and dissociation (B) of [^{3}H]DHA from WT and mutant β_2AR was determined using membrane preparations of COS-1 cells. Association was initiated by adding 0.5 nM of [^{3}H]DHA to membranes at room temperature. Dissociation assays were performed by pre-incubating membranes with 0.5 nM of [^{3}H]DHA for one hour at room temperature. Subsequent [^{3}H]DHA re-association was inhibited using 10 μM of propranolol in the absence or presence of test compounds at the concentrations shown. Data are presented as the mean ± SEM of 3-4 independent experiments performed in triplicate.

Table 4.2 The effects of the vestibule mutations on the affinity and binding kinetics of [^{3}H]DHA

Human β_2AR	K_D (nM)	n	Log_{10} K_{on}	K_{on} (x 10^8 M^{-1} min^{-1})	n	Log_{10} K_{off}	K_{off} (min^{-1})	n
WT	0.17 ± 0.02	3	8.32 ± 0.17	2.09	3	-1.42 ± 0.03	0.038	4
F193^{ECL2}A	0.76 ± 0.14*	3	8.39 ± 0.07	2.45	3	-0.64 ± 0.14*	0.229	3
F193^{ECL2}I	0.86 ± 0.04*	3	8.30 ± 0.03	2.00	3	-1.13 ± 0.09	0.074	3
Y308$^{7.35}$A	0.81 ± 0.17*	3	8.35 ± 0.10	2.24	3	-0.83 ± 0.04*	0.148	3
H296$^{6.58}$A	0.44 ± 0.07	3	8.70 ± 0.08	5.01	3	-1.22 ± 0.14	0.060	3

K_D, concentration of [^{3}H]DHA required to occupy 50% of total receptors, data fitted to a single binding site.
K_{on}, association rate of [^{3}H]DHA, data fitted to a non-linear regression using one concentration of radioligand.
K_{off}, dissociation rate of [^{3}H]DHA, data fitted to a non-linear regression using a single exponential decay function.
*$P < 0.05$ compared to WT by one-way ANOVA with Dunnett's multiple comparison test.
Data are presented as the mean ± SEM for n repeats, performed in duplicate or triplicate.

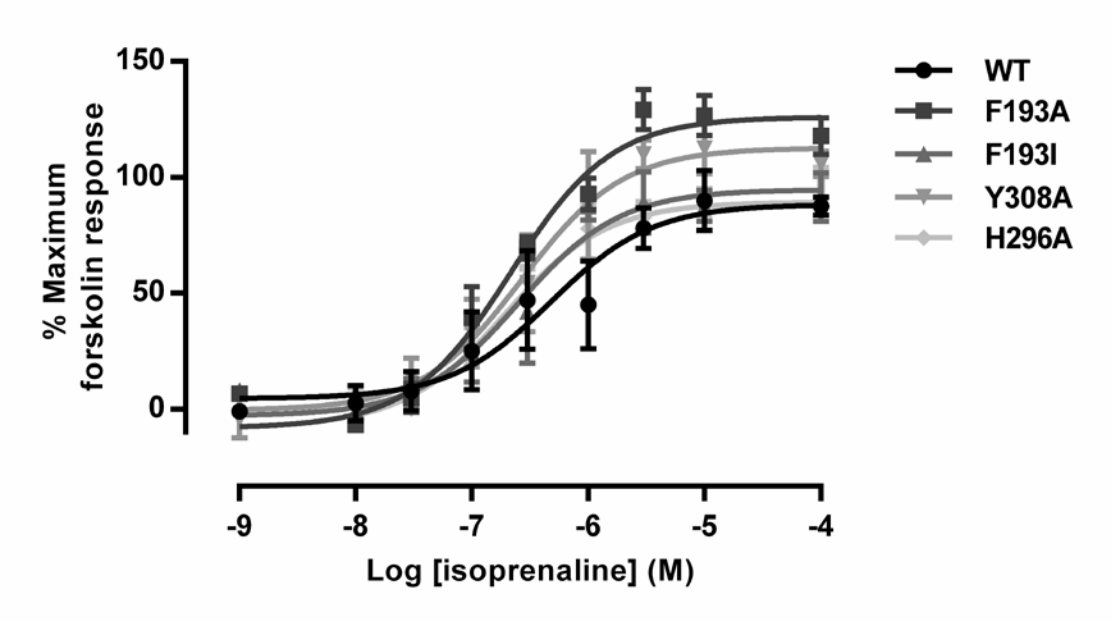

Figure 4.3 The effects of the vestibule mutations on isoprenaline-mediated receptor activation

Isoprenaline-mediated receptor activation on WT and mutant β_2AR was examined in stable CHO cells transiently transfected with the BRET cAMP sensor CAMYEL. cAMP production was measured after a 10 min incubation with increasing concentrations of isoprenaline in the presence of 40 μM of IBMX. Data are presented as the mean ± SEM of 4-5 independent experiments performed in triplicate.

Table 4.3 The effects of the vestibule mutations on the affinity and potency of isoprenaline

Human β_2AR	pK_i	K_i (nM)	n	pEC_{50}	EC_{50} (nM)	E_{max} (% forskolin)	n
WT	6.4 ± 0.1	398	3	6.5 ± 0.5	316	87.6 ± 3.9	4
F193^{ECL2}A	5.1 ± 0.1*	7943	3	6.7 ± 0.1	200	118.0 ± 7.8	3
F193^{ECL2}I	5.2 ± 0.4*	6310	3	6.6 ± 0.2	251	91.5 ± 10.5	4
Y308$^{7.35}$A	5.5 ± 0.1*	3162	3	6.7 ± 0.3	200	105.8 ± 5.4	5
H296$^{6.58}$A	5.7 ± 0.1 $^{P = 0.07}$	1995	3	7.1 ± 0.3	79	90.6 ± 13.0	4

pK_i, negative $\log_{10}$ of the inhibition constant K_i, the concentration of ligand required to occupy 50% of total receptors, calculated from IC_{50} values using the Cheng and Prusoff equation $K_i = IC_{50}/(1+([L]/K_D))$ where [L] is the concentration of the radioligand used and K_D is the dissociation rate constant of the radioligand.

EC_{50}, the concentration of isoprenaline resulting in 50% of the maximum cAMP production.

E_{max}, the maximum amount of cAMP produced from the highest concentration of isoprenaline, expressed as percentage maximum stimulation with 10 μM of forskolin.

*$P < 0.05$ compared to WT by one-way ANOVA with Dunnett's multiple comparison test.

Data are presented as the mean ± SEM for n independent experiments performed in duplicate or triplicate.

in affinity, the mutations F193^{ECL2}A, F193^{ECL2}I, Y308$^{7.35}$A and H296$^{6.58}$A did not significantly affect the potency or the maximum response of isoprenaline in cAMP production (P > 0.05) (Table 4.3**,** Figure 4.3).

4.3.2 The role of the D192^{ECL2}-K305$^{7.32}$ salt bridge in ligand binding kinetics and receptor activation

To examine the role of the D192^{ECL2}-K305$^{7.32}$ salt bridge in ligand binding and receptor activation, the side chains were either individually replaced with alanine (D192^{ECL2}A and K305$^{7.32}$A) or the positively charged lysine was replaced with a negatively charged aspartic acid (K305$^{7.32}$D). A reciprocal mutant that should recapitulate the salt bridge (D192^{ECL2}K/K305$^{7.32}$D) was also constructed.

The mutation of either D192^{ECL2} or K305$^{7.32}$ to alanine did not significantly alter the affinity of [^{3}H]DHA (P > 0.05) (Table 4.4). Additionally, the charge reversal produced with the K305$^{7.32}$D mutation also did not significantly alter the affinity of [^{3}H]DHA (P > 0.05) (Table 4.4). However, the affinity of [^{3}H]DHA was significantly decreased by 2.8 fold with the D192^{ECL2}K/K305$^{7.32}$D reciprocal mutant (P < 0.05) (Table 4.4). Similar to the vestibule mutations, none of the D192^{ECL2}-K305$^{7.32}$ salt bridge mutations affected the association rate of [^{3}H]DHA (P > 0.05) (Table 4.4, Figure 4.4). The K305$^{7.32}$D mutant produced the largest increase in the dissociation rate of [^{3}H]DHA from the receptor (2.8 fold, P < 0.05), followed by the K305$^{7.32}$A mutant (2.4 fold, P <0.05) (Table 4.4, Figure 4.4). In contrast, the D192^{ECL2}A mutant did not change the dissociation rate of [^{3}H]DHA (P > 0.05) (Table 4.4, Figure 4.4) and the reciprocal mutant D192^{ECL2}K/K305$^{7.32}$D had WT [^{3}H]DHA dissociation rate (Table 4.4, Figure 4.4)

Removal of one of the salt bridge interaction partners by the D192^{ECL2}A or the K305$^{7.32}$A mutation did not change the affinity of isoprenaline when compared to the WT receptor ($P > 0.05$) (Table 4.5). However, the mutation K305$^{7.32}$D led to a 5 fold decrease in isoprenaline affinity ($P < 0.05$, Table 4.5). The affinity for isoprenaline was also decreased by 10 fold in the D192^{ECL2}K/K305$^{7.32}$D reciprocal mutant ($P < 0.05$) (Table 4.5). Similar to the vestibule mutations, all of the mutations tested which disrupt the D192^{ECL2}-K305$^{7.32}$ salt bridge interaction have little effect on the potency and maximum response of isoprenaline in cAMP assays ($P > 0.05$) (Table 4.5, Figure 4.5).

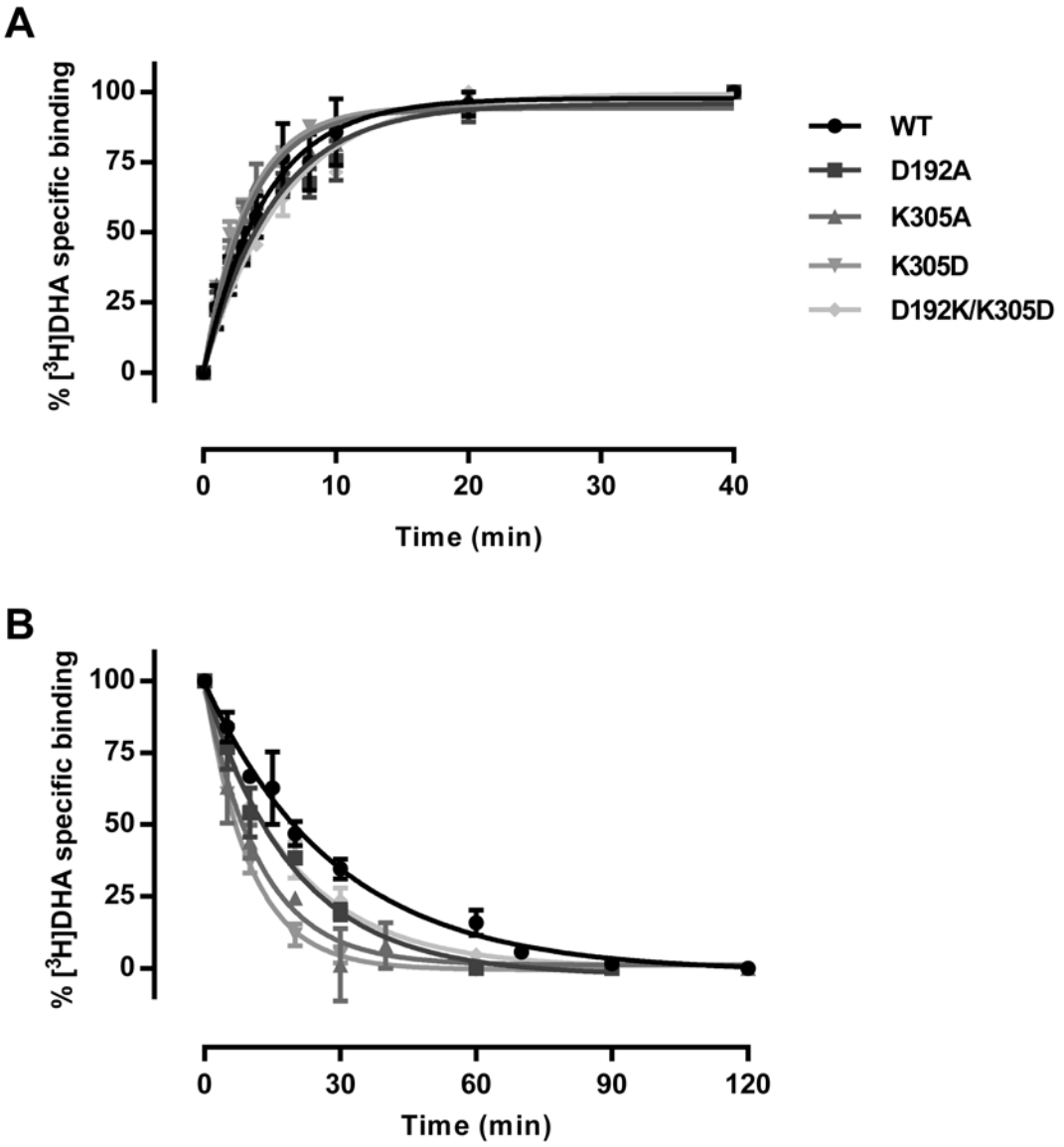

Figure 4.4 The effects of the D192^{ECL2}-K305$^{7.32}$ salt bridge mutations on [^{3}H]DHA binding kinetics

Association (A) and dissociation (B) of [^{3}H]DHA from WT and mutant β_2AR was determined using membrane preparations of COS-1 cells. Association was initiated by adding 0.5 nM of [^{3}H]DHA to membranes at room temperature. Dissociation assays were performed by pre-incubating membranes with 0.5 nM of [^{3}H]DHA for one hour at room temperature. Subsequent [^{3}H]DHA re-association was inhibited using 10 μM of propranolol in the absence or presence of test compounds at the concentrations shown. Data represent mean ± SEM of 3-4 independent experiments performed in triplicate.

Table 4.4 The effects of D192^{ECL2}-K305$^{7.32}$ salt bridge mutations on the affinity and binding kinetics of [^{3}H]DHA

Human β_2AR	K_D (nM)	n	Log K_{on}	K_{on} (x 10^8 M^{-1} min^{-1})	n	Log K_{off}	K_{off} (min^{-1})	n
WT	0.18 ± 0.02	3	8.51 ± 0.12	3.24	3	-1.45 ± 0.04	0.035	4
D192^{ECL2}A	0.38 ± 0.01	3	8.44 ± 0.11	2.75	3	-1.28 ± 0.04	0.052	3
K305$^{7.32}$A	0.27 ± 0.09	4	8.63 ± 0.13	4.27	3	-1.08 ± 0.06*	0.083	3
K305$^{7.32}$D	0.34 ± 0.02	3	8.63 ± 0.05	4.27	3	-1.01 ± 0.02*	0.098	3
D192^{ECL2}K/K305$^{7.32}$D	0.50 ± 0.08*	3	8.40 ± 0.06	2.51	3	-1.31 ± 0.08	0.049	3

K_D, concentration of [^{3}H]DHA required to occupy 50% of total receptors, data fitted to a single binding site.
K_{on}, association rate of [^{3}H]DHA, data fitted to a non-linear regression using one concentration of radioligand.
K_{off}, dissociation rate of [^{3}H]DHA, data fitted to a non-linear regression using a single exponential decay function.
*$P < 0.05$ compared to WT by one-way ANOVA with Dunnett's multiple comparison test.
Data are presented as the mean ± SEM for n repeats, performed in duplicate or triplicate.

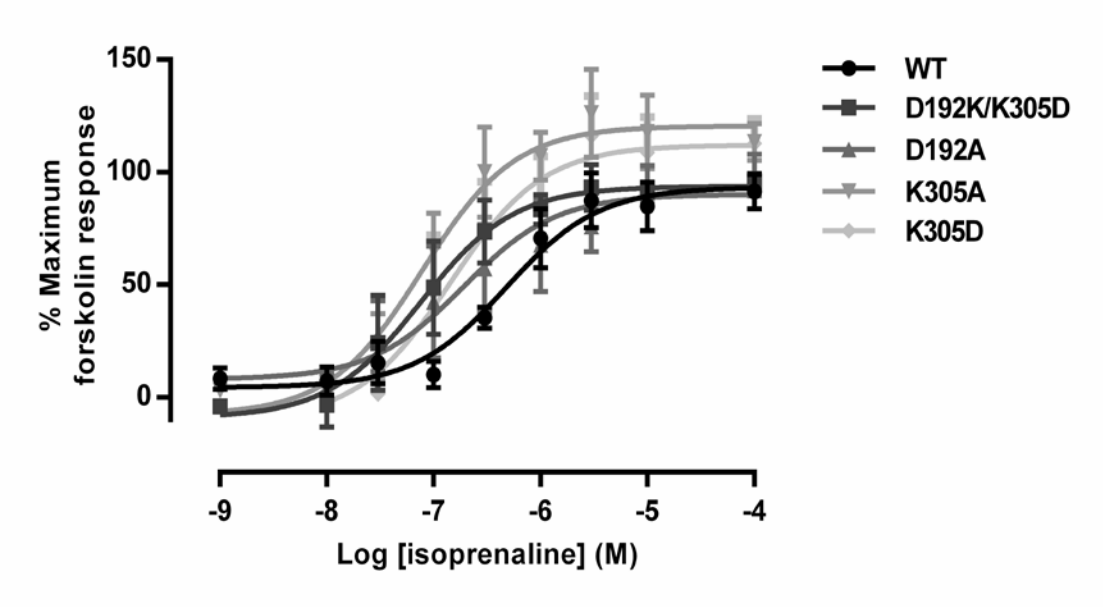

Figure 4.5 The effects of the D192^{ECL2}-K305$^{7.32}$ salt bridge mutations on isoprenaline-mediated receptor activation

Isoprenaline-mediated receptor activation on WT and mutant β_2AR was examined in stable CHO cells transiently transfected with the BRET cAMP sensor CAMYEL. cAMP production was measured after a 10 min incubation with increasing concentrations of isoprenaline in the presence of 40 μM of IBMX. Data are presented as the mean ± SEM of 4-5 independent experiments performed in triplicate.

Table 4.5 The effects of the D192^{ECL2}-K305$^{7.32}$ salt bridge mutations on the affinity and potency of isoprenaline

Human β_2AR	pK_i	K_i (nM)	n	pEC_{50}	EC_{50} (nM)	E_{max} (% forskolin)	n
WT	6.7 ± 0.1	200	3	6.3 ± 0.2	501	91.4 ± 7.7	4
D192^{ECL2}A	6.6 ± 0.1	251	3	6.6 ± 0.4	251	98.8 ± 9.3	4
K305$^{7.32}$A	6.2 ± 0.1	631	3	7.2 ± 0.2	63	113.4 ± 8.2	5
K305$^{7.32}$D	6.0 ± 0.1*	1000	3	7.0 ± 0.4	100	112.9 ± 10.8	4
D192^{ECL2}K/K305$^{7.32}$D	5.7 ± 0.2*	1995	3	7.2 ± 0.3	63	96.4 ± 3.6	4

pK_i, negative $\log_{10}$ of the inhibition constant K_i, the concentration of ligand required to occupy 50% of total receptors, calculated from IC_{50} values using the Cheng and Prusoff equation $K_i = IC_{50}/(1+([L]/K_D))$ where [L] is the concentration of the radioligand used and K_D is the dissociation rate constant of the radioligand.

EC_{50}, the concentration of isoprenaline resulting in 50% of the maximum cAMP production.

E_{max}, the maximum amount of cAMP produced from the highest concentration of isoprenaline, expressed as percentage maximum stimulation with 10 μM of forskolin.

*$P < 0.05$ compared to WT by one-way ANOVA with Dunnett's multiple comparison test.

Data are presented as the mean ± SEM for n independent experiments performed in duplicate or triplicate.

4.4 Discussion

Previous computational studies proposed a ligand binding mechanism at the β_2AR which involves a metastable binding site at the extracellular vestibule of the receptor (Dror *et al.*, 2011; Gonzalez *et al.*, 2011; Plazinska *et al.*, 2015; Wang and Duan, 2009). Simulations of ligand association suggested that ligand binding at the β_2AR starts with the interaction of the ligand with hydrophobic residues that form the vestibule, in particular F193^{ECL2}, A200$^{5.39}$, H296$^{6.58}$, V297$^{6.59}$ and Y308$^{7.35}$ (Dror *et al.*, 2011). The association of ligands at the extracellular vestibule has been suggested to increase the probability of orthosteric ligands to enter the orthosteric pocket due to a conformational change of the receptor where F193^{ECL2} and Y308$^{7.35}$ separate to allow the ligand to enter the orthosteric pocket (Dror *et al.*, 2011). During ligand binding in these simulations, the D192^{ECL2}-K305$^{7.32}$ salt bridge located next to F193^{ECL2} and Y308$^{7.35}$ was observed to break and form multiple times (Dror *et al.*, 2011). Similar to simulations of ligand association, simulations of ligand dissociation suggested that orthosteric antagonists preferentially leave the β_2AR via the same pathway (Gonzalez *et al.*, 2011; Plazinska *et al.*, 2015; Wang and Duan, 2009).

In this study, none of the vestibule or the D192^{ECL2}-K305$^{7.32}$ salt bridge mutants tested affected the association rate of orthosteric antagonist [^{3}H]DHA at the β_2AR. Dror *et al*. (2011) noted that although the transition of ligands from the extracellular vestibule to the orthosteric pocket is accompanied by the conformational change in which F193^{ECL2} and Y308$^{7.35}$ separate to allow the ligand to traverse down into the orthosteric pocket, this event does not appear to be rate-limiting because F193^{ECL2} and Y308$^{7.35}$ can be seen to remain separated on

occasions while ligands waited in the extracellular vestibule to enter the binding pocket. Therefore, the removal of their side chains may not affect the association rate of orthosteric ligands. An alternative explanation for the unchanged [^{3}H]DHA association rate observed with the mutants is that ligand entry may occur via one or more different pathway(s). Wang and Duan (2009) suggested that while ligand exit from the β_2AR occurs primarily through the opening formed by ECL2 and TM5-7, ligand entry may occur via the alternate opening formed by ECL2, TM2-3 and TM7. However, ligand association simulations were not performed in the study by Wang and Duan (2009). Instead, the idea that ligand entry occurs via the alternate pathway was inferred indirectly from the observation that ligand dissociation from a model of an apo-β_2AR structure occurs primarily via the alternate pathway (Wang and Duan, 2009).

Crystallography data suggest that activation of the β_2AR causes a conformational change of the receptor whereby F193^{ECL2} and Y308$^{7.35}$ move closer together to restrict the entry and exit of ligands from the orthosteric pocket of the receptor (Rasmussen *et al.*, 2011b). This observation is supported by mutagenesis data which showed that the mutation Y308$^{7.35}$A was able to decrease the ability of the $G_{\alpha s}$ mimetic nanobody Nb80 to retard the association rate of [^{3}H]DHA at the β_2AR (DeVree *et al.*, 2016). In their analysis of the active and inactive β_2AR crystal structures, DeVree *et al.* (2016) noted that the capping of the orthosteric binding pocket by F193^{ECL2} and Y308$^{7.35}$ is reinforced by K305$^{7.32}$, which redirects its interaction from D192^{ECL2} to the backbone oxygen of F193^{ECL2} following receptor activation. The ability of K305$^{7.32}$ to switch its interacting partner from D192^{ECL2} to

F193^{ECL2} is supported by an NMR study which showed that the D192^{ECL2}-K305$^{7.35}$ salt bridge interaction is weakened in active β_2ARs (Bokoch *et al.*, 2010).

While none of the vestibule or the D192^{ECL2}-K305$^{7.32}$ salt bridge mutants tested affected the association rate of [^{3}H]DHA, the F193^{ECL2}A, Y308$^{7.35}$A, K305$^{7.32}$A and K305$^{7.32}$D mutants all increased the rate of [^{3}H]DHA dissociation. These data suggest that the binding of [^{3}H]DHA may cause the same extracellular conformational changes as seen in the active structures of the β_2AR, where access to and from the orthosteric pocket is closed off by the relative movement of F193^{ECL2} and Y308$^{7.35}$ towards each other with a charge redistribution of K305$^{7.35}$ from D192^{ECL2} to the backbone carbonyl group of F193^{ECL2} stabilising the interaction between F193^{ECL2} and Y308$^{7.35}$. Therefore, removal of these side chains increased the dissociation rate of [^{3}H]DHA, but not its association rate. Although it can be argued that neutral antagonists such as DHA should not promote an active state, it has been shown that alprenolol is able to promote $G_{\alpha s}$ coupling to the β_2AR in the absence of free nucleotides (Yao *et al.*, 2009), which is the case in this study as crude membrane preparations were used in the binding assays. Alprenolol is an unsaturated analogue of DHA which has been shown to behave identically to DHA at the β_2AR in simulations studies (Dror et al., 2011), so it could be extrapolated that DHA will also promote $G_{\alpha s}$ binding resulting in an "active" structure.

The role of the residues on the extracellular vestibule in the kinetics of orthosteric ligand binding is demonstrated in this study. The idea that F193^{ECL2} and Y308$^{7.35}$ form a gate which closes upon ligand binding at the β_2AR is supported by the data which show that the dissociation rate of [^{3}H]DHA is affected to a similar extent in both the F193^{ECL2}A and Y308$^{7.35}$A mutants. The dissociation data

also provides evidence to support the role of K305$^{7.32}$ in maintaining the F193^{ECL2}-Y305$^{7.35}$ gate in a closed conformation, as both K305$^{7.32}$A and K305$^{7.32}$D, but not D192^{ECL2}A, increased the dissociation rate of [^{3}H]DHA. While the D192^{ECL2}-K305$^{7.32}$ salt bridge was observed to be exclusively broken during ligand exit in the simulations performed by Wang and Duan (2009), the data here indicate that the breakage of this salt bridge may not favour ligand dissociation, as the D192^{ECL2}A mutation has no effect on [^{3}H]DHA dissociation. However, the loss of D192^{ECL2} as an interacting partner of K305$^{7.32}$ may increase the interaction between K305$^{7.32}$ and F193^{ECL2}, compensating for the loss of the D192^{ECL2}-K305$^{7.32}$ salt bridge. The increase in the dissociation rate of [^{3}H]DHA caused by the K305$^{7.32}$A and K305$^{7.32}$D mutations is likely due to the loss of the interactions that reinforce the packing of the F193^{ECL2}-Y305$^{7.35}$ gate. While H296$^{6.58}$ was proposed to contribute to the formation of the hydrophobic extracellular vestibule and ligands were observed to make initial contact with H296$^{6.58}$ prior to entering the orthosteric binding pocket in molecular dynamics simulations (Dror *et al.*, 2011), the mutation of this residue has little effect on the association and dissociation rates of [^{3}H]DHA, suggesting that this residue provides little contribution to the control of ligand binding kinetics at the β_2AR.

In addition to increasing the dissociation rate of [^{3}H]DHA, the mutation F193^{ECL2}A also decreased its affinity, as would be expected if the dissociation rate was increased while the association rate remained unchanged. The affinity of isoprenaline was also decreased at the F193^{ECL2}A mutant. This could indicate that like [^{3}H]DHA, the dissociation but not the association rate of isoprenaline is increased at the β_2AR. In an alprenolol-bound β_2AR crystal structure, the side chain

of F193^{ECL2} can be seen to extend into the orthosteric pocket such that it is favourable for orthosteric ligand interactions (PDB ID 3NYA) (Wacker *et al.*, 2010). In addition, the side chain of F193^{ECL2} interacted with the inverse agonist carazolol in an inactive β_2AR crystal structure (PDB ID 2RH1) (Cherezov *et al.*, 2007). Therefore, the increase in the dissociation rate of [^{3}H]DHA and the decrease in the affinity of [^{3}H]DHA and isoprenaline at the F193^{ECL2}A mutant may be due to the loss of direct interactions. Unlike the F193^{ECL2}A mutant, the F193^{ECL2}I mutant showed WT [^{3}H]DHA association and dissociation rates, but has decreased affinity for both [^{3}H]DHA and isoprenaline. As affinity is a ratio of the dissociation and association rates of a ligand, the results obtained with the F193^{ECL2}I mutant was not expected and further investigation of this mutant is needed.

The affinity of [^{3}H]DHA and isoprenaline was also decreased at the D192^{ECL2}K/K305$^{7.32}$D reciprocal mutant which should recapitulate the salt bridge interaction, but not at the single mutants D192^{ECL2}A, K305$^{7.32}$A and K305$^{7.32}$D. This suggests that introducing a positively charged residue such as lysine at position 192 potentially changed the structure of the ECL2, affecting the ability of F193^{ECL2} to interact with [^{3}H]DHA and isoprenaline in the binding pocket and therefore reduced their affinity. The single mutant D192^{ECL2}K would be useful to test this hypothesis.

Similar to F193^{ECL2}A, Y308$^{7.35}$A also increased the dissociation rate of [^{3}H]DHA and decreased the affinity of both [^{3}H]DHA and isoprenaline. Analysis of the active and inactive β_2AR crystal structures (PDB ID 2RH1, 3NYA and 3P0G) suggests that unlike the side chain of F193^{ECL2} which extends into the orthosteric binding pocket, the side chain of Y308$^{7.35}$ extends sideways which could potentially create a

physical barrier to ligand dissociation. In addition, a crystal structure of isoprenaline-bound β_1AR showed that isoprenaline binds in the orthosteric pocket and does not interact with ECL2 residues nor the residue analogous to Y308$^{7.35}$, F325$^{7.35}$ (Warne *et al.*, 2011). Therefore, the decrease in the affinity of isoprenaline observed with the Y308$^{7.35}$A mutant could potentially be due to the loss of impedance to ligand dissociation.

In this study, mutations of F193^{ECL2}, H296$^{6.58}$, Y308$^{7.35}$ and the D192^{ECL2}-K305$^{7.32}$ salt bridge have little effect on the potency and the maximum response of isoprenaline. This is in agreement with a previous study which showed that mutations of extracellular residues H296$^{6.58}$A, K305$^{7.32}$A, K305$^{7.32}$D, Y308$^{7.35}$F and H296$^{6.58}$K-K305$^{7.32}$D have little effect on the overall efficacy of the agonist salmeterol (Baker, 2005).

A metastable binding site located at the trajectory of orthosteric binding pathway has been reported not only for family A GPCRs such as the M_2 and M_3 muscarinic acetylcholine receptors (mAChRs), D_2 and D_3 dopamine receptors and adenosine A_{2A} receptor, but also for family F GPCRs such as the bitter taste receptor (Guo *et al.*, 2016; Kruse *et al.*, 2012; Sabbadin *et al.*, 2015; Sandal *et al.*, 2015; Thomas *et al.*, 2016). The metastable binding sites that have been predicted for family A GPCRs vary in the location, suggesting that ligand entry and exit from these receptors may occur via distinct pathways. For example, like the β_2AR, the metastable binding sites for the M_2 and M_3 mAChRs have been proposed to be formed by residues from the ECL2 and the top of TM6 and 7 (Kruse *et al.*, 2012), while the metastable binding site for the adenosine A_{2A} receptor includes residues from the ECL2 and TM2, 6 and 7 (Guo *et al.*, 2016; Sabbadin *et al.*, 2015) and the

metastable binding site for the D_2 and D_3 dopamine receptors is formed by residues from the ECL2 and TM2 and 7 (Thomas *et al.*, 2016). However, a common observation is that the vestibules of these receptors form a lid-like structure over the orthosteric binding pocket which restricts ligand exit from the receptor.

The metastable binding site of family A GPCRs is important not only for the binding of orthosteric ligands, but also for allosteric interactions. A potent allosteric modulator of the M_2 mAChR, LY2119620, has been shown to bind to a site identified as the metastable binding site for orthosteric ligands of the receptor (Kruse *et al.*, 2012; Kruse *et al.*, 2013; Redka *et al.*, 2008). This observation provides a structural rationale for the changes in the kinetics of orthosteric ligands in the presence of allosteric modulators. Allosteric ligands which stabilise the vestibule in a closed conformation will retard orthosteric ligand dissociation, whereas allosteric ligands which stabilise the vestibule in an open conformation will increase ligand dissociation.

This study describes the contribution of extracellular residues in orthosteric ligand binding and activation of the β_2AR. The data in this study provide pharmacological evidence to support the existence of a metastable binding site at the β_2AR which is located at the extracellular end of orthosteric ligand binding trajectory of the β_2AR.

CHAPTER 5

Characterisation of the extracellular allosteric binding site of the β_2 adrenoceptors

5.1 Introduction

Many allosteric modulators of α branch family A GPCRs bind to the extracellular domain of the receptors. For example, allosteric modulators of the mAChRs bind to the ECL2 and the top of TM6 and 7 (Gnagey *et al.*, 1999; Huang *et al.*, 2005; Jager *et al.*, 2007; Kruse *et al.*, 2013; May *et al.*, 2007; Voigtländer *et al.*, 2003), while allosteric modulators of the α_{1A}AR and the D_2 dopamine receptor interact with residues located at the top of TM2 (Campbell, 2015; Lane *et al.*, 2014). These data suggest that an extracellular allosteric binding site may also exist for the closely related β_2AR. Docking of allosteric modulators THRX100361 and tacrine into β_2AR crystal structures supported this idea, as an allosteric binding site which is formed by residues from ECL2 and 3 and the top of TM6 and 7, including D192^{ECL2}, F193^{ECL2}, F194^{ECL2}, T195^{ECL2}, A200$^{5.39}$, N293$^{6.55}$, H296$^{6.58}$, I303^{ECL3}, K305$^{7.32}$, Y308$^{7.35}$ and I309$^{7.36}$, has been predicted in Chapter 3.

Molecular dynamics studies suggest that the allosteric binding site of the M_2 mAChR and the D_2 dopamine receptor is located on the extracellular end of their orthosteric ligand binding pathway (Kruse *et al.*, 2012; Thomas *et al.*, 2016). In Chapter 4, it was shown that extracellular residues F193^{ECL2}, Y308$^{7.35}$ and K305$^{7.32}$ play a role in the binding kinetics of β_2AR orthosteric ligands. In addition, molecular dynamics studies have proposed that β_2AR orthosteric ligand entry and

exit at occurs from the opening between ECL2 and TM5-7 through the extracellular vestibule. Taken together, these data suggest that like the M_2 mAChR and the D_2 dopamine receptor, the extracellular vestibule of the β_2AR is also important for both orthosteric and allosteric ligand interactions.

In this chapter, the proposed allosteric binding site of THRX100361 and tacrine at the β_2AR was characterised using the mutant receptors previously shown in Chapter 4 to play a role in the binding kinetics of orthosteric ligands. It was hypothesised that allosteric modulators THRX100361 and tacrine bind to the extracellular vestibule of the β_2AR.

5.2 Methods

5.2.1 Experimental protocols

In addition to F193^{ECL2}A, K305$^{7.32}$A, Y308$^{7.35}$A and H296$^{6.58}$A generated and characterised in Chapter 4, the double and triple mutants H296$^{6.58}$A/K305$^{7.32}$A, K305$^{7.32}$A/Y308$^{7.35}$A and H296$^{6.58}$A/K305$^{7.32}$A/Y308$^{7.35}$A were also generated using the primers listed in Table 5.1. The same primers but different templates were used for the K305$^{7.32}$A/Y308$^{7.35}$A and H296$^{6.58}$A/K305$^{7.32}$A/Y308$^{7.35}$A mutants.

The affinity of isoprenaline, THRX100361 and tacrine at WT and mutant human β_2ARs and their effects on [^{3}H]DHA dissociation were investigated using equilibrium competition and kinetics dissociation binding assays performed with COS-1 cell membranes as described in section 2.2.6. Binding assays were performed in a total volume of 500 µL of 75 mM TRIS, pH 7.4 at room temperature. In competition assays, membranes were incubated with increasing concentrations of the proposed modulators and 0.5 nM of [^{3}H]DHA for 1 hour. In kinetics dissociation assays, membranes were equilibrated with 0.5 nM of [^{3}H]DHA for 1 hour and re-association of [^{3}H]DHA was prevented using 10 µM of propranolol. Non-specific binding was determined using 10 µM of propranolol.

The effects of the proposed allosteric modulators on receptor activation were investigated using a BRET-based cAMP assay as described in section 2.2.8.1. The BRET sensor CAMYEL was transiently transfected into the CHO cells stably expressing WT or mutant human β_2ARs as described in 2.2.7.1. On the day of the assay, cells were incubated with the allosteric modulators for 30 min prior to

Table 5.1 Human β_2AR mutagenic primers

β_2AR mutants	Template cDNA	Primers	
H296$^{6.58}$A/K305$^{7.32}$A	K305$^{7.32}$A	F	CATCGTTAACATTGTGGCTGTGATCCAGGATAACCTCATCCG
		R	GTTATCCTGGATCACAGCCACAATGTTAACGATGAAGAAGGG
K305$^{7.32}$A/Y308$^{7.35}$A	K305$^{7.32}$A	F	CGTGCGGAAGTTGCCATCCTCCTAAATTGGATAGG
		R	CCTATCCAATTTAGGAGGATGGCAACTTCCGCACG
H296$^{6.58}$A/K305$^{7.32}$A/Y308$^{7.35}$A	H296$^{6.58}$A/K305$^{7.32}$A	F	CGTGCGGAAGTTGCCATCCTCCTAAATTGGATAGG
		R	CCTATCCAATTTAGGAGGATGGCAACTTCCGCACG

F, forward or sense primer.

R, reverse or antisense primer.

The nucleotides of the mutated residues are underlined.

stimulation with increasing concentrations of isoprenaline to initiate cAMP production. The assays were carried out in 100 µL of HBSS, in the presence of 40 µM of IBMX at pH 7.4 and 37°C. Emission signals of RLuc and YFP were measured sequentially after a 15 min incubation with isoprenaline at 37°C, using the BRET1 filter set (475/25 and 535/30 nm).

5.2.2 Data analysis

GraphPad Prism 6 was used to plot and analyse the binding and functional data. Competition binding data were fit to one-site fit K_i equation and dissociation binding data were fit to a one-site exponential decay. Isoprenaline concentration response curves were fitted to the log (agonist) vs. response (three parameters) equation. Statistical analyses were performed using one-way ANOVA followed by the Dunnett's multiple comparisons test. Statistical analyses of the pEC_{50} ratio data were performed using one-sample t-tests which compare the values to the ratio of the control, which has a value of 0.The kinetics binding data were transformed into $\log_{10}$ values to normalise the distribution of the data.

5.3 Results

Docking of THRX100361 and tacrine into the active and inactive state human β_2AR crystal structures suggested that an allosteric binding pocket existed within the vestibule of the receptor, which included residues from the ECL2 and the top of TM6 and 7 (Chapter 3). As allosteric modulators of the M_2 mAChR and the D_2 dopamine receptor have been suggested to bind to the extracellular end of their orthosteric binding pathway (Campbell, 2015; Kruse *et al.*, 2012; Kruse *et al.*, 2013) and that F193^{ECL2}, Y308$^{7.35}$ and K305$^{7.32}$ formed the gate for orthosteric ligand exit at the β_2AR (Chapter 4), the involvement of these residues in the modulatory effects of THRX100361 and tacrine at the β_2AR was investigated. The role of H296$^{6.58}$ in mediating the allosteric effects of THRX100361 and tacrine was also investigated as it has been suggested by docking to interact with these modulators (Chapter 3). Double and triple mutants H296$^{6.58}$A/K305$^{7.32}$A, K305$^{7.32}$A/Y308$^{7.35}$A and H296$^{6.58}$A/K305$^{7.32}$A/Y308$^{7.35}$A were also constructed to further characterise the allosteric binding site of THRX100361 and tacrine.

5.3.1 Equilibrium binding assays

As a control, competition binding assays were performed to investigate the contribution of the mutated residues on the affinity of orthosteric agonist isoprenaline. As shown in Chapter 4, the mutations F193^{ECL2}A and Y308$^{7.35}$A decreased the affinity of isoprenaline by 21 and 23 fold respectively, whereas H296$^{6.58}$A, K305$^{7.32}$A/Y308$^{7.35}$A and H296$^{6.58}$A/K305$^{7.32}$A/Y308$^{7.35}$A decreased the affinity of isoprenaline by 2 to 3 fold ($P < 0.05$) (Table 5.2). The mutation K305$^{7.32}$A did not change the affinity of isoprenaline ($P > 0.05$) (Table 5.2). The double

mutant H296$^{6.58}$A/K305$^{7.32}$A showed WT isoprenaline affinity despite the decrease in affinity seen with the H296$^{6.58}$A mutant.

Competition binding assays were also performed to investigate the effects of the mutations on the apparent affinity of THRX100361 and tacrine. The mutation H296$^{6.58}$A significantly decreased the apparent affinity of THRX100361 by 5 fold, whereas the double mutant K305$^{7.32}$A/Y308$^{7.35}$A increased the apparent affinity of THRX100361 by 6 fold (P < 0.05) (Table 5.2). Unlike THRX100361, all of the mutations tested significantly decreased the apparent affinity of tacrine. The mutations K305$^{7.32}$A, Y308$^{7.35}$A, H296$^{6.58}$A and H296$^{6.58}$A/K305$^{7.32}$A/Y308$^{7.35}$A decreased the affinity of tacrine by approximately 3 fold while F193^{ECL2}A decreased the affinity of tacrine by 5 fold (P < 0.05) (Table 5.2).

5.3.2 Kinetics dissociation binding assays

Previous docking of THRX100361 into an active state β_2AR crystal structure suggested that THRX100361 interacted with N293$^{6.55}$, H296$^{6.58}$, I303^{ECL3}, K305$^{7.32}$ and Y308$^{7.35}$ (Table 3.4**,** Figure 3.8), whereas docking into an inactive structure suggested interactions with T195^{ECL2}, F194^{ECL2}, N293$^{6.55}$, K305$^{7.32}$ and Y308$^{7.35}$ (Table 3.6**,** Figure 3.10). Kinetics dissociation binding assays were performed to investigate the effects of the proposed allosteric site mutations on the ability of THRX100361 to modulate [^{3}H]DHA dissociation. The assays were performed using 1 mM of THRX100361 because it is a poor modulator which only slowed the dissociation rate of [^{3}H]DHA at this concentration (Table 3.1**,** Figure 3.3). The limited solubility of THRX100361 prevented testing at higher concentrations.

Table 5.2 The effects of allosteric site mutations on ligand binding at equilibrium

Human β_2AR	Isoprenaline			THRX100361			Tacrine		
	pK_i	K_i (μM)	n	pK_i	K_i (μM)	n	pK_i	K_i (μM)	n
WT	6.5 ± 0.1	0.3	3	†4.2 ± 0.1	63.1	3	4.8 ± 0.1	20.0	3
F193^{ECL2}A	5.2 ± 0.1*	6.3	3	†4.3 ± 0.1	50.1	3	4.0 ± 0.1*	100.0	3
K305$^{7.32}$A	6.3 ± 0.1	0.5	3	†4.2 ± 0.2	63.1	3	4.3 ± 0.1*	50.1	4
Y308$^{7.35}$A	5.6 ± 0.1*	6.9	3	††3.9 ± 0.2	125.9	3	4.2 ± 0.1*	63.1	4
H296$^{6.58}$A	6.1 ± 0.1*	0.8	3	††3.5 ± 0.1*	316.2	4	4.2 ± 0.1*	63.1	4
H296$^{6.58}$A/K305$^{7.32}$A	6.3 ± 0.1	0.5	3	4.5 ± 0.2	39.8	3	ND		
K305$^{7.32}$A/Y308$^{7.35}$A	6.1 ± 0.1*	0.8	3	4.8 ± 0.1*	10.0	3	ND		
H296$^{6.58}$A/K305$^{7.32}$A/Y308$^{7.35}$A	6.2 ± 0.1*	0.6	3	4.6 ± 0.2	25.1	3	4.3 ± 0.1*	50.1	3

pK_i, $-\log_{10} K_i$.

K_i, calculated inhibitory constant or the concentration of ligand required to occupy 50% of receptors. K_i values were calculated from observed IC_{50} values using the Cheng and Prusoff equation $K_i = IC_{50}/(1+([L]/K_D))$ where [L] is the concentration of the radioligand used and K_D is the dissociation rate constant of the radioligand.

ND, not determined.

* $P < 0.05$ compared to control by one-way ANOVA with Dunnett's multiple comparison test.

Data are presented as the mean ± SEM of independent experiments performed in duplicate.

† Data have previously been presented in Leonar (2011).

†† Data generated in part by Mr Tony Ngo.

As shown previously, in the absence of the modulators, the mutations F193^{ECL2}A, K305$^{7.32}$A and Y308$^{7.35}$A significantly increased the dissociation rate of [^{3}H]DHA from the β_2AR (Table 4.2**,** Table 4.4). The mutation K305$^{7.32}$A did not affect the ability of THRX100361 to modulate [^{3}H]DHA dissociation ($P > 0.05$) (Table 5.3**,** Figure 5.1). The mutations H296$^{6.58}$A and Y308$^{7.35}$A, however, decreased the ability of THRX100361 to modulate [^{3}H]DHA dissociation by 1.6 and 1.8 fold respectively ($P < 0.05$) (Table 5.3**,** Figure 5.1).

In the absence of the modulators, the double mutant H296$^{6.58}$A/K305$^{7.32}$A increased the dissociation rate of [^{3}H]DHA by 3 fold, while the double and triple mutants K305$^{7.32}$A/Y308$^{7.35}$A and H296$^{6.58}$A/K305$^{7.32}$A/Y308$^{7.35}$A increased the dissociation rate of [^{3}H]DHA by 5.5 and 6.5 fold respectively when compared to WT receptor ($P < 0.05$) (Log_{10} K_{off} WT = -1.44 ± 0.02, H296$^{6.58}$A/K305$^{7.32}$A = -0.98 ± 0.07, K305$^{7.32}$A/Y308$^{7.35}$A = -0.73 ± 0.10, H296$^{6.58}$A/K305$^{7.32}$A/Y308$^{7.35}$A = -0.66 ± 0.11, mean ± SEM, n = 3-5). Interestingly, the double mutant H296$^{6.58}$A/K305$^{7.32}$A did not change the ability of THRX100361 to modulate [^{3}H]DHA dissociation when compared to WT receptor, suggesting that K305$^{7.32}$A counteracted the effect of H296$^{6.58}$A. However, K305$^{7.32}$A was unable to counteract the effect of Y308$^{7.35}$A as the double mutant K305$^{7.32}$A/Y308$^{7.35}$A also decreased the ability of THRX100361 to modulate [^{3}H]DHA dissociation by 1.5 fold when compared to the WT receptor ($P < 0.05$) (Table 5.3**,** Figure 5.1). Similarly, the ability of THRX100361 to modulate [^{3}H]DHA dissociation was decreased by 1.7 fold at the H296$^{6.58}$A/K305$^{7.32}$A/Y308$^{7.35}$A triple mutant ($P < 0.05$) (Table 5.3**,** Figure 5.1). Although docking did not suggest an interaction between F193^{ECL2} and THRX100361, the mutation F193^{ECL2}A significantly decreased the ability of

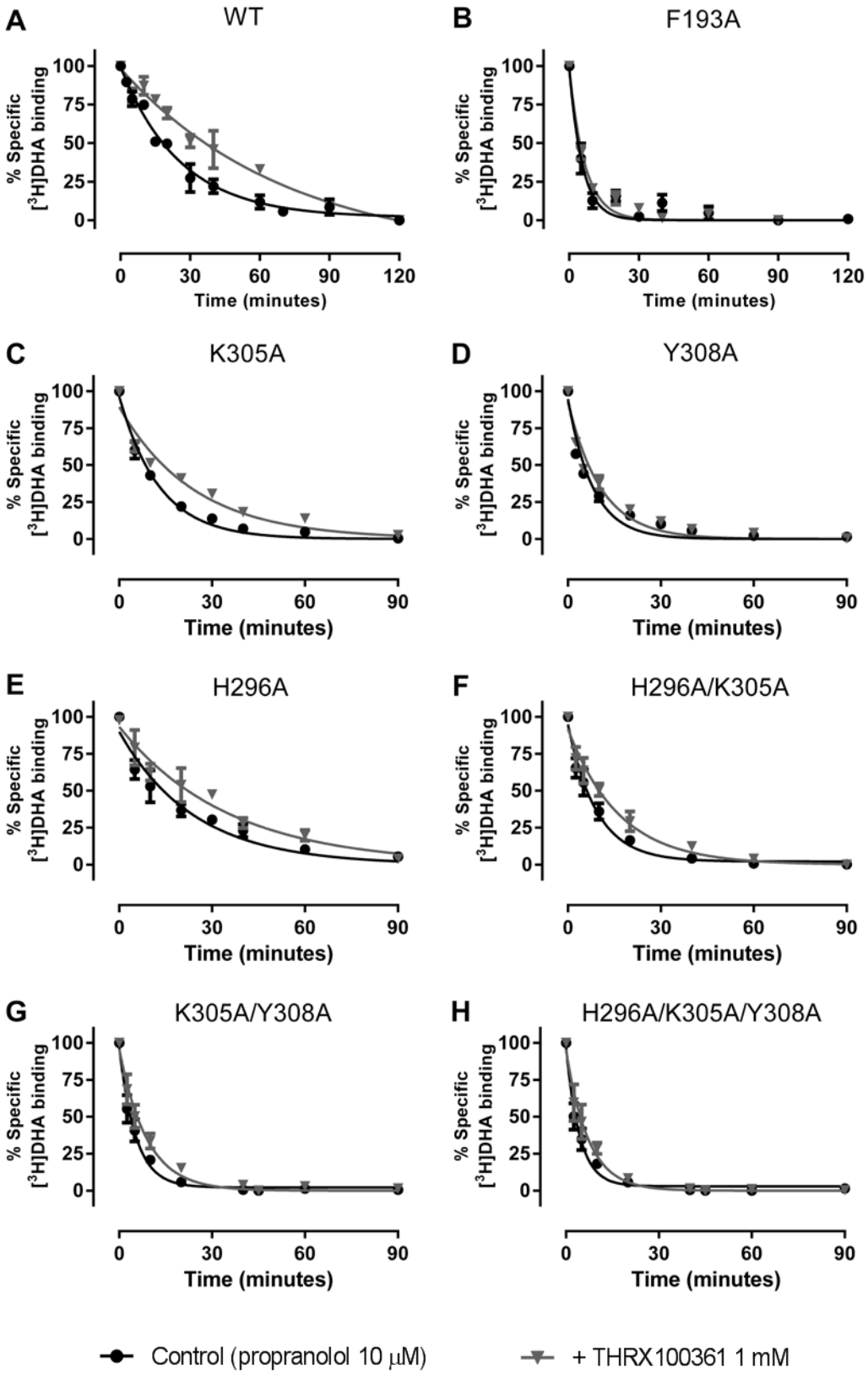
A
WT
B
F193A
C
K305A
D
Y308A
E
H296A
F
H296A/K305A
G
K305A/Y308A
H
H296A/K305A/Y308A
% Specific [3H]DHA binding
Time (minutes)
Control (propranolol 10 μM)
+ THRX100361 1 mM

Figure 5.1 The effects of allosteric binding site mutations on the modulatory action of THRX100361 on [^{3}H]DHA dissociation

The dissociation of [^{3}H]DHA from WT (A), F193^{ECL2}A (B), K305$^{7.32}$A (C), Y308$^{7.35}$A (D), H296$^{6.58}$A (E), H296$^{6.58}$A/K305$^{7.32}$A (F), K305$^{7.32}$A/Y308$^{7.35}$A (G) and H296$^{6.58}$A/K305$^{7.32}$A/Y308$^{7.35}$A (H) β_2AR in the absence and presence of 1 mM of THRX100361. Membrane preparations of COS-1 cells expressing WT or mutant β_2AR were pre-incubated with 0.5 nM of [^{3}H]DHA for 1 hour at room temperature. Subsequent [^{3}H]DHA re-association was inhibited using 10 μM of propranolol in the absence or presence of 1 mM of THRX100361. Data are presented as the mean ± SEM of 3-5 independent experiments performed in duplicate of triplicate.

Table 5.3 The effects of allosteric site mutations on the modulatory action of THRX100361 on [^{3}H]DHA dissociation

Human β_2AR	K_{off} (min^{-1})	K_{obs} (min^{-1})	K_{obs}/K_{off}	Log_{10} K_{obs}/K_{off}	n
WT†	0.036 ± 0.002	0.015 ± 0.003	0.43 ± 0.08	-0.39 ± 0.09	4
F193^{ECL2}A	0.200 ± 0.046	0.149 ± 0.012	0.74 ± 0.06	-0.13 ± 0.04*	3
K305$^{7.32}$A††	0.079 ± 0.004	0.042 ± 0.003	0.53 ± 0.05	-0.28 ± 0.04	3
Y308$^{7.35}$A††	0.125 ± 0.016	0.095 ± 0.013	0.76 ± 0.01	-0.12 ± 0.01*	3
H296$^{6.58}$A††	0.040 ± 0.004	0.028 ± 0.001	0.70 ± 0.03	-0.16 ± 0.02*	3
H296$^{6.58}$A/K305$^{7.32}$A	0.107 ± 0.017	0.062 ± 0.009	0.59 ± 0.04	-0.23 ± 0.03	3
K305$^{7.32}$A/Y308$^{7.35}$A	0.198 ± 0.050	0.124 ± 0.025	0.64 ± 0.05	-0.20 ± 0.03*	3
H296$^{6.58}$A/K305$^{7.32}$A/Y308$^{7.35}$A	0.235 ± 0.066	0.177 ± 0.064	0.72 ± 0.06	-0.14 ± 0.03*	3

K_{off}, dissociation rate of [^{3}H]DHA.

K_{obs}, dissociation rate of [^{3}H]DHA in the presence of 1 mM of THRX100361.

* $P \leq 0.05$ compared to WT by one-way ANOVA with Dunnett's multiple comparison test.

Data are presented as the mean ± SEM of n independent experiments performed in duplicate or triplicate.

† Data have previously been presented in Leonar (2011).

†† Data generated by Mr Tony Ngo.

THRX100361 to modulate [^{3}H]DHA dissociation by 1.7 fold ($P < 0.05$) (Table 5.3**,** Figure 5.1).

Kinetics dissociation binding assays were also performed using tacrine to investigate the effects of the proposed allosteric binding site mutations on the ability of tacrine to modulate [^{3}H]DHA dissociation. As tacrine is a more potent modulator compared to THRX100361, three different concentrations of tacrine were used in these assays – 10, 30 and 100 μM. Previous docking of tacrine into an active state β_2AR crystal structure suggested that tacrine binds allosterically to D192^{ECL2}, F194^{ECL2}, K305$^{7.32}$, Y308$^{7.35}$ and I309$^{7.36}$ (Table 3.5**,** Figure 3.9), whereas docking into an inactive state crystal structure suggested that tacrine interacts with F193^{ECL2}, N293$^{6.55}$, A200$^{5.39}$, H296$^{6.58}$ and Y308$^{7.35}$ (Table 3.6**,** Figure 3.10).

In contrast to the lack of effect on the modulation of THRX100361 seen with the K305$^{7.32}$A mutant, the modulatory effect of 100 μM of tacrine was decreased by 2.5 fold with this mutant ($P < 0.05$) (Table 5.4, Figure 5.2). Although the Y308$^{7.35}$A mutant decreased the modulatory effect of 10 μM of tacrine on [^{3}H]DHA dissociation ($P < 0.05$), it has no effect at 30 μM and 100 μM suggesting that Y308$^{7.35}$ has a minor role in mediating the allosteric effect of tacrine on [^{3}H]DHA dissociation (Table 5.4, Figure 5.2). Similar to THRX100361, both F193^{ECL2}A and H296$^{6.58}$A negatively affected the ability of tacrine to modulate [^{3}H]DHA dissociation. F193^{ECL2}A decreased the ability of 10 and 30 μM of tacrine to modulate [^{3}H]DHA dissociation by approximately 1.5 fold and 100 μM of tacrine by 2.9 fold, whereas H296$^{6.58}$A completely abolished the ability of all 3 concentrations of tacrine to modulate [^{3}H]DHA dissociation ($P < 0.05$) (Table 5.4, Figure 5.2).

Table 5.4 The effects of allosteric site mutations on the modulatory action of tacrine on [^{3}H]DHA dissociation

Human β_2AR	[Tacrine] (μM)	K_{off} (min^{-1})	K_{obs} (min^{-1})	K_{obs}/K_{off}	Log_{10} K_{obs}/K_{off}	n
WT†	0 (control)	0.023 ± 0.004				5
	10		0.014 ± 0.001	0.67 ± 0.04	-0.17 ± 0.03	3
	30		0.010 ± 0.001	0.54 ± 0.02	-0.27 ± 0.02	3
	100		0.007 ± 0.001	0.25 ± 0.04	-0.61 ± 0.07	3
F193^{ECL2}A	0 (control)	0.148 ± 0.001				3
	10		0.156 ± 0.011	1.06 ± 0.09	0.02 ± 0.04*	3
	30		0.122 ± 0.010	0.82 ± 0.03	-0.09 ± 0.02*	3
	100		0.107 ± 0.009	0.72 ± 0.03	-0.15 ± 0.02*	3
K305$^{7.32}$A	0 (control)	0.055 ± 0.004				4
	10		0.041 ± 0.002	0.81 ± 0.05	-0.09 ± 0.03	3
	30		0.032 ± 0.004	0.63 ± 0.08	-0.21 ± 0.05	3
	100		0.022 ± 0.009	0.63 ± 0.09	-0.43 ± 0.05*	3
Y308$^{7.35}$A	0 (control)	0.070 ± 0.004				4
	10		0.018 ± 0.002	0.87 ± 0.02	-0.06 ± 0.01*	3
	30		0.046 ± 0.004	0.66 ± 0.06	-0.18 ± 0.03	3
	100		0.061 ± 0.003	0.25 ± 0.02	-0.60 ± 0.03	3
H296$^{6.58}$A	0 (control)	0.028 ± 0.001				5
	10		0.028 ± 0.002	1.01 ± 0.02	0.01 ± 0.01*	3
	30		0.026 ± 0.003	0.95 ± 0.06	-0.02 ± 0.03*	3
	100		0.028 ± 0.001	0.96 ± 0.02	-0.01 ± 0.01*	3

K_{off}, dissociation rate of [^{3}H]DHA.

K_{obs}, dissociation rate of [^{3}H]DHA in the presence of various concentrations of tacrine.

* $P < 0.05$ compared to respective WT in the presence of the same concentration of tacrine by one-way ANOVA with Dunnett's multiple comparison test.

Data are presented as the mean ± SEM of n independent experiments performed in duplicate.

† *WT data have previously been presented in* Table 3.1.

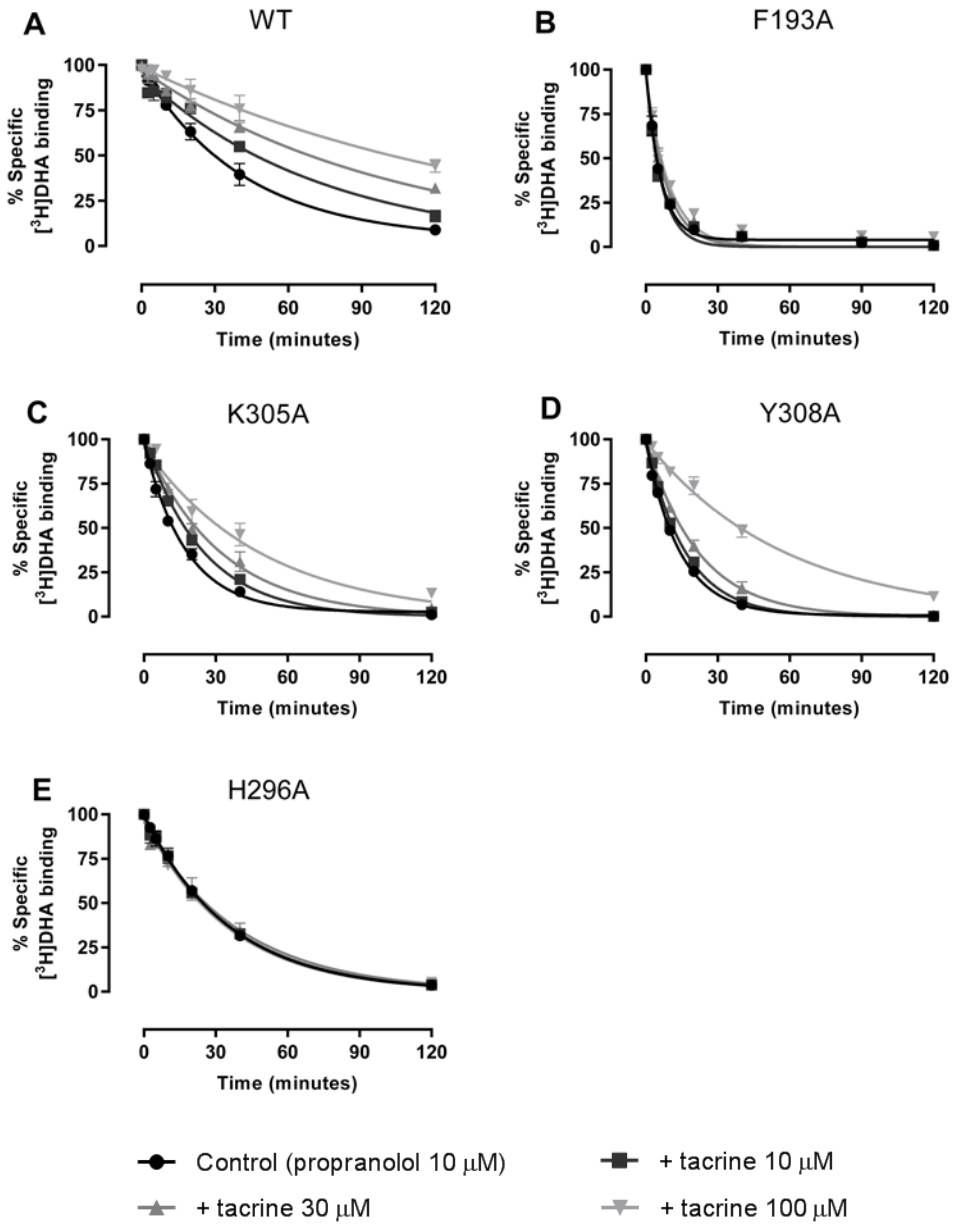

Figure 5.2 The effects of allosteric binding site mutations on the modulatory action of tacrine on [^{3}H]DHA dissociation

The dissociation of [^{3}H]DHA from WT (A), F193^{ECL2}A (B), K305$^{7.32}$A (C), Y308$^{7.35}$A (D), and H296$^{6.58}$A (E) β_2AR in the absence and presence of increasing concentrations of tacrine. Membrane preparations of COS-1 cells expressing WT or mutant human β_2AR were pre-incubated with 0.5 nM of [^{3}H]DHA for 1 hour at room temperature. Subsequent [^{3}H]DHA re-association was inhibited using 10 μM of propranolol in the absence or presence of various concentrations of tacrine. Data are presented as the mean ± SEM of 3-5 independent experiments performed in duplicate.

5.3.3 cAMP assays

The effects of the allosteric site mutations on the ability of THRX100361 and tacrine to modulate isoprenaline-mediated cAMP production were investigated using CHO cells stably transfected with the β_2AR and the BRET CAMYEL cAMP assay. The expression levels of the β_2AR in the stable cell clones used in this study are (sites/cell, min-max): WT 16655-37600, K305$^{7.32}$A 8248-32540, Y308$^{7.35}$A 15482-22672, H296$^{6.58}$A 6744-10767. The average expression level of the H296$^{6.58}$A mutant is significantly lower compared to the WT receptor (mean ± SEM, n = 3-4, $P < 0.05$).

In Chapter 4, the mutations F193^{ECL2}A, K305$^{7.32}$A, Y308$^{7.35}$A and H296$^{6.58}$A were shown to have no effect on the potency and maximum response of isoprenaline (Table 4.3**,** Table 4.5). In this study, however, the maximum response of isoprenaline at the H296$^{6.58}$A mutant was significantly lower compared to the WT receptor in the data set obtained for tacrine (Table 5.6**,** Figure 5.4), but not in the data set obtained for THRX100361 (Table 5.5**,** Figure 5.3). In addition, the potency of isoprenaline at the K305$^{7.32}$A mutant is markedly different in the data set obtained for THRX100361 and tacrine. In the absence of the modulators, the potency of isoprenaline is 10 fold higher in the data set obtained for tacrine ($P < 0.05$) (Table 5.5**,** Table 5.6). These results suggest that a larger sample size is needed to reduce inter assay variabilities.

At 600 μM, THRX100361 reduced the potency of isoprenaline at WT β_2AR by 4 fold (pEC_{50} ratio, $P < 0.05$) without affecting the maximum response (Table 5.5**,** Figure 5.3). The mutations K305$^{7.32}$A, Y308$^{7.35}$A and H296$^{6.58}$A decreased the ability of THRX100361 to modulate the potency of isoprenaline (Table 5.5**,** Figure

5.3). In addition, THRX100361 (600 μM) also reduced the maximum response of isoprenaline at the K305$^{7.32}$A and Y308$^{7.35}$A mutants by approximately 50% ($P \leq 0.05$), while having no effect at the H296$^{6.58}$A mutant (Table 5.5**,** Figure 5.3).

Similar to THRX100361, 300 μM and 600 μM of tacrine reduced the potency of isoprenaline by 2.5 and 4 fold respectively (pEC_{50} ratio, $P < 0.05$) without affecting the maximum response (Table 5.6**,** Figure 5.4). The Hill coefficient of the isoprenaline response curves in the absence or presence of increasing concentrations of tacrine for the K305$^{7.32}$A, Y308$^{7.35}$A and H296$^{6.58}$A mutants are not significantly different from the WT receptor ($P > 0.05$). The mutations K305$^{7.32}$A, Y308$^{7.35}$A and H296$^{6.58}$A decreased the ability of tacrine to modulate the potency of isoprenaline. Unlike THRX100361, tacrine (600 μM) reduced the maximum response of isoprenaline at the K305$^{7.32}$A ($P = 0.05$), but not the Y308$^{7.35}$A mutant and did not affect the maximum response of isoprenaline at the H296$^{6.58}$A mutant (Table 5.6**,** Figure 5.4).

Table 5.5 The effects of allosteric site mutations on the ability of THRX100361 to modulate β_2AR function

β_2AR	[THRX100361] (μM)	pEC_{50} (M)	EC_{50} (nM)	pEC_{50} ratio (Δ)	% Potency	Emax (% forskolin)	n
WT	0 (control)	7.0 ± 0.3	100	0		100.8 ± 8.1	10
	300	6.5 ± 0.3	316	0.4 ± 0.3	39.8	64.7 ± 16.0	5
	600	7.1 ± 0.1	79	0.6 ± 0.1*	25.1	84.7 ± 8.1	3
K305A	0 (control)	7.2 ± 0.3	63	0		105.4 ± 9.7	4
	300	7.0 ± 0.5	100	0.2 ± 0.3	63.1	90.7 ± 16.4	4
	600	7.1 ± 0.6	79	0.2 ± 0.3	63.1	47.3 ± 18.9†	3
Y308A	0 (control)	7.3 ± 0.4	50	0		101.1 ± 4.4	5
	300	6.9 ± 0.3	126	0.4 ± 0.5	39.8	106.5 ± 6.8	4
	600	6.7 ± 0.4	200	0.3 ± 0.4	50.1	58.5 ± 12.8†	3
H296A	0 (control)	7.2 ± 0.4	63	0		75.5 ± 5.6	6
	300	6.8 ± 0.4	158	0.3 ± 0.3	50.1	83.0 ± 12.6	5
	600	7.0 ± 0.7	100	0.4 ± 0.6	39.8	62.6 ± 11.2	3

pEC_{50}, negative log of the concentration of isoprenaline resulting in 50% of the maximum cAMP production.
pEC_{50} ratio (Δ), pEC_{50} control - pEC_{50} in the presence of the modulator.
% Potency, relative potency of isoprenaline in the presence of the modulator as % control ((antilog –Δ) x 100%).
E_{max}, the maximum amount of cAMP produced from the highest concentration of isoprenaline, expressed as percentage maximum stimulation with 10 μM of forskolin.
* $P < 0.05$ compared to WT control by one sample t test.
† $P \leq 0.05$ compared to control by one-way ANOVA with Dunnett's multiple comparison test.
Data are presented as the mean ± SEM of n independent experiments performed in triplicate.

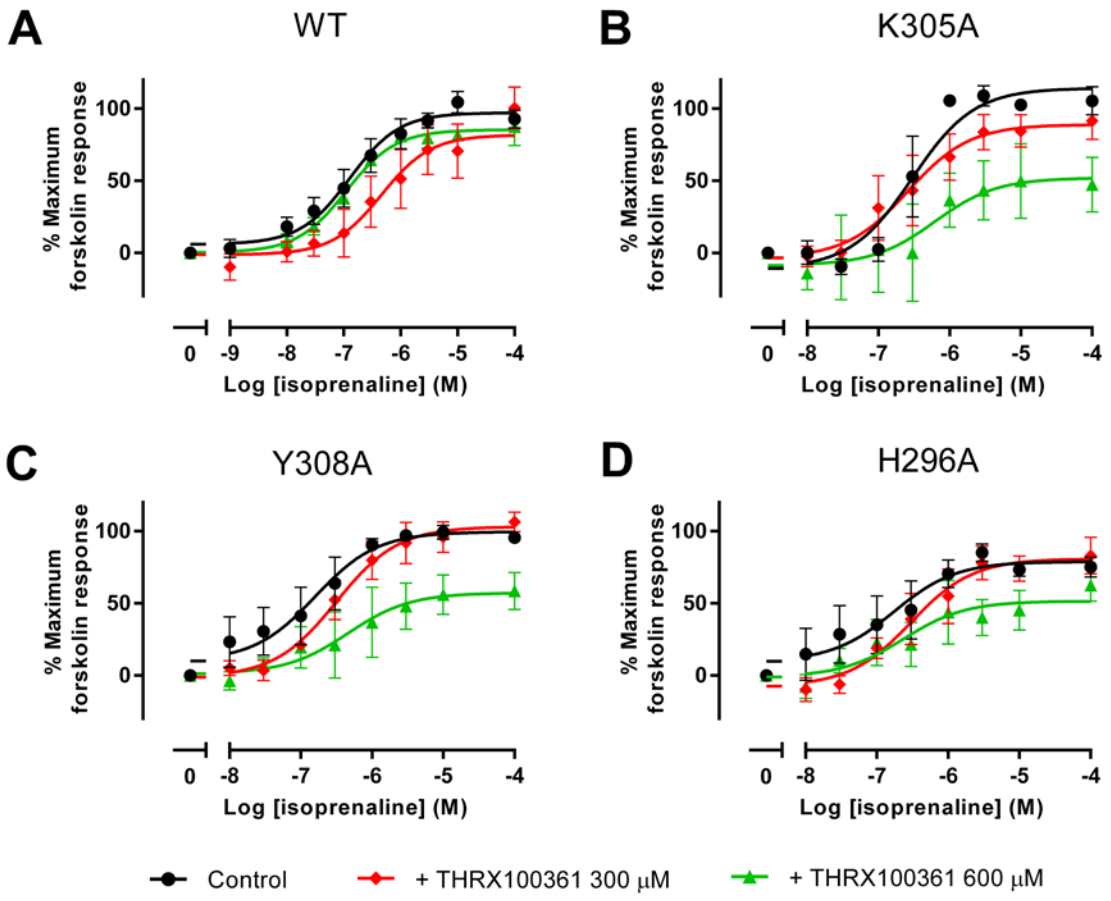

Figure 5.3 The effects of allosteric site mutations on the ability of THRX100361 to modulate β_2AR function

CHO cells stably expressing WT (A), K305A (B), Y308A (C) or H296A (D) human β_2AR were transfected with the BRET cAMP sensor CAMYEL. Cells were pre-incubated for 30 min with or without THRX100361 and stimulated with increasing concentrations of isoprenaline. cAMP production was measured after a 15 min incubation with isoprenaline in the presence of 40 µM of IBMX. Data are presented as the mean ± SEM of 3-8 independent experiments performed in triplicate.

Table 5.6 The effects of allosteric site mutations on the ability of tacrine to modulate β_2AR function

β_2AR	[Tacrine] (μM)	pEC_{50} (M)	EC_{50} (nM)	pEC_{50} ratio (Δ)	% Potency	Emax (% forskolin)	n
WT	0 (control)	7.1 ± 0.2	79	0		95.4 ± 2.8	7
	100	7.0 ± 0.3	100	0.2 ± 0.3	63.1	92.3 ± 1.5	6
	300	6.8 ± 0.2	158	0.4 ± 0.1*	39.8	88.1 ± 7.8	6
	600	6.7 ± 0.2	200	0.6 ± 0.2*	25.1	83.3 ± 5.4	6
K305A	0 (control)	8.2 ± 0.2§	6	0		103.4 ± 3.4	4
	100	7.9 ± 0.4	13	0.2 ± 0.4	63.1	86.4 ± 4.6	4
	300	8.0 ± 0.2	10	0.2 ± 0.3	63.1	86.1 ± 6.9	4
	600	8.1 ± 0.2	8	0.1 ± 0.2	79.4	76.2 ± 11.4†	4
Y308A	0 (control)	7.4 ± 0.2	40	0		90.4 ± 3.1	3
	100	7.3 ± 0.1	50	0.2 ± 0.3	63.1	84.9 ± 2.3	3
	300	7.5 ± 0.2	32	0.1 ± 0.1	79.4	80.3 ± 3.4	3
	600	7.4 ± 0.3	40	0.1 ± 0.1	79.4	81.8 ± 6.1	3
H296A	0 (control)	7.3 ± 0.3	50	0		67.6 ± 9.1§	5
	100	7.2 ± 0.2	63	0.1 ± 0.3	79.4	70.2 ± 7.7	5
	30	7.4 ± 0.2	40	0.1 ± 0.1	79.4	71.8 ± 10.8	4
	600	7.3 ± 0.2	50	0.1 ± 0.1	79.4	67.5 ± 8.8	4

pEC_{50}, negative log of the concentration of isoprenaline resulting in 50% of the maximum cAMP production.
pEC_{50} ratio (Δ), pEC_{50} control - pEC_{50} in the presence of the modulator.
% Potency, relative potency of isoprenaline in the presence of the modulator as % control ((antilog –Δ) x 100%).
E_{max}, the maximum amount of cAMP produced from the highest concentration of isoprenaline, expressed as percentage maximum stimulation with 10 μM of forskolin.
* $P < 0.05$ compared to control by one sample t test.
§ $P < 0.05$ compared to WT control by one-way ANOVA with Dunnett's multiple comparison test.
† $P = 0.05$ compared to K305A control by one-way ANOVA with Dunnett's multiple comparison test.
Data are presented as the mean ± SEM of n independent experiments performed in triplicate.

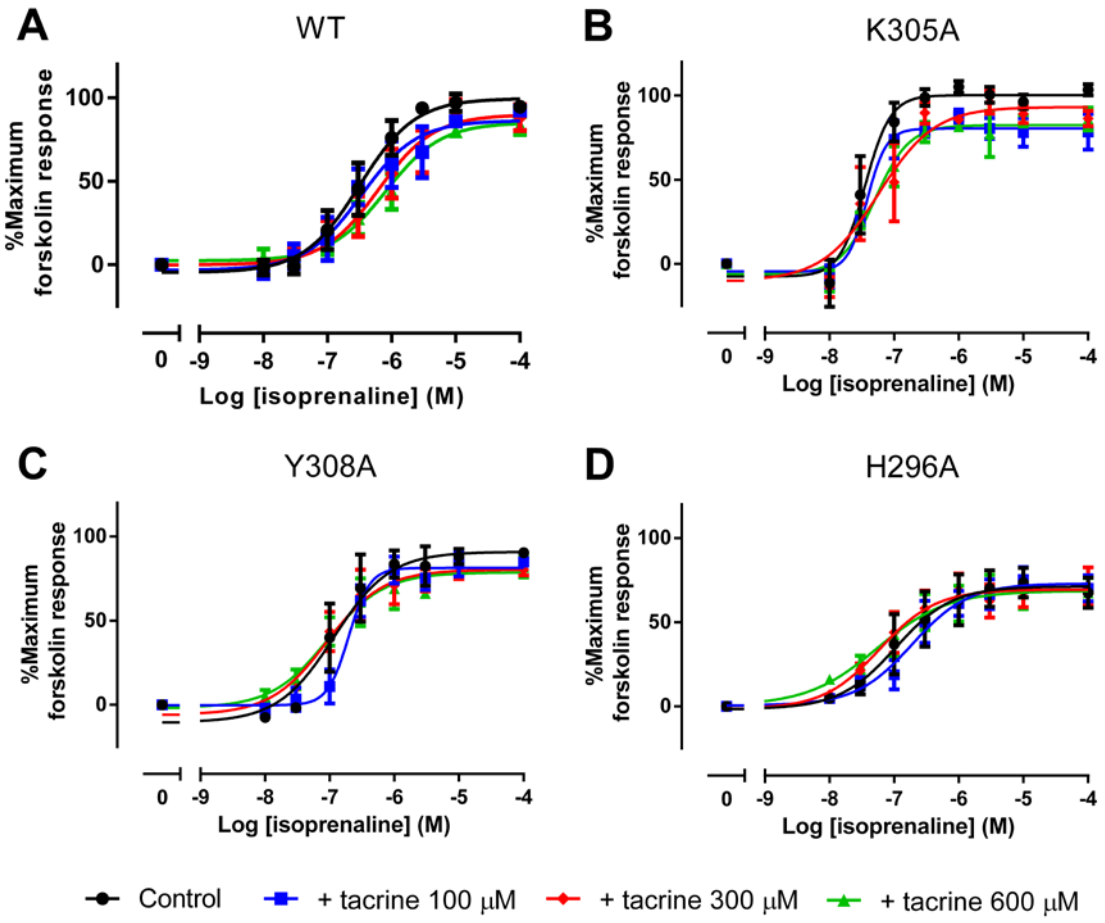

Figure 5.4 The effects of allosteric site mutations on the ability of tacrine to modulate β_2AR function

CHO cells stably expressing WT (A), K305$^{7.32}$A (B), Y308$^{7.35}$A (C) or H296$^{6.58}$A (D) human β_2AR were transfected with the BRET cAMP sensor CAMYEL. Cells were pre-incubated for 30 min with or without tacrine and stimulated with increasing concentrations of isoprenaline. cAMP production was measured after a 15 min incubation with isoprenaline in the presence of 40 μM of IBMX. Data are presented as the mean ± SEM of 3-7 independent experiments performed in triplicate.

5.4 Discussion

Allosteric modulators of small molecule-neurotransmitter binding family A GPCRs such as the mAChRs, D_2 dopamine and α_{1A}AR have been shown to bind to the extracellular region of the receptors. The docking of THRX100361 and tacrine predicted that these modulators also bind to the extracellular region of the β_2AR, making interactions with residues from the ECL2 and the top of TM6 and 7 (Chapter 3). The characterisation of this extracellular region of the β_2AR suggests that it plays a role in the kinetics of orthosteric ligand binding (Chapter 4).

In line with the docking of THRX100361 into an inactive β_2AR structure which predicted that it interacts with D192^{ECL2}, F193^{ECL2}, A200$^{5.39}$, H296$^{6.58}$ and Y308$^{7.35}$ (Chapter 3), the mutations F193^{ECL2}A, Y308$^{7.35}$A and H296$^{6.58}$ decreased the ability of THRX100361 to modulate [^{3}H]DHA dissociation. As predicted by the docking study, the mutation K305$^{7.32}$A has no effect on the ability of THRX100361 to modulate [^{3}H]DHA dissociation. These data suggest that the allosteric modulation of [^{3}H]DHA dissociation by THRX100361 is mediated by F193^{ECL2}, H296$^{6.58}$ and Y308$^{7.35}$. In addition, the ability of THRX100361 to modulate the dissociation of [^{3}H]DHA was decreased to the same extent by each of the F193^{ECL2}A, H296$^{6.58}$A and Y308$^{7.35}$A mutant, suggesting that these residues contribute equally to the allosteric effect of THRX100361 on [^{3}H]DHA dissociation.

Docking of tacrine into the inactive β_2AR crystal structure predicted that it also interacts at the same region as THRX100361, making interactions with F193^{ECL2}, A200$^{5.39}$, N293$^{6.55}$, H296$^{6.58}$ and Y305$^{7.35}$ (Chapter 3). The single mutation H296$^{6.58}$A is sufficient to completely abolish the allosteric effect of tacrine on [^{3}H]DHA dissociation, even at the highest concentration tested of 100 μM,

suggesting that it plays a major role in the binding of tacrine or the transfer of the conformational effect of tacrine on [^{3}H]DHA binding. In addition, the mutation F193^{ECL2}A also significantly reduced the ability of tacrine to modulate [^{3}H]DHA dissociation. However, this mutation has less effect at higher concentrations (30 μM and 100 μM) compared to H296$^{6.58}$A, suggesting that H296$^{6.58}$ has a major contribution in mediating the allosteric effect of tacrine on [^{3}H]DHA dissociation. Although docking did not identify an interaction with K305$^{7.32}$, the mutation of this residue to alanine also decreased the allosteric effect of 100 μM of tacrine on [^{3}H]DHA dissociation. In contrast, the mutation Y308$^{7.35}$A has no effect on the ability of tacrine to modulate [^{3}H]DHA dissociation at 30 μM and 100 μM, suggesting that Y308$^{7.35}$ has a small contribution to the allosteric effect of tacrine on [^{3}H]DHA dissociation.

The mutations K305$^{7.32}$A, Y308$^{7.35}$A and H296$^{6.58}$A eliminated the inhibitory effect of both THRX100361 and tacrine on the potency of isoprenaline. However, the mutations K305$^{7.32}$A and Y308$^{7.35}$A have complex consequence on the modulatory effect of THRX100361 on isoprenaline-mediated receptor activation. THRX100361 decreased the maximum response of isoprenaline at the K305$^{7.32}$A and Y308$^{7.35}$A mutants, but not at the WT receptor or the H296$^{6.58}$A mutant. A possible explanation for this observation is that pre-incubation of THRX100361 in the assays blocked the entry of isoprenaline into the orthosteric pocket of the receptor and reduced the maximum response of isoprenaline. The effect of these mutations on the modulatory effect of THRX100361 and tacrine in β_2AR function needs to be further investigated, including co-addition of the modulator and isoprenaline in the assay.

The data in this study suggest that THRX100361 and tacrine bind to the same region of the β_2AR. While they do not interact with identical residues, there is an overlap in the binding site of these allosteric modulators. This allosteric site is in the same region as the binding site of the M_2 mAChR allosteric modulator LY2119620 determined by crystallography (Kruse *et al.*, 2013). Three out of four allosteric residues shown to form an allosteric binding site at the β_2AR, F193^{ECL2}, H296$^{6.58}$ and Y308$^{7.35}$, correspond to Y177^{ECL2}, N410$^{6.58}$ and W422$^{7.35}$ respectively at the M_2 mAChR, suggesting that the β_2AR and the mAChRs share a homologous allosteric binding site.

W422$^{7.35}$ at the M_2 mAChR has been identified as a common orthosteric and allosteric binding site (Jager *et al.*, 2007; Kruse *et al.*, 2013). At the M_2 mAChR crystal structure, W422$^{7.35}$ was observed to interact with both iperoxo and LY2119620, acting as a lid that separates the two ligands (Kruse *et al.*, 2013). In addition, the mutation W422$^{7.35}$A not only decreased the affinity of orthosteric agonist acetylcholine and reduced receptor activation by partial agonist pilocarpine, but also attenuated the binding cooperativity between allosteric modulator naphmethonium and acetylcholine and reversed the cooperativity between naphmethonium and partial agonist pilocarpine (Jager *et al.*, 2007). W422$^{7.35}$ has also been found to control the degree of $G_{\alpha i}$ coupling at the M_2 mAChR (Bock *et al.*, 2012). Similarly, Y308$^{7.35}$ is also important for both allosteric and orthosteric ligand interactions at the β_2AR. The mutation Y308$^{7.35}$A decreased the affinity of orthosteric agonist isoprenaline and antagonist [^{3}H]DHA (Chapter 4), as well as the ability of THRX100361 to modulate [^{3}H]DHA dissociation. Furthermore, the mutation Y308$^{7.35}$F at the β_2AR enabled $G_{\alpha s}$-biased agonist (R,R')-4'-

aminofenoterol to activate $G_{\alpha i}$ signalling (Woo *et al.*, 2014) and decreased the association rate of [^{3}H]DHA from active β_2AR (DeVree *et al.*, 2016). Taken together, these data suggest that there is a conservation of a general mechanism of receptor modulation between the β_2AR and the M_2 mAChR which is mediated by aromatic residues located at the top of TM7.

The allosteric effect of tacrine on [^{3}H]DHA dissociation was strongly mediated by H296$^{6.58}$. Interestingly, H296$^{6.58}$ has been implicated in the binding of salmeterol at the β_2AR (Baker *et al.*, 2015). Salmeterol is a long-acting bivalent β_2AR agonist used clinically to manage the symptoms of asthma and COPD and has a high β_2AR/β_2AR selectivity of over 1000 fold (Baker *et al.*, 2015; Ball *et al.*, 1987; Mann *et al.*, 1996). Salmeterol was made by linking a phenol ring to salbutamol through a butyl-hexyl linker ($CH_{3(6)}OCH_{3(4)}$) (Bradshaw *et al.*, 1987). Salmeterol is slightly smaller in size compared to the bitopic β_2AR allosteric modulator THRX198321. Docking of THRX198321 into an active state β_2AR crystal structure suggests that a phenol ring on its allosteric moiety interacts with H296$^{6.58}$ (Chapter 3). The mutation of H296$^{6.58}$ to a corresponding lysine residue on the β_1AR or to alanine has been shown to decrease the affinity of salmeterol (Baker *et al.*, 2015). Given the role of H296$^{6.58}$ in allosteric modulation of the β_2AR and the mAChRs, the possibility of salmeterol to interact allosterically at the β_2AR should be investigated.

In contrast to the β_2AR and the mAChRs, mutagenesis studies suggest that allosteric modulation at the α_{1A}AR is mediated by the TM2 residue F86$^{2.64}$, as the mutation of this residue to alanine has been shown to decrease the ability of 9-aminoacridine to modulate the dissociation rate of orthosteric antagonist

[^{3}H]prazosin (Campbell, 2015). 9-aminoacridine is a planar analogue of tacrine, with a phenol ring in place of the saturated cyclohexane. Both tacrine and 9-aminoacridine are potent negative modulators of the α_{1A}AR and have been predicted to interact in the same manner at the α_{1A}AR (Campbell, 2015). Docking of tacrine and 9-aminoacridine into a homology model of the α_{1A}AR predicted that they also interact with F308$^{7.35}$ (Campbell, 2015), a residue that is important for allosteric modulation of the β_2AR and the mAChRs. However, the contribution of this residue in the allosteric effects of tacrine and 9-aminoacridine at the α_{1A}AR has not been verified in mutagenesis studies. An allosteric binding site which involves TM2 residues has also been reported for the D_2 dopamine receptor (Lane *et al.*, 2014). Taken together, these data suggest that β_2AR and the mAChRs share a common allosteric binding site that is distinct from the D_2 dopamine receptor and may be shared by the α_{1A}AR.

The residues that mediate the allosteric effects of THRX100361 and/or tacrine on [^{3}H]DHA dissociation such as F193^{ECL2}, Y308$^{7.35}$ and K305$^{7.32}$ have been shown in Chapter 4 to affect the dissociation rate of [^{3}H]DHA and are predicted to form the metastable binding site of the β_2AR. Simulation studies at the M_3 mAChR and the D_2 dopamine receptor have shown that orthosteric ligands of these receptors associate with the extracellular vestibule of the receptors prior to entering the orthosteric pocket and these regions of the receptors have also been shown to be involved in allosteric binding of small molecule ligands (Kruse *et al.*, 2012; Thomas *et al.*, 2016). The ability of the vestibule to recognise both orthosteric and allosteric ligands suggest that orthosteric and allosteric ligands must share similar inherent properties. This idea is also supported by the data which show that the β_2AR

agonist BA can modulate the M_2/M_3 mAChRs and the M_2/M_3 mAChR antagonist THRX100361 can modulate the β_2AR (Steinfeld *et al.*, 2011). In fact, like many orthosteric ligands of the β_2AR, THRX100361 and tacrine both have a basic nitrogen and one or more phenol ring(s).

The ability of the extracellular vestibule to bind both orthosteric and allosteric ligands also suggests that allosteric binding sites are likely low affinity binding sites for orthosteric ligands and that allosteric modulators remain at the metastable binding site because they have higher affinity for the metastable site compared to the orthosteric site. The docking of THRX100361 into the active state β_2AR crystal structure in the absence of bound orthosteric ligand supports this idea, as THRX100361 can be seen to bind in the orthosteric pocket, although these orthosteric poses were not frequently observed and were scored less compared to the allosteric poses (Chapter 3). In addition, orthosteric ligands of the M_2 mAChR N-methylscopolamine and oxotremorine-M have been shown in binding studies to bind weakly at the allosteric site of the receptor (Redka *et al.*, 2008).

In summary, this study is the first to characterise an extracellular allosteric binding site at the β_2AR. This allosteric site is homologous to the allosteric site of the mAChRs, suggesting a conservation of allosteric mechanism between these receptors. This study also showed that the allosteric site of the β_2AR exists on the extracellular end of the orthosteric ligand binding pathway. The data presented in this study will be useful in the development of novel allosteric modulators of the β_2AR.

CHAPTER 6

Pharmacological characterisation of PMX53 interactions at the complement 5a receptor

6.1 Introduction

The complement system is a major component of innate and adaptive immunity (Carroll, 2004; Dunkelberger and Song, 2009). C5a is one of the most potent pro-inflammatory peptides generated following activation of the complement system (Ember *et al.*, 1994; Okusawa *et al.*, 1988). Elevated C5a levels in the circulation have been associated with many inflammatory disorders, such as rheumatoid arthritis, inflammatory bowel disease, psoriasis and macular degeneration (Grant *et al.*, 2002; Liu *et al.*, 2011; Ternowitz *et al.*, 1987; Woodruff *et al.*, 2003; Woodruff *et al.*, 2002).

PMX53 (AcF[OPdChaWR]) is a cyclic peptide-mimetic which acts as a non-competitive C5aR antagonist in assays measuring myeloperoxidase release from PMNs (Finch *et al.*, 1999; March *et al.*, 2004; Paczkowski *et al.*, 1999). PMX53 has been shown to improve clinical outcome in many animal models of inflammatory disorders, including arthritis, sepsis, immune complex disorder and inflammatory bowel disease (Short *et al.*, 1999; Woodruff *et al.*, 2003; Woodruff *et al.*, 2002). Early phase clinical trials of PMX53 have been carried out for rheumatoid arthritis and psoriasis (Kohl, 2006; Vergunst *et al.*, 2007). While PMX53 was efficacious in psoriasis, there was no clear efficacy in the rheumatoid arthritis trial (Kohl, 2006; Vergunst *et al.*, 2007). Further development of PMX53 and its analogue PMX205

has not been announced since the lapse of the patent and efforts to commercialise the first C5aR antagonist are currently ongoing.

Despite substantial preclinical and clinical studies being carried out on PMX53, the precise molecular mechanism of C5aR inhibition with this antagonist has not been established. PMX53 was originally developed from the modification of a linear partial agonist derived from the C-terminal tail of C5a, MeFKPdChaFr (Drapeau *et al.*, 1993). The substitution of tryptophan at position F_5 of the partial agonist MeFKPdChaFr resulted in the first antagonist of the C5aR MeFKPdChaWr (Konteatis *et al.*, 1994), further substitution of which resulted in PMX53, one of the most potent cyclic peptide antagonists of the C5aR (Paczkowski *et al.*, 1999). Despite being developed from an agonist, PMX53 inhibits C5a-mediated myeloperoxidase release from PMNs in an apparently non-competitive manner (March *et al.*, 2004; Paczkowski *et al.*, 1999).

PMX53 binds to the human and rat C5aR with an affinity of 90 nM and 40 nM respectively, whereas its affinity for the mouse C5aR is approximately 400 fold less at 36 μM (Woodruff *et al.*, 2001). However, PMX53 shows *in vivo* efficacy in various mouse models of inflammatory diseases despite low binding affinity at the mouse C5aR (Bao *et al.*, 2005; Girardi *et al.*, 2006; Kim *et al.*, 2004; Woodruff *et al.*, 2001) and the reasons for this are not understood. Analysis of the sequence alignment of human, rat and mouse C5aRs showed that the highest sequence variation between the species can be found on the ECL2 where the sequence conservation is less than 50% (Figure 6.1). Mutations of ECL2 residues have been shown to cause constitutive activity at the C5aR, suggesting that the ECL2 serves as a negative regulator of receptor function (Klco *et al.*, 2005). In addition, the mutation of R175

on the ECL2 has been shown to decrease the potency of PMX53 and C5a (Cain *et al.*, 2003; Higginbottom *et al.*, 2005).

The apparent non-competitive mechanism of PMX53 inhibition led to the hypothesis that PMX53 is a negative allosteric modulator of the C5aR. To test this hypothesis and to identify the possible binding site of PMX53, homology models of human and mouse C5aR were built and docking was performed. Mutagenesis studies were also carried out to characterise the binding site of PMX53 at the C5aR.

```
Human       MDSFNYTTPDYGHYDDKDTLDLNTPVDKTSN-TLRVPDILALVIFAVVFLVGVLGNALVVWVTAFEAKR   68
Rat         MDPISNDSSEITYDYSDGTPNPDMPADGVYIPKMEPGDIAALIIYLAVFLVGVTGNALVVWVTAFEAKR   69
Mouse       MDPIDNSSFEINYDH-YGTMDPNIPADGIHLPKRQPGDVAALIIYSVVFLVGVPGNALVVWVTAFEARR   68
                                                                  TM1

Human       TINAIWFLNLAVADFLSCLALPILFTSIVQHHHWPFGGAACSILPSLILLNMYASILLLATISADRFLL  137
Rat         TVNAIWFLNLAVADLLSCLALPILFTSIVKHNHWPFGDQACIVLPSLILLNMYSSILLLATISADRFLL  138
Mouse       AVNAIWFLNLAVADLLSCLALPVLFTTVLNHNYWYFDATACIVLPSLILLNMYASILLLATISADRFLL  137
                        TM2                                       TM3

Human       VFKPIWCQNFRGAGLAWIACAVAWGLALLLTIPSFLYRVVREEYFPPKVLCGVDYSHDK-RRERAVAIV  205
Rat         VFKPIWCQKFRRPGLAWMACGVTWVLALLLTIPSFVFRRIHKDPYSDSILCNIDYSKGPFFIEKAIAIL  207
Mouse       VFKPIWCQKVRGTGLAWMACGVAWVLALLLTIPSFVYREAYKDFYSEHTVCGINYGGGSFPKEKAVAIL  206
                                  TM4                                ECL2

Human       RLVLGFLWPLLTLTICYTFILLRTWSRRATRSTKTLKVVVAVVASFFIFWLPYQVTGIMMSFLEPSSPT  274
Rat         RLMVGFVLPLLTLNICYTFLLIRTWSRKATRSTKTLKVVMAVVTCFFVFWLPYQVTGVILAWLPRSSST  277
Mouse       RLMVGFVLPLLTLNICYTFLLLRTWSRKATRSTKTLKVVMAVVICFFIFWLPYQVTGVMIAWLPPSSPT  275
                        TM5                                TM6

Human       FLLLKKLDSLCVSFAYINCCINPIIYVVAGQGFQGRLRKSLPSLLRNVLTEESVVRESKSFTRSTVDTM  343
Rat         FQSVERLNSLCVSLAYINCCVNPIIYVMAGQGFHGRLRRSLPSIIRNVLSEDSLGRDSKSFTRSTMDTS  345
Mouse       LKRVEKLNSLCVSLAYINCCVNPIIYVMAGQGFHGRLLRSLPSIIRNALSEDSVGRDSKTFTPSTTDTS  344
                           TM7

Human       AQKTQAV  350
Rat         TQKSQAV  352
Mouse       TRKSQAV  351
```

Figure 6.1 Sequence alignment of human, rat and mouse complement 5a receptors

The putative transmembrane (TM) domains of the C5aRs are underlined. The residues on the second extracellular loop (ECL2) are highlighted in blue. Residues that are the same in human and rat but different in the mouse C5aR are highlighted in red. Sequence alignment was performed using Clustal Omega (http://www.ebi.ac.uk/Tools/msa/clustalo/).

6.2 Methods

6.2.1 Human polymorphonuclear leukocyte isolation

Approximately 25 mL of human venous blood was drawn from the cubital veins of healthy volunteers using 23 gauge butterfly needles. This procedure was carried out according to the UNSW human research ethics approvals HC13289 and HC15070. The blood was drawn into 9 mL Vacuette® tubes containing acid citrate dextrose (ACD) solution B and the tubes were immediately inverted several times to mix the blood with the ACD solution. The blood was then carefully layered onto an equal volume of Ficoll-Paque Plus (GE Healthcare, UK) and centrifuged at 400 x g for 30 min at room temperature. The mixture separated into four distinct layers following centrifugation. The top three layers were removed while the remaining bottom layer containing red blood cells and polymorphonuclear leukocytes (PMNs) was further processed. After removal of the top three layers, the red blood cells were lysed through the addition of 35 mL of ice-cold milliQ water to the tube, which was then shaken vigorously for 40 s and 3.5 mL of ice-cold 10X PBS was added to the tube to restore isotonicity. The mixture was then centrifuged at 700 x g for 20 min at 4°C. The resulting supernatant was then removed, leaving approximately 5 mL of solution. The red blood cells were lysed again as described above until no red blood cells were visible in the tube. This process was repeated up to 4 times. The purified PMNs were then resuspended in assay buffers to the final concentration required for each assay.

6.2.2 U937 cell differentiation

The human monocytic lymphoma cell line, U937, was maintained in Roswell Park Memorial Institute (RPMI)-1640 medium supplemented with 10% (v/v) of heat inactivated FBS at 37 ℃ and 5% CO_2. U937 cells were differentiated by incubation in 1 mM dibutyryl cAMP (Sigma-Aldrich, USA) for 72 hours in order to differentiate the cells into C5a-responsive macrophage-like cells.

6.2.3 Generation of CHO cells stably expressing human C5aR

CHO cells stably expressing human C5aR were used in Eu-EP54 competition binding assays. These stable CHO cells were generated using wild type (WT) human C5aR cDNA as outlined in section 2.2.2**.** The membrane preparation used in the dissociation kinetics binding assays was obtained by homogenisation of these stable cells as described in section 2.2.5**.**

6.2.4 Site-directed mutagenesis

The primers used to construct the mutant human and mouse C5aRs can be found in Table 6.1**.** The mutant human and mouse C5aRs were generated using site-directed mutagenesis as described in section 2.2.3. The corresponding WT receptor for each species was used as the template to generate the hC5aR $L187^{ECL2}V$ and $D191^{ECL2}N$, and mC5aR $V187^{ECL2}L$ and $N191^{ECL2}D$ mutants. The hC5aR $L187^{ECL2}V/D191^{ECL2}N$ double mutant was constructed using $D191^{ECL2}N$ as the template receptor, while the mC5aR $V187^{ECL2}L/N191^{ECL2}D$ double mutant was constructed using the $N191^{ECL2}D$ as the template receptor.

Table 6.1 C5aR mutagenesis primers

Species	Mutation	Primer	
Human	L187^{ECL2}V	F	CACCAAAGGTGGTGTGTGGCGTGGACTACAG
		R	CTGTAGTCCACGCCACACACCACCTTTGGTG
	D191^{ECL2}N	F	GTGTTGTGTGGCGTGAACTACAGCCACGACAAAC
		R	GTTTGTCGTGGCTGTAGTTCACGCCACACAACAC
	L187^{ECL2}V/D191^{ECL2}N	F	GTGGTGTGTGGCGTGAACTACAGCCACGACAAAC
		R	GTTTGTCGTGGCTGTAGTTCACGCCACACACCAC
Mouse	V187^{ECL2}L	F	GGACTTCTACTCAGAGCACACTCTATGTGGTATTAACTATGG
		R	CCATAGTTAATACCACATAGAGTGTGCTCTGAGTAGAAGTCC
	N191^{ECL2}D	F	GCACACTGTATGTGGTATTGACTATGGTGGGGGTAGC
		R	GCTACCCCCACCATAGTCAATACCACATACAGTGTGC
	V187^{ECL2}L/N191^{ECL2}D	F	GCACACTCTATGTGGTATTGACTATGGTGGGGGTAGC
		R	GCTACCCCCACCATAGTCAATACCACATAGAGTGTGC

F, forward or sense primer.

R, reverse or antisense primer.

The nucleotides of the mutated residues are underlined.

6.2.5 EP54 synthesis and purification

EP54 (YSFKPMPLaR) was prepared using a standard solid-phase peptide synthesis (SPPS) approach. Briefly, 300 mg of 2-chlorotritylchloride was weighed into a 10 mL polypropylene syringe equipped with a porous polypropylene frit (Torviq SF-1000). The resin was initially swelled with dichloromethane (DCM) for 30 min and washed with *N,N*-dimethylformamide (DMF). The C-terminal arginine (4 equivalents) was attached to the resin using diisopropylethylamine (DIPEA) (6 equivalents). Iterative peptide elongation was performed consisting of N-terminal Fmoc deprotection using piperidine in DMF (1:5, v/v) followed by washing with DMF. Amino acid coupling was performed using 6 equivalents of DIPEA, 4 equivalents of 1-hydroxybenzotriazole hydrate (HOBt), 3.95 equivalents of *N,N,N′,N′*-tetramethyl-O-(1*H*-benzotriazol-1-yl)uronium hexafluorophosphate, O-(benzotriazol-1-yl)-*N,N,N′,N′*-tetramethyluronium hexafluorophosphate (HBTU) and 4 equivalents of the relevant C-terminally unprotected amino acid in DMF for 45 min. After the final coupling and deprotection, the solid phase-coupled peptide was washed with DCM then dried. The peptide was cleaved from the resin using a cocktail of trifluoroacetic acid/triisopropylsilane/water (90:5:5, v/v/v) for 3 hours. The peptide was precipitated using cold diethyl ether and washed with diethyl ether. The peptide was then dried, resuspended in pure water and lyophilised yielding a white precipitate. The peptide was purified by reversed-phase semi-preparative HPLC (A = H_2O, B = acetonitrile, both with 0.1% formic acid, isocratic 5% B for 5 min, gradient 5-40% B over 5 min, isocratic 40% B for 12.5 min and gradient 40-80% B over 2.5 min) yielding EP54 as a white fluffy powder after lyophilisation. Peptide purity was calculated from the high

performance liquid chromatography (HPLC) trace by dividing the area of the peak for the peptide over the area of all detected peaks.

6.2.6 Europium labelling of EP54

EP54 was fluorescently labelled with Europium (Eu^{3+}) using the Perkin Elmer Delfia Eu-labelling kit (1244-302) according to the manufacturer's guidelines. Briefly, 50 nmol of EP54 (2 mg/mL) was added to 50 nmol of the Eu-labelling reagent in 100 mM of Na_2CO_3 at pH 9. The reaction was incubated overnight at 4°C. The labelled peptide was separated from the unlabelled peptide and free europium by HPLC, running from 10 to 60% B at 1 mL/min over 45 min (A = 20 mM triethylammonium acetate (TEA) pH 7.2; B = 20 mM TEA in 90% acetonitrile).

6.2.7 Eu-EP54 competition binding assays

Europium-labelled peptides were competed against unlabelled peptide to determine the binding capabilities of the labelled peptides in Millipore Multiscreen BV 96-well filter plates. Labelled peptides were incubated with 1 mM of unlabelled peptide and 2 x 10^5 CHO cells stably transfected with human C5aR in a volume of 200 µL for 1 hour at 4°C with gentle shaking. A negative control of cells and unlabelled peptide was included to correct for auto-fluorescence. The reaction was terminated by filtration and the samples were washed three times with 200 µL of ice-cold PBS. Following this, 150 µL of enhancement solution was added to the samples and incubated for 15 min at room temperature with slow shaking. Fluorescence was measured using a Fluostar Optima plate reader, with 355 nm excitation and 620 nm emission filters, 200 µs delay and 400 µs integration time.

6.2.8 FITC labelling of ahxEP54

EP54 was N-terminally labelled with fluorescein isothiocyanate (FITC) via a six-carbon linker aminohexanoic acid (ahx). ahxEP54 was synthesised using a solid phase peptide synthesis approach as described in section 6.2.5 and cleaved from the resin by incubating with hexafluoroisopropanol/DCM (1:4, v/v) for 15 min. The peptide was precipitated using diethyl ether, washed with diethyl ether and dried. Acetonitrile was added dropwise to 2 mg/mL of ahxEP54 in Na_2CO_3 at pH 9 until the peptide was completely dissolved, 200 µL of 1 mg/mL FITC in acetonitrile was then added to the peptide solution and stirred gently overnight at room temperature. The peptide was then lyophilised and subsequently treated with trifluoroacetic acid/triisopropylsilane/water (95:2.5:2.5, v/v/v) for 3 hours to remove the peptide protecting groups. The peptide was precipitated using cold diethyl ether, washed with diethyl ether, dried and lyophilised. The peptide was finally purified with HPLC (A = H_2O, B = acetonitrile, both with 0.1% formic acid, isocratic 5% B for 5 min, gradient 5-45% B over 5 min, isocratic 45% B for 20 min and gradient 40-80% B over 5 min) yielding FITC-ahxEP54 (>85%) after lyophilisation.

6.2.9 FITC-ahxEP54 binding assay

Binding assays were performed using FITC-ahxEP54 to characterise this fluorescent derivative of EP54. Increasing concentrations of FITC-ahxEP54 (1.25 – 40 µM) were competed against 100 nM of recombinant human C5a on 2 x 10^5 of either human PMNs or differentiated U937 cells using standard C5aR binding buffer consisting of 50 mM HEPES, 1 mM $CaCl_2$, 5 mM $MgCl_2$ and 0.5% BSA, pH 7.4

at 4°C for 1 hour with gentle shaking. The reaction was performed on 96-well filter plates in a total volume of 200 µL and was terminated by filtration. The cells were washed twice with ice-cold PBS. Fluorescence was measured in 200 µL of PBS with excitation and emission filters set at 490 and 515 nm respectively.

6.2.10 Myeloperoxidase release assay

Myeloperoxidase (MPO) activity was measured as described previously (Pulli *et al.*, 2013). The assay was performed in Hank's Balanced Salt Solution containing 0.1% gelatine at pH 7.4. Briefly, 20 µL of human PMNs (1 x 10^5 cells) were plated onto a 96-well plate. To these cells, 10 µL of cytochalasin B were added at a final concentration of 5 µg/mL and incubated at 37°C for 10 min. 10 µL of EP54 or FITC-ahxEP54 were then added at 4X concentration and incubated at 37°C for 5 min. 40 µL of 1.5 mM H_2O_2 was then added to the wells followed by 110 µL of 3,3',5,5'-tetramethylbenzidine (TMB) solution (2.9 mM TMB in 14.5% DMSO and 150 mM sodium phosphate buffer at pH 5.4). The plate was incubated at 37°C for 5 min. The reaction was stopped by addition of 50 µL of 2 M H_2SO_4. MPO activity was measured by reading absorbance at 450 nm.

6.2.11 ^{125}I[C5a] receptor binding assays

Radioligand binding assays were performed using Bolton-Hunter labelled ^{125}I[human C5a] (2200 Ci/mmol) (Perkin Elmer, Waltham, USA). Association binding assays were performed by adding 2 x 10^5 human PMNs to 50 mM HEPES, 1 mM $CaCl_2$, 5 mM $MgCl_2$ and 0.5% BSA, pH 7.4 at 4°C. Dissociation assays were

initially performed using 2 x 10^5 human PMNs in 50 mM HEPES, 1 mM $CaCl_2$, 5 mM $MgCl_2$ and 0.5% BSA, pH 7.4 for 1 hour at 4°C in a total reaction volume of 200 µL, on Millipore multiscreen 96 well filter plates fitted with HVPP 0.45 µm membranes. ^{125}I[C5a] dissociation was attempted with either 100 nM of recombinant human C5a or 1 mM of EP54. Since dissociation could not be initiated with these assay conditions, different buffers were tested. The buffers tested include 50 mM TRIS, 50 mM TRIS with 5 mM EGTA and 50 mM TRIS with 1 mM $CaCl_2$ and 5 mM $MgCl_2$, all in the presence of 0.5% BSA at pH 7.4. Dissociation binding assays were also attempted at room temperature without success. Other parameters tested include increasing the reaction volume from 200 to 500 µL. Since the reaction volume was too large for the filter plates, the assays were subsequently carried out in 5 mL polypropylene tubes and filtered through Whatman GF/C glass fibre filters soaked in 0.1% PEI. Dissociation assays were also carried out with CHO cell membranes expressing human C5aR without success.

6.2.12 cAMP assays

The ability of C5a to activate the C5aR and the inhibitory effect of PMX53 were measured using cAMP assays as described in section 2.2.8.2. CHO cells were transiently transfected with WT or mutant C5aR cDNA using jetPEI as described in section 2.2.7.1. On the day of the assay, cells were washed with 40 µL of HBSS and serum starved in 40 µL of HBSS, pH 7.4, for 30 min at 37°C and 5% CO_2 in the absence or presence of PMX53. 10 µL of IBMX and coelenterazine-h in HBSS were added to a final concentration of 40 µM and 5 µM respectively and incubated for 5 min at 37°C. 25 µL of increasing concentrations of purified or recombinant human

C5a were added to stimulate cAMP production. This was immediately followed by the addition of 25 µL of forskolin. Emission signals of RLuc and YFP were measured sequentially after a 5 min incubation at 37°C.

6.2.13 Homology modelling

A master alignment of closely related receptors was generated using Clustal Omega accessed through The European Bioinformatics Institute website (http://www.ebi.ac.uk/Tools/msa/clustalo/). Homology models of human and mouse C5aR were generated using MODELLER as implemented in Discovery Studio 4.0. Five homology models of human and mouse C5aR were built from four closely related receptors – neurotensin receptor NTSR1 (PDB ID 4GRV (White *et al.*, 2012)), chemokine receptor CXCR4 (PDB ID 3ODU and 4EA3 (Wu *et al.*, 2010)), opioid receptor-like OPRL1 (PDB ID 4EA3 (Thompson *et al.*, 2012)) and δ-opioid receptor OPRD1 (PDB ID 4RWD (Fenalti *et al.*, 2015)). The co-crystallised ligands were copied from the templates during model generation and the optimisation level was set to high. All other parameters were kept at default values. One hundred models were generated from each template. The highest scoring model from each template was minimised using the CHARMM force field to convergence using 10,000 steps and a gradient of 0.1 kcal mol^{-1} $Å^{-1}$. All other parameters were left at default values and the ligand from the template structure was left in the binding pocket during minimisation. The minimisation was performed in 3 steps starting with the hydrogens, followed by the side chains and the backbone of the receptor. During minimisation, the atoms that are not being minimised were constrained and kept immobile. After minimisation, the models were assessed for

fitness. This includes assessments of the stereo-chemical accuracy of the model such as Ramachandran analysis, analysis of bond planarities, lengths and angles, torsion angles and chirality of C_α-atoms.

6.2.14 Docking

Docking of PMX53 into the homology models of human and mouse C5aRs was carried out as described in section 2.2.9, using GOLD through Accelrys Discovery Studio 4.0. PMX53 was sketched in AccelrysDraw 4.1 and minimised using the CHARMM forcefield to convergence using 10,000 steps and a gradient of 0.1 kcal mol^{-1} $Å^{-1}$. The binding pocket for PMX53 was determined from the receptor cavities. All docking parameters were left at default values except for "Detect Cavity" and "Early Termination" which were set to false. Each docking run generated 100 poses which were then clustered at heavy atoms root mean square deviation of 3Å.

6.2.15 Data analysis

GraphPad Prism 6 was used to plot and analyse the binding and functional data. The association binding data were fitted by non-linear regression using one concentration of radioligand. Concentration response curves of agonists were fitted to the log (agonist) vs. response (three parameters) equation. The measure of PMX53 potency or the negative logarithm of the concentration of antagonist needed to shift the dose response curve by a factor of 2 (pA_2) was calculated from the Gaddum/Schild pEC_{50} shift equation $r = 1 + [B]/K_B$, where r is the ratio of the

agonist concentrations producing matched responses in the absence and presence of antagonist, B is the concentration of the antagonist and K_B is the equilibrium dissociation constant of the antagonist for the receptor. PMX53 inhibition curves were fitted to the log (inhibitor) vs. response (three parameters) equation. Statistical analyses were performed using one-way ANOVA followed by the Dunnett's multiple comparisons test.

6.3 Results

PMX53 is a non-competitive inhibitor of the C5aR with high affinity for human and rat, but not mouse C5aR (Woodruff *et al.*, 2001). The highest variation in the sequence of the C5aR from the three species can be found on the ECL2, suggesting that PMX53 may bind to the ECL2. In addition, the ECL2 of the C5aR has been shown to be a negative regulator of receptor function (Klco *et al.*, 2005). Taken together, these data suggest that PMX53 may be a negative allosteric modulator which binds to the ECL2 of the C5aR. To investigate this, homology models of human and mouse C5aR were built and PMX53 was subsequently docked into the homology models. The residues predicted to interact with PMX53 were then mutated and the interactions of PMX53 at the mutant receptors were characterised.

6.3.1 Binding assays

Binding assays are routinely used to study receptor-ligand interactions. The only commercially available labelled ligand for the C5aR is [^{125}I]C5a supplied by Perkin Elmer. Unfortunately, the availability of [^{125}I]C5a throughout this study was sporadic due to world-wide supply issues of recombinant human C5a. Therefore, the development of alternative labelled ligands was explored for further characterisation of the interactions between PMX53 and the C5aR.

Fluorescently-labelled ligands are attractive alternatives to radiolabelled ligands because they eliminate the potential hazards associated with radiation and may be particularly useful compared to isotopes with short half-lives, such as ^{125}I. One of the most popular peptide labelling strategies is to attach a fluorophore to a

reactive amino acid side chain, for example lysine, or to the N terminus of the peptide (Durroux *et al.*, 1999; Harikumar *et al.*, 2006; Hoffman *et al.*, 1996). In this study, EP54 (YSFKPMPLaR) was labelled with europium and fluorescein using two different methods. EP54 is a decapeptide agonist of the C5aR derived from the C-terminal tail of C5a and is commonly used in C5aR research (Finch *et al.*, 1997; March *et al.*, 2004; Ulrich *et al.*, 2000; Vogen *et al.*, 1999). In addition, its relative smaller size compared to C5a allows for a more targeted labelling.

6.3.1.1 EP54 synthesis

EP54 synthesis was performed using a standard solid phase peptide synthesis approach as described in section 6.2.5. Pure EP54 (> 85%) was obtained by HPLC. High resolution mass spectrometry was performed to confirm the molecular weight of EP54 – calculated mass 1209.65, mass found 1209.65. ^{1}H and ^{13}C NMR as well as Fourier transform infrared spectroscopy were also performed to characterise the peptide - ^{1}H-NMR (600 MHz, D_2O, δ) 0.83 (4H, d, *J* = 6.5 Hz), 0.87 (4H, d, *J* = 6.5 Hz), 1.26-1.30 (2H, m), 1.33 (4H, d, *J* = 7.2 Hz), 1.44-1.68 (13H, m), 1.78-2.02 (11H, m), 2.05 (3H, s), 2.17-2.25 (2H, m), 2.50-2.65 (3H, m), 2.88-3.00 (8H, m), 3.10 (3H, t, *J* = 7.6 Hz), 3.49-3.69 (7H, m), 3.73-3.77 (1H, m), 4.09-4.14 (1H, m), 4.24-4.28 (1H, m), 6.75 (2H, d, *J* = 8.7 Hz), 6.99 (2H, d, J = 8.7 Hz), 7.18-7.30 (6H, m); ^{13}C-NMR (151 MHz, D_2O, δ) 14.28. 16.75, 20.77, 21.67, 22.05, 24.20, 24.34, 24.54, 24.72, 26.36, 28.77, 29.33, 29.83, 36.21, 37.02, 39.16, 39.74, 40.56, 47.95, 49.81, 50.38, 50.84, 52.58, 54.22, 54.83, 54.94, 60.10, 60.45, 61.13, 115.80, 128.72, 129.19, 130.76, 155.07, 156.66, 170.23, 170.79, 170.99, 171.80, 172.14, 173.83, 173.86, 174.58, 177.88. IR (neat) cm^{-1} 3286.4 (m), 3202.3 (w), 3067.4 (w), 2956.7

(m), 2928 (w), 2872.6 (w), 1622.5 (s), 1540.6 (w), 1516.3 (m), 1452 (m), 1390.1 (w), 1341.5 (w), 1244.1 (m), 1211 (w), 1076 (s). The characterisation data confirmed the presence of EP54.

6.3.1.2 Europium labelling of EP54

Lanthanides such as europium (Eu^{3+}) have been used to label proteins and peptides for use in binding studies (Appell *et al.*, 1998; Gao *et al.*, 2004; Zhang *et al.*, 2012b). In this study, EP54 (YSFKPMPLaR) was labelled with the europium-chelate of N^1-(p-isothiocyanatobenzyl)-diethylenetriamine-N^1,N^2,-N^3,N^4-tetraacetic acid (DTTA). The isothiocyanate group reacts with primary aliphatic amino groups on the peptide at alkaline pH to form a covalent bond. For EP54, this means that the resulting labelled peptide will be a mixture of peptide labelled at the amino terminal tyrosine, at K4 and a combination of both. Following the labelling reaction, Eu-EP54 was separated from unlabelled EP54 using reversed phase high performance liquid chromatography. As a control, unlabelled EP54 was injected into the column and eluted approximately 17.5 min after sample injection (Figure 6.2A). This was confirmed by mass spectrometry where a peptide with a molecular weight of 1209 Da was detected in the sample. Compared to the chromatogram of the unlabelled peptide, two additional peaks were present in the crude Eu-EP54 sample at 9 and 19 min (Figure 6.2B). Unfortunately, mass spectrometry performed on the eluted samples did not provide conclusive evidence of the presence of labelled EP54. The peaks were then collected and assayed for Eu^{3+} fluorescence. From this assay, sample 9, 19 and 24 were further tested in competition binding assays as they had a large fluorescence reading

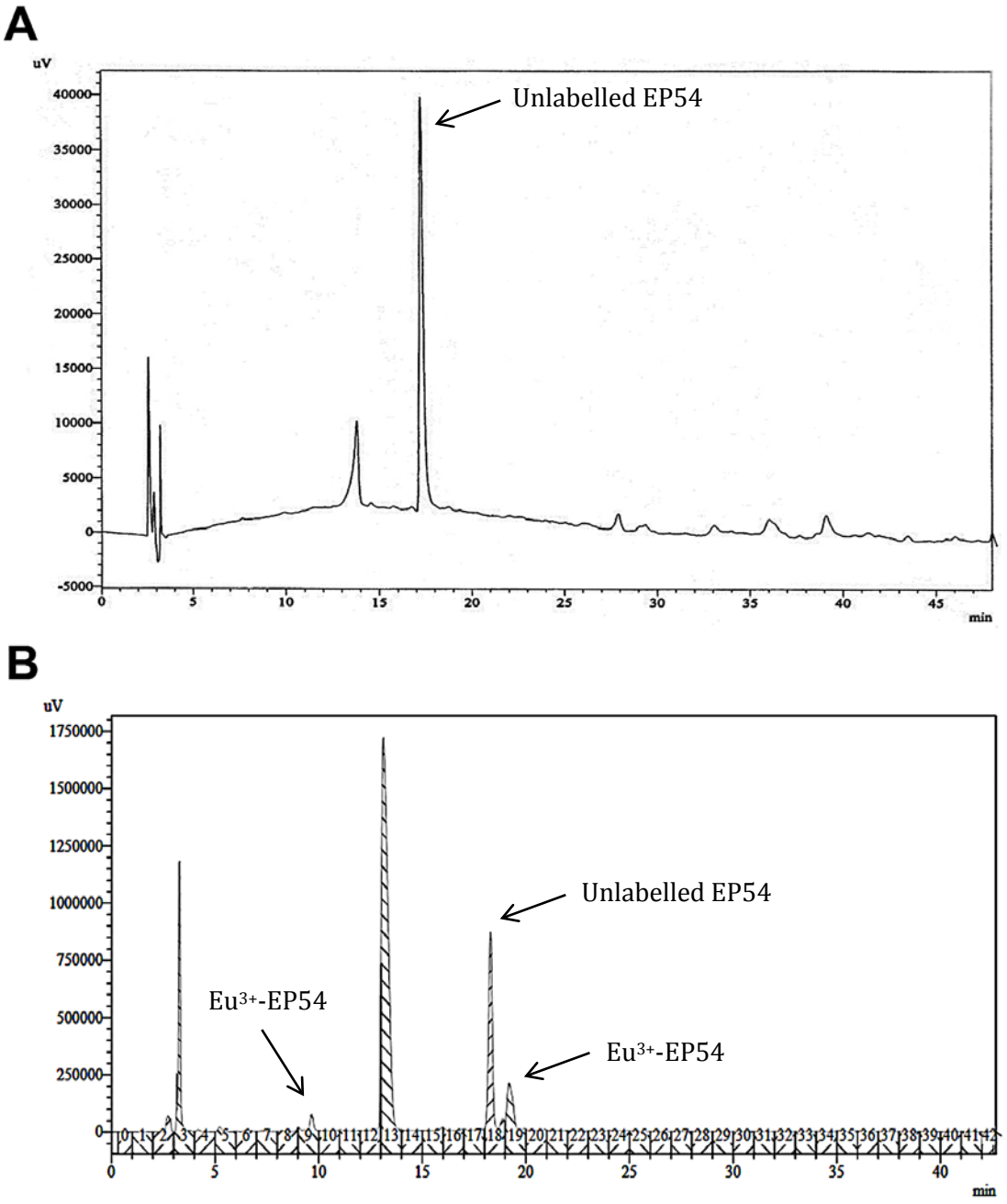

Figure 6.2 HPLC chromatogram of EP54 and Eu-EP54

Reversed phase HPLC was performed using purified EP54 (A) and crude Eu-EP54 (B). The HPLC was performed with a 1 mL/min linear gradient of 10 to 60% B over 45 min (A = 20 mM triethylammonium acetate, pH 7.2, in H_2O; B = 20 mM triethylammonium acetate, pH 7.2, in 90% acetonitrile).

(Figure 6.3). Sample numbers correspond to the elution time on the HPLC column.

Of the three samples tested, only sample 19 displayed specific binding to human C5aR as shown by a substantially larger fluorescence signal after washing to remove unbound ligand (Figure 6.4). Although sample 9 and 24 had large fluorescence signals in the Eu^{3+} fluorescence assay, they did not display specific binding to human C5aR (Figure 6.4). It is possible that sample 9 and 24 contained EP54 that has been labelled at K4, since this residue has previously been shown to be important for the binding of EP54 at the C5aR (Vogen *et al.*, 1999). Further chemical characterisation needs to be performed on sample 19 to confirm the species present.

Eu^{3+} labelling using this commercial kit required a large amount of peptide and resulted in poor yield of the fluorescent peptide which showed specific binding to the C5aR. This method of labelling is also not cost effective as fluorescence measurements using this method rely on the use of proprietary enhancement solution to release the europium from the DTTA cage. Therefore, an alternative method of fluorescent labelling was sought.

6.3.1.3 Fluorescein labelling of EP54

An alternative method to obtain specific labelling of EP54 is to perform fluorescence conjugation on the amino terminus of the peptide in the presence of a protecting group at the lysine residue to avoid non-specific labelling. EP54 was fluorescently labelled with fluorescein isothiocyanate (FITC) on the amino terminus of EP54 in the presence of a six-carbon linker aminohexanoic acid (ahx).

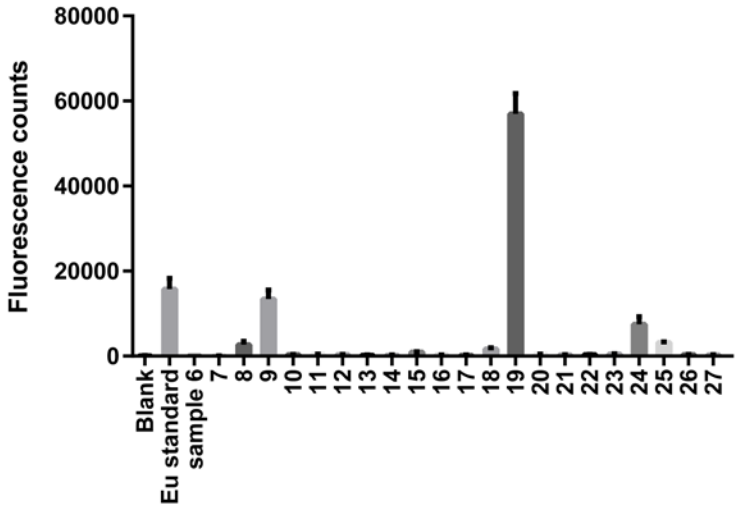

Figure 6.3 Fluorescence assay of crude Eu-EP54 HPLC fractions

Samples collected from the HPLC fractions of crude Eu-EP54 were assayed for Eu^{3+} fluorescence. Samples were diluted 1:10,000 in a total volume of 200 µL in the europium enhancement solution and incubated for 15 min with gentle shaking at room temperature. Fluorescence was measured using 355 nm excitation and 620 nm emission filter.

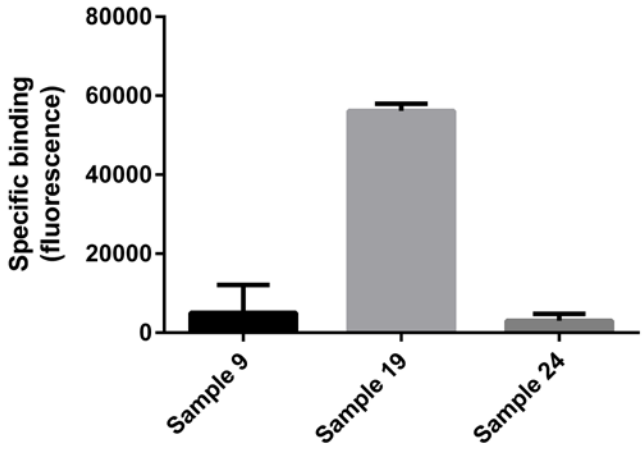

Figure 6.4 Competition binding using Eu-EP54 HPLC fractions

HPLC fractions from crude Eu-EP54 were competed against unlabelled EP54. Labelled peptide was incubated with 2 x 10^4 CHO cells stably transfected with human C5aR in a total volume of 200 µL for 1 hour at 4°C in the presence or absence of 1 mM of unlabelled EP54. Reaction was stopped by filtration, washed and the samples were assayed for fluorescence by addition of enhancement solution. Each bar is the mean ± SEM of specific binding (total binding minus binding in the presence of unlabelled peptide) from a single experiment preformed in duplicate.

This linker was introduced to minimise the potential of the fluorophore to interfere with the binding of EP54 at the C5aR. AhxEP54 has been shown to have similar affinity and potency to that of EP54 in human PMNs (Finch, 1998). FITC-ahxEP54 was purified from unlabelled ahxEP54 using HPLC. FITC-ahxEP54 was eluted at 16.8 min following sample injection and unlabelled ahxEP54 was eluted prior to FITC-ahxEP54 at 16.2 min (Figure 6.5). Mass spectrometry performed on the largest peak confirmed the presence of FITC-ahxEP54 with a molecular mass of 1710.8 g/mol. In addition, fluorescence spectroscopy was also performed on FITC-ahxEP54 to confirm the presence of the FITC. FITC-ahxEP54 produced a peak emission wavelength at 515 nm when excited at 480 nm, which is a characteristic excitation and emission spectrum of FITC.

Binding assays and myeloperoxidase release assays were performed to characterise FITC-ahxEP54. Unfortunately, no specific binding was detected with FITC-ahxEP54. Functional assay measuring myeloperoxidase release from human PMNs showed that the potency of FITC-ahxEP54 was decreased by approximately 30 fold compared to the unlabelled peptide EP54 (Figure 6.6). It is likely that the addition of FITC at this position disrupts the interaction between EP54 and the C5aR. A possible solution to this problem would be to optimise the length of the FITC-EP54 linker. Alternatively, N-terminally labelled Eu^{3+}-EP54 could be synthesised, eliminating the need to separate the three species of Eu^{3+}-EP54 generated using the isothiocyanate reaction.

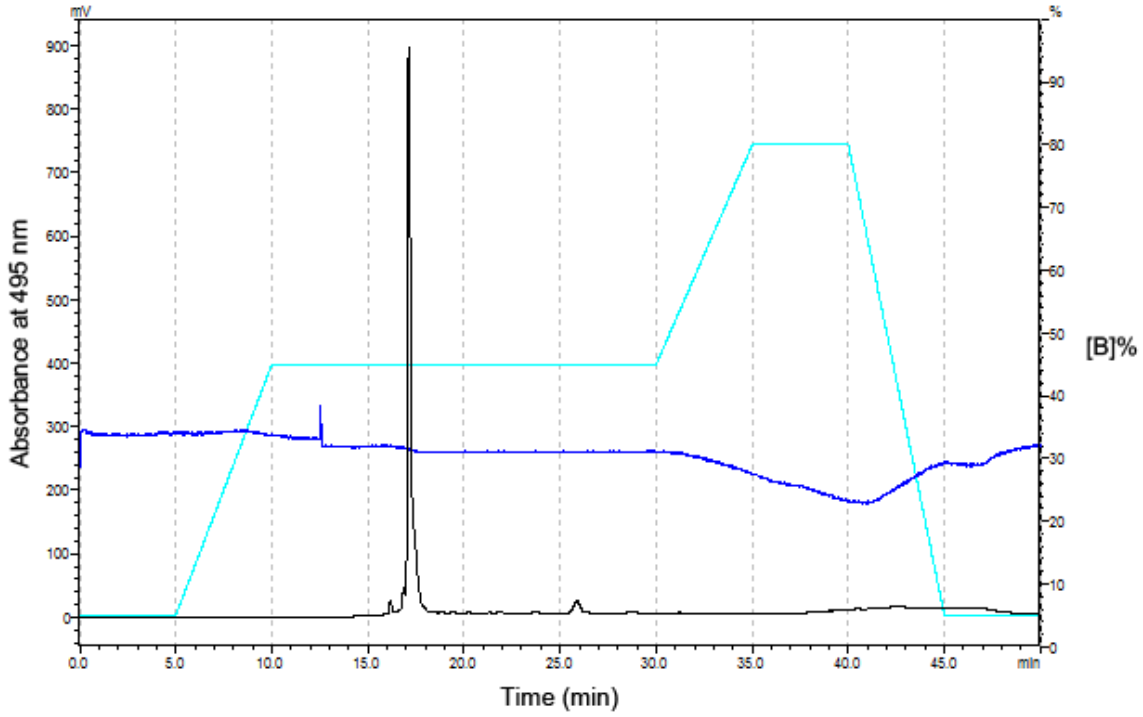

Figure 6.5 HPLC chromatogram of FITC-ahxEP54

Reversed phase HPLC was performed to purify FITC-ahxEP54. The HPLC was performed with a flow rate of 1 mL/min, isocratic 5% B for 5 min, gradient 5-45% B over 5 min, isocratic 45% B for 20 min and gradient 40-80% B over 5 min (A = H_2O, B = acetonitrile, both with 0.1% formic acid).

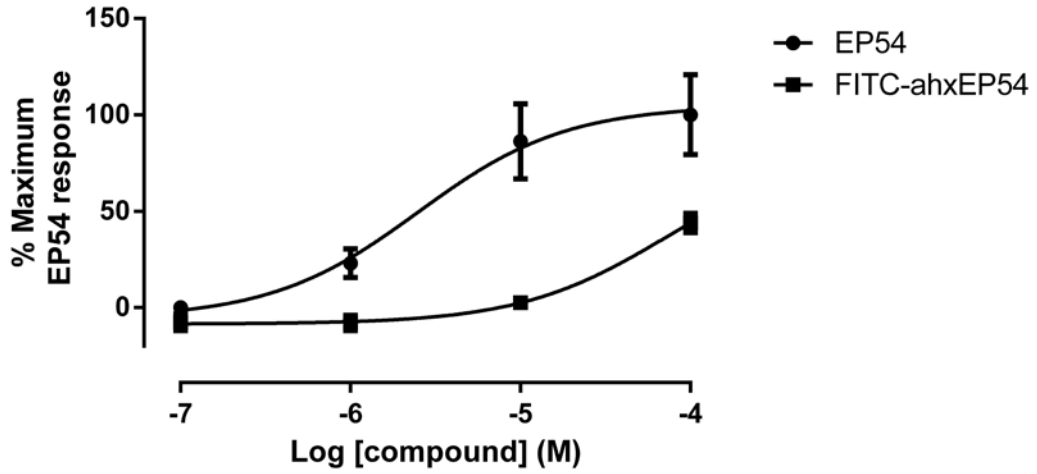

Figure 6.6 FITC-ahxEP54 myeloperoxidase release assay

Myeloperoxidase release following stimulation of human PMNs with unlabelled EP54 and FITC-ahxEP54 was measured. Briefly, 1 x 10^5 PMNs were pre-incubated with 5 μg/mL of cytochalasin B in Hank's balanced salt solution at pH 7.4 for 10 min. The cells were then incubated with increasing concentrations of EP54 or FITC-ahxEP54 for a further 5 min. To this, 1.5 mM of H_2O_2 was added followed by tetramethylbenzidine (TMB) solution containing 2.9 mM of TMB in 14.5% DMSO and 150 mM of sodium phosphate solution at pH 5.4 and the plate was incubated for a further 5 min. The reaction was terminated by addition of 2M H_2SO_4. Absorbance was then measured at 450 nM. Data are presented as the mean ± SEM of a single experiment performed in triplicate.

6.3.1.4 [^{125}I]C5a binding assay

Dissociation kinetics binding assays are commonly used to detect allosterism. To investigate the non-competitive action of PMX53, dissociation kinetics binding assays were performed. Although [^{125}I]C5a is routinely used in competition binding assays (Finch *et al.*, 1997; Sumichika *et al.*, 2002; Woodruff *et al.*, 2001), only one study had reported the binding kinetics of [^{125}I]C5a at human PMNs (Huey and Hugli, 1985). [^{125}I]C5a associated with the C5aR but did not significantly dissociate from the receptor despite extensive optimisation of the assay conditions (Figure 6.7, Figure 6.8). C5aR binding assays reported in the literature were performed using a buffer which comprises of 50 mM HEPES, 1 mM $CaCl_2$, 5 mM $MgCl_2$ and 0.5% BSA at pH 7.4, and this buffer was the buffer initially used for the dissociation assays in this study. The assay parameters were then changed in an attempt to optimise [^{125}I]C5a dissociation which included changing the buffer, reaction volume, cell numbers, temperature, the unlabelled ligand used as well as using cell membranes instead of whole cells. The other buffers used include 50 mM TRIS, 50 mM TRIS with 5 mM EGTA and lastly 50 mM TRIS with 1 mM $CaCl_2$ and 5 mM $MgCl_2$, all in the presence of 0.5% BSA. Unfortunately, none of the conditions tested resulted in a timely dissociation of [^{125}I]C5a (Figure 6.7). The association of [^{125}I]C5a at the C5aR could be measured in the initial buffer used, using either $2x10^5$ (Figure 6.8A) or $1x10^4$ (Figure 6.8B) human PMNs, as well as in 50 mM TRIS buffer using CHO cell membranes expressing human C5aR (Figure 6.8C), with maximum binding observed at approximately 20 min. These association data show the specific binding of [^{125}I]C5a to the C5aR expressed in human PMNs and in the CHO cell membranes.

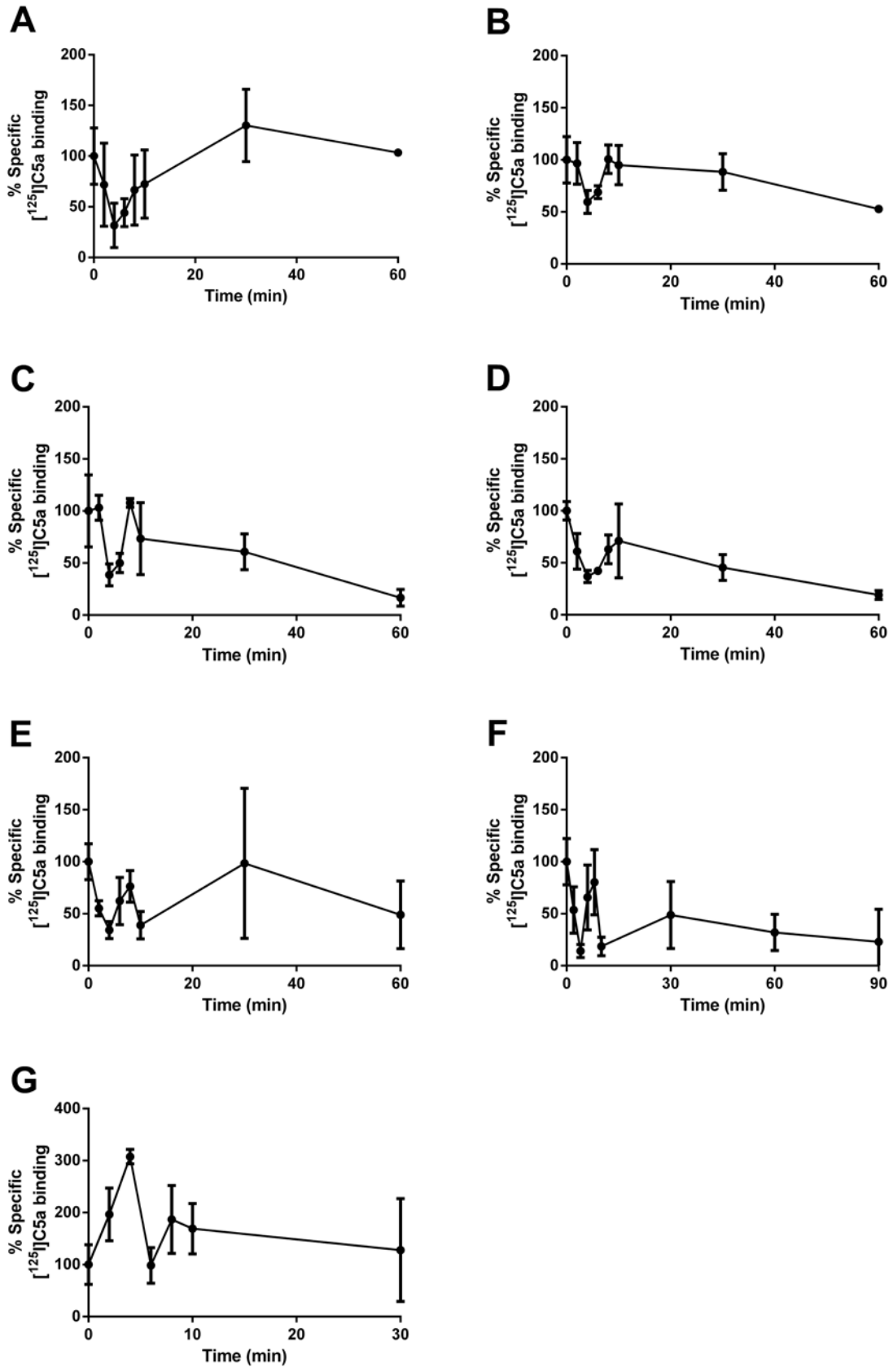
A
B
C
D
E
F
G
% Specific [125I]C5a binding
Time (min)

Figure 6.7 [^{125}I] C5a dissociation binding assays

Dissociation binding assays were performed using the following conditions: (A) 2 x 10^5 human PMNs in 50 mM HEPES, 1 mM $CaCl_2$, 5 mM $MgCl_2$ and 0.5% BSA, pH 7.4 at 4°C using 50 nM of recombinant human C5a (rhC5a) as the unlabelled ligand to prevent [^{125}I]C5a re-association in a total volume of 200 µL, (B) 1 x 10^4 human PMNs in 50 mM HEPES, 1 mM $CaCl_2$, 5 mM $MgCl_2$ and 0.5% BSA, pH 7.4 at 4°C using 50 nM of rhC5a as the unlabelled ligand in a total volume of 200 µL, (C) CHO cell membranes stably expressing human C5aR in 50 mM TRIS, 1 mM $CaCl_2$, 5 mM $MgCl_2$ and 0.5% BSA, pH 7.4 at room temperature using 50 nM of rhC5a as the unlabelled ligand in a total volume of 200 µL, (D) CHO cell membranes stably expressing human C5aR in 50 mM TRIS, 1 mM $CaCl_2$, 5 mM $MgCl_2$ and 0.5% BSA, pH 7.4 at room temperature using 10 µM of EP54 in a total volume of 200 µL, (E) CHO cell membranes stably expressing human C5aR in 50 mM TRIS, 1 mM $CaCl_2$, 5 mM $MgCl_2$ and 0.5% BSA, pH 7.4 at room temperature using 10 µM of EP54 in a total volume of 500 µL, (F) CHO cell membranes stably expressing human C5aR in 50 mM TRIS, 5 mM EGTA and 0.5% BSA, pH 7.4 at room temperature using 10 µM of EP54 in a total volume of 500 µL and (G) CHO cell membranes stably expressing human C5aR in 50 mM HEPES, 1 mM $CaCl_2$, 5 mM $MgCl_2$ and 0.5% BSA, pH 7.4 at 4°C using 50 nM of rhC5a as the cold ligand. In these assays, human PMNs or CHO cells stably expressing human C5aR were pre-incubated with 50 pM of [^{125}I]C5a for 1 hour. Subsequent [^{125}I]C5a re-association was inhibited using ligands as indicated. Data are presented as the mean ± SEM of a single experiment performed in duplicate or triplicate.

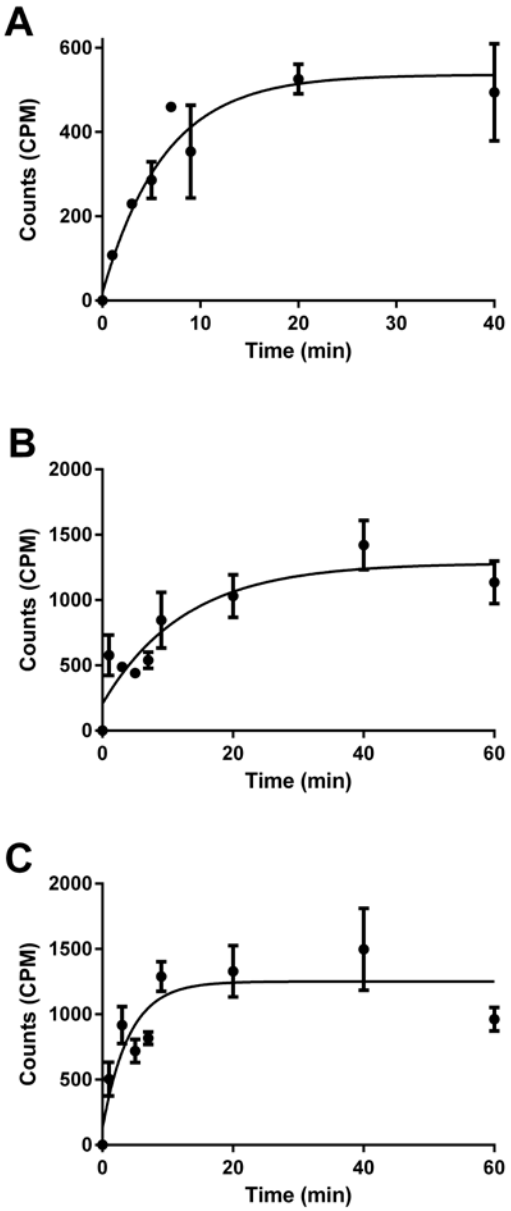

Figure 6.8 [^{125}I] C5a association binding assays

[^{125}I]C5a association binding assays were performed using (A) 2 x 10^5 human PMNs in 50 mM HEPES, 1 mM $CaCl_2$, 5 mM $MgCl_2$ and 0.5% BSA, pH 7.4 at 4°C, (B) 1 x 10^4 human PMNs in 50 mM HEPES, 1 mM $CaCl_2$, 5 mM $MgCl_2$ and 0.5% BSA, pH 7.4 at 4°C and (C) membrane preparation of CHO cells stably transfected with human C5aR in 50 mM TRIS, 1 mM $CaCl_2$, 5 mM $MgCl_2$ and 0.5% BSA, pH 7.4 at room temperature. In these assays, PMNs or membranes were added to 50 pM of [^{125}I]C5a at the indicated time. Data are presented as the mean ± SEM of a single experiment performed in duplicate.

6.3.2 cAMP assays

In the absence of binding assays, cAMP assays were used to characterise the binding and potency of PMX53 at WT C5a. The C5aR primarily couples to the $G_{\alpha i}$ G protein which inhibits the function of adenylate cyclase, resulting in decreased intracellular cAMP levels (Skokowa *et al.*, 2005; Vanek *et al.*, 1994). In these assays, the ability of C5a to inhibit forskolin-induced cAMP production and the ability of PMX53 to inhibit the action of C5a were measured in CHO cells transiently transfected with C5aR. Due to supply issues with commercially available recombinant human C5a, both purified human (Complement Technology Inc., Texas, USA) and recombinant C5a (Sigma Aldrich, St Louis, USA) were used in this study as indicated. In contrast to purified human C5a, recombinant human C5a is not glycosylated at position N_{64} (Fernandez and Hugli, 1978). The potencies of the purified human C5a and recombinant human C5a were identical (pEC_{50} (M) purified human C5a = 10.2 ± 0.2, recombinant human C5a = 10.4 ± 0.2, mean ± SEM, n = 4-7).

6.3.2.1 Activation of human and mouse C5aR by C5a

The ability of C5a to activate $G_{\alpha i}$ was investigated using the cAMP assay. Purified human C5a has the same potency on WT human and mouse C5aR (pEC_{50} (M) human C5aR = 10.2 ± 0.2, mouse C5aR = 10.5 ± 0.2, mean ± SEM, n = 4) (Figure 6.9). However, the maximum response of purified human C5a was significantly lower at the mouse receptors compared to the human receptors ($P < 0.05$) (Emax (% forskolin) human C5aR = 60.1 ± 1.7, mouse C5aR = 32.1 ± 4.5, mean ± SEM, n = 4) (Figure 6.9). Recombinant human C5a has been shown to have the same affinity,

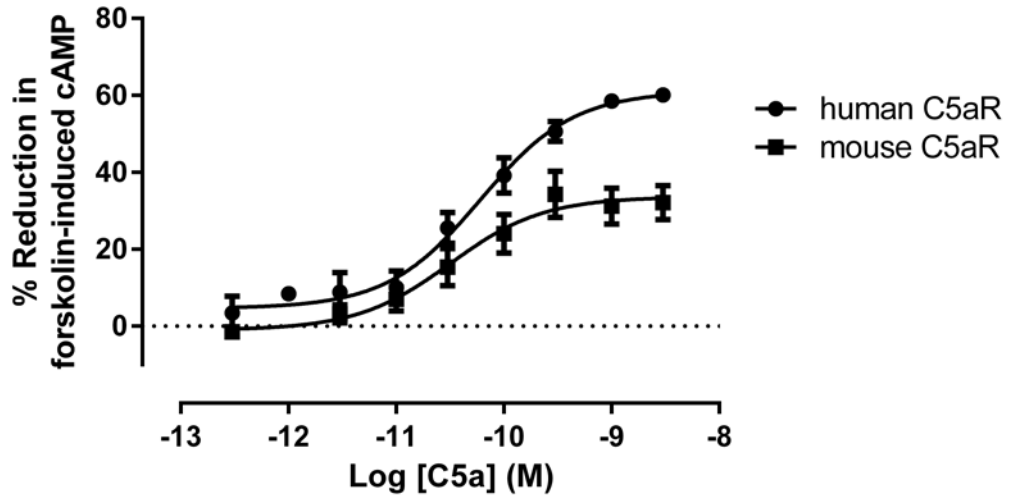

Figure 6.9 The potency and efficacy of C5a at human and mouse C5aR

CHO cells were transiently transfected with either wild type human (A) or mouse (B) C5aR and the BRET cAMP sensor CAMYEL. cAMP levels were measured after a 5 min incubation of cells with increasing concentrations of purified human C5a and 10 μM of forskolin in the presence of 40 μM of IBMX. Data were normalised to stimulation with 10 μM forskolin (0%) and unstimulated cells (100%). Data are presented as the mean ± SEM of 3-4 independent experiments performed in triplicate.

potency and efficacy for human and mouse C5aR (Schatz-Jakobsen *et al.*, 2014; Woodruff *et al.*, 2001). The mouse C5aR construct used in the current study contained an mCherry tag on the C-terminal domain of the receptor. It is therefore possible that the decrease in the maximum response of C5a is caused by quenching of the luminescence signal produced by the BRET sensors since the emission spectrum of YFP (emission max 535 nm) overlaps with the excitation spectrum of mCherry (excitation max 587 nm).

6.3.2.2 The potency of PMX53 at human and mouse C5aR

The ability of PMX53 to inhibit C5a-mediated receptor activation was also investigated using the cAMP assay. In this assay, the pIC_{50} (M) value for PMX53 inhibition of receptor activation by 0.3 nM of purified human C5a (E_{max} 80%) on the WT human C5aR was 5.8 ± 0.1 (mean ± SEM, n = 6) (Figure 6.10). Unfortunately, the same assay could not be performed on the WT and mutant mouse C5aR due to the small window of detection. This study needs to be repeated using the mouse C5aR construct without the mCherry tag.

6.3.2.3 Inhibition of C5a-mediated receptor activation by PMX53

PMX53 is described in the literature as a non-competitive antagonist of the C5aR in studies investigating myeloperoxidase release following stimulation of PMNs with C5a as a measure of receptor activation (March *et al.*, 2004; Paczkowski *et al.*, 1999). In this study measuring cAMP production, PMX53 behaved as a competitive antagonist at the C5aR (Figure 6.11). At the concentrations tested of

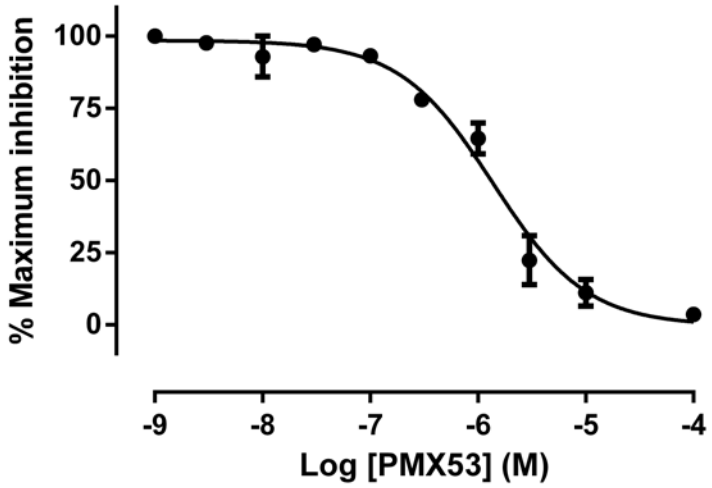

Figure 6.10 PMX53 inhibition of C5a-mediated cAMP production

CHO cells were transiently transfected with wild type human C5aR and the BRET cAMP sensor CAMYEL. The cells were pre-incubated with increasing concentrations of PMX53 for 30 min. cAMP levels were measured after a 5 min incubation with 0.3 nM of purified human C5a and 10 μM of forskolin in the presence of 40 μM of IBMX. Data was normalised to the maximum response obtained with 0.3 nM of purified human C5a. Data are presented as the mean ± SEM of 5-6 independent experiments performed in triplicate.

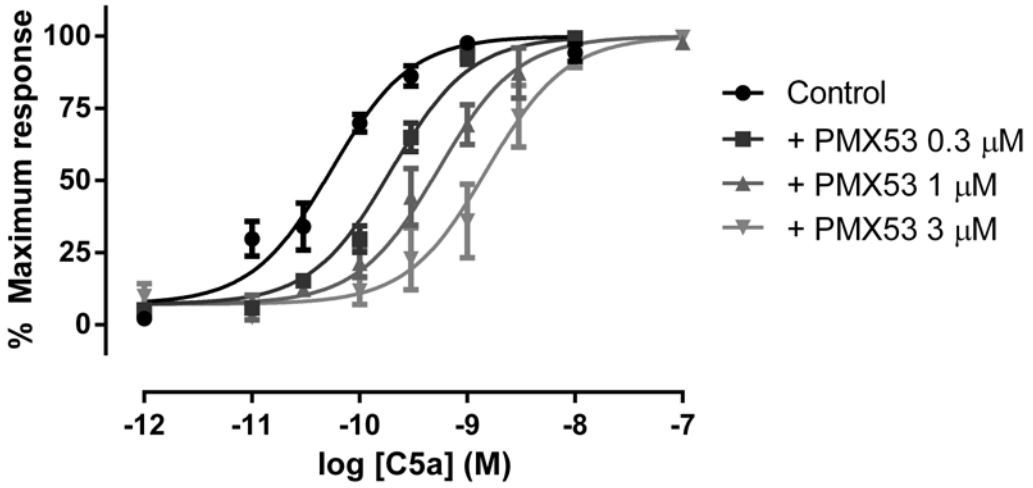

Figure 6.11 Inhibition of C5a-mediated receptor activation by PMX53

Concentration response curves for recombinant human C5a were obtained in the absence or presence of increasing concentrations of PMX53. CHO cells were transiently transfected with wild type human C5aR and the BRET cAMP sensor CAMYEL. The cells were pre-incubated with PMX53 for 30 min. cAMP levels were measured after a 5 min incubation with increasing concentrations of recombinant human C5a and 10 μM of forskolin in the presence of 40 μM of IBMX. Data was normalised to maximum stimulation with C5a. Data are presented as the mean ± SEM of 5 independent experiments performed in triplicate.

0.3 to 3 μM, PMX53 caused a rightward parallel shift of the C5a concentration response curve (C5a pEC_{50} (M) control = 10.3 ± 0.1, +PMX53 0.3 μM = 9.7 ± 0.1, +PMX53 1 μM = 9.4 ± 0.2, +PMX53 3 μM = 8.9 ± 0.2, mean ± SEM, n = 5). The pA_2 value (M) calculated using the Gaddum/Schild pEC_{50} shift equation was 6.9 ± 0.1 with a Hill slope of 1.

6.3.3 C5aR homology models

To date, a crystal structure of the C5aR is not publicly available. Therefore, homology models of human and mouse C5aR were built for use in the docking of PMX53. Homology modelling remains the most popular and successful method for generating 3D models of GPCRs (Kufareva *et al.*, 2014). Briefly, homology model generation consists of the following steps: identification of template protein, sequence alignment between target and template protein, model generation and refinement and model quality assessment.

The structures of close relatives of the C5aR that have been solved and were available in the Protein Data Bank (PDB) (http://www.rcsb.org/pdb/) at the time of this study included the chemokine receptors CXCR4 and CCR5 and all four subtypes of the opioid receptors. Although neurotensin receptor 1 (NTSR1) is not closely related to the C5aR by sequence homology, recent re-classification of family A GPCRs by ligand similarity has placed NTSR1 as one of the closest relatives of the C5aR (Figure 1.3) (Lin *et al.*, 2013). This classification of GPCRs was used as a basis for template selection. Five homology models of human and mouse C5aR were constructed based on five crystal structures of four closely related receptors. The template receptors used were the NTSR1 (PDB ID 4GRV), the chemokine receptor

CXCR4 (PDB ID 3ODU and 3OE0), the opioid receptor-like OPRL1 (PDB ID 4EA3) and the δ-opioid receptor OPRD1 (PDB ID 4RWD). Two structures of CXCR4 were used in this study – one crystallised in the presence of a small molecule antagonist (PDB ID 3ODU) and the other in the presence of a 16-amino acid peptide antagonist (PDB ID 3OE0) to investigate if the size of the ligand in the template receptor influences the quality of the homology model. The CCR5 receptor was not used as a template because it is relatively distant to the C5aR according to receptor classification based on both sequence and ligand similarity. The details of the template receptors are listed in Table 6.2.

Following template selection, a master alignment was generated using Clustal Omega from closely related receptors to increase the accuracy of the alignment. The master alignment was generated by alignment of the following receptors: hC5aR, mC5aR, rC5aR, C5aR2, formyl peptide receptor 1 (hFPR1), formyl peptide receptor-like 1 (hFPRL1), opioid receptor-like 1 (hORL1), δ-opioid receptor (hODRD1), κ-opioid receptor (hOPRK1), μ-opioid receptor (hOPRM1), chemokine receptors hCCR5, hCXCR1 and hCXCR4 and the rat neurotensin receptor 1 (rNSTR1). The C3a receptor was not included in the master alignment because it has an unusually large ECL2. The sequence alignment was further refined by hand editing to maximise the alignment of conserved sequences and to minimise gaps. The master alignment is shown in Figure 6.12**.**

The homology models of human and mouse C5aR were generated using MODELLER as implemented in Discovery Studio 4.0. The highest scoring model (out of 100) from each template was then minimised using the CHARMM force field. The models were also checked for abnormalities in the protein structure


rNTSR1 ------MHLNSSVPQGTPGEPDAQPFSGPQSEMEATFLALSLSNGSGNTSESDTAGPNSDLDVNTDIYSKVLVTAIYLA 73
hFPR1 ----------METNSSLPTNISGGTPAVSAGYLFLDIITYLVFAV 35
hFPRL1 ----------METNFSTPLNEYEEVSYESAGYTVLRILPLVVLGV 35
hC5aR2 ----------MGNDSVSYEYGDYSDLSDRPVDCLDGACLAIDPLRVAPLPLYAA 44
hC5aR1 ----------MDSFNYTTPDYGHYDDKDTLDLNTPVDKTSNTLRVPDILALVIFAV 46
mC5aR ----------MDPIDNSSFEINYDHYGTMDPNIPADGIHLPKRQPGDVAALIIYSV 46
rC5aR ----------MDPISNDSSEITYDYSDGTPNPDMPADGVYIPKMEPGDIAALIIYLA 47
hOPRL1 ----------MEPLFPAPFWEVIYGSHLQGNLSLLSPNHSLLPPHLLLNASHGAFLPLGLKVTIVGLYLA 60
hOPRK1 ----------MDSPIQIFRGEPGPTCAPSACLPPNSSAWFPGWAEPDSNGSAGSEDAQLEPAHISPAIPVIITAVYSV 68
hOPRD1 ----------MEPAPSAGAELQPPLFANASDAYPSACPSAGANASGPPGARSASSLALAIAITALYSA 58
hOPRM1 MDSSAAPTNASNCTDALAYSSCSPAPSPGSWVNLSHLDGNLSDPCGPNRTDLGGRDSLCPPTGSPSMITAITIMALYSI 79
hCCR5 ----------MDYQVSSPIYDINYYTSEPCQKINVKQIAARLLPPLYSL 39
hCXCR4 ----------MEGISSIPLPLLQIYTSDNYTEEMGSGDYDSMKEPCFREENANFNKIFLPTIYSI 47
hCXCR1 ----------MSNITDPQMWDFDDLNFTGMPPADEDYSPCXLETETLNKYVVIIAYAL 48
rNTSR1 LFVVGTVGNSVTAFTLARKKSLQSLQSTVHYHLGSLALSDLLILLLAMPVELYNFIWVHHPWAFGDAGCRGYYFLRDAC 152
hFPR1 TFVLGVLGNGLVIWVAGFR-MTHTVTTISYL---NLAVADFCFT-STLPFFMV-RKAMGGHWPFGWFLCKFVFTIVDIN 108
hFPRL1 TFVLGVLGNGLVIWVAGFR-MTRTVTTICYL---NLALADFSFT-ATLPFLIV-SMAMGEKWPFGWFLCKLIHIVVDIN 108
hC5aR2 IFLVGVPGNAMVAWVAGKV-ARRRVGATWLL---HLAVADLLCC-LSLPILAV-PIARGGHWPYGAVGCRALPSIILLT 117
hC5aR1 VFLVGVLGNALVVWVTAFE-AKRTINAIWFL---NLAVADFLSC-LALPILFT-SIVQHHHWPFGGAACSILPSLILLN 119
mC5aR VFLVGVPGNALVVWVTAFE-ARRAVNAIWFL---NLAVADLLSC-LALPVLFT-TVLNHNYWYFDATACIVLPSLILLN 119
rC5aR VFLVGVTGNALVVWVTAFE-AKRTVNAIWFL---NLAVADLLSC-LALPILFT-SIVKHNHWPFGDQACIVLPSLILLN 120
hOPRL1 VCVGGLLGNCLVMYVILRHTKMKTATNIYIF---NLALADTLVL-LTLPFQGT-DILL-GFWPFGNALCKTVIAIDYYN 133
hOPRK1 VFVVGLVGNSLVMFVIIRYTKMKTATNIYIF---NLALADALVT-TTMPFQST-VYLM-NSWPFGDVLCKIVISIDYYN 141
hOPRD1 VCAVGLLGNVLVMFGIVRYTKMKTATNIYIF---NLALADALAT-STLPFQSA-KYLM-ETWPFGELLCKAVLSIDYYN 131
hOPRM1 VCVVGLFGNFLVMYVIVRYTKMKTATNIYIF---NLALADALAT-STLPFQSV-NYLM-GTWPFGTILCKIVISIDYYN 152
hCCR5 VFIFGFVGNMLVILILINCKRLKSMTDIYLL---NLAISDLFFL-LTVPFWAH--YAA-AQWDFGNTMCQLLTGLYFIG 111
hCXCR4 IFLTGIVGNGLVILVMGYQKKLRSMTDKYRL---HLSVADLLFV-ITLPFWAV--DAV-ANWYFGNFLCKAVHVIYTVN 119
hCXCR1 VFLLSLLGNSLVMLVILYSRVGRSVTDVYLL---NLALADLLFA-LTLPIWAA--SKV-NGWIFGTFLCKVVSLLKEVN 120
1.50
2.50

```
rNTSR1    TYATALNVASLSVERYLAICHPFKAKTLMSRSRTKKFISAIWLASALLAIPMLFTMGLQNRSGDGTHPGGLVCTPIVDT  231
hFPR1     LFGSVFLIALIALDRCVCVLHPVWTQNHRTVSLAKKVIIGPWVMALLLTLPVIIRVTTVPGK-----TGTVACTFNFSP  182
hFPRL1    LFGSVFLIGFIALDRCICVLHPVWAQNHRTVSLAMKVIVGPWILALVLTLPVFLFLTTVTIP-----NGDTYCTFNFAS  182
hC5aR2    MYASVLLLAALSADLCFLALGPAWWSTVQRACGVQVACGAAWTLALLLTVPSAIYRRLHQEH----FPARLQCVVDYGG  192
hC5aR1    MYASILLLATISADRFLLVFKPIWCQNFRGAGLAWIACAVAWGLALLLTIPSFLYRVVREEY----FPPKVLCGVDYSH  194
mC5aR     MYASILLLATISADRFLLVFKPIWCQKVRGTGLAWMACGVAWVLALLLTIPSFVYREAYKDF----YSEHTVCGINYGG  194
rC5aR     MYSSILLLATISADRFLLVFKPIWCQKFRRPGLAWMACGVTWVLALLLTIPSFVFRRIHKDP----YSDSILCNIDYSK  195
hOPRL1    MFTSTFTLTAMSVDRYVAICHPIRALDVRTSSKAQAVNVAIWALASVVGVPVAIMGSAQVED------EEIECLVEIPT  206
hOPRK1    MFTSIFTLTMMSVDRYIAVCHPVKALDFRTPLKAKIINICIWLLSSSVGISAIVLGGTKVRE----DVDVIECSLQFPD  216
hOPRD1    MFTSIFTLTMMSVDRYIAVCHPVKALDFRTPAKAKLINICIWVLASGVGVPIMVMAVTRPRD------GAVVCMLQFPS  204
hOPRM1    MFTSIFTLCTMSVDRYIAVCHPVKALDFRTPRNAKIINVCNWILSSAIGLPVMFMATTKYRQ------GSIDCTLTFSH  225
hCCR5     FFSGIFFIILLTIDRYLAVVHAVFALKARTVTFGVVTSVITWVVAVFASLPGIIFTRSQKEG------LHYTCSSHFPY  184
hCXCR4    LYSSVLILAFISLDRYLAIVHATNSQRPRKLLAEKVVYVGVWIPALLLTIPDFIFANVSEAD----D--RYICDRFYPN  192
hCXCR1    FYSGILLLACISVDRYLAIVHATRTLTQKRHL-VKFVCLGCWGLSMNLSLPFFLFRQAYHPN----N-SSPVCYEVLGN  193
                       3.50                          4.50

rNTSR1    -------------ATVKVVIQVNTFMSFLFPMLVISILNTVIANKLTVMVHQAAEQGRVCTVGTHNGLEHSTFNMTIEP  297
hFPR1     WTNDPKERINVAVAMLTVRGIIRFIIGFSAPMSIVAVSYGLIATKIHKQGLI-----------------------KS--  236
hFPRL1    WGGTPEERLKVAITMLTARGIIRFVIGFSLPMSIVAICYGLIAAKIHKKGMI-----------------------KS--  236
hC5aR2    ---SS--------STENAVTAIRFLFGFLGPLVAVASCHSALL--CWAARRC-----------------------RP--  233
hC5aR1    ---DK--------RRERAVAIVRLVLGFLWPLLTLTICYTFILLRTWSRRAT-----------------------RS--  237
mC5aR     ---GSF-------PKEKAVAILRLMVGFVLPLLTLNICYTFLLLRTWSRKAT-----------------------RS--  238
rC5aR     ---GPF-------FIEKAIAILRLMVGFVLPLLTLNICYTFLLIRTWSRKAT-----------------------RS--  239
hOPRL1    ---PQD-------YWGPVFAICIFLFSFIVPVLVISVCYSLMIRRLRGVRLL-----------------------SGSR  252
hOPRK1    ---DDYS------WWDLFMKICVFIFAFVIPVLIIIVCYTLMILRLKSVRLL-----------------------SGSR  263
hOPRD1    ---PSW-------YWDTVTKICVFLFAFVVPILIITVCYGLMLLRLRSVRLL-----------------------SGSK  250
hOPRM1    ---PTW-------YWENLLKICVFIFAFIMPVLIITVCYGLMILRLKSVRML-----------------------SGSK  271
hCCR5     ---SQYQ------FWKNFQTLKIVILGLVLPLLVMVICYSGILKTLLRCRN-------------------------EK  228
hCXCR4    ------D------LWVVVFQFQHIMVGLILPGIVILSCYCIIISKLSHSKG-------------------------H-  232
hCXCR1    ---D-TA------KWRMVLRILPHTFGFIVPLFVMLFCYGFTLRTLFKAHM-----------------------G-  235
                                  5.50
```

```
rNTSR1    GRVQALRHGVLVLRAVVIAFVVCWLPYHVRRLMFCYISDEQWTT--FLFDFYHYFYMLTNALFYVSSAINPILYNLVSA  374
hFPR1     ------SRPLRVLSFVAAAFFLCWSPYQVVALIATVRIREL-LQGM--YKEIGIAVDVTSALAFFNSCLNPMLYVFMGQ  306
hFPRL1    ------SRPLRVLTAVVASFFICWFPFQLVALLGTVWLKEMLFYGK--YKIIDILVNPTSSLAFFNSCLNPMLYVFVGQ  307
hC5aR2    ------L-----GTAIVVGFFVCWAPYHLLGLVLTVAAPNSAL-----LARALRAEPLIVGLALAHSCLNPMLFLYFGR  296
hC5aR1    ------TKTLKVVVAVVASFFIFWLPYQVTGIMMSFLEPSSPT-----FLLLKKLDSLCVSFAYINCCINPIIYVVAGQ  305
mC5aR     ------TKTLKVVMAVVICFFIFWLPYQVTGVMIAWLPPSSPT-----LKRVEKLNSLCVSLAYINCCVNPIIYVMAGQ  306
rC5aR     ------TKTLKVVMAVVTCFFVFWLPYQVTGVILAWLPRSSST-----FQSVERLNSLCVSLAYINCCVNPIIYVMAGQ  307
hOPRL1    EKDRNLRRITRLVLVVVAVFVGCWTPVQVFVLAQGLGVQP------SS-ETAVAILRFCTALGYVNSCLNPILYAFLDE  324
hOPRK1    EKDRNLRRITRLVLVVVAVFVVCWTPIHIFILVEALGSTS------HS-TAALSSYYFCIALGYTNSSLNPILYAFLDE  335
hOPRD1    EKDRSLRRITRMVLVVVGAFVVCWAPIHIFVIVWTLVDID------RRDPLVVAALHLCIALGYANSSLNPVLYAFLDE  323
hOPRM1    EKDRNLRRITRMVLVVVAVFIVCWTPIHIYVIIKALVTIP------ET-TFQTVSWHFCIALGYTNSCLNPVLYAFLDE  343
hCCR5     KR----HRAVRLIFTIMIVYFLFWAPYNIVLLLNTFQEFF-GLNNCSSSNRLDQAMQVTETLGMTHCCINPIIYAFVGE  302
hCXCR4    QK----RKALKTTVILILAFFACWLPYYIGISIDSFILLEIIKQGCEFENTVHKWISITEALAFFHCCLNPILYAFLGA  307
hCXCR1    QK----HRAMRVIFAVVLIFLLCWLPYNLVLLADTLMRTQVIQESCERRNNIGRALDATEILGFLHSCLNPIIYAFIGQ  310
                                 6.50                                          7.50

rNTSR1    NFRQVFLSTLACLCPGWRHRRKKRPTFSRKPN----SM-----SSNHAFSTSATRETLY--  424
hFPR1     DFRERLIHALPASLERALTEDST----QTSDT-ATNSTLPSAEVELQAK------------  350
hFPRL1    DFRERLIHSLPTSLERALSEDSA----PTNDT-AANSASPPAETELQAM------------  351
hC5aR2    A---QLRRSLPAACHWALRESQG----QDESVDSKKSTSHDLVSEMEV------------  337
hC5aR1    GFQGRLRKSLPSLLRNVLTEESV----VRESKSFTRSTVDTMAQKTQAV------------  350
mC5aR     GFHGRLLRSLPSIIRNALSEDSV----GRDSKTFTPSTTDTSTRKSQAV------------  351
rC5aR     GFHGRLRRSLPSIIRNVLSEDSL----GRDSKSFTRSTMDTSTQKSQAV------------  352
hORL1     NFKACFRKFCCASALRRDVQVSDR---VRSIAKDVALACKT-SETVPRPA-----------  370
hOPRK1    NFKRCFRDFCFPLKMRMERQSTSR---VRNTVQDPAYLRDI--DGMNKPV-----------  380
hOPRD1    NFKRCFRQLCRKPCGRPDPSSFSR---AREATARERVTACTPSDGPGGGAAA---------  372
hOPRM1    NFKRCFREFCIPTSSNIEQQNSTR---IRQNTRDHPSTANTV-DRTNHQLENLEAETAPLP  400
hCCR5     KFRNYLLVFFQKHIAKRFCKCCSI--FQQEAPERASS-VYTRSTGEQEISVGL--------  352
hCXCR4    KFKTSAQHALTSVSRGSSLK---I--LSKGKRGGHSSVSTESES--SSFHSS---------  352
hCXCR1    NFRHGFLKILAMHGLV-SKE---F--LAR-----HRVTSYTSSS--VNVSSNL--------  350
```

Figure 6.12 Master alignment for C5aR homology modelling

The master alignment used for C5aR homology modelling was generated using sequences from closely related receptors such as the neurotensin receptor 1 (NTSR1), C5aR2, formyl peptide receptor 1 (FPR1), formyl peptide receptor-like 1 (FPRL1), opioid receptor-like 1 (ORL1), δ-opioid receptor (OPRD1), κ-opioid receptor (OPRK1), μ-opioid receptor (OPRM1), chemokine receptors CCR5, CXCR1 and CXCR4. The species of the receptors used are denoted by the letter next to the receptor name – h, m and r for human, mouse and rat respectively. The highly conserved residues are highlighted in red and the Ballesteros-Weinstein numbers are shown as text. Clustal Omega was used to generate this alignment (http://www.ebi.ac.uk/Tools/msa/clustalo/).

Table 6.2 Template receptors for C5aR homology models

Receptor	PDB ID	Species	Sequence identity (%)		Resolution (Å)	Crystallised ligand
			human C5aR	mouse C5aR		
NTSR1	4GRV (White *et al.*, 2012)	rat	23.8	23.1	2.8	Neurotensin (NTS_{8-13})
CXCR4	3ODU (Wu *et al.*, 2010)	human	25.9	26.8	2.5	Small molecule antagonist IT1t
CXCR4	3OE0 (Wu *et al.*, 2010)	human	25.9	26.8	2.9	16 amino acid cyclic peptide antagonist CVX15
OPRL1	4EA3 (Thompson *et al.*, 2012)	human	24.0	23.1	3.0	Small molecule antagonist C-24
OPRD1	4RWD (Fenalti *et al.*, 2015)	human	24.6	24.0	2.7	Tetrapeptide antagonist DIPP-NH_2

using the validate protein structure tool in Discovery Studio 4.0. In general, the homology models had good structures and were comparable to the template receptors. The protein health reports for the human and mouse C5aR homology models are presented in Table 6.3 and Table 6.4 respectively. There were few variations in the backbone structure of the models from the different templates (Figure 6.13). The largest variation in the models occurred in the ECL2 (Figure 6.13). The ECL2 has a similar conformation in all of the models. However, in both human and mouse C5aR models based on both CXCR4 structures as well as the mouse C5aR based on OPRL1, the ECL2 adopted a distinct anti-parallel beta sheet conformation (Figure 6.13). While a previous human C5aR homology model with *de novo* loop generation did not report an anti-parallel beta sheet conformation for the ECL2 (Nikiforovich *et al.*, 2008), a more recent C5aR model based on the CXCR1 receptor in which the ECL2 was subjected to all atom folding simulations using molecular dynamics suggested that the ECL2 of the C5aR adopts an anti-parallel beta sheet conformation (Rana and Sahoo, 2015). In addition, all five template receptors used to generate the C5aR models in this study have ECL2s which form anti-parallel beta sheets (Fenalti *et al.*, 2015; Thompson *et al.*, 2012; White *et al.*, 2012; Wu *et al.*, 2010), suggesting that this ECL2 conformation may be common for γ branch peptide binding family A GPCRs.

6.3.4 Docking into C5aR homology models

One of the most common methods to test the quality of a homology model is to perform docking. The aims of these docking experiments were to identify the best template for the C5aR and to identify the potential binding site for PMX53. First,

Table 6.3 Human C5aR homology model validation

		NTSR1 (4GRV)		CXCR4 (3ODU)		CXCR4 (3OE0)		OPRL1 (4EA3)		OPRD1 (4RWD)	
		T[a]	M[b]	T	M	T	M	T	M	T	M
Number of residues		299	292	302	305	289	295	278	280	300	294
Ramachandran analysis[c]	A	94.8%	95.0%	97.8%	97.8%	94.9%	93.8%	96.4%	96.0%	98.5%	95.5%
	M	4.8%	4.2%	1.8%	1.5%	3.9%	5.4%	3.6%	3.2%	1.5%	3.8%
	D	0.4%	0.8%	0.4%	0.7%	1.2%	0.8%	0.0%	0.8%	-	0.8%
Side-chain deviations[d]		53	69	53	81	70	69	16	79	30	74
Peptide planarity violations[e]		3	11	6	3	9	11	-	11	1	9
Cis peptides		4	2	-	-	-	-	1	1	1	1
CA-CA distance violations[f]		1	1	1	-	2	5	-	2	1	-

[a] Template receptor.
[b] Highest scoring homology model (out of 100) after minimisation with CHARMm force field.
[c] The main chain conformation of each residue as defined by the φ and ψ angles was checked against the Ramachandran map (Ramachandran *et al.*, 1963). Percentage residues in the allowed (A), marginal (M) and disallowed (D) regions are shown. Glycine and proline residues were excluded from this analysis.
[d] The number of residues with side-chain conformations that deviated from the Lovell, Word and Richardson rotamer library (Lovell *et al.*, 2000).
[e] The number of peptide bonds with ω angles that deviate from 0˚ or 180˚ by 15˚.
[f] The number of peptide bonds within the protein structure in which the distance between two consecutive C-alpha atoms deviates from 3.8 Å for a peptide bond in a standard trans conformation and 2.9 Å for a peptide bond in a cis conformation.

Table 6.4 Mouse C5aR homology model validation

		NTSR1 (4GRV)		CXCR4 (3ODU)		CXCR4 (3OE0)		OPRL1 (4EA3)		OPRD1 (4RWD)	
		T[a]	M[b]	T	M	T	M	T	M	T	M
Number of residues		299	296	302	307	289	297	278	281	300	295
Ramachandran analysis[c]	A	94.8%	96.5%	97.8%	93.8%	95.0%	94.9%	96.4%	95.2%	98.5%	98.1%
	M	4.8%	2.3%	1.8%	4.8%	3.9%	3.9%	3.6%	3.2%	1.5%	1.5%
	D	0.4%	1.2%	0.4%	1.5%	1.2%	1.2%	0.0%	1.6%	0.0%	0.4%
Side-chain deviations[d]		53	59	53	76	70	72	16	86	30	65
Peptide planarity violations[e]		3	18	6	14	9	12	-	13	1	8
Cis peptides		4	3	-	-	-	-	1	-	1	1
CA-CA distance violations[f]		1	2	1	1	1	1	-	1	-	-

[a] Template receptor.
[b] Highest scoring homology model (out of 100) after minimisation with CHARMm force field.
[c] The main chain conformation of each residue as defined by the φ and ψ angles was checked against the Ramachandran map (Ramachandran *et al.*, 1963). Percentage residues in the allowed (A), marginal (M) and disallowed (D) regions are shown. Glycine and proline residues were excluded from this analysis.
[d] The number of residues with side-chain conformations that deviated from the Lovell, Word and Richardson rotamer library (Lovell *et al.*, 2000).
[e] The number of peptide bonds with ω angles that deviate from 0˚ or 180˚ by 15˚.
[f] The number of peptide bonds within the protein structure in which the distance between two consecutive C-alpha atoms deviates from 3.8 Å for a peptide bond in a standard trans conformation and 2.9 Å for a peptide bond in a cis conformation.

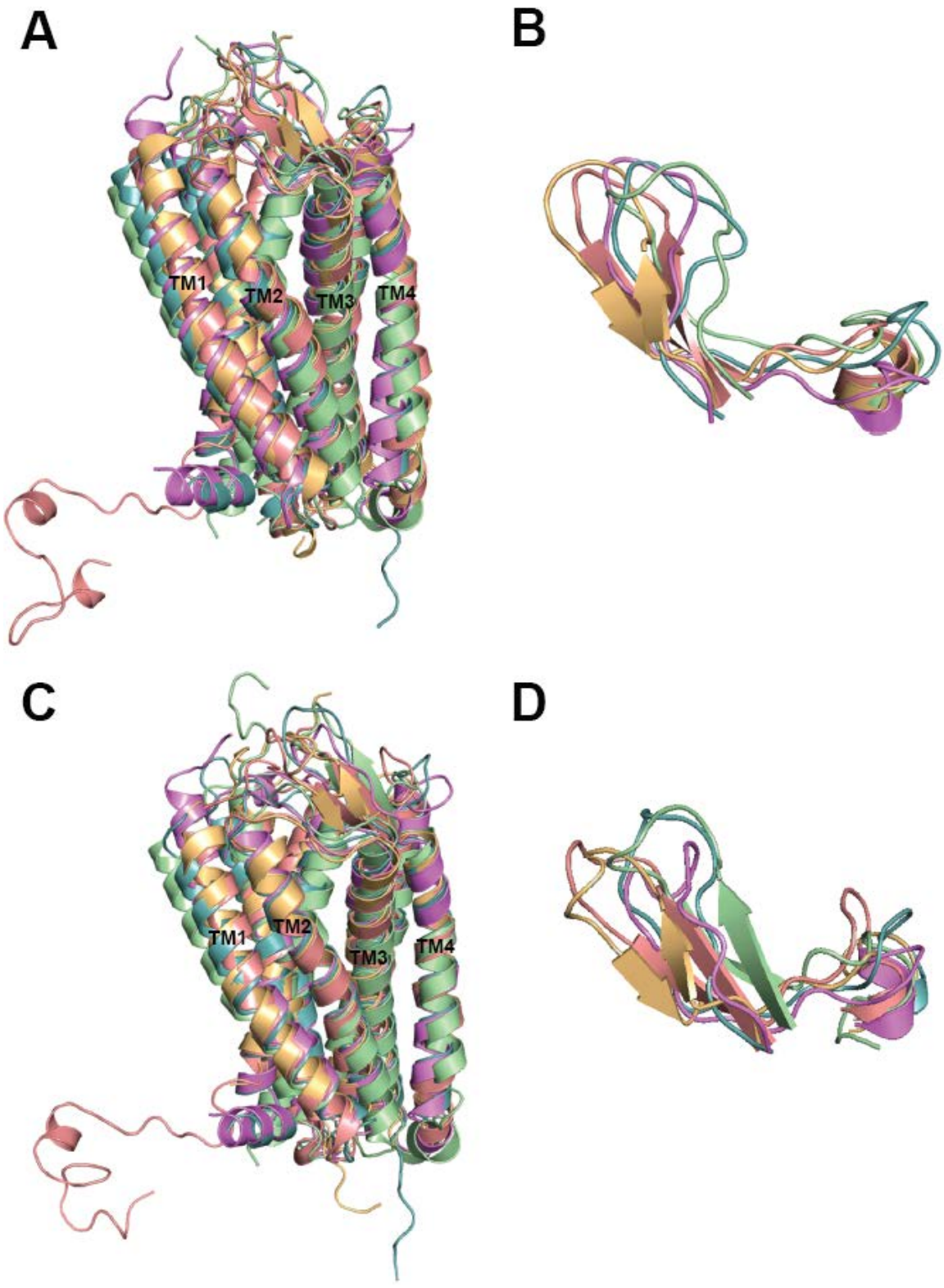
A
TM1
TM2
TM3
TM4
B
C
TM1
TM2
TM3
TM4
D

Figure 6.13 Homology models of human and mouse C5aR

Superimposition of human (A) and mouse (C) C5aR homology models based on various template receptors. The ECL2 of the human (B) and mouse (D) C5aR homology models are shown in separate panels for clarity. The homology models based on the neurotensin receptor NTSR1 (PDB ID 4GRV) is shown in green, chemokine receptor CXCR4 (PDB ID 3ODU) in pink, chemokine receptor CXCR4 (PDB ID 3OE0) in gold, opioid receptor-like OPRL1 (PDB ID 4EA3) in teal and δ-opioid receptor OPRD1 (PDB ID 4RWD) in purple.

docking was performed using small molecule antagonists NDT9520492 and W54011. In general, docking of these antagonists into the C5aR homology models suggested that they bind in the transmembrane domain of the receptor. However, the results varied for each model and the lack of mutagenesis data for C5aR small molecule antagonists precluded their use in testing the quality of the homology models. In contrast, mutagenesis data for linear hexapeptide ligands of the C5aR are available, such as antagonist MeFKPdChaWr and agonist MeFKPdChaChar. However, docking of these linear peptides into the C5aR models using GOLD were unsuccessful despite extensive attempts to optimise the docking conditions. The linear hexapeptides are highly flexible and docking of these peptides would require molecular dynamics simulation to address the conformational flexibility issue.

Unlike the linear hexapeptides, PMX53 is conformationally constrained as a result of its cyclisation and docked well into the homology models. First, the interactions of PMX53 in all 5 human C5aR models were analysed. In these dockings, the poses generated were clustered based on a root mean square deviation of the heavy atoms of PMX53 of 3 Å. In all of the models, except for the model based on the CXCR4 receptor crystallised with the cyclic peptide antagonist (PDB ID 3OE0), the first PMX53 pose which is the highest scored pose did not belong to the largest docking cluster. Therefore, in each of these models, the first pose was compared to the highest scoring pose of the largest cluster (Table 6.5). Although the interactions of PMX53 were not identical in these poses, PMX53 bound to the same region of each receptor model (Table 6.5).

Table 6.5 Docking of PMX53 into human C5aR homology models

Template	Docking clusters[a]	Interactions[b]	
NTSR1 (4GRV)	| **1** 6 8 10 13 | 2 4 | **3** 9 15 20 23 31 32 | 5 7 17 43 | 11 12 22 | 14 | 16 48 | 18 34 35 | 9 28 71 | 21 25 47 | 24 | 26 36 41 79 | 27 37 61 | 29 46 75 89 90 | 30 | 33 | 38 66 | 39 55 59 67 | 40 | 42 50 | 44 68 70 | 45 85 92 | 49 | 51 | 52 | 53 | 54 57 58 | 56 | 60 | 62 | 63 | 64 | 65 78 | 69 | 72 73 77 81 82 84 87 93 99 | 74 | 76 91 | 80 | 83 | 86 | 88 | 94 | 95 | 96 98 | 97 | 100 |	Pose number, Goldscore[c]	1, 64.1
		H-bond	AcF1§-R175^{ECL2}, Orn2§-K280$^{7.33}$, P3-D282$^{7.35}$, dCha4§-D282$^{7.35}$, W5-T29$^{N\text{-}term}$§, R6-M264$^{6.57}$§, R6-M265$^{6.58}$§
		Charge	AcF1-R175^{ECL2}
		Hydrophobic	AcF1-I116$^{3.32}$, dCha4-H99^{ECL1}, W5-K28$^{N\text{-}term}$, W5-L278$^{7.31}$
		Pose number, Goldscore	3, 60.7
		H-bond	AcF1-L278$^{7.31}$§, Orn2§-M265$^{6.58}$, Orn2§-K280$^{7.33}$, W5-S95$^{2.63}$§, W5-H99^{ECL1}§, W5§-H99^{ECL1}, R6§-S30$^{N\text{-}term}$, R6-I96$^{2.64}$§, R6§-D282$^{7.35}$
		Charge	R6-D37$^{1.32}$
		Hydrophobic	P3-M265$^{6.58}$, W5-W102^{ECL1}
CXCR4 (3ODU)	| **1** 3 4 12 13 16 17 23 70 74 87 | **2** 7 11 18 32 34 38 50 53 56 60 91 | 5 6 14 27 39 41 67 79 | 8 | 9 | 10 15 19 21 24 25 42 44 46 47 48 66 71 76 84 | 20 59 | 22 33 | 26 | 28 29 | 30 31 83 93 | 35 52 | 36 | 37 | 40 | 43 | 45 | 49 85 | 51 | 54 | 55 | 57 58 62 65 68 72 73 75 78 80 81 82 90 | 61 | 63 | 64 | 69 | 77 94 | 86 | 88 92 98 | 89 | 95 | 96 | 97 | 99 | 100 |	Pose number, Goldscore	1, 66.1
		H-bond	AcF1-R206$^{5.42}$, AcF1-Y258$^{6.51}$, dCha4§-D282$^{7.35}$, W5§-R175^{ECL2}, W5§-G189^{ECL2}, R6§-V190^{ECL2}§
		Charge	W5-R175^{ECL2}, R6-E180^{ECL2}, R6-D191^{ECL2}
		Hydrophobic	AcF1-A203$^{5.39}$, AcF1-M265$^{6.58}$, P3-Y258$^{6.51}$, P3-V286$^{7.39}$, W5-L92$^{2.60}$, W5-W102^{ECL1}, W5-P113$^{3.29}$
		Pose number, Goldscore	2, 58.8
		H-bond	Orn2§-R198$^{5.34}$, dCha4§-D282$^{7.35}$, W5§-R175^{ECL2}, W5§-G189^{ECL2}, R6-L187^{ECL2}§, R6§-V190^{ECL2}
		Charge	R6-D191^{ECL2}
		Hydrophobic	AcF1-M265$^{6.58}$, AcF1-A203$^{5.39}$, P3-V286$^{7.39}$, W5-L187^{ECL2}

Template	Docking clusters	Interactions	
CXCR4 (3OE0)	| **1** 2 4 5 6 7 8 10 11 12 13 15 18 19 23 24 26 28 29 30 34 37 38 43 44 47 53 54 64 70 | 3 75 78 | 9 14 27 35 46 81 | 16 89 | 17 21 25 33 39 45 48 52 55 66 69 73 83 | 20 22 31 36 40 49 51 56 60 62 65 72 82 84 95 | 32 | 41 61 | 42 | 50 | 57 | 58 92 | 59 | 63 | 67 79 | 68 | 71 76 96 | 74 80 87 | 77 | 85 91 94 | 86 98 | 88 | 90 93 97 | 99 | 100 |	Pose number, Goldscore	1, 61.2
		H-bond	AcF1§-Y258$^{6.51}$, P3-Y258$^{6.51}$, W5§-R175^{ECL2}, R6-D191^{ECL2}
		Charge	
		Hydrophobic	AcF1-M264$^{6.57}$, P3-M120$^{3.35}$, P3-Y258$^{6.51}$, dCha4-V286$^{7.39}$, W5-L92$^{2.60}$, W5-H100^{ECL1}, W5-C188^{ECL2}
OPRL1 (4EA3)	| **1** 12 20 26 47 | 2 5 9 10 22 43 49 79 | 3 19 33 40 | 4 7 | 6 59 | 8 13 21 31 35 50 | **11** 14 15 16 17 25 28 29 36 37 | 18 32 63 64 83 | 23 | 24 38 | 27 39 48 84 87 | 30 | 34 44 | 41 62 69 | 42 45 | 46 53 86 | 51 92 | 52 68 71 73 | 54 58 65 66 | 55 57 | 56 | 60 76 85 91 | 61 81 | 67 72 | 70 | 74 | 75 82 93 95 | 77 | 78 | 80 88 89 94 96 100 | 90 | 97 99 | 98 |	Pose number, Goldscore	1, 60.4
		H-bond	AcF1§-S171$^{4.60}$, dCha4§-Y192^{ECL2}, R6-S95$^{2.63}$, R6-C188^{ECL2}§, R6§-R175^{ECL2}
		Charge	W5-K279$^{7.32}$, W5-D282$^{7.35}$
		Hydrophobic	AcF1-Y174$^{4.63}$, AcF1-V202$^{5.38}$, P3-R206$^{5.42}$, W5-M265$^{6.58}$, W5-K279$^{7.32}$
		Pose number, Goldscore	11, 48.4
		H-bond	P3§-Y258$^{6.51}$, W5-Y290$^{7.43}$
		Hydrophobic	P3-M265$^{6.58}$, W5-I116$^{3.32}$

Template	Docking clusters	Interactions	
OPRD1 (4RWD)	| **1** 3 | 2 6 | 4 27 | 5 | **7** 22 28 | 8 | 9 | 10 | 11 | 12 | 13 23 | 14 | 15 | 16 52 74 | 17 18 | 19 | 20 | 21 | 24 44 | 25 | 26 31 | 29 | 30 | 32 | 33 | 34 41 | 35 | 36 62 | 37 | 38 43 | 39 | 40 66 | 42 | 45 89 | 46 | 47 51 72 | 48 | 49 | 50 | 53 | 54 | 55 68 | 56 | 57 67 76 | 58 61 73 | 59 | 60 | 63 | 64 | 65 | 69 | 70 79 | 71 | 75 80 | 77 | 78 | 81 | 82 | 83 | 84 | 85 | 86 90 | 87 | 88 | 91 92 96 | 93 | 94 | 95 98 99 | 97 | 100 |	Pose number, Goldscore	1, 58.5
		H-bond	AcF1§-A203$^{5.39}$§, AcF1-R206$^{5.42}$, AcF1-Y258$^{6.51}$, W5-C188^{ECL2}§
		Hydrophobic	AcF1-Y258$^{6.51}$, AcF1-M265$^{6.58}$, P3-I116$^{3.32}$, P3-Y258$^{6.51}$, dCha4-V286$^{7.39}$, W5-C188^{ECL2}
		Pose number, Goldscore	7, 44.6
		H-bond	AcF1§-K279$^{7.32}$, R6-D282$^{7.35}$
		Charge	AcF1-E180^{ECL2}, R6-D282$^{7.35}$
		Hydrophobic	P3-W102^{ECL1}, P3-L187^{ECL2}, P3-C188^{ECL2}, dCha4-V190^{ECL2}, W5-I116$^{3.32}$, W5-Y258$^{6.51}$, W5-V286$^{7.39}$

[a] Docking clusters, 100 poses from each docking run were clustered at root mean square deviation of 3 Å. The highest scoring pose and the highest scoring pose of the largest cluster is highlighted in bold.

[b] The first letter represents an amino acid on PMX53 while the second letter represents an amino acid from the C5aR. The residue number for PMX53 is shown as a subscript. Superscripts denote Ballesteros-Weinstein residue numbering.

[c] GoldScore, scoring function in GOLD which is a weighted sum of the intramolecular van der Waals forces, internal torsion of the ligand, van der Waals forces between the ligand and the receptor and H-bond interactions between the ligand and the receptor. A positive number indicates favourable interactions.

§ Interaction was with a backbone atom of the amino acid.

In all 5 human C5aR models, PMX53 can be seen to interact with residues from the ECL2, TM6 and TM7 (Table 6.5). However, the interacting residues were not the same. The cluster size was the smallest in the human C5aR based on the δ-opioid receptor (PDB ID 4RWD) with an average cluster size of 2 poses (Table 6.5), indicating that these poses likely did not represent the binding of PMX53. In addition, the Goldscores of the highest scoring pose in the human C5aR based on the δ-opioid receptor were also the lowest out of the 5 homology models generated in this study (Table 6.5). In all of the models, except for the model based on the δ-opioid receptor, PMX53 can be seen to interact with $R175^{ECL2}$, a residue which has been shown to reduce the potency of the non-acetylated analogue of PMX53 by 131 fold when mutated into an aspartic acid (Higginbottom *et al.*, 2005).

The human C5aR homology models based on two different CXCR4 receptors co-crystallised with either a small molecule antagonist or a 16 amino acid cyclic peptide antagonist gave similar PMX53 docking results. The highest scoring pose from the model based on the CXCR4 receptor co-crystallised with a small molecule antagonist (PDB ID 3ODU) suggested that PMX53 interacted with residues from the top of TM2 to TM7 as well as residues from ECL1 and ECL2 (Table 6.5**,** Figure 6.14). Similarly, the highest scoring pose from the model based on the CXCR4 receptor co-crystallised with a peptide antagonist (PDB ID 3OE0) showed that PMX53 also bound with the same orientation at the receptor and gave similar binding interactions (Table 6.5**,** Figure 6.14). However, the docking score was higher in the homology model based on the template receptor crystallised with a small molecule ligand compared to the cyclic peptide antagonist. The common residues implicated in PMX53 interactions at these models were $L92^{2.60}$, $R175^{ECL2}$,

D191^{ECL2}, Y258$^{6.51}$ and V286$^{7.39}$. The root mean square deviation of the heavy atoms between the two highest scoring poses from the two models was 2.6 Å (Figure 6.14).

Previous mutagenesis data combined with the sequence alignment between human and mouse C5aR suggest that the ECL2 may be a possible interaction site. PMX53 has a lower affinity for mouse C5aR compared to human and rat C5aR. The largest variation in the sequence alignment between human, rat and mouse C5aR can be found on the ECL2. Of all the ECL2 residues, L187^{ECL2}, D191^{ECL2} and S193^{ECL2} are the only residues that are the same in human and rat but different in the mouse receptor, suggesting the involvement of these residues in the binding of PMX53. In addition, R175^{ECL2} of the human C5aR has been shown to contribute to the potency of the non-acetylated form of PMX53 (Higginbottom *et al.*, 2005). Therefore, particular attention was paid to these four residues when analysing the docking interactions. In all of the homology models, S193^{ECL2} on the human C5aR and the corresponding residue G193^{ECL2} on the mouse C5aR pointed away from the binding pocket. All 5 human C5aR homology models showed different levels of frequency of interaction between PMX53 and R175^{ECL2}, L187^{ECL2} and D191^{ECL2}. The frequency of interaction was defined as the number of poses in which PMX53 interacted with particular residues of the C5aR out of 100 poses generated from the docking run. Out of all the human C5aR homology models, only two models showed high frequency of interactions between PMX53 and R175^{ECL2}, L187^{ECL2} and D191^{ECL2} on the human receptor but not with the corresponding residues on the mouse receptor. These were the human C5aR based on the CXCR4 receptor crystallised with a small molecule antagonist (PDB ID 3ODU) and the CXCR4

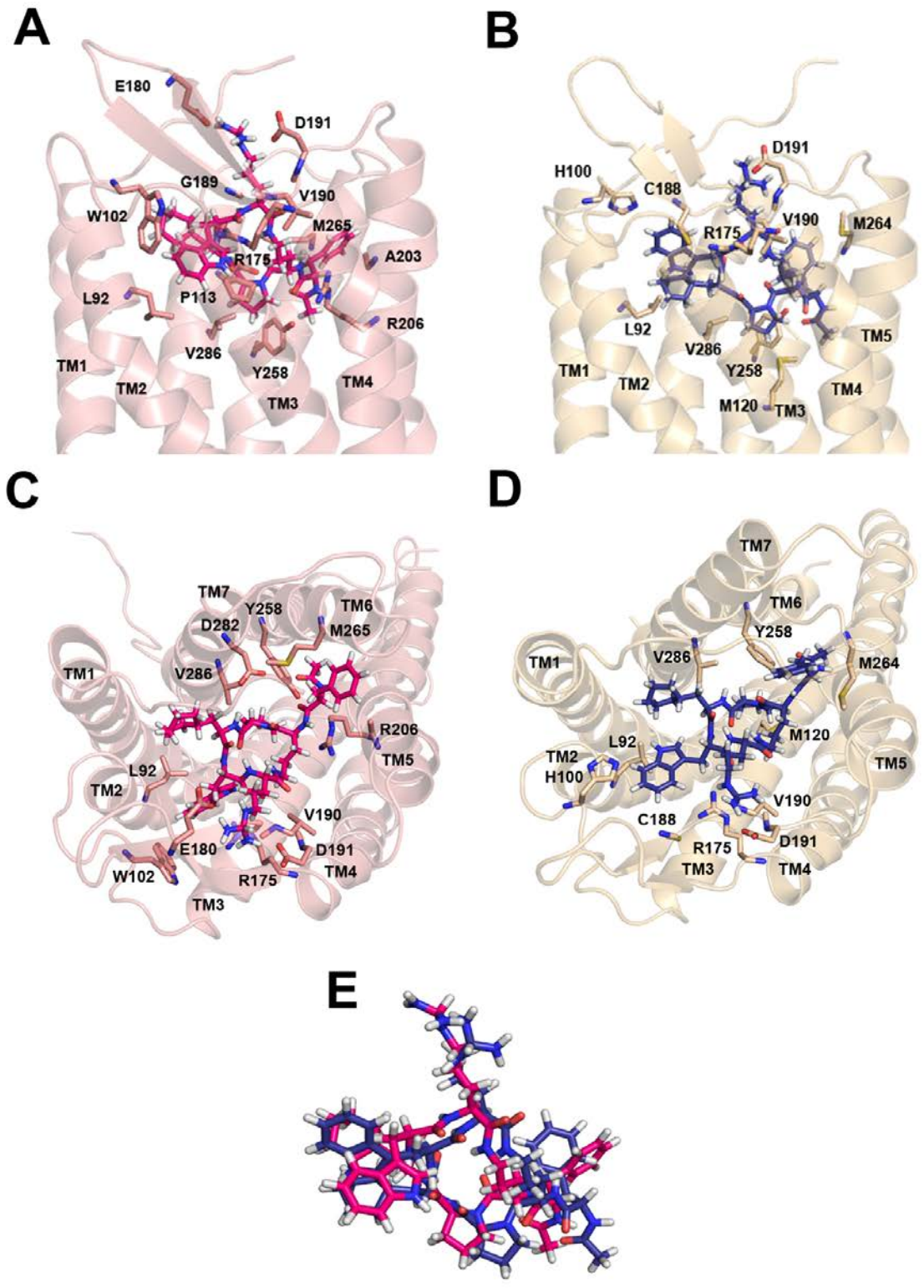
A
E180
D191
G189
V190
W102
M265
R175
A203
L92
P113
R206
V286
TM1
Y258
TM2
TM4
TM3
B
D191
H100
C188
V190
M264
R175
L92
TM5
V286
TM1
Y258
TM2
TM4
M120
TM3
C
TM7
Y258
TM6
D282
M265
TM1
V286
R206
TM5
L92
TM2
V190
E180
D191
W102
R175
TM4
TM3
D
TM7
TM6
Y258
TM1
V286
M264
M120
L92
TM2
H100
TM5
V190
C188
R175
D191
TM3
TM4
E

Figure 6.14 Docking of PMX53 into human C5aR homology models

PMX53 was docked into human C5aR homology models based on the CXCR4 receptor crystallised with a small molecule antagonist (PDB ID 3ODU) (A, C) or with a 16-amino acid peptide antagonist (PDB ID 3OE0) (B, D). The highest scoring pose (out of 100) is shown. The homology model based on the CXCR4 receptor co-crystallised with a small molecule antagonist is shown in pink and the model based on the CXCR4 receptor co-crystallised with a 16-amino acid cyclic peptide antagonist is shown in yellow. PMX53 is coloured in magenta or blue and is shown in stick representation. The side chains of interacting amino acids are shown as sticks with oxygen atoms in red, nitrogens in blue and hydrogens in white. Superimposition of the highest scoring docking pose of PMX53 from the two homology models (E).

receptor crystallised with a 16-amino acid cyclic antagonist (PDB ID 3OE0). In both models, PMX53 showed high frequency of interactions with R175^{ECL2}, L187^{ECL2} and D191^{ECL2} on the human receptor but not with the corresponding residues on the mouse receptor. In particular, both models showed a high frequency of interaction between PMX53 and D191^{ECL2} of the human receptor, but no interaction with N191^{ECL2} of the mouse receptor. Although PMX53 did not interact with L187^{ECL2} in the top scoring pose of both models, the interaction with this residue is frequently observed in the human C5aR models based on both CXCR4 receptors, but not in the mouse C5aR models. The frequencies of interactions between PMX53 and the selected ECL2 residues on the C5aR are summarised in Table 6.6. In addition to R175^{ECL2}, D192^{ECL2} and L187^{ECL2}, high frequencies of PMX53 interactions (≥30%) were observed with L92$^{2.60}$, I96$^{2.64}$, W102^{ECL1}, P113$^{3.29}$, E180^{ECL2}, C188^{ECL2}, G189^{ECL2}, V190^{ECL2}, R198$^{5.34}$, R206$^{5.42}$, M265$^{6.58}$, K279$^{7.32}$, D282$^{7.35}$ and V286$^{7.39}$ in the human C5aR based on the CXCR4 receptor crystallised with a small molecule antagonist. High frequencies of PMX53 interactions were also observed with L92$^{2.60}$, H100^{ECL2}, M120$^{3.36}$, E180^{ECL2}, V190^{ECL2}, Y192^{ECL2}, R198$^{5.34}$, A203$^{5.39}$, R206$^{5.42}$, L207$^{5.43}$, Y258$^{6.51}$, M264$^{6.57}$ and V286$^{7.39}$ in the mouse C5aR based on the CXCR4 crystallised with a 16-amino acid peptide antagonist.

To further investigate the binding site of PMX53 on the C5aR, the docking results from the corresponding mouse C5aR homology models based on the two CXCR4 receptors were analysed. Docking of PMX53 into the corresponding mouse C5aR homology models suggested that PMX53 adopted a different binding mode at the mouse receptor compared to the human receptor. Firstly, the cluster sizes of the docked poses at the mouse homology models were considerably smaller

Table 6.6 Frequency of PMX53 interactions with selected ECL2 residues

NTSR1 (4GRV)[a]				CXCR4 (3ODU)[a]				CXCR4 (3OE0)[a]				OPRL1 (4EA3)[a]				OPRD1 (4RWD)[a]			
Human		Mouse		Human		Mouse		Human		Mouse		Human		Mouse		Human		Mouse	
Residue	F	Residue	F	Residue	F	Residue	F	Residue	F	Residue	F	Residue	F	Residue	F	Residue	F	Residue	F
R175	61	R175	77	R175	65	R175	13	R175	63	R175	5	R175	46	R175	23	R175	12	R175	0
L187	21	V187	12	L187	52	V187	12	L187	61	V187	27	L187	28	V187	39	L187	43	V187	35
D191	1	N191	1	D191	70	N191	0	D191	54	N191	0	D191	7	N191	3	D191	2	N191	0
S193	0	G193	0	S193	0	G193	1	S193	1	G193	0	S193	0	G193	0	S193	0	G193	0

[a] Template used for homology modelling.

F, Frequency of interactions, defined as the number of poses in which PMX53 interacted with the abovementioned residues on the C5aR, out of 100 poses generated from the docking run.

with fewer poses per cluster compared to the human homology models (Table 6.7). In addition, PMX53 interacted with different amino acids on the mouse homology models compared to the human homology models (Table 6.7). Unlike in the human homology models where the binding of PMX53 to the human C5aR homology models based on the two CXCR4 receptor crystal structures gave similar results, the binding of PMX53 to the corresponding mouse C5aR homology models was different in these models (Table 6.7).

To validate the homology models and to investigate the binding site of PMX53 at the C5aR, the following residues on the human C5aR were mutated to the corresponding mouse residue – L187^{ECL2}V, D191^{ECL2}N and the double mutant L187^{ECL2}V/D191^{ECL2}N. The reciprocal mutations were also made on the mouse C5aR – V187^{ECL2}L, N191^{ECL2}D and V187^{ECL2}L/N191^{ECL2}D.

6.3.5 Characterisation of the inhibitory action of PMX53 on mutant C5aRs

The ability of PMX53 to inhibit C5a-mediated receptor activation was investigated using the BRET cAMP assay. None of the human and mouse C5aR mutants tested affected the potency or the maximum response of purified human C5a (Table 6.8**,** Figure 6.15). In this assay, the pIC_{50} (M) value for PMX53 inhibition of receptor activation by 0.3 nM of purified human C5a on the WT human C5aR was 5.8 ± 0.1 (mean ± SEM, n = 6) (Figure 6.16). Surprisingly, the mutation D191^{ECL2}N significantly increased the potency of PMX53 when compared to the WT receptor (pIC_{50} (M) = 6.2 ± 0.1, mean ± SEM, n = 5, $P < 0.05$) (Figure 6.16). In contrast, the L187^{ECL2}V and L187^{ECL2}V/D191^{ECL2}N mutants did not significantly change the potency of PMX53. The pIC_{50} (M) values of PMX53 for these mutants

were 5.7 ± 0.1 and 6.1 ± 0.1 respectively (mean ± SEM, n = 5) (Figure 6.16). The same assay could not be performed on the mouse C5aR because of a small window of detection, presumably due to interference from the mCherry fluorescence tag.

Table 6.7 Docking of PMX53 into mouse C5aR homology models

Template	Docking clusters[a]	Interactions[b]	
CXCR4 (3ODU)	| 1 5 11 | 2 36 54 | 3 6 24 58 90 | 4 | 7 18 34 | 8 15 26 33 | 9 | 10 47 | 12 | 13 35 | 14 31 | 16 23 25 65 76 | 17 21 22 29 38 39 53 | 19 48 50 | 20 | 27 | 28 52 56 73 77 84 85 88 96 | 30 | 32 | 37 | 40 | 41 | 42 83 | 43 | 44 | 45 | 46 | 49 72 | 51 | 55 69 | 57 | 59 | 60 | 61 | 62 | 63 | 64 | 66 80 | 67 70 75 82 | 68 79 | 71 | 74 | 78 | 81 91 | 86 95 97 | 87 93 | 89 | 92 | 94 | 98 99 | 100 |	Pose number. Goldscore[c] H-bond π-charge Hydrophobic	1. 57.7 AcF1-H29$^{N\text{-term}}$, AcF1§-K277$^{7.29}$, O2§-E280$^{7.32}$, P3-E280$^{7.32}$, W5-R207$^{5.42}$ P3-P113$^{3.29}$, W5-M120$^{3.36}$, W5-R207$^{5.42}$
		Pose number, Goldscore H-bond Hydrophobic	28, 36.7 Orn2§-R207$^{5.42}$, P3§-Y259$^{6.51}$, dCha4§-R207$^{5.42}$, AcF1-L92$^{2.60}$, AcF1-V96$^{2.64}$, AcF1-L112$^{3.28}$, P3-I116$^{3.32}$, P3-V287$^{7.39}$, dCha4-M120$^{3.36}$, dCha4-F212$^{5.47}$, dCha4-W256$^{6.48}$, W5-A204$^{5.39}$, W5-L208$^{5.43}$, W5-I266$^{6.58}$
CXCR4 (3OE0)	| 1 9 | 2 | 3 19 85 | 4 31 | 5 18 | 6 11 | 7 | 8 14 45 | 10 21 43 | 12 23 37 44 68 72 | 13 28 52 60 | 15 58 | 16 36 | 17 | 20 | 22 | 24 32 38 50 53 62 73 | 25 | 26 29 30 46 55 66 74 82 87 | 27 51 | 33 | 34 | 35 78 | 39 76 | 40 | 41 | 42 | 47 | 48 57 79 | 49 | 54 | 56 | 59 | 61 | 63 | 64 | 65 | 67 84 | 69 | 70 | 71 | 75 | 77 | 80 | 81 | 83 | 86 | 88 | 89 | 90 | 91 93 | 92 | 94 95 99 | 96 | 97 | 98 | 100 |	Pose number, Goldscore H-bond Hydrophobic	1, 52.7 P3-E280$^{7.32}$, W5§-S284$^{7.36}$, R6-Y44$^{1.39}$, R6§-S284$^{7.36}$ AcF1-I190^{ECL2}, dCha4-P31$^{N\text{-term}}$, W5-K32$^{N\text{-term}}$, W5-P35$^{1.30}$, W5-K281$^{7.33}$, W5-S284$^{7.36}$, W5-L285$^{7.37}$
		Pose number, Goldscore H-bond Charge Hydrophobic	26, 37.0 dCha4§-E280$^{7.32}$, R6-V96$^{2.64}$§, R6-N98$^{2.66}$§ R6-D180^{ECL2} AcF1-I116$^{3.32}$, AcF1-L117$^{3.33}$, P3-V287$^{7.39}$, dCha4-P31$^{N\text{-term}}$, W5-K32$^{N\text{-term}}$, W5-P35$^{1.30}$, W5-K281$^{7.33}$

[a] Docking clusters, 100 poses generated from each docking run were clustered at root mean square deviation of 3 Å. The highest scoring pose of the largest cluster is highlighted in bold.
[b] The first letter represents an amino acid on PMX53 while the second letter represents an amino acid from the C5aR. The residue number for PMX53 is shown as a subscript. Superscripts denote Ballesteros-Weinstein residue numbering.
[c] GoldScore, scoring function in GOLD which is a weighted sum of the intramolecular van der Waals forces, internal torsion of the ligand, van der Waals forces between the ligand and the receptor and H-bond interactions between the ligand and the receptor. A positive number indicates favourable interactions.
[§] Interaction was with a backbone atom of the amino acid.

Table 6.8 The potency and efficacy of C5a at wild type and mutant human and mouse C5aR

Species	Receptor	pEC_{50}	E_{max}	n
Human	WT	10.2 ± 0.2	60.1 ± 1.7	4
	$L187^{ECL2}V$	10.3 ± 0.1	57.6 ± 5.5	3
	$D191^{ECL2}N$	10.5 ± 0.1	53.7 ± 3.9	4
	$L187^{ECL2}V/D191^{ECL2}N$	10.6 ± 0.1	53.2 ± 4.0	4
Mouse	WT	10.5 ± 0.2	32.1 ± 4.5*	4
	$V187^{ECL2}L$	10.3 ± 0.1	21.6 ± 3.2*	4
	$N191^{ECL2}D$	10.2 ± 0.3	22.0 ± 0.9*	4
	$V187^{ECL2}L/N191^{ECL2}D$	10.7 ± 0.1	27.7 ± 6.6*	3

pEC_{50}, negative log of the concentration of purified human C5a resulting in 50% reduction of forskolin-induced cAMP production.

E_{max}, the maximum reduction in forskolin-induced cAMP production from the highest concentration of purified human C5a, normalised to stimulation with 10 μM forskolin (0%) and unstimulated cells (100%).

* $P < 0.05$ compared to human WT C5aR by one-way ANOVA with Dunnett's multiple comparison test.

Data are presented as the mean ± SEM n of independent experiments performed in triplicate.

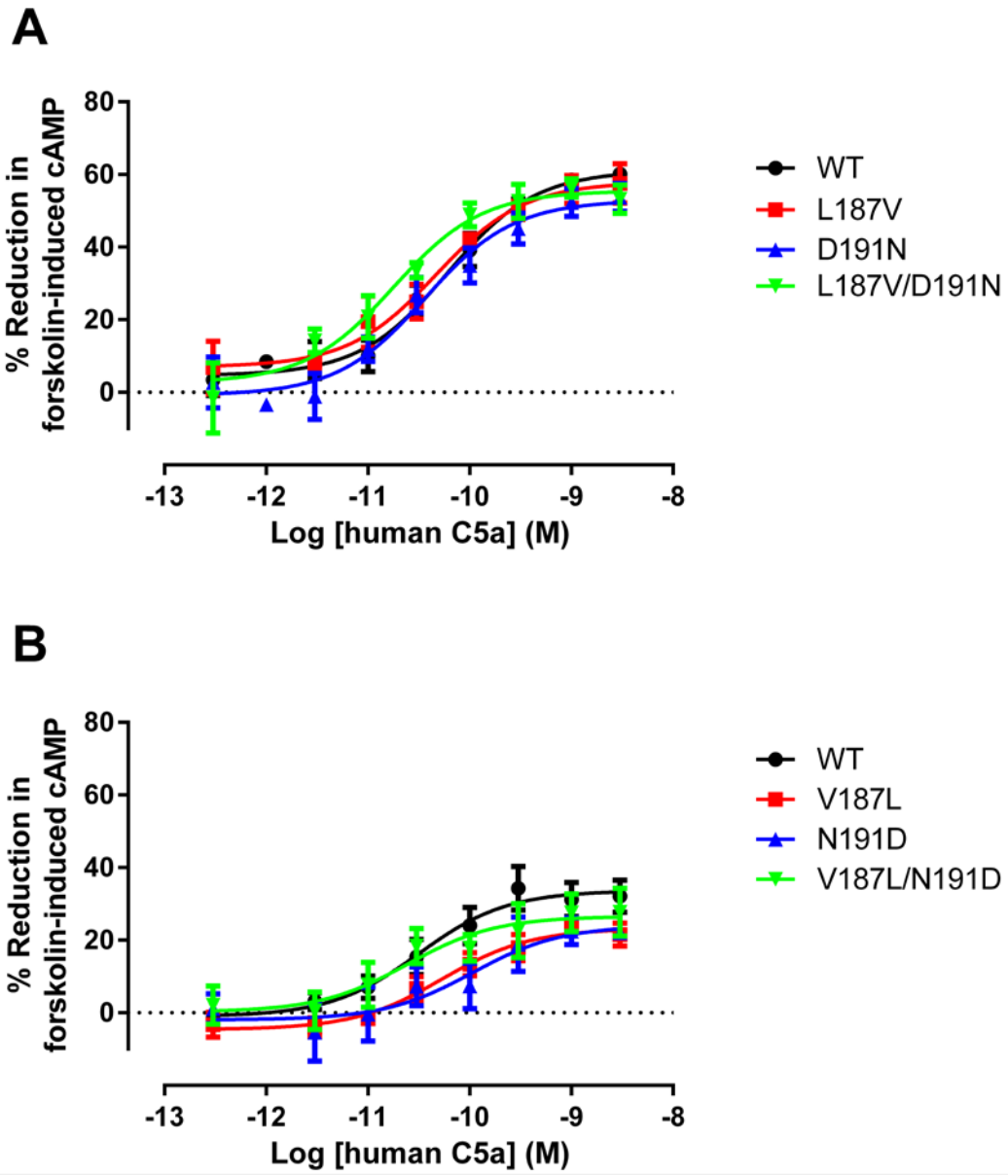

Figure 6.15 The effect of ECL2 mutations on the potency of C5a at human and mouse C5aR.

CHO cells were transiently transfected with either WT or mutant human (A) or mouse (B) C5aR and the BRET cAMP sensor CAMYEL. cAMP levels were measured after a 5 min incubation with increasing concentrations of purified human C5a and 10 μM of forskolin in the presence of 40 μM of IBMX. Data were normalised to stimulation with 10 μM forskolin (0%) and unstimulated cells (100%). Data are presented as the mean ± SEM of 3-4 independent experiments performed in triplicate.

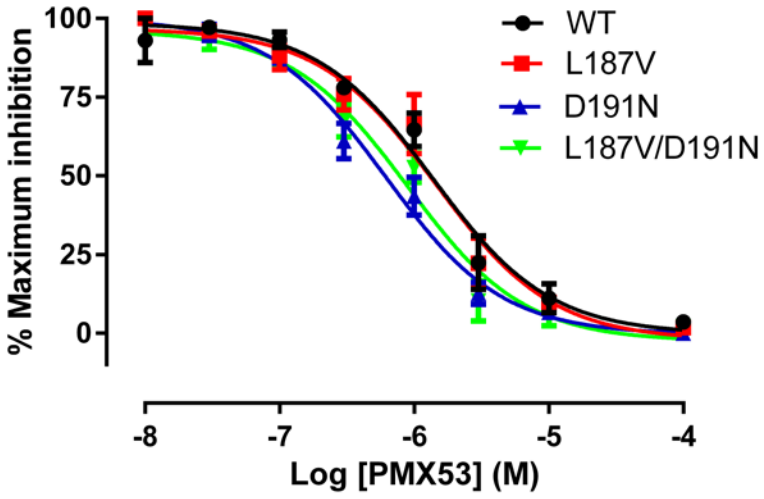

Figure 6.16 The effect of ECL2 mutations on the inhibition of C5a-mediated cAMP production by PMX53

CHO cells were transiently transfected with WT or mutant human C5aR and the BRET cAMP sensor CAMYEL. Cells were pre-incubated with increasing concentrations of PMX53 for 30 min. cAMP levels were measured after a 5 min incubation with 0.3 nM of purified human C5a and 10 µM of forskolin in the presence of 40 µM of IBMX. Data was normalised to maximum response with 0.3 nM of purified human C5a. Data are presented as the mean ± SEM of 5-6 independent experiments performed in triplicate.

6.4 Discussion

PMX53 is the most widely used antagonist in studies investigating the role of the complement peptide C5a in disease (Benson *et al.*, 2015; Iyer *et al.*, 2011; Li *et al.*, 2014a; Li *et al.*, 2014b; Woodruff *et al.*, 2003; Woodruff *et al.*, 2006). Despite being developed from the C-terminal tail of the endogenous peptide C5a, PMX53 inhibits C5a-mediated myeloperoxidase release from PMNs in a non-competitive manner (March *et al.*, 2004; Paczkowski *et al.*, 1999). The ECL2 of the C5aR has been shown to negatively modulate receptor activation (Klco *et al.*, 2005). Taken together with the data which suggest that PMX53 may bind to the ECL2, PMX53 was proposed to be a negative allosteric modulator of the C5aR.

Dissociation kinetics binding assays are routinely used to detect allosteric modulators because allosteric ligands that modulate the binding of orthosteric ligands may change the binding kinetics of the orthosteric ligands (Christopoulos and Kenakin, 2002). To investigate the modulatory effect of PMX53 on C5a, dissociation binding assays were attempted. Unfortunately, the effect of PMX53 on the dissociation rate of C5a could not be investigated in this study because [^{125}I]C5a did not readily dissociate from the C5aR. Huey and Hugli (1985) reported that the dissociation of [^{125}I]C5a from human PMNs occurs with a half-life of binding of approximately 5 min at 0°C. This dissociation could not be replicated in this study despite extensive attempts at optimisation of the experimental conditions. However, one parameter not tested in this study is the effect of sodium on the dissociation of [^{125}I]C5a. Huey and Hugli (1985) used RPMI media in the binding assay, which contained sodium ions. The allosteric effects of sodium on ligand binding have been described in the literature for many GPCRs, including

peptide binding receptors such as the vasopressin 1b receptor and the neurotensin 1 receptor as well as small molecule-binding receptors such as the adenosine A_{2A} receptor and the dopamine D_2 receptor (Koshimizu *et al.*, 2016; Liu *et al.*, 2012; Martin *et al.*, 1999; Neve, 1991). In addition, sodium has been shown to increase the dissociation rate of antagonist [^{3}H]yohimbine from the α_2 adrenoceptors (Horstman *et al.*, 1990). Therefore, the effect of sodium on the dissociation of [^{125}I]C5a from the C5aR should be investigated.

In addition to binding assays, receptor allosterism can also be detected using functional assays. Interestingly, PMX53 showed competitive antagonism in the cAMP assay. In contrast to myeloperoxidase release assays in PMNs where the maximum response of C5a was depressed in the presence of PMX53 (March *et al.*, 2004; Paczkowski *et al.*, 1999), addition of PMX53 in cAMP assays caused a parallel rightward shift of the concentration response curve of C5a. An allosteric modulator with a neutral cooperativity for ligand efficacy, but negatively modulating ligand affinity can produce a dextral displacement of the concentration response curves (Gregory *et al.*, 2010). However, this observation does not suggest an allosteric mechanism of action for PMX53. A hallmark of receptor allosterism is saturability of the observed effects which means that the dextral displacement of the concentration response curves will eventually approach a saturable limit (Christopoulos and Kenakin, 2002). In previous studies, 100 nM of PMX53 was able to depress the maximum response of C5a by as much as 80% (March *et al.*, 2004; Paczkowski *et al.*, 1999). In this study, 3 μM of PMX53 produced a parallel rightward shift in the concentration response curve of C5a with no visible sign of saturation and a Hill slope of unity. Therefore, these data suggest that PMX53

behaved as a classical competitive antagonist in the cAMP assay, which is in agreement with its origin as a peptide modified from the C-terminal tail of C5a.

Using an *in vitro* calcium assay as a surrogate marker for receptor residence time, Seow *et al*. (2016) suggested that the half-life of binding of PMX53 at the C5aR is 18.2 hours. A long receptor residence time can also be implied from the pharmacokinetics profile of PMX53. Once daily dosing of PMX53 was proven to be efficacious in numerous rat models of inflammation, despite a short plasma half-life of 20-70 min and a bioavailability of less than 2% (Morgan *et al.*, 2008; Strachan *et al.*, 2001; Woodruff *et al.*, 2003; Woodruff *et al.*, 2006; Woodruff *et al.*, 2002). In the absence of labelled PMX53, the residence time of PMX53 could be measured using a competition-association binding assay (Guo *et al.*, 2012; Motulsky and Mahan, 1984). Using this assay, the association and dissociation rate constants of an unlabelled ligand can be determined by competing the unlabelled ligand with a labelled orthosteric ligand in a standard association binding assay (Guo *et al.*, 2012; Motulsky and Mahan, 1984).

The difference in the action of PMX53 in the cAMP assay performed in this study and the myeloperoxidase release assays performed in previous studies by March *et al.* (2004) and Paczkowski *et al*. (1999) could be due to hemi-equilibrium. Hemi-equilibrium is likely to be observed in functional assays with short incubation times, whereby a competitive antagonist produces a depression in the maximum response due to insufficient agonist-antagonist-receptor re-equilibration time between the addition of agonist to initiate a response and the measurement of the response (Charlton and Vauquelin, 2010). However, this depression in maximum response may not be observed in a cellular system with a

higher receptor density despite the response being measured at hemi-equilibrium conditions, as simulated by Riddy *et al*. (2015) using a combined operational/hemi-equilibrium model of competitive antagonism, possibly due to the presence of spare receptors. The agonist-antagonist-receptor re-equilibration time in the myeloperoxidase and the cAMP assays were 10 and 5 min respectively. Therefore, if the residence time of PMX53 at the C5aR is truly in excess of 18 hours, it is likely that the C5a responses in the presence of PMX53 were measured at hemi-equilibrium conditions in both assays. The differences in the behaviour of PMX53 in the myeloperoxidase and cAMP assays could be attributed to the cellular systems used, in particular receptor density. While the level of C5aR expression in human PMNs has been determined (Huey and Hugli, 1985), the number of C5aR expressed in the CHO cells following transient transfections as performed in this study needs to be determined to help elucidate the molecular basis of the difference in PMX53 behaviour in the myeloperoxidase versus the cAMP assays. In addition, a more direct measurement of the residence time of PMX53 at the C5aR will shed more light on the molecular basis of the action of PMX53.

In this study, homology models of the C5aR were generated based on the structures of receptors that are closely related to the C5aR, either by sequence homology or ligand similarity. The hypothesis of this study was that PMX53 interacts with the human C5aR at $L187^{ECL2}$, $D191^{ECL2}$ and $S193^{ECL2}$. These residues differ in the mouse but not in rat or human C5a and they may account for the difference in the affinity of PMX53 between the three species. Based on this hypothesis, the chemokine CXCR4 receptor provided the best template for the C5aR as PMX53 frequently interacted with $L187^{ECL2}$ and $D191^{ECL2}$ at the human

C5aR model but not with the equivalent residues at the mouse C5aR model. This may have biased the template selection. However, out of all the template receptors used, CXCR4 is the closest relative of the C5aR by both sequence homology and ligand similarity and the quality of a homology model has been shown to be directly proportional to the sequence identity between the template and the model receptor (Bordoli *et al.*, 2008). Since the resolution of the template receptors used ranges from 2.5 to 3.0 Å, template resolution is expected to have little impact on the differences in the quality of the models generated in this study. Although there is little difference in PMX53 docking between the model based on the CXCR4 receptor crystallised with a small molecule antagonist and the CXCR4 receptor crystallised with a 16-amino acid peptide antagonist, the Goldscore was higher in the model based on the CXCR4 receptor crystallised with a small molecule antagonist, suggesting that the binding pocket of the model based on the CXCR4 receptor crystallised with a small molecule antagonist may accommodate PMX53 better than the model based on the CXCR4 receptor crystallised with a 16-amino acid peptide antagonist.

The highest ranked docking pose of PMX53 at the human C5aR model based on the CXCR4 receptor crystallised with a small molecule antagonist suggested that PMX53 binds across the upper region of the TM domain and ECL regions of the C5aR, with the N-terminal AcF1 binding in the region between TM5 and TM6, and the C-terminal R6 interacting with $D191^{ECL2}$. This mode of PMX53 binding is similar to that reported by Tamamis *et al*. (2014) using a model based on bovine rhodopsin with *de novo* loop generation. However, PMX53 adopted a more stretched conformation and bound approximately one helix turn deeper in the

study conducted by Tamamis *et al*. (2014). In the highest ranked pose of the rhodopsin based model, AcF1 pointed towards the TM helix core while R6 lay at the extracellular face of the receptor, in between TM7 and ECL2 and strong polar interactions were observed between Orn2-R206$^{5.42}$, dCha4-R206$^{5.42}$, W5-H194^{ECL2}, R6-D282$^{7.35}$, R6-D191^{ECL2}, R6-L287$^{7.40}$ and R6-Y258$^{6.51}$ (Tamamis *et al.*, 2014). Similarly, docking of PMX53 into the human C5aR model based on the CXCR4 receptor crystallised with a small molecule antagonist also identified high frequency of interactions with D191^{ECL2}, R206$^{5.42}$ and D282$^{7.35}$, whereas the docking of PMX53 into the human C5aR model based on the CXCR4 receptor crystallised with a 16-amino acid peptide antagonist identified high frequency of interactions with D191^{ECL2}, R206$^{5.42}$ and Y258$^{6.51}$, but not with D282$^{7.35}$. Although docking identified high frequencies of interactions with L187^{ECL2} in both human C5aR models based on the CXCR4 receptor structures, this interaction was not observed in the highest scoring pose at the CXCR4 based nor at the rhodopsin model used by Tamamis *et al.* (2014), suggesting that this interaction may not be critical for the binding of PMX53 at the C5aR. Overall, the docking of PMX53 into the human C5aR models based on the CXCR4 receptor is largely in agreement with previously published data (Tamamis *et al.*, 2014).

Using a homology model based on the chemokine CXCR1 receptor, Rana *et al*. (2016) suggested that PMX53 occupies the extracellular region of the C5aR, interacting solely with residues from the N-terminus and all three extracellular loops. This result is not in agreement with the data presented in this study and also in the study by Tamamis *et al*. (2014). Rana *et al*. (2016) suggested that W5 of PMX53 occupied the same pocket as K5 of the C5aR peptide agonist

NISHKDMQLGR, making a strong π-π interaction with F275^{ECL3}. Similarly, in an earlier study using the same homology model, Rana *et al*. (2015) suggested that the equivalent lysine residue of EP54 (YSFKPMPLaR), K4, also made a strong interaction with F275^{ECL3}. This result is not supported by a mutagenesis study where K4 of EP54 was suggested to interact with E199$^{5.35}$ located at the top of TM5 (Vogen *et al.*, 1999). Vogen *et al*. (1999) showed that the mutation of K4 to an aspartic acid significantly decreased the affinity of EP54 at the WT C5aR and that this decrease in affinity was not observed at the mutant E199$^{5.35}$K mutant C5aR, suggesting that K4 of EP54 interacts with E199$^{5.35}$. K4 of EP54 is analogous to Orn2 in PMX53. In the highest scoring pose of the largest cluster based on the CXCR4 receptor crystallised with a small molecule antagonist, Orn2 of PMX53 can be seen to interact with R198$^{5.34}$, which more closely reflects the mutagenesis data by Vogen *et al*. (1999). In addition, the data presented in this chapter and in the study by Tamamis *et al.* (2014) both identified ECL2 residues G189^{ECL2} and V190^{ECL2} as interacting partners for W_5 of PMX53.

A mutagenesis study has identified several key residues that play a role in the interaction of the non-acetylated analogue of PMX53 at the C5aR (Higginbottom *et al.*, 2005). In the study, the mutations I116$^{3.32}$A and V286$^{7.39}$A were found to decrease the affinity of the non-acetylated analogue of PMX53 by 6 and 2 fold respectively (Higginbottom *et al.*, 2005). The largest effect was observed with the mutation R175^{ECL2}D where the potency of the non-acetylated analogue of PMX53 was decreased by 131 fold and the ligand was converted to a weak partial agonist (Higginbottom *et al.*, 2005). This data provides further evidence that PMX53 is not an allosteric modulator, but instead an orthosteric antagonist. In addition,

I116$^{3.32}$A, E199$^{5.35}$K, R206$^{5.42}$A and D282$^{7.35}$A were found to have a small but significant effect on the potency of the non-acetylated analogue of PMX53. The docking of PMX53 into the human C5aR based on the CXCR4 receptor crystallised with a small molecule antagonist did not identify an interaction between PMX53 and I116$^{3.32}$, suggesting that the increase in the affinity and potency of the non-acetylated analogue of PMX53 at the I116$^{3.32}$A mutant may be due to a conformational change caused by the mutation. However, in agreement with these mutagenesis data, the docking of PMX53 identified high frequencies of interactions with R175^{ECL2}, R206$^{5.42}$, D282$^{7.35}$ and V286$^{7.39}$. These data suggest that PMX53 binding at the C5aR can be modelled accurately from a homology model based on the CXCR4 receptor.

Contrary to the prediction that the mutation of D191^{ECL2} to the corresponding mouse residue would lead to a decrease in the affinity and therefore the potency of PMX53, the mutation D191^{ECL2}N increased the potency of PMX53. The docking of PMX53 at the human C5aR model suggested that the side chain of R6 was positioned between two negatively charged amino acids D191^{ECL2} and E180^{ECL2}. It is possible that the interaction of R6 with E180^{ECL2} in the absence of D191^{ECL2} enables PMX53 to interact better with its TM interaction partners such as R175^{ECL2} and D282$^{7.35}$, mutations of which have been shown to decrease the potency of the non-acetylated analogue of PMX53 (Higginbottom *et al.*, 2005). Further mutagenesis and receptor binding studies need to be performed to fully characterise the contribution of D191^{ECL2} in the binding of PMX53.

The residues suggested to interact with PMX53 in the docking studies have also been implicated in the binding of C5a. The mutations R175^{ECL2}A, R175^{ECL2}D,

D282$^{7.35}$A, D282$^{7.35}$R and V286$^{7.39}$A have been shown to decrease the affinity of C5a at the human C5aR (Cain *et al.*, 2001a; Cain *et al.*, 2003; Higginbottom *et al.*, 2005). The role of R175^{ECL2} and D282$^{7.35}$ on the C5a-mediated receptor activation has also been described in the literature (Cain *et al.*, 2001a; Cain *et al.*, 2003). The mutant C5aR R175^{ECL2}A can be weakly activated by C5a but strongly activated by a mutant C5a peptide, suggesting that C5a makes a specific interaction with R175^{ECL2} when bound to the receptor (Cain *et al.*, 2003). Meanwhile, the mutation D282$^{7.35}$A has a decreased response to C5a, but not C5a-desArg (Cain *et al.*, 2001a). In addition, the mutation of C5a at position R74 to alanine decreased receptor activation at the WT receptor by 60 fold, but only by 2 fold at the D282$^{7.35}$A mutant (Cain *et al.*, 2001a). Similarly, the C5a R74D mutant was inactive at the WT and D282$^{7.35}$A mutant, but active at the D282$^{7.35}$R mutant (Cain *et al.*, 2001a). All of these data suggest the importance of R175^{ECL2}, D282$^{7.35}$ and V286$^{7.39}$ in the binding and/or activity of C5a at the C5aR. As PMX53 was developed through the modification of an agonist based on the C-terminal tail of C5a, combined with a mutagenesis study which suggested that PMX53 can be converted to a partial agonist at the R175^{ECL2}D mutant (Higginbottom *et al.*, 2005), this overlap in binding site was not unexpected. Combined with the observation that PMX53 produced a parallel rightward shift in the concentration response curve of C5a, these data strongly suggest that PMX53 is a competitive antagonist and not an allosteric modulator of the C5aR.

Allosteric modulation of the C5aR by a small molecule ligand has been described by Moriconi *et al.* (2014). DF2593A was rationally designed to target the binding pocket of the C5aR which corresponds to the allosteric binding pocket of

the closely related CXCR1 receptor. This pocket, formed by TM 1,2,3,6 and 7, was initially identified through the docking of repertaxin into a rhodopsin-based model of the CXCR1 receptor and subsequently confirmed by mutagenesis (Bertini *et al.*, 2004). DF2593A has no apparent affinity at the C5aR as shown in competition binding assays using [^{125}I]C5a and did not compete for binding with unlabelled C5a (Moriconi *et al.*, 2014). Docking of DF2593A into a homology model based on the CXCR1 receptor predicted direct interactions with D82$^{2.50}$, I116$^{3.32}$, N119$^{3.35}$, Y258$^{6.51}$, D282$^{7.35}$ and Y290$^{7.43}$ (Moriconi *et al.*, 2014). D82$^{2.50}$ was shown to mediate C5aR activation by C5a but was not involved in the binding of C5a (Monk *et al.*, 1994) and thus the interaction of DF2593A with D82$^{2.50}$ was proposed to inhibit C5a-mediated receptor activation by locking the receptor in an inactive conformation (Moriconi *et al.*, 2014). However, the contribution of D82$^{2.50}$ to the binding of DF2593A has not been investigated. In addition, the interaction of DF2593A with D282$^{7.35}$ should also be investigated as this residue has been shown to interact with C5a (Cain *et al.*, 2001a) and was frequently observed to interact with PMX53 in this study, suggesting that DF2593A may not be an allosteric modulator. In agreement with the docking results, the mutation N119$^{3.35}$A decreased the potency of DF2593A. Furthermore, mutation of the hydrophobic residues capping the binding pocket of DF2593A, L41$^{1.36}$, F93$^{2.61}$, I96$^{2.64}$, L278$^{7.31}$ and Y258$^{6.51}$, also decreased the potency of the ligand, suggesting a role of these residues in maintaining the shape of the binding pocket (Moriconi *et al.*, 2014). Interestingly, Y251$^{6.51}$ of the closely related chemokine CCR5 receptor has been shown to mediate the binding of the clinically approved allosteric modulator maraviroc (Kondru *et al.*, 2008), suggesting a possible conservation of an allosteric binding site between peptide binding receptors.

In summary, contrary to the previously published data which identified PMX53 as a non-competitive antagonist of the C5aR, the data presented in this study strongly suggest that PMX53 is a competitive antagonist of the C5aR with a long receptor residence time which interacts with residues implicated in the binding of C5a at the C5aR.

CHAPTER 7

General discussion and future directions

There is increasing interest in the role of the extracellular domain of family A GPCRs in ligand binding and receptor activation. In α branch family A GPCRs, this interest largely stems from the discovery that allosteric modulators of the mAChRs bind to the residues on the ECL2-3 and the upper region of TM6-7 (Avlani *et al.*, 2007; Gnagey *et al.*, 1999; Huang *et al.*, 2005; Jager *et al.*, 2007; Kruse *et al.*, 2013; May *et al.*, 2007; Trankle *et al.*, 2003; Voigtländer *et al.*, 2003). This region has also been shown to regulate the kinetics of orthosteric ligand binding and unbinding and therefore ligand residence time (Dror *et al.*, 2011; Gonzalez *et al.*, 2011; Kruse *et al.*, 2012; Plazinska *et al.*, 2015; Thomas *et al.*, 2016; Wang and Duan, 2009).

This thesis is the first to characterise a binding site for small molecule allosteric ligands at the β_2AR, which is distinct from the intracellular allosteric binding site for Zn^{2+} (Swaminath *et al.*, 2003). The allosteric binding site of the β_2AR identified in this study is made up of residues from the ECL2 and the top of TM6 and 7, in particular $F193^{ECL2}$, $H296^{6.58}$, $K305^{7.32}$ and $Y308^{7.35}$. The characterisation of this extracellular allosteric binding site will be useful for future *in silico* drug discovery and rational design of β_2AR allosteric modulators. For example, the data generated in this thesis can be used to develop complex-based pharmacophores, which could then be used in virtual screenings to identify novel β_2AR modulators.

The characterisation of the β_2AR allosteric binding site also adds to current understanding of allosteric mechanisms across the small molecule neurotransmitter-binding family A GPCRs. The data in this thesis showed that the allosteric binding site of the β_2AR corresponds to the allosteric binding site of the mAChRs (Gnagey *et al.*, 1999; Huang *et al.*, 2005; Jager *et al.*, 2007; Kruse *et al.*, 2012; May *et al.*, 2007; Voigtländer *et al.*, 2003). However, allosteric modulators of the α_{1A}AR and the D_2 dopamine receptor have been found to interact with residues at the top of TM2 (Campbell, 2015; Lane *et al.*, 2014), whereas allosteric modulators of the A_1 and A_3 adenosine receptors have been found to interact with residues within TM1,2,3,5 and 7 (Gao *et al.*, 2003; Kourounakis *et al.*, 2001). These sites are distinct from the allosteric site of the β_2AR and mAChRs, suggesting a conservation of allosteric binding sites across several, but not all family A GPCRs.

It has previously been postulated that allosteric modulators have the potential to increase receptor subtype selectivity because allosteric sites would have been under less evolutionary pressure and are therefore less conserved than the orthosteric site (Christopoulos, 2002; Gentry *et al.*, 2015). However, the data presented in this study suggest that like orthosteric sites, allosteric sites of closely related receptors may also be conserved. For example, the allosteric binding site of tacrine at the β_2AR identified in this study is the same site as that previously identified at the M_2 mAChR (Trankle *et al.*, 2005). In addition, tacrine can also modulate antagonist binding at the α_{1A}AR and its binding site at the α_{1A}AR may overlap with the β_2AR (Campbell, 2015). Therefore, the allosteric binding site of these small molecule neurotransmitter-binding GPCRs may not be as diverse as previously thought.

Recent advances in structural biology and computational modelling have enabled high detail simulations of ligand binding and unbinding at GPCRs (Dror *et al.*, 2011; Gonzalez *et al.*, 2011; Guo *et al.*, 2016; Kruse *et al.*, 2012; Plazinska *et al.*, 2015; Sabbadin *et al.*, 2015; Sandal *et al.*, 2015; Thomas *et al.*, 2016; Wang and Duan, 2009). These computational studies provide insights into the previously unknown mechanism of ligand entry and exit from GPCRs which includes a metastable binding site located at the extracellular vestibule of these receptors. Molecular dynamics studies investigating ligand binding and unbinding at the β_2AR and the M_2 and M_3 mAChRs suggested that orthosteric ligands pause at the extracellular vestibule formed by residues from the ECL2 and the top of TM6 and 7 prior to their entry into the orthosteric binding pocket and that ligand exit from the receptors occur through the same pathway (Dror *et al.*, 2011; Gonzalez *et al.*, 2011; Kruse *et al.*, 2012; Plazinska *et al.*, 2015; Wang and Duan, 2009). The data presented in this thesis provide the pharmacological evidence for the existence of this metastable binding site at the β_2AR, supporting a role for F193^{ECL2} and Y308$^{7.35}$ as gatekeepers for ligand entry and exit from the receptor and K305$^{7.32}$ as a regulator of the gate formed by F193^{ECL2} and Y308$^{7.32}$. The mechanism of orthosteric ligand binding which involves a metastable binding site at the extracellular vestibule of the receptor has been proposed for other GPCRs such as the β_1AR, M_2/M_3 mAChRs, D_2/D_3 dopamine receptors and adenosine A_{2A} receptor (Dror *et al.*, 2011; Guo *et al.*, 2016; Kruse *et al.*, 2012; Sabbadin *et al.*, 2015; Thomas *et al.*, 2016). Taken together, these data suggest that orthosteric ligand binding at GPCRs is a multi-step process controlled by residues located at the extracellular region of the receptors.

The data presented in this thesis also showed that an allosteric binding site of the β_2AR coincides with the extracellular vestibule of the receptor, with the binding site of THRX100361 and tacrine overlapping with the ligand entry pathway formed by the residues from the ECL2 and TM6 and 7. Despite this, the orthosteric ligand isoprenaline was able to activate the β_2AR in the presence of pre-bound THRX100361 and tacrine. This suggests that more than one ligand entry pathway may be present. Previous molecular dynamics studies support this idea, as residues lining the ECL2 and the top of TM2, 3 and 7 have been suggested to form a minor ligand entry/exit pathway (Gonzalez *et al.*, 2011; Wang and Duan, 2009).

The overlap in the allosteric and orthosteric binding site of the β_2AR suggests that allosteric and orthosteric ligands may share common properties. For example, like many orthosteric ligands of the βAR, THRX100361 and tacrine both contain a basic nitrogen and one or more phenol ring(s). In support of this, orthosteric ligands of the mAChR have been shown to be able to bind weakly to the allosteric site of the receptor (Redka *et al.*, 2008). Therefore, for orthosteric ligands to bind to the receptor, they must first be "captured" by the vestibule before binding in the orthosteric pocket. Furthermore, the β_2AR agonist BA is an allosteric modulator of the M_2/M_3 mAChRs while the muscarinic antagonist THRX100361 is an allosteric modulator of the β_2AR (Chapter 3; Steinfeld *et al*. 2011). The reciprocal modulation of the β_2AR and M_2/M_3 mAChRs by these ligands suggests that allosteric modulators of these receptors share similar inherent properties with their orthosteric ligands.

While sharing structural characteristics, allosteric modulators have low apparent affinity for the orthosteric binding site and therefore remain at the vestibule and cannot progress to the orthosteric site. A structural basis for the modulatory effects of allosteric ligands can therefore be proposed from this study. Allosteric modulators that potentiate the residence time of orthosteric ligands may do so either by directly blocking orthosteric ligand exit or promoting a "closed" vestibule, while allosteric modulators that decrease residence time may do so by keeping the vestibule in an "open" conformation.

This ability of modulators to modulate orthosteric ligand residence time has been suggested to potentially increase receptor subtype selectivity through cooperativity-driven selectivity between the orthosteric and the allosteric sites (Christopoulos, 2002; Gentry *et al.*, 2015). While the data presented in this study suggest that like orthosteric sites, allosteric sites of closely related receptors may also be conserved. Therefore, increased receptor subtype selectivity from allosteric modulators may be more readily achieved through cooperativity-driven selectivity. For example, tiochrome is a functionally selective M_4 mAChR allosteric modulator which displays equal affinity for the allosteric binding site of M_1-M_4 mAChRs (Lazareno *et al.*, 2004).

In family A GPCRs, the ECL2 is the most divergent structure that shares few similarities between different receptor groups in family A GPCRs. As shown in chapters 3-5 and other studies, the ECL2 plays an important role in the function as well as the binding of orthosteric and allosteric ligands at many family A GPCRs (Avlani *et al.*, 2007; Campbell *et al.*, 2014; Jager *et al.*, 2007; Klco *et al.*, 2005; Voigtländer *et al.*, 2003). The data in this thesis show that the ECL2 of the β_2AR

plays a role in both orthosteric and allosteric ligand interactions. Similarly, the ECL2 is also important for the interaction of the peptide-mimetic antagonist PMX53 at the C5aR.

PMX53 is one of the most widely used C5aR antagonists in research investigating the role of C5a in disease. While previously described as a non-competitive antagonist (March *et al.*, 2004; Paczkowski *et al.*, 1999), this study shows that PMX53 is most likely a competitive antagonist of the C5aR. This discrepancy can be explained by the long residence time of PMX53 at the C5aR. While the residence time of PMX53 remains to be measured directly, evidence which suggests that PMX53 has a long residence time at the C5aR exists. Using a calcium release assay as a surrogate readout, the residence time of PMX53 at the C5aR was recently estimated to be in excess of 18 hours (Seow *et al.*, 2016). The antagonism of the C5aR by PMX53 was shown to be superior compared to equipotent small molecule antagonists W54011 and JJ47 because of its residence time, which was estimated to be 15 and 30 fold longer compared to W54011 and JJ47 respectively (Seow *et al.*, 2016). While the plasma concentrations of W54011 and JJ47 peaked at 2 to 3 hours following oral administrations, PMX53 could not be detected in the plasma after oral administrations (Seow *et al.*, 2016). Despite this, the ability of PMX53 to antagonise C5aR agonist-mediated paw swelling in rats was evident 16 hours post antagonist administration, while W54011 and JJ47 were no longer efficacious 2 hours post-administration (Seow *et al.*, 2016). Other studies have also shown that once daily dosing of PMX53 was effective in rat models of arthritis, inflammatory bowel disease and neuro-inflammation (Morgan *et al.*, 2008; Strachan *et al.*, 2001; Woodruff *et al.*, 2003; Woodruff *et al.*, 2006; Woodruff

et al., 2002). Taken together, these data suggest a long residence time of PMX53 at the C5aR. The cAMP study performed with PMX53 in this study highlights the importance of considering residence time in the pharmacological characterisation of a ligand, as agonist-antagonist-receptor re-equilibration time in functional assays with short incubation times can determine the outcome of the responses measured.

PMX53 is one of the most potent C5aR antagonists ever developed but currently remains as a research tool. As ligand-receptor residence time is governed by the interaction of the ligand with the receptor (Gillard *et al.*, 2002; Vilums *et al.*, 2015), future studies investigating the residue(s) responsible for conferring the long residence time of PMX53 will be useful for the design of next generation C5aR antagonists. This study has provided the tools that can aid in this process, which include accurate homology models of the C5aR and the prediction of the binding of PMX53 at these models.

The kinetics of ligand binding was a previously under-appreciated parameter in drug discovery. However, the kinetics of ligand binding is increasingly recognised to play an important role in receptor-ligand interactions. Firstly, the residence time of a drug at its target receptor has been correlated with increased functional efficacy (Guo *et al.*, 2012; Sykes *et al.*, 2009) and improved clinical outcomes (Casarosa *et al.*, 2009; Seow *et al.*, 2016). Secondly, ligand binding kinetics has been exploited to improve receptor subtype selectivity and reduce off-target side effects (Disse *et al.*, 1993). Most recently, residence time has been shown to play a role not only in the duration of action of ligands, but also in the determination of signalling outcomes (Klein Herenbrink *et al.*, 2016). Ligands with

long residence time at the D_2 dopamine receptor have been shown to display bias in multiple signalling pathways and changes in the magnitude and direction of bias were observed with these ligands over time, suggesting that residence time plays a role in the recruitment of signalling molecules (Klein Herenbrink *et al.*, 2016). Therefore, the kinetics of ligand binding is an important parameter to consider in pharmacological characterisation of ligands as well as in drug development.

In summary, using the β_2AR and the C5aR as examples, this thesis describes the importance of the extracellular region of family A GPCRs in orthosteric and allosteric ligand interactions. The results presented in this thesis characterised for the first time an extracellular allosteric binding site at the β_2AR which is amenable to modulation by small molecule ligands and the role that this region plays in the control of orthosteric ligand binding kinetics. This thesis also investigated the molecular mechanism of action of the highly potent C5aR antagonist, PMX53, highlighting the importance of ligand-receptor residence time in the pharmacological characterisation of candidate drug molecules. The data presented in this thesis is useful for future drug design and development for the β_2AR and the C5aR.

References

Aaron SD, Vandemheen KL, Fergusson D, Maltais F, Bourbeau J, Goldstein R*, et al.* (2007). Tiotropium in combination with placebo, salmeterol, or fluticasone–salmeterol for treatment of chronic obstructive pulmonary disease: a randomized trial *Ann Intern Med* 146**:** 545-555.

Abdul-Ridha A, Lane JR, Mistry SN, López L, Sexton PM, Scammells PJ*, et al.* (2014). Mechanistic insights into allosteric structure-function relationships at the M_1 muscarinic acetylcholine receptor. *J Biol Chem* 289**:** 33701-33711.

Ager RR, Fonseca MI, Chu SH, Sanderson SD, Taylor SM, Woodruff TM*, et al.* (2010). Microglial C5aR (CD88) expression correlates with amyloid-β deposition in murine models of Alzheimer's disease. *J Neurochem* 113**:** 389-401.

Ahn S, Nelson CD, Garrison TR, Miller WE & Lefkowitz RJ (2003). Desensitization, internalization, and signaling functions of β-arrestins demonstrated by RNA interference. *Proc Natl Acad Sci USA* 100**:** 1740-1744.

Ahn S, Shenoy SK, Wei H & Lefkowitz RJ (2004). Differential kinetic and spatial patterns of β-arrestin and G protein-mediated ERK activation by the angiotensin II receptor. *J Biol Chem* 279**:** 35518-35525.

Akam EC, Challiss RAJ & Nahorski SR (2001). $G_{q/11}$ and $G_{i/o}$ activation profiles in CHO cells expressing human muscarinic acetylcholine receptors: dependence on agonist as well as receptor-subtype. *Br J Pharmacol* 132**:** 950-958.

Altenbach C, Kusnetzow AK, Ernst OP, Hofmann KP & Hubbell WL (2008). High-resolution distance mapping in rhodopsin reveals the pattern of helix movement due to activation. *Proc Natl Acad Sci USA* 105**:** 7439-7444.

Amatruda TT, Gerard NP, Gerard C & Simon MI (1993). Specific interactions of chemoattractant factor receptors with G-proteins. *J Biol Chem* 268**:** 10139-10144.

Andersson KE & Wyllie MG (2003). Ejaculatory dysfunction: why all alpha-blockers are not equal. *BJU Int* 92**:** 876-877.

Andrews G, Jones C & Wreggett KA (2008). An intracellular allosteric site for a specific class of antagonists of the CC chemokine G protein-coupled receptors CCR4 and CCR5. *Mol Pharmacol* 73**:** 855-867.

Appell KC, Chung TDY, Solly KJ & Chelsky D (1998). Biological characterization of neurokinin antagonists discovered through screening of a combinatorial library. *J Biomol Screen* 3**:** 19-27.

Arumugam TV, Shiels IA, Woodruff TM, Reid RC, Fairlie DP & Taylor SM (2002). Protective effect of a new C5a receptor antagonist against ischemia-reperfusion injury in the rat small intestine. *J Surg Res* 103**:** 260-267.

Avlani VA, Gregory KJ, Morton CJ, Parker MW, Sexton PM & Christopoulos A (2007). Critical role for the second extracellular loop in the binding of both orthosteric and allosteric G protein-coupled receptor ligands. *J Biol Chem* 282**:** 25677-25686.

Baker JG (2005). The selectivity of β-adrenoceptor antagonists at the human β_1, β_2 and β_3 adrenoceptors. *Br J Pharmacol* 144**:** 317-322.

Baker JG (2010). The selectivity of β-adrenoceptor agonists at human β_1-, β_2- and β_3-adrenoceptors. *Br J Pharmacol* 160**:** 1048-1061.

Baker JG, Proudman RGW & Hill SJ (2015). Salmeterol's extreme β_2 selectivity is due to residues in both extracellular loops and transmembrane domains. *Mol Pharmacol* 87**:** 103-120.

Ball D, Coleman R, Denyer L, Nials A & Sheldrick K (1987). In vitro characterisation of the β_2-adrenoceptor agonist, salmeterol. *Br J Pharmacol* 92**:** 591P.

Ballesteros JA & Weinstein H (1995). Integrated methods for the construction of three-dimensional models and computational probing of structure-function relations in G protein-coupled receptors. In Methods in Neurosciences. ed Stuart C.S. Academic Press, 366-428.

Bamberg CE, Mackay CR, Lee H, Zahra D, Jackson J, Lim YS*, et al.* (2010). The C5a receptor (C5aR) C5L2 is a modulator of C5aR-mediated signal transduction. *J Biol Chem* 285**:** 7633-7644.

Bao L, Osawe I, Puri T, Lambris JD, Haas M & Quigg RJ (2005). C5a promotes development of experimental lupus nephritis which can be blocked with a specific receptor antagonist. *Eur J Immunol* 35**:** 2496-2506.

Bateman ED, Hurd SS, Barnes PJ, Bousquet J, Drazen JM, FitzGerald M*, et al.* (2008). Global strategy for asthma management and prevention: GINA executive summary. *Eur Respir J* 31**:** 143-178.

Bateman ED, Kornmann O, Ambery C & Norris V (2013). Pharmacodynamics of GSK961081, a bi-functional molecule, in patients with COPD. *Pulm Pharmacol Ther* 26**:** 581-587.

Benovic JL, Kuhn H, Weyand I, Codina J, Caron MG & Lefkowitz RJ (1987). Functional desensitization of the isolated β-adrenergic receptor by the β-adrenergic receptor kinase: potential role of an analog of the retinal protein arrestin (48-kDa protein). *Proc Natl Acad Sci USA* 84**:** 8879-8882.

Benson MJ, Thomas NK, Talwar S, Hodson MP, Lynch JW, Woodruff TM*, et al.* (2015). A novel anticonvulsant mechanism via inhibition of complement receptor C5aR1 in murine epilepsy models. *Neurobiol Dis* 76**:** 87-97.

Berman HM, Westbrook J, Feng Z, Gilliland G, Bhat TN, Weissig H*, et al.* (2000). The Protein Data Bank. *Nucleic Acids Res* 28**:** 235-242.

Bertini R, Allegretti M, Bizzarri C, Moriconi A, Locati M, Zampella G*, et al.* (2004). Noncompetitive allosteric inhibitors of the inflammatory chemokine receptors CXCR1 and CXCR2: Prevention of reperfusion injury. *Proc Natl Acad Sci USA* 101**:** 11791-11796.

Birnbaumer L & Zurita AR (2010). On the roles of Mg in the activation of G proteins. *J Recept and Signal Transduct* 30**:** 372-375.

Blair JB, James ME & Foster JL (1979). Adrenergic control of glycolysis and pyruvate kinase activity in hepatocytes from young and old rats. *J Biol Chem* 254**:** 7585-7590.

Bock A, Merten N, Schrage R, Dallanoce C, Batz J, Klockner J*, et al.* (2012). The allosteric vestibule of a seven transmembrane helical receptor controls G-protein coupling. *Nat Commun* 3**:** 1044.

Bokisch VA & Muller-Eberhard HJ (1970). Anaphylatoxin inactivator of human plasma: its isolation and characterization as a carboxypeptidase. *J Clin Invest* 49**:** 2427-2436.

Bokoch MP, Zou Y, Rasmussen SGF, Liu CW, Nygaard R, Rosenbaum DM*, et al.* (2010). Ligand-specific regulation of the extracellular surface of a G-protein-coupled receptor. *Nature* 463**:** 108-112.

Bordoli L, Kiefer F, Arnold K, Benkert P, Battey J & Schwede T (2008). Protein structure homology modeling using SWISS-MODEL workspace. *Nat Protocols* 4**:** 1-13.

Boulay F, Mery L, Tardif M, Brouchon L & Vignais P (1991). Expression cloning of a receptor for C5a anaphylatoxin on differentiated HL-60 cells. *Biochemistry* 30**:** 2993-2999.

Bradley ME, Bond ME, Manini J, Brown Z & Charlton SJ (2009). SB265610 is an allosteric, inverse agonist at the human CXCR2 receptor. *Br J Pharmacol* 158**:** 328-338.

Bradshaw J, Brittain R, Coleman R, Jack D, Kennedy I, Lunts L*, et al.* (1987). The design of salmeterol, a long-acting selective β_2-adrenoceptor agonist. *Br J Pharmacol* 92**:** 590P.

Braun M & Davis AE, III (1998). Cultured human glomerular mesangial cells express the C5a receptor. *Kidney Int* 54**:** 1542-1549.

Bubeck P, Grötzinger J, Winkler M, Köhl J, Wollmer A, Klos A*, et al.* (1994). Site-specific mutagenesis of residues in the human C5a anaphylatoxin which are involved in possible interaction with the C5a receptor. *Eur J Biochem* 219**:** 897-904.

Buck E, Bourne H & Wells JA (2005). Site-specific disulfide capture of agonist and antagonist peptides on the C5a receptor. *J Biol Chem* 280**:** 4009-4012.

Buhl AM, Avdi N, Worthen GS & Johnson GL (1994). Mapping of the C5a receptor signal transduction network in human neutrophils. *Proc Natl Acad Sci USA* 91**:** 9190-9194.

Burford NT, Clark MJ, Wehrman TS, Gerritz SW, Banks M, O'Connell J*, et al.* (2013). Discovery of positive allosteric modulators and silent allosteric modulators of the μ-opioid receptor. *Proc Natl Acad Sci USA* 110**:** 10830-10835.

Burgmer U, Schulz U, Trankle C & Mohr K (1998). Interaction of Mg^{2+} with the allosteric site of muscarinic M_2 receptors. *Naunyn Schmiedebergs Arch Pharmacol* 357**:** 363-370.

Bylund DB (1988). Subtypes of α_2-adrenoceptors: pharmacological and molecular biological evidence converge. *Trends Pharmacol Sci* 9**:** 356-361.

Cain S, Coughlan T & Monk P (2001a). Mapping the ligand-binding site on the C5a receptor: arginine 74 of C5a contacts aspartate 282 of the C5a receptor. *Biochemistry* 40**:** 14047 - 14052.

Cain S, Higginbottom A & Monk P (2003). Characterisation of C5a receptor agonists from phage display libraries. *Biochem Pharmacol* 66**:** 1833 - 1840.

Cain SA & Monk PN (2002). The orphan receptor C5L2 has high affinity binding sites for complement fragments C5a and C5a des-Arg74. *J Biol Chem* 277**:** 7165-7169.

Cain SA, Woodruff TM, Taylor SM, Fairlie DP, Sanderson SD & Monk PN (2001b). Modulation of ligand selectivity by mutation of the first extracellular loop of the human C5a receptor. *Biochem Pharmacol* 61**:** 1571-1579.

Campbell AP (2015). Identification of novel sites of interaction for α_1 adrenoceptors. PhD thesis. UNSW Australia: Sydney.

Campbell AP, MacDougall IJ, Griffith R & Finch AM (2014). An aspartate in the second extracellular loop of the α_{1B} adrenoceptor regulates agonist binding. *Eur J Pharmacol* 733**:** 90-96.

Canals M, Lane JR, Wen A, Scammells PJ, Sexton PM & Christopoulos A (2012). A Monod-Wyman-Changeux mechanism can explain G protein-coupled receptor (GPCR) allosteric modulation. *J Biol Chem* 287**:** 650-659.

Carlsson J, Coleman RG, Setola V, Irwin JJ, Fan H, Schlessinger A*, et al.* (2011). Ligand discovery from a dopamine D_3 receptor homology model and crystal structure. *Nat Chem Biol* 7**:** 769-778.

Carpenter EP, Beis K, Cameron AD & Iwata S (2008). Overcoming the challenges of membrane protein crystallography. *Curr Opin Struct Biol* 18**:** 581-586.

Carroll MC (2004). The complement system in regulation of adaptive immunity. *Nat Immunol* 5**:** 981-986.

Carstairs JR, Nimmo AJ & Barnes PJ (1985). Autoradiographic visualization of β-adrenoceptor subtypes in human lung. *Am Rev Respir Dis* 132**:** 541-547.

Casarosa P, Bouyssou T, Germeyer S, Schnapp A, Gantner F & Pieper M (2009). Preclinical evaluation of long-acting muscarinic antagonists: comparison of tiotropium and investigational drugs. *J Pharmacol Exp Ther* 330**:** 660-668.

Cavasotto CN & Phatak SS (2009). Homology modeling in drug discovery: current trends and applications. *Drug Discov Today* 14**:** 676-683.

Cazzola M, Centanni S, Santus P, Verga M, Mondoni M, di Marco F*, et al.* (2004). The functional impact of adding salmeterol and tiotropium in patients with stable COPD. *Resp Med* 98**:** 1214-1221.

Cazzola M & Matera MG (2007). Review: Safety of long-acting β_2-agonists in the treatment of asthma. *Therapeutic Advances in Respiratory Disease* 1**:** 35-46.

Chan WY, McKinzie DL, Bose S, Mitchell SN, Witkin JM, Thompson RC*, et al.* (2008). Allosteric modulation of the muscarinic M_4 receptor as an approach to treating schizophrenia. *Proc Natl Acad Sci USA* 105**:** 10978-10983.

Charlton SJ & Vauquelin G (2010). Elusive equilibrium: the challenge of interpreting receptor pharmacology using calcium assays. *Br J Pharmacol* 161**:** 1250-1265.

Chen NJ, Mirtsos C, Suh D, Lu YC, Lin WJ, McKerlie C*, et al.* (2007). C5L2 is critical for the biological activities of the anaphylatoxins C5a and C3a. *Nature* 446**:** 203-207.

Cheng Y-C & Prusoff WH (1973). Relationship between the inhibition constant (K_I) and the concentration of inhibitor which causes 50 per cent inhibition (I_{50}) of an enzymatic reaction. *Biochem Pharmacol* 22**:** 3099-3108.

Cherezov V, Rosenbaum DM, Hanson MA, Rasmussen SGF, Thian FS, Kobilka TS*, et al.* (2007). High-resolution crystal structure of an engineered human β_2-adrenergic G protein–coupled receptor. *Science* 318**:** 1258-1265.

Cheung YD, Barnett DB & Nahorski SR (1982). [^{3}H]Rauwolscine and [^{3}H]yohimbine binding to rat cerebral and human platelet membranes: possible heterogeneity of α_2-adrenoceptors. *Eur J Pharmacol* 84**:** 79-85.

Chien EY, Liu W, Zhao Q, Katritch V, Han GW, Hanson MA*, et al.* (2010). Structure of the human dopamine D_3 receptor in complex with a D_2/D_3 selective antagonist. *Science* 330**:** 1091-1095.

Chowdhury BA & Dal Pan G (2010). The FDA and safe use of long-acting β-agonists in the treatment of asthma. *N Engl J Med* 362**:** 1169-1171.

Christopoulos A (2002). Allosteric binding sites on cell-surface receptors: novel targets for drug discovery. *Nat Rev Drug Discov* 1**:** 198-210.

Christopoulos A, Changeux JP, Catterall WA, Fabbro D, Burris TP, Cidlowski JA*, et al.* (2014). International Union of Basic and Clinical Pharmacology. XC. multisite pharmacology: recommendations for the nomenclature of receptor allosterism and allosteric ligands. *Pharmacol Rev* 66**:** 918-947.

Christopoulos A & Kenakin T (2002). G protein-coupled receptor allosterism and complexing. *Pharmacol Rev* 54**:** 323-374.

Copeland RA (2016). The drug-target residence time model: a 10-year retrospective. *Nat Rev Drug Discov* 15**:** 87-95.

Copeland RA, Pompliano DL & Meek TD (2006). Drug-target residence time and its implications for lead optimization. *Nat Rev Drug Discov* 5**:** 730-739.

Copik AJ, Baldys A, Nguyen K, Sahdeo S, Ho H, Kosaka A*, et al.* (2015). Isoproterenol acts as a biased agonist of the α_{1A}-adrenoceptor that selectively activates the MAPK/ERK pathway. *PLoS ONE* 10**:** e0115701.

Cotecchia S, Schwinn DA, Randall RR, Lefkowitz RJ, Caron MG & Kobilka BK (1988). Molecular cloning and expression of the cDNA for the hamster α_1-adrenergic receptor. *Proc Natl Acad Sci USA* 85**:** 7159-7163.

Crane J, Pearce N, Flatt A, Burgess C, Jackson R, Kwong T*, et al.* (1989). Prescribed fenoterol and death from asthma in New Zealand, 1981-83: case-control study. *Lancet* 1**:** 917-922.

Crass T, Bautsch W, Cain SA, Pease JE & Monk PN (1999). Receptor activation by human C5a des Arg74 but not intact C5a is dependent on an interaction between Glu199 of the receptor and Lys68 of the ligand. *Biochemistry* 38**:** 9712-9717.

Daaka Y, Luttrell LM & Lefkowitz RJ (1997). Switching of the coupling of the β_2-adrenergic receptor to different G proteins by protein kinase A. *Nature* 390**:** 88-91.

Davis AM, Teague SJ & Kleywegt GJ (2003). Application and limitations of X-ray crystallographic data in structure-based ligand and drug design. *Angew Chem Int Ed Engl* 42**:** 2718-2736.

de Kruijf P, Lim HD, Roumen L, Renjaän VA, Zhao J, Webb ML*, et al.* (2011). Identification of a novel allosteric binding site in the CXCR2 chemokine receptor. *Mol Pharmacol* 80**:** 1108-1118.

de Kruijf P, van Heteren J, Lim HD, Conti PGM, van der Lee MMC, Bosch L*, et al.* (2009). Nonpeptidergic allosteric antagonists differentially bind to the CXCR2 chemokine receptor. *J Pharmacol Exp Ther* 329**:** 783-790.

DeMartino JA, Konteatis ZD, Siciliano SJ, Van Riper G, Underwood DJ, Fischer PA*, et al.* (1995). Arginine 206 of the C5a receptor is critical for ligand recognition and receptor activation by C-terminal hexapeptide analogs. *J Biol Chem* 270**:** 15966-15969.

DeMartino JA, Van Riper G, Siciliano SJ, Molineaux CJ, Konteatis ZD, Rosen H*, et al.* (1994). The amino terminus of the human C5a receptor is required for high affinity C5a binding and for receptor activation by C5a but not C5a analogs. *J Biol Chem* 269**:** 14446-14450.

DeVree BT, Mahoney JP, Vélez-Ruiz GA, Rasmussen SGF, Kuszak AJ, Edwald E*, et al.* (2016). Allosteric coupling from G protein to the agonist-binding pocket in GPCRs. *Nature* 535**:** 182-186.

Diaz P, Phatak SS, Xu J, Astruc-Diaz F, Cavasotto CN & Naguib M (2009). 6-Methoxy-N-alkyl isatin acylhydrazone derivatives as a novel series of potent selective cannabinoid receptor 2 inverse agonists: design, synthesis, and binding mode prediction. *J Med Chem* 52**:** 433-444.

Disse B, Reichl R, Speck G, Traunecker W, Rominger KL & Hammer R (1993). Ba 679 BR, a novel long-acting anticholinergic bronchodilator. *Life Sci* 52**:** 537-544.

Dore AS, Okrasa K, Patel JC, Serrano-Vega M, Bennett K, Cooke RM*, et al.* (2014). Structure of class C GPCR metabotropic glutamate receptor 5 transmembrane domain. *Nature* 511**:** 557-562.

Drapeau G, Brochu S, Godin D, Levesque L, Rioux F & Marceau F (1993). Synthetic C5a receptor agonists. Pharmacology, metabolism and in vivo cardiovascular and hematologic effects. *Biochem Pharmacol* 45**:** 1289-1299.

Dror RO, Pan AC, Arlow DH, Borhani DW, Maragakis P, Shan Y*, et al.* (2011). Pathway and mechanism of drug binding to G-protein-coupled receptors. *Proc Natl Acad Sci USA* 108**:** 13118-13123.

Ducharme FM, Ni Chroinin M, Greenstone I & Lasserson TJ (2010). Addition of long-acting β_2-agonists to inhaled corticosteroids versus same dose inhaled corticosteroids for chronic asthma in adults and children. *Cochrane Database Syst Rev*.

Dunham TD & Farrens DL (1999). Conformational changes in rhodopsin: movement of helix F detected by site-specific chemical labling and fluorescence spectroscopy. . *J Biol Chem* 274**:** 1683-1690.

Dunkelberger JR & Song W-C (2009). Complement and its role in innate and adaptive immune responses. *Cell Res* 20**:** 34-50.

Durroux T, Peter M, Turcatti G, Chollet A, Balestre MN, Barberis C*, et al.* (1999). Fluorescent pseudo-peptide linear vasopressin antagonists: design, synthesis, and applications. *J Med Chem* 42**:** 1312-1319.

Ember JA, Sanderson SD, Hugli TE & Morgan EL (1994). Induction of interleukin-8 synthesis from monocytes by human C5a anaphylatoxin. *Am J Pathol* 144**:** 393-403.

Emorine LJ, Marullo S, Briend-Sutren MM, Patey G, Tate K, Delavier-Klutchko C*, et al.* (1989). Molecular characterization of the human β_3-adrenergic receptor. *Science* 245**:** 1118-1121.

Farrens DL, Altenbach C, Yang K, Hubbell WL & Khorana HG (1996). Requirement of rigid-body motion of transmembrane helices for light activation of rhodopsin. *Science* 274**:** 768-770.

Farzan M, Schnitzler CE, Vasilieva N, Leung D, Kuhn J, Gerard C*, et al.* (2001). Sulfated tyrosines contribute to the formation of the C5a docking site of the human C5a anaphylatoxin receptor. *J Exp Med* 193**:** 1059-1066.

Fatkenheuer G, Pozniak AL, Johnson MA, Plettenberg A, Staszewski S, Hoepelman AI*, et al.* (2005). Efficacy of short-term monotherapy with maraviroc, a new CCR5 antagonist, in patients infected with HIV-1. *Nat Med* 11**:** 1170-1172.

Fenalti G, Zatsepin NA, Betti C, Giguere P, Han GW, Ishchenko A*, et al.* (2015). Structural basis for bifunctional peptide recognition at human δ-opioid receptor. *Nat Struct Mol Biol* 22**:** 265-268.

Ferguson SSG, Ménard L, Barak LS, Koch WJ, Colapietro A-M & Caron MG (1995). Role of phosphorylation in agonist-promoted β_2-adrenergic receptor sequestration: rescue of a sequestration-defective mutant receptor by βARK1. *J Biol Chem* 270**:** 24782-24789.

Fernandez HN & Hugli TE (1978). Primary structural analysis of the polypeptide portion of human C5a anaphylatoxin. Polypeptide sequence determination and assignment of the oligosaccharide attachment site in C5a. *J Biol Chem* 253**:** 6955-6964.

Finch A, Wong A, Paczkowski N, Wadi S, Craik D, Fairlie D*, et al.* (1999). Low-molecular-weight peptidic and cyclic antagonists of the receptor for the complement factor C5a. *J Med Chem* 42**:** 1965 - 1974.

Finch AM (1998). Pharmacological activity of C5a and peptide analogues of C5a. PhD thesis. The University of Queensland: Brisbane.

Finch AM, Vogen SM, Sherman SA, Kirnarsky L, Taylor SM & Sanderson SD (1997). Biologically active conformer of the effector region of human C5a and modulatory effects of N-terminal receptor binding determinants on activity. *J Med Chem* 40**:** 877-884.

Fredriksson R, Lagerström MC, Lundin L-G & Schiöth HB (2003). The G-protein-coupled receptors in the human genome form five main families. Phylogenetic analysis, paralogon groups, and fngerprints. *Mol Pharmacol* 63**:** 1256-1272.

Gao F, Sexton PM, Christopoulos A & Miller LJ (2008). Benzodiazepine ligands can act as allosteric modulators of the Type 1 cholecystokinin receptor. *Bioorg Med Chem Lett* 18**:** 4401-4404.

Gao H, Neff TA, Guo R-F, Speyer CL, Sarma JV, Tomlins S*, et al.* (2005). Evidence for a functional role of the second C5a receptor C5L2. *FASEB J* 19**:** 1003-1005.

Gao X, Hsu CK, Heinz LJ, Morin J, Shi Y, Shukla NK*, et al.* (2004). Europium-labeled melanin-concentrating hormone analogues: ligands for measuring binding to melanin-concentrating hormone receptors 1 and 2. *Anal Biochem* 328**:** 187-195.

Gao Z-G & Ijzerman AP (2000). Allosteric modulation of A_{2A} adenosine receptors by amiloride analogues and sodium ions. *Biochem Pharmacol* 60**:** 669-676.

Gao Z-G, Van Muijlwijk-Koezen JE, Chen A, Müller CE, Ijzerman AP & Jacobson KA (2001). Allosteric modulation of A_3 adenosine receptors by a series of 3-(2-pyridinyl)isoquinoline derivatives. *Mol Pharmacol* 60**:** 1057-1063.

Gao ZG, Kim SK, Gross AS, Chen A, Blaustein JB & Jacobson KA (2003). Identification of essential residues involved in the allosteric modulation of the human A_3 adenosine receptor. *Mol Pharmacol* 63**:** 1021-1031.

Garland SL (2013). Are GPCRs Still a Source of New Targets? *J Biomol Screen* 18**:** 947-966.

Gasque P, Chan P, Fontaine M, Ischenko A, Lamacz M, Gotze O*, et al.* (1995). Identification and characterization of the complement C5a anaphylatoxin receptor on human astrocytes. *J Immunol* 155**:** 4882-4889.

Gentry PR, Sexton PM & Christopoulos A (2015). Novel allosteric modulators of G protein-coupled receptors. *J Biol Chem* 290**:** 19478-19488.

Gerard NP, Bao L, He XP, Eddy RL, Shows TB & Gerard C (1993). Human chemotaxis receptor genes cluster at 19q13.3-13.4. Characterization of the human C5a receptor gene. *Biochemistry* 32**:** 1243-1250.

Gerard NP, Hodges MK, Drazen JM, Weller PF & Gerard C (1989). Characterization of a receptor for C5a anaphylatoxin on human eosinophils. *J Biol Chem* 264**:** 1760-1766.

Gerber B, Meng E, Doetsch V, Baranski T & Bourne H (2001). An activation switch in the ligand binding pocket of the C5a receptor. *J Biolog Chem* 276**:** 3394 - 3400.

Gerlach LO, Skerlj RT, Bridger GJ & Schwartz TW (2001). Molecular interactions of cyclam and bicyclam non-peptide antagonists with the CXCR4 chemokine receptor. *J Biol Chem* 276**:** 14153-14160.

Gether U, Lin S, Ghanouni P, Ballesteros JA, Weinstein H & Kobilka BK (1997). Agonists induce conformational changes in transmembrane domains III and VI of the β_2 adrenoceptor. *EMBO J* 16**:** 6737-6747.

Gether U, Lin S & Kobilka BK (1995). Fluorescent labeling of purified β_2 adrenergic receptor: evidence for ligand-specific conformational changes *J Biol Chem* 270**:** 28268-28275.

Ghosh E, Kumari P, Jaiman D & Shukla AK (2015). Methodological advances: the unsung heroes of the GPCR structural revolution. *Nat Rev Mol Cell Biol* 16**:** 69-81.

Giembycz MA & Raeburn D (1991). Putative substrates for cyclic nucleotide-dependent protein kinases and the control of airway smooth muscle tone. *J Auton Pharmacol* 11**:** 365-398.

Gillard M, Van Der Perren C, Moguilevsky N, Massingham R & Chatelain P (2002). Binding characteristics of cetirizine and levocetirizine to human H_1 histamine receptors: contribution of Lys^{191} and Thr^{194}. *Mol Pharmacol* 61**:** 391-399.

Girardi G, Berman J, Redecha P, Spruce L, Thurman JM, Kraus D*, et al.* (2003). Complement C5a receptors and neutrophils mediate fetal injury in the antiphospholipid syndrome. *J Clin Invest* 112**:** 1644-1654.

Girardi G, Yarilin D, Thurman JM, Holers VM & Salmon JE (2006). Complement activation induces dysregulation of angiogenic factors and causes fetal rejection and growth restriction. *J Exp Med* 203**:** 2165-2175.

Gnagey AL, Seidenberg M & Ellis J (1999). Site-directed mutagenesis reveals two epitopes involved in the subtype selectivity of the allosteric interactions of gallamine at muscarinic acetylcholine receptors. *Mol Pharmacol* 56**:** 1245-1253.

Gomez-Cambronero J, Di Fulvio M & Knapek K (2007). Understanding phospholipase D (PLD) using leukocytes: PLD involvement in cell adhesion and chemotaxis. *J Leukoc Biol* 82**:** 272-281.

Gonzalez A, Perez-Acle T, Pardo L & Deupi X (2011). Molecular basis of ligand dissociation in β-adrenergic receptors. *PLoS ONE* 6**:** e23815.

Goodman OB, Krupnick JG, Santini F, Gurevich VV, Penn RB, Gagnon AW*, et al.* (1996). β-Arrestin acts as a clathrin adaptor in endocytosis of the β_2-adrenergic receptor. *Nature* 383**:** 447-450.

Goodman WG, Frazao JM, Goodkin DA, Turner SA, Liu W & Coburn JW (2000). A calcimimetic agent lowers plasma parathyroid hormone levels in patients with secondary hyperparathyroidism. *Kidney Int* 58**:** 436-445.

Granier S, Manglik A, Kruse AC, Kobilka TS, Thian FS, Weis WI*, et al.* (2012). Structure of the δ-opioid receptor bound to naltrindole. *Nature* 485**:** 400-404.

Grant EP, Picarella D, Burwell T, Delaney T, Croci A, Avitahl N*, et al.* (2002). Essential role for the C5a receptor in regulating the effector phase of synovial infiltration and joint destruction in experimental arthritis. *J Exp Med* 196**:** 1461-1471.

Gregory KJ, Sexton PM & Christopoulos A (2010). Overview of receptor allosterism. In Current Protocols in Pharmacology. John Wiley & Sons, Inc.

Gunst SJ & Stropp JQ (1988). Effect of Na-K adenosinetriphosphatase activity on relaxation of canine tracheal smooth muscle. *J Appl Physiol* 64**:** 635-641.

Guo D, Mulder-Krieger T, AP IJ & Heitman LH (2012). Functional efficacy of adenosine A_{2A} receptor agonists is positively correlated to their receptor residence time. *Br J Pharmacol* 166**:** 1846-1859.

Guo D, Pan AC, Dror RO, Mocking T, Liu R, Heitman LH*, et al.* (2016). Molecular basis of ligand dissociation from the adenosine A_{2A} receptor. *Mol Pharmacol* 89**:** 485-491.

Guo RF, Riedemann NC & Ward PA (2004). Role of C5a-C5aR interaction in sepsis. *Shock* 21**:** 1-7.

Haga K, Kruse A, Asada H, Yurugi-Kobayashi T, Shiroishi M, Zhang C*, et al.* (2012). Structure of the human M_2 muscarinic acetylcholine receptor bound to an antagonist. *Nature* 482**:** 547 - 551.

Hagemann I, Miller D, Kico J, Nikiforovich G & Baranski T (2008). Structure of the complement factor 5a receptor-ligand complex studied by disulfide trapping and molecular modeling. *J Biol Chem* 283**:** 7763 - 7775.

Hagemann IS, Narzinski KD, Floyd DH & Baranski TJ (2006). Random mutagenesis of the complement factor 5a (C5a) receptor N terminus provides a structural constraint for C5a docking. *J Biol Chem* 281**:** 36783-36792.

Hall RA, Ostedgaard LS, Premont RT, Blitzer JT, Rahman N, Welsh MJ*, et al.* (1998). A C-terminal motif found in the β_2-adrenergic receptor, $P2Y_1$ receptor and cystic fibrosis transmembrane conductance regulator determines binding to the Na^+/H^+ exchanger regulatory factor family of PDZ proteins. *Proc Natl Acad Sci USA* 95**:** 8496-8501.

Haney S & Hancox RJ (2005). Rapid onset of tolerance to β-agonist bronchodilation. *Respir Med* 99**:** 566-571.

Haney S & Hancox RJ (2007). Overcoming β-agonist tolerance: high dose salbutamol and ipratropium bromide. Two randomised controlled trials. *Respir Res* 8**:** 19.

Hansel TT, Neighbour H, Erin EM, Tan AJ, Tennant RC, Maus JG*, et al.* (2005). Glycopyrrolate causes prolonged bronchoprotection and bronchodilatation in patients with asthma. *Chest* 128**:** 1974-1979.

Hanson MA, Roth CB, Jo E, Griffith MT, Scott FL, Reinhart G*, et al.* (2012). Crystal structure of a lipid G protein-coupled receptor. *Science* 335**:** 851-855.

Harikumar KG, Hosohata K, Pinon DI & Miller LJ (2006). Use of probes with fluorescence indicator distributed throughout the pharmacophore to examine the peptide agonist-binding environment of the family B G protein-coupled secretin receptor. *J Biol Chem* 281**:** 2543-2550.

Hausdorff WP, Bouvier M, O'Dowd BF, Irons GP, Caron MG & Lefkowitz RJ (1989). Phosphorylation sites on two domains of the β_2-adrenergic receptor are involved in distinct pathways of receptor desensitization. *J Biol Chem* 264**:** 12657-12665.

Healy DP, Munzel PA & Insel PA (1985). Localization of β_1- and β_2-adrenergic receptors in rat kidney by autoradiography. *Circ Res* 57**:** 278-284.

Heitz A, Schwartz J & Velly J (1983). β-Adrenoceptors of the human myocardium: determination of β_1 and β_2 subtypes by radioligand binding. *Br J Pharmacol* 80**:** 711-717.

Higginbottom A, Cain S, Woodruff T, Proctor L, Madala P, Tyndall J*, et al.* (2005). Comparative agonist/antagonist responses in mutant human C5a receptors define the ligand binding site. *J Biol Chem* 280**:** 17831 - 17840.

Hillmen P, Young NS & Schubert J (2006). The complement inhibitor eculizumab in paroxysmal nocturnal hemoglobinuria. *N Engl J Med* 355**:** 1233-1243.

Hinkle RT, Hodge KMB, Cody DB, Sheldon RJ, Kobilka BK & Isfort RJ (2002). Skeletal muscle hypertrophy and anti-atrophy effects of clenbuterol are mediated by the β_2-adrenergic receptor. *Muscle Nerve* 25**:** 729-734.

Hoffman JF, Linderman JJ & Omann GM (1996). Receptor up-regulation, internalization, and interconverting receptor states. Critical components of a quantitative description of N-formyl peptide-receptor dynamics in the neutrophil. *J Biol Chem* 271**:** 18394-18404.

Hollenstein K, Kean J, Bortolato A, Cheng RK, Dore AS, Jazayeri A*, et al.* (2013). Structure of class B GPCR corticotropin-releasing factor receptor 1. *Nature* 499**:** 438-443.

Horstman DA, Brandon S, Wilson AL, Guyer CA, Cragoe EJ & Limbird LE (1990). An aspartate conserved among G-protein receptors confers allosteric regulation of α_2-adrenergic receptors by sodium. *J Biol Chem* 265**:** 21590-21595.

Hothersall JD, Brown AJ, Dale I & Rawlins P (2016). Can residence time offer a useful strategy to target agonist drugs for sustained GPCR responses? *Drug Discov Today* 21**:** 90-96.

Huang R, Lian JP, Robinson D & Badwey JA (1998). Neutrophils stimulated with a variety of chemoattractants exhibit rapid activation of p21-activated kinases (Paks): separate signals are required for activation and inactivation of paks. *Mol Cell Biol* 18**:** 7130-7138.

Huang W, Manglik A, Venkatakrishnan AJ, Laeremans T, Feinberg EN, Sanborn AL*, et al.* (2015). Structural insights into μ-opioid receptor activation. *Nature* 524**:** 315-321.

Huang XP, Prilla S, Mohr K & Ellis J (2005). Critical amino acid residues of the common allosteric site on the M_2 muscarinic acetylcholine receptor: more similarities than differences between the structurally divergent agents gallamine and bis(ammonio)alkane-type hexamethylene-bis-[dimethyl-(3-phthalimido-propyl)ammonium]dibromide. *Mol Pharmacol* 68**:** 769-778.

Huber-Lang MS, Riedeman NC, Sarma JV, Younkin EM, McGuire SR, Laudes IJ*, et al.* (2002). Protection of innate immunity by C5aR antagonist in septic mice. *FASEB J* 16**:** 1567-1574.

Huey R & Hugli TE (1985). Characterization of a C5a receptor on human polymorphonuclear leukocytes (PMN). *J Immunol* 135**:** 2063-2068.

Ignatowska-Jankowska BM, Baillie GL, Kinsey S, Crowe M, Ghosh S, Owens RA*, et al.* (2015). A cannabinoid CB1 receptor-positive allosteric modulator reduces neuropathic pain in the mouse with no psychoactive effects. *Neuropsychopharmacol* 40**:** 2948-2959.

Im WB, Chio CL, Alberts GL & Dinh DM (2003). Positive allosteric modulator of the human 5-HT_{2C} receptor. *Mol Pharmacol* 64**:** 78-84.

Inoue H, Nojima H & Okayama H (1990). High efficiency transformation of Escherichia coli with plasmids. *Gene* 96**:** 23-28.

Irannejad R, Tomshine JC, Tomshine JR, Chevalier M, Mahoney JP, Steyaert J*, et al.* (2013). Conformational biosensors reveal adrenoceptor signalling from endosomes. *Nature* 495**:** 534-538.

Iyer A, Woodruff TM, Wu MC, Stylianou C, Reid RC, Fairlie DP*, et al.* (2011). Inhibition of inflammation and fibrosis by a complement C5a receptor antagonist in DOCA-salt hypertensive rats. *J Cardiovasc Pharmacol* 58**:** 479-486.

Jaakola VP, Griffith MT, Hanson MA, Cherezov V, Chien EY, Lane JR*, et al.* (2008). The 2.6 angstrom crystal structure of a human A_{2A} adenosine receptor bound to an antagonist. *Science* 322**:** 1211-1217.

Jager D, Schmalenbach C, Prilla S, Schrobang J, Kebig A, Sennwitz M*, et al.* (2007). Allosteric small molecules unveil a role of an extracellular E2/transmembrane helix 7 junction for G protein-coupled receptor activation. *J Biol Chem* 282**:** 34968-34976.

Jiang LI, Collins J, Davis R, Lin K-M, DeCamp D, Roach T*, et al.* (2007). Use of a cAMP BRET sensor to characterize a novel regulation of cAMP by the sphingosine 1-phosphate/G_{13} pathway. *J Biol Chem* 282**:** 10576-10584.

Johswich K, Martin M, Thalmann J, Rheinheimer C, Monk PN & Klos A (2006). Ligand specificity of the anaphylatoxin C5L2 receptor and its regulation on myeloid and epithelial cell lines. *J Biol Chem* 281**:** 39088-39095.

Jones G, Willett P & Glen RC (1995). Molecular recognition of receptor sites using a genetic algorithm with a description of desolvation. *J Mol Biol* 245**:** 43-53.

Jones G, Willett P, Glen RC, Leach AR & Taylor R (1997). Development and validation of a genetic algorithm for flexible docking. *J Mol Biol* 267**:** 727-748.

Kalant D, Cain SA, Maslowska M, Sniderman AD, Cianflone K & Monk PN (2003). The chemoattractant receptor-like protein C5L2 binds the C3a des-Arg77/acylation-stimulating protein. *J Biol Chem* 278**:** 11123-11129.

Kalant D, MacLaren R, Cui W, Samanta R, Monk PN, Laporte SA*, et al.* (2005). C5L2 is a functional receptor for acylation-stimulating protein. *J Biol Chem* 280**:** 23936-23944.

Kane BE, Grant MKO, El-Fakahany EE & Ferguson DM (2008). Synthesis and evaluation of xanomeline analogs - Probing the wash-resistant phenomenon at the M_1 muscarinic acetylcholine receptor. *Bioorg Med Chem* 16**:** 1376-1392.

Kastl SP, Speidl WS, Kaun C, Rega G, Assadian A, Weiss TW*, et al.* (2006). The complement component C5a induces the expression of plasminogen activator inhibitor-1 in human macrophages via NF-κB activation. *J Thromb Haemost* 4**:** 1790-1797.

Kawai M, Quincy DA, Lane B, Mollison KW, Luly JR & Carter GW (1991). Identification and synthesis of a receptor binding site of human anaphylatoxin C5a. *J Med Chem* 34**:** 2068-2071.

Kew KM, Mavergames C & Walters JA (2013). Long-acting β_2-agonists for chronic obstructive pulmonary disease. *Cochrane Database Syst Rev***:** CD010177.

Kiefer-Day JS, Campbell HE, Towles J & el-Fakahany EE (1991). Muscarinic subtype selectivity of tetrahydroaminoacridine: possible relationship to its capricious efficacy. *Eur J Pharmacol* 203**:** 421-423.

Kiener HP, Baghestanian M, Dominkus M, Walchshofer S, Ghannadan M, Willheim M*, et al.* (1998). Expression of the C5a receptor (CD88) on synovial mast cells in patients with rheumatoid arthritis. *Arthritis Rheum* 41**:** 233-245.

Kilts JD, Gerhardt MA, Richardson MD, Sreeram G, Mackensen GB, Grocott HP*, et al.* (2000). β_2-Adrenergic and several other G protein–coupled receptors in human atrial membranes activate both G_s and G_i. *Circ Res* 87**:** 705-709.

Kim AHJ, Dimitriou ID, Holland MCH, Mastellos D, Mueller YM, Altman JD*, et al.* (2004). Complement C5a receptor is essential for the optimal generation of antiviral CD8+ T cell responses. *J Immunol* 173**:** 2524-2529.

Kingston RE, Chen CA & Okayama H (2001). Calcium phosphate transfection. In Current Protocols in Immunology. John Wiley & Sons, Inc.

Klco JM, Wiegand CB, Narzinski K & Baranski TJ (2005). Essential role for the second extracellular loop in C5a receptor activation. *Nat Struct Mol Biol* 12**:** 320-326.

Klein Herenbrink C, Sykes DA, Donthamsetti P, Canals M, Coudrat T, Shonberg J*, et al.* (2016). The role of kinetic context in apparent biased agonism at GPCRs. *Nat Commun* 7**:** 10842.

Knaus GA, Knaus H-G & Saria A (1991). Complex allosteric interaction of heparin with neurokinin-1 receptors. *Eur J Pharmacol* 207**:** 267-270.

Kobilka BK, Dixon RA, Frielle T, Dohlman HG, Bolanowski MA, Sigal IS*, et al.* (1987). cDNA for the human β_2-adrenergic receptor: a protein with multiple membrane-spanning domains and encoded by a gene whose chromosomal location is shared with that of the receptor for platelet-derived growth factor. *Proc Natl Acad Sci USA* 84**:** 46-50.

Kohl J (2006). Drug evaluation: the C5a receptor antagonist PMX-53. *Curr Opin Mol Ther* 8**:** 529-538.

Kolakowski LF, Jr. (1994). GCRDb: a G-protein-coupled receptor database. *Recept Channels* 2**:** 1-7.

Kolb P, Rosenbaum DM, Irwin JJ, Fung JJ, Kobilka BK & Shoichet BK (2009). Structure-based discovery of β_2-adrenergic receptor ligands. *Proc Natl Acad Sci USA* 106**:** 6843-6848.

Kondru R, Zhang J, Ji C, Mirzadegan T, Rotstein D, Sankuratri S*, et al.* (2008). Molecular interactions of CCR5 with major classes of small-molecule anti-HIV CCR5 antagonists. *Mol Pharmacol* 73**:** 789-800.

Konteatis ZD, Siciliano SJ, Van Riper G, Molineaux CJ, Pandya S, Fischer P*, et al.* (1994). Development of C5a receptor antagonists. Differential loss of functional responses. *J Immunol* 153**:** 4200-4205.

Koshimizu T-a, Kashiwazaki A & Taniguchi J (2016). Combined sodium ion sensitivity in agonist binding and internalization of vasopressin V1b receptors. *Sci Rep* 6**:** 25327.

Kourounakis A, Visser C, de Groote M & AP IJ (2001). Differential effects of the allosteric enhancer (2-amino-4,5-dimethyl-trienyl)[3-trifluoromethyl) phenyl]methanone (PD81,723) on agonist and antagonist binding and function at the human wild-type and a mutant (T277A) adenosine A_1 receptor. *Biochem Pharmacol* 61**:** 137-144.

Krejci A & Tucek S (2001). Changes of cooperativity between N-methylscopolamine and allosteric modulators alcuronium and gallamine induced by mutations of external loops of muscarinic M_3 receptors. *Mol Pharmacol* 60**:** 761-767.

Kruse A, Hu J, Pan A, Arlow D, Rosenbaum D, Rosemond E*, et al.* (2012). Structure and dynamics of the M_3 muscarinic acetylcholine receptor. *Nature* 482**:** 552 - 556.

Kruse AC, Ring AM, Manglik A, Hu J, Hu K, Eitel K*, et al.* (2013). Activation and allosteric modulation of a muscarinic acetylcholine receptor. *Nature* 504**:** 101-106.

Kufareva I, Katritch V, Stevens Raymond C & Abagyan R (2014). Advances in GPCR modeling evaluated by the GPCR Dock 2013 assessment: meeting new challenges. *Structure* 22**:** 1120-1139.

Lacy M, Jones J, Whittemore SR, Haviland DL, Wetsel RA & Barnum SR (1995). Expression of the receptors for the C5a anaphylatoxin, interleukin-8 and FMLP by human astrocytes and microglia. *J Neuroimmunol* 61**:** 71-78.

Lagerstrom MC & Schioth HB (2008). Structural diversity of G protein-coupled receptors and significance for drug discovery. *Nat Rev Drug Discov* 7**:** 339-357.

Lam AR, Bhattacharya S, Patel K, Hall SE, Mao A & Vaidehi N (2011). Importance of receptor flexibility in binding of cyclam compounds to the chemokine receptor CXCR4. *J Chem Inf Model* 51**:** 139-147.

Lands AM, Arnold A, McAuliff JP, Luduena FP & Brown TG (1967a). Differentiation of receptor systems activated by sympathomimetic amines. *Nature* 214**:** 597-598.

Lands AM, Luduena FP & Buzzo HJ (1967b). Differentiation of receptors responsive to isoproterenol. *Life Sci* 6**:** 2241-2249.

Lane JR, Donthamsetti P, Shonberg J, Draper-Joyce CJ, Dentry S, Michino M*, et al.* (2014). A new mechanism of allostery in a G protein–coupled receptor dimer. *Nat Chem Biol* 10**:** 745-752.

Langin D, Portillo MP, Saulnier-Blache JS & Lafontan M (1991). Coexistence of three β-adrenoceptor subtypes in white fat cells of various mammalian species. *Eur J Pharmacol* 199**:** 291-301.

Langmead CJ, Fry VAH, Forbes IT, Branch CL, Christopoulos A, Wood MD*, et al.* (2006). Probing the molecular mechanism of interaction between 4-n-butyl-1-[4-(2-methylphenyl)-4-oxo-1-butyl]-piperidine (AC-42) and the muscarinic M_1 receptor: direct pharmacological evidence that AC-42 is an allosteric agonist. *Mol Pharmacol* 69**:** 236-246.

Larsson P, Wallner B, Lindahl E & Elofsson A (2008). Using multiple templates to improve quality of homology models in automated homology modeling. *Prot Sci* 17**:** 990-1002.

Larsson S & Svedmyr N (1977). Tremor caused by sympathomimetics is mediated by β_2-adrenoreceptors. *Scand J Respir Dis* 58**:** 5-10.

Laudes IJ, Chu JC, Huber-Lang M, Guo RF, Riedemann NC, Sarma JV*, et al.* (2002). Expression and function of C5a receptor in mouse microvascular endothelial cells. *J Immunol* 169**:** 5962-5970.

Lazareno S, Doležal V, Popham A & Birdsall NJM (2004). Thiochrome enhances acetylcholine affinity at muscarinic M_4 receptors: receptor subtype selectivity via cooperativity rather than affinity. *Mol Pharmacol* 65**:** 257-266.

Lazareno S, Popham A & Birdsall NJ (2002). Analogs of WIN 62,577 define a second allosteric site on muscarinic receptors. *Mol Pharmacol* 62**:** 1492-1505.

Lazareno S, Popham A & Birdsall NJM (2000). Allosteric interactions of staurosporine and other indolocarbazoles with N-[methyl-^{3}H]scopolamine and acetylcholine at muscarinic receptor subtypes: identification of a second allosteric site. *Mol Pharmacol* 58**:** 194-207.

Leach K, Valant C, Sexton PM & Christopoulos A (2010). Measurement of ligand–G protein-coupled receptor interactions. In G Protein-Coupled Receptors. Wiley-Blackwell, 1-29.

Lee DK, George SR, Cheng R, Nguyen T, Liu Y, Brown M*, et al.* (2001). Identification of four novel human G protein-coupled receptors expressed in the brain. *Mol Brain Res* 86**:** 13-22.

Lefkowitz RJ, Pierce KL & Luttrell LM (2002). Dancing with different partners: protein kinase A phosphorylation of seven membrane-spanning receptors regulates their G protein-coupling specificity. *Mol Pharmacol* 62**:** 971-974.

Legendre CM, Licht C, Muus P, Greenbaum LA, Babu S, Bedrosian C*, et al.* (2013). Terminal complement inhibitor eculizumab in atypical hemolytic–uremic syndrome. *N Engl J Med* 368**:** 2169-2181.

Leonar E (2011). Allosteric modulation of β_2-adrenoceptors. Honours thesis. UNSW Australia: Sydney.

Leppik RA, Mynett A, Lazareno S & Birdsall NJM (2000). Allosteric interactions between the antagonist prazosin and amiloride analogs at the human α_{1A}-adrenergic receptor. *Mol Pharmacol* 57**:** 436-445.

Li G, Fan RM, Chen JL, Wang CM, Zeng YC, Han C*, et al.* (2014a). Neuroprotective effects of argatroban and C5a receptor antagonist (PMX53) following intracerebral haemorrhage. *Clin Exp Immunol* 175**:** 285-295.

Li L, Xiong ZY, Qian ZM, Zhao TZ, Feng H, Hu S*, et al.* (2014b). Complement C5a is detrimental to histological and functional locomotor recovery after spinal cord injury in mice. *Neurobiol Dis* 66**:** 74-82.

Liapakis G, Ballesteros JA, Papachristou S, Chan WC, Chen X & Javitch JA (2000). The forgotten serine: a critical role for Ser-$203^{5.42}$ in ligand binding to and activation of the β_2-adrenergic receptor. *J Biol Chem* 275**:** 37779-37788.

Lin DCH, Guo Q, Luo J, Zhang J, Nguyen K, Chen M*, et al.* (2012). Identification and pharmacological characterization of multiple allosteric binding sites on the free fatty acid 1 receptor. *Mol Pharmacol* 82**:** 843-859.

Lin F-T, Krueger KM, Kendall HE, Daaka Y, Fredericks ZL, Pitcher JA*, et al.* (1997). Clathrin-mediated endocytosis of the β-adrenergic receptor is regulated by phosphorylation/dephosphorylation of β-arrestin 1. *J Biol Chem* 272**:** 31051-31057.

Lin H, Sassano MF, Roth BL & Shoichet BK (2013). A pharmacological organization of G protein-coupled receptors. *Nat Methods* 10**:** 140-146.

Litschig S, Gasparini F, Rueegg D, Stoehr N, Flor PJ, Vranesic I*, et al.* (1999). CPCCOEt, a noncompetitive metabotropic glutamate receptor 1 antagonist, inhibits receptor signaling without affecting glutamate binding. *Mol Pharmacol* 55**:** 453-461.

Liu B, Wei L, Meyerle C, Tuo J, Sen HN, Li Z*, et al.* (2011). Complement component C5a promotes expression of IL-22 and IL-17 from human T cells and its implication in age-related macular degeneration. *J Transl Med* 9**:** 1-12.

Liu W, Chun E, Thompson AA, Chubukov P, Xu F, Katritch V*, et al.* (2012). Structural basis for allosteric regulation of GPCRs by sodium ions. *Science* 337**:** 232-236.

Lomasney JW, Cotecchia S, Lorenz W, Leung WY, Schwinn DA, Yang-Feng TL*, et al.* (1991). Molecular cloning and expression of the cDNA for the α_{1A}-adrenergic receptor: the gene for which is located on human chromosome 5. *J Biol Chem* 266**:** 6365-6369.

Longhurst PA & Levendusky M (1999). Pharmacological characterization of β-adrenoceptors mediating relaxation of the rat urinary bladder in vitro. *Br J Pharmacol* 127**:** 1744-1750.

Lougheed MD, Lemiere C, Ducharme FM, Licskai C, Dell SD, Rowe BH*, et al.* (2012). Canadian Thoracic Society 2012 guideline update: diagnosis and management of asthma in preschoolers, children and adults. *Can Respir J* 19**:** 127-164.

Lovell SC, Word JM, Richardson JS & Richardson DC (2000). The penultimate rotamer library. *Proteins: Struct Funct Genet* 40**:** 389-408.

Mahajan SD, Parikh NU, Woodruff TM, Jarvis JN, Lopez M, Hennon T*, et al.* (2015). C5a alters blood-brain barrier integrity in a human invitro model of systemic lupus erythematosus. *Immunology* 146**:** 130-143.

Mahmoud S, Margas W, Trapella C, Caló G & Ruiz-Velasco V (2010). Modulation of silent and constitutively active nociceptin/orphanin FQ receptors by potent receptor antagonists and Na^+ ions in rat sympathetic neurons. *Mol Pharmacol* 77**:** 804-817.

Manglik A, Kruse AC, Kobilka TS, Thian FS, Mathiesen JM, Sunahara RK*, et al.* (2012). Crystal structure of the μ-opioid receptor bound to a morphinan antagonist. *Nature* 485**:** 321-326.

Mann RD, Kubota K, Pearce G & Wilton L (1996). Salmeterol: a study by prescription event monitoring in a UK cohort of 15,407 patients. *J Clin Epidemiol* 49**:** 247-250.

March D, Proctor L, Stoermer M, Sbaglia R, Abbenante G, Reid C*, et al.* (2004). Potent cyclic antagonists of the complement C5a receptor on human polymorphonuclear leukocytes. Relationships between structure and activity. *Mol Pharmacol* 65**:** 868 - 879.

Martin S, Botto JM, Vincent JP & Mazella J (1999). Pivotal role of an aspartate residue in sodium sensitivity and coupling to G proteins of neurotensin receptors. *Mol Pharmacol* 55**:** 210-215.

May LT, Avlani VA, Langmead CJ, Herdon HJ, Wood MD, Sexton PM*, et al.* (2007). Structure-function studies of allosteric agonism at M_2 muscarinic acetylcholine receptors. *Mol Pharmacol* 72**:** 463-476.

Mery L & Boulay F (1994). The NH_2-terminal region of C5aR but not that of FPR is critical for both protein transport and ligand binding. *J Biol Chem* 269**:** 3457-3463.

Michielan L, Bacilieri M, Schiesaro A, Bolcato C, Pastorin G, Spalluto G*, et al.* (2008). Linear and nonlinear 3D-QSAR approaches in tandem with ligand-based homology modeling as a computational strategy to depict the pyrazolo-triazolo-pyrimidine antagonists binding site of the human adenosine A_{2A} receptor. *J Chem Inf Model* 48**:** 350-363.

Millman EE, Rosenfeld JL, Vaughan DJ, Nguyen J, Dai W, Alpizar-Foster E*, et al.* (2004). Endosome sorting of β_2-adrenoceptors is GRK5 independent. *Br J Pharmacol* 141**:** 277-284.

Mirzadegan T, Benko G, Filipek S & Palczewski K (2003). Sequence analyses of G-protein-coupled receptors: similarities to rhodopsin. *Biochemistry* 42**:** 2759-2767.

Mitchell R, McCulloch D, Lutz E, Johnson M, MacKenzie C, Fennell M*, et al.* (1998). Rhodopsin-family receptors associate with small G proteins to activate phospholipase D. *Nature* 392**:** 411-414.

Mohler H, Fritschy JM & Rudolph U (2002). A new benzodiazepine pharmacology. *J Pharmacol Exp Ther* 300**:** 2-8.

Mollison KW, Mandecki W, Zuiderweg ER, Fayer L, Fey TA, Krause RA*, et al.* (1989). Identification of receptor-binding residues in the inflammatory complement protein C5a by site-directed mutagenesis. *Proc Natl Acad Sci USA* 86**:** 292-296.

Monk PN, Barker MD, Partridge LJ & Pease JE (1995). Mutation of glutamate 199 of the human C5a receptor defines a binding site for ligand distinct from the receptor N terminus. *J Biol Chem* 270**:** 16625-16629.

Monk PN, Pease JE, Marland G & Barker MD (1994). Mutation of aspartate 82 of the human C5a receptor abolishes the secretory response to human C5a in transfected rat basophilic leukemia cells. *Eur J Immunol* 24**:** 2922-2925.

Morgan EL, Ember JA, Sanderson SD, Scholz W, Buchner R, Ye RD*, et al.* (1993). Anti-C5a receptor antibodies. Characterization of neutralizing antibodies specific for a peptide, C5aR$_{9\text{-}29}$, derived from the predicted amino-terminal sequence of the human C5a receptor. *J Immunol* 151**:** 377-388.

Morgan M, Bulmer AC, Woodruff TM, Proctor LM, Williams HM, Stocks SZ*, et al.* (2008). Pharmacokinetics of a C5a receptor antagonist in the rat after different sites of enteral administration. *Eur J Pharm Sci* 33**:** 390-398.

Moriconi A, Cunha TM, Souza GR, Lopes AH, Cunha FQ, Carneiro VL*, et al.* (2014). Targeting the minor pocket of C5aR for the rational design of an oral allosteric inhibitor for inflammatory and neuropathic pain relief. *Proc Natl Acad Sci USA* 111**:** 16937-16942.

Motulsky HJ & Mahan LC (1984). The kinetics of competitive radioligand binding predicted by the law of mass action. *Mol Pharmacol* 25**:** 1-9.

Moukhametzianov R, Warne T, Edwards PC, Serrano-Vega MJ, Leslie AG, Tate CG*, et al.* (2011). Two distinct conformations of helix 6 observed in antagonist-bound structures of a β_1-adrenergic receptor. *Proc Natl Acad Sci USA* 108**:** 8228-8232.

Mullmann TJ, Siegel MI, Egan RW & Billah MM (1990). Complement C5a activation of phospholipase D in human neutrophils. A major route to the production of phosphatidates and diglycerides. *J Immunol* 144**:** 1901-1908.

Mundell SJ, Loudon RP & Benovic JL (1999). Characterization of G protein-coupled receptor regulation in antisense mRNA-expressing cells with reduced arrestin levels. *Biochemistry* 38**:** 8723-8732.

Murphy TJ & Bylund DB (1988). Characterization of α_2 adrenergic receptors in the OK cell, an opossum kidney cell line. *J Pharmacol Exp Ther* 244**:** 571-578.

Narlawar R, Lane JR, Doddareddy M, Lin J, Brussee J & Ijzerman AP (2010). Hybrid ortho/allosteric ligands for the adenosine A_1 receptor. *J Med Chem* 53**:** 3028-3037.

Nelson HS, Weiss ST, Bleecker ER, Yancey SW & Dorinsky PM (2006). The salmeterol multicenter asthma research trial: a comparison of usual pharmacotherapy for asthma or usual pharmacotherapy plus salmeterol. *Chest* 129**:** 15-26.

Neve KA (1991). Regulation of dopamine D_2 receptors by sodium and pH. *Mol Pharmacol* 39**:** 570-578.

Nicholls DJ, Tomkinson NP, Wiley KE, Brammall A, Bowers L, Grahames C*, et al.* (2008). Identification of a putative intracellular allosteric antagonist binding-site in the CXC chemokine receptors 1 and 2. *Mol Pharmacol* 74**:** 1193-1202.

Niederbichler AD, Hoesel LM, Westfall MV, Gao H, Ipaktchi KR, Sun L*, et al.* (2006). An essential role for complement C5a in the pathogenesis of septic cardiac dysfunction. *J Exp Med* 203**:** 53-61.

Nikiforovich G, Marshall G & Baranski T (2008). Modeling molecular mechanisms of binding of the anaphylatoxin C5a to the C5a receptor. *Biochemistry* 47**:** 3117 - 3130.

Nishimune A, Suzuki F, Yoshiki H, Morishima S & Muramatsu I (2010). Identification of cysteine-rich epidermal growth factor-like domain 1α (CRELD1α) as a novel α_{1A}-adrenoceptor-down-regulating protein and establishment of an α_{1L}-adrenoceptor-expressing cell line. *J Pharmacol Sci* 113**:** 169-181.

Nishiyama K & Hirai K (2015). In vitro comparison of duration of action of melatonin agonists on melatonin MT_1 receptor: possible link between duration of action and dissociation rate from receptor. *Eur J Pharmacol* 757**:** 42-52.

Nobles KN, Xiao K, Ahn S, Shukla AK, Lam CM, Rajagopal S*, et al.* (2011). Distinct phosphorylation sites on the β_2-adrenergic receptor establish a barcode that encodes differential functions of β-arrestin. *Sci Signal* 4**:** ra51.

Ohno M, Hirata T, Enomoto M, Araki T, Ishimaru H & Takahashi TA (2000). A putative chemoattractant receptor, C5L2, is expressed in granulocyte and

immature dendritic cells, but not in mature dendritic cells. *Mol Immunol* 37**:** 407-412.

Okada T, Sugihara M, Bondar AN, Elstner M, Entel P & Buss V (2004). The retinal conformation and its environment in rhodopsin in light of a new 2.2 Å crystal structure. *J Mol Biol* 342**:** 571-583.

Okinaga S, Slattery D, Humbles A, Zsengeller Z, Morteau O, Kinrade MB*, et al.* (2003). C5L2, a nonsignaling C5A binding protein. *Biochemistry* 42**:** 9406-9415.

Okusawa S, Yancey KB, van der Meer JW, Endres S, Lonnemann G, Hefter K*, et al.* (1988). C5a stimulates secretion of tumor necrosis factor from human mononuclear cells in vitro. Comparison with secretion of interleukin 1β and interleukin 1α. *J Exp Med* 168**:** 443-448.

Paczkowski NJ, Finch AM, Whitmore JB, Short AJ, Wong AK, Monk PN*, et al.* (1999). Pharmacological characterization of antagonists of the C5a receptor. *Br J Pharmacol* 128**:** 1461-1466.

Padro CJ (2013). A study of the distal molecular mechanism by which β_2 adrenergic receptor stimulation on a B cell regulates IgE production.The Ohio State University: Columbus.

Palczewski K, Kumasaka T, Hori T, Behnke CA, Motoshima H, Fox BA*, et al.* (2000). Crystal structure of rhodopsin: a G protein-coupled receptor. *Science* 289**:** 739-745.

Palmer TM, Gettys TW & Stiles GL (1995). Differential interaction with and regulation of multiple G-proteins by the rat A_3 adenosine receptor. *J Biol Chem* 270**:** 16895-16902.

Park SH, Das BB, Casagrande F, Tian Y, Nothnagel HJ, Chu M*, et al.* (2012). Structure of the chemokine receptor CXCR1 in phospholipid bilayers. *Nature* 491**:** 779-783.

Patel SN, Berghout J, Lovegrove FE, Ayi K, Conroy A, Serghides L*, et al.* (2008). C5 deficiency and C5a or C5aR blockade protects against cerebral malaria. *J Exp Med* 205**:** 1133-1143.

Pearce BD & Potter LT (1988). Effects of tetrahydroaminoacridine on M_1 and M_2 muscarine receptors. *Neurosci Lett* 88**:** 281-285.

Pease JE, Burton DR & Barker MD (1994). Generation of chimeric C5a/formyl peptide receptors: towards the identification of the human C5a receptor binding site. *Eur J Immunol* 24**:** 211-215.

Perez-Aso M, Segura V, Montó F, Barettino D, Noguera MA, Milligan G*, et al.* (2013). The three α_1-adrenoceptor subtypes show different spatio-temporal mechanisms of internalization and ERK1/2 phosphorylation. *BBA Mol Cell Res* 1833**:** 2322-2333.

Perez DM, Piascik MT & Graham RM (1991). Solution-phase library screening for the identification of rare clones: isolation of an α_{1D}-adrenergic receptor cDNA. *Mol Pharmacol* 40**:** 876-883.

Perianayagam MC, Balakrishnan VS, King AJ, Pereira BJ & Jaber BL (2002). C5a delays apoptosis of human neutrophils by a phosphatidylinositol 3-kinase-signaling pathway. *Kidney Int* 61**:** 456-463.

Perianayagam MC, Balakrishnan VS, Pereira BJ & Jaber BL (2004). C5a delays apoptosis of human neutrophils via an extracellular signal-regulated kinase and Bad-mediated signalling pathway. *Eur J Clin Invest* 34**:** 50-56.

Petrash AC & Bylund DB (1986). α_2-Adrenergic receptor subtypes indicated by [^{3}H]yohimbine binding in human brain. *Life Sci* 38**:** 2129-2137.

Plazinska A, Plazinski W & Jozwiak K (2015). Agonist binding by the β_2-adrenergic receptor: an effect of receptor conformation on ligand association–dissociation characteristics. *Eur Biophys J* 44**:** 149-163.

Poon G (2005). Cinacalcet hydrochloride (Sensipar). *Proceedings (Baylor University Medical Center)* 18**:** 181-184.

Pulli B, Ali M, Forghani R, Schob S, Hsieh KLC, Wojtkiewicz G*, et al.* (2013). Measuring myeloperoxidase activity in biological samples. *PLoS ONE* 8**:** e67976.

Qaseem A, Wilt TJ, Weinberger SE, Hanania NA, Criner G, van der Molen T*, et al.* (2011). Diagnosis and management of stable chronic obstructive pulmonary disease: a clinical practice guideline update from the American College of Physicians, American College of Chest Physicians, American Thoracic Society, and European Respiratory Society. *Ann Intern Med* 155**:** 179-191.

Ramachandran GN, Ramakrishnan C & Sasisekharan V (1963). Stereochemistry of polypeptide chain configurations. *J Mol Biol* 7**:** 95-99.

Ramos-Jimenez J, Soria-Jasso LE, Lopez-Colombo A, Reyes-Esparza JA, Camacho J & Arias-Montano JA (2007). Histamine augments β_2-adrenoceptor-induced cyclic AMP accumulation in human prostate cancer cells DU-145 independently of known histamine receptors. *Biochem Pharmacol* 73**:** 814-823.

Rana S & Sahoo AR (2015). Model structures of inactive and peptide agonist bound C5aR: insights into agonist binding, selectivity and activation. *Biochem and Biophys Rep* 1**:** 85-96.

Rana S, Sahoo AR & Majhi BK (2016). Structural complexes of the agonist, inverse agonist and antagonist bound C5a receptor: insights into pharmacology and signaling. *Mol Biosyst* 12**:** 1586-1599.

Rasmussen S, DeVree B, Zou Y, Kruse A, Chang K, Kobilka T*, et al.* (2011a). Crystal structure of the β_2 adrenergic receptor-G_s protein complex. *Nature* 477**:** 549 - 555.

Rasmussen SGF, Choi HJ, Fung JJ, Pardon E, Casarosa P, Chae PS*, et al.* (2011b). Structure of a nanobody-stabilized active state of the β_2 adrenoceptor. *Nature* 469**:** 175-180.

Redka DyS, Pisterzi LF & Wells JW (2008). Binding of orthosteric ligands to the allosteric site of the M_2 muscarinic cholinergic receptor. *Mol Pharmacol* 74**:** 834-843.

Regard JB, Sato IT & Coughlin SR (2008). Anatomical profiling of G protein-coupled receptor expression. *Cell* 135**:** 561-571.

Riddy DM, Valant C, Rueda P, Charman WN, Sexton PM, Summers RJ*, et al.* (2015). Label-free kinetics: exploiting functional hemi-equilibrium to derive rate constants for muscarinic receptor antagonists. *Mol Pharmacol* 88**:** 779-790.

Ring AM, Manglik A, Kruse AC, Enos MD, Weis WI, Garcia KC*, et al.* (2013). Adrenaline-activated structure of β_2-adrenoceptor stabilized by an engineered nanobody. *Nature* 502**:** 575-579.

Rittirsch D, Flierl MA, Nadeau BA, Day DE, Huber-Lang M, Mackay CR*, et al.* (2008). Functional roles for C5a receptors in sepsis. *Nat Med* 14**:** 551-557.

Rollins TE, Siciliano S, Kobayashi S, Cianciarulo DN, Bonilla-Argudo V, Collier K*, et al.* (1991). Purification of the active C5a receptor from human polymorphonuclear leukocytes as a receptor-G_i complex. *Proc Natl Acad Sci USA* 88**:** 971-975.

Rook JM, Noetzel MJ, Pouliot WA, Bridges TM, Vinson PN, Cho HP, *et al.* (2013). Unique signaling profiles of positive allosteric modulators of metabotropic glutamate receptor subtype 5 determine differences in in vivo activity. *Biol Psychiatry* 73**:** 501-509.

Rosethorne EM, Bradley ME, Gherbi K, Sykes DA, Sattikar A, Wright JD*, et al.* (2016). Long receptor residence time of C26 contributes to super agonist activity at the human β_2 adrenoceptor. *Mol Pharmacol* 89**:** 467-475.

Ruiz-Gómez A & Mayor Jr F (1997). β-adrenergic receptor kinase (GRK2) colocalizes with β-adrenergic receptors during agonist-induced receptor internalization. *J Biol Chem* 272**:** 9601-9604.

Sabbadin D, Ciancetta A, Deganutti G, Cuzzolin A & Moro S (2015). Exploring the recognition pathway at the human A_{2A} adenosine receptor of the endogenous agonist adenosine using supervised molecular dynamics simulations. *MedChemComm* 6**:** 1081-1085.

Salchow K, Bond ME, Evans SC, Press NJ, Charlton SJ, Hunt PA*, et al.* (2010). A common intracellular allosteric binding site for antagonists of the CXCR2 receptor. *Br J Pharmacol* 159**:** 1429-1439.

Šali A & Blundell TL (1993). Comparative protein modelling by satisfaction of spatial restraints. *J Mol Biol* 234**:** 779-815.

Salih H, Anghelescu I, Kezic I, Sinha V, Hoeben E, Van Nueten L*, et al.* (2015). Pharmacokinetic and pharmacodynamic characterisation of JNJ-40411813, a positive allosteric modulator of $mGluR_2$, in two randomised, double-blind phase-I studies. *J Psychopharmacol* 29**:** 414-425.

Samama P, Cotecchia S, Costa T & Lefkowitz RJ (1993). A mutation-induced activated state of the β_2-adrenergic receptor. Extending the ternary complex model. *J Biol Chem* 268**:** 4625-4636.

Sandal M, Behrens M, Brockhoff A, Musiani F, Giorgetti A, Carloni P*, et al.* (2015). Evidence for a transient additional ligand binding site in the TAS2R46 bitter taste receptor. *J Chem Theory Comput* 11**:** 4439-4449.

Schatz-Jakobsen JA, Yatime L, Larsen C, Petersen SV, Klos A & Andersen GR (2014). Structural and functional characterization of human and murine C5a anaphylatoxins. *Acta Crystallogr D Biol Crystallogr* 70**:** 1704-1717.

Schwinn DA, Lomasney JW, Lorenz W, Szklut PJ, Fremeau RT, Jr., Yang-Feng TL*, et al.* (1990). Molecular cloning and expression of the cDNA for a novel α_1-adrenergic receptor subtype. *J Biol Chem* 265**:** 8183-8189.

Scola A-M, Higginbottom A, Partridge LJ, Reid RC, Woodruff T, Taylor SM*, et al.* (2007). The role of the N-terminal domain of the complement fragment receptor C5L2 in ligand binding. *J Biol Chem* 282**:** 3664-3671.

Scola A-M, Johswich K-O, Morgan BP, Klos A & Monk PN (2009). The human complement fragment receptor, C5L2, is a recycling decoy receptor. *Mol Immunol* 46**:** 1149-1162.

Seow V, Lim J, Cotterell AJ, Yau MK, Xu W, Lohman RJ*, et al.* (2016). Receptor residence time trumps drug-likeness and oral bioavailability in determining efficacy of complement C5a antagonists. *Sci Rep* 6**:** 24575.

Shenoy SK, Drake MT, Nelson CD, Houtz DA, Xiao K, Madabushi S*, et al.* (2006). β-Arrestin-dependent, G protein-independent ERK1/2 activation by the β_2 adrenergic receptor. *J Biol Chem* 281**:** 1261-1273.

Shimamura T, Shiroishi M, Weyand S, Tsujimoto H, Winter G, Katritch V*, et al.* (2011). Structure of the human histamine H_1 receptor complex with doxepin. *Nature* 475**:** 65-70.

Short A, Wong AK, Finch AM, Haaima G, Shiels IA, Fairlie DP*, et al.* (1999). Effects of a new C5a receptor antagonist on C5a- and endotoxin-induced neutropenia in the rat. *Br J Pharmacol* 126**:** 551-554.

Sibley DR & Creese I (1983). Regulation of ligand binding to pituitary D_2 dopaminergic receptors. Effects of divalent cations and functional group modification. *J Biol Chem* 258**:** 4957-4965.

Siciliano SJ, Rollins TE & Springer MS (1990). Interaction between the C5a receptor and G_i in both the membrane-bound and detergent-solubilized states. *J Biol Chem* 265**:** 19568-19574.

Siddappa NB, Avinash A, Venkatramanan M & Ranga U (2007). Regeneration of commercial nucleic acid extraction columns without the risk of carryover contamination. *Biotechniques* 42**:** 186, 188-192.

Simon V, Robin MT, Legrand C & Cohen-Tannoudji J (2003). Endogenous G protein-coupled receptor kinase 6 triggers homologous β-adrenergic receptor desensitization in primary uterine smooth muscle cells. *Endocrinol* 144**:** 3058-3066.

Siu FY, He M, de Graaf C, Han GW, Yang D, Zhang Z*, et al.* (2013). Structure of the human glucagon class B G-protein-coupled receptor. *Nature* 499**:** 444-449.

Skokowa J, Ali SR, Felda O, Kumar V, Konrad S, Shushakova N*, et al.* (2005). Macrophages induce the inflammatory response in the pulmonary arthus reaction through $G_{\alpha i2}$ activation that controls C5aR and Fc receptor cooperation. *J Immunol* 174**:** 3041-3050.

Sorbi C, Franchini S, Tait A, Prandi A, Gallesi R, Angeli P*, et al.* (2009). 1,3-Dioxolane-based ligands as rigid analogues of naftopidil: structure-affinity/activity relationships at α_1 and 5-HT_{1A} receptors. *Chem Med Chem* 4**:** 393-399.

Soriano-Ursua M, McNaught-Flores D, Correa-Basurto J, Arias-Montano J & Trujillo-Ferrara J (2013). Histamine modulates isoproterenol efficacy at the β_2 adrenoceptor: inferences regarding allosteric modulation by imidazole-containing compounds. *Biochemistry and Physiology* 2**:** 1000114.

Soudijn W, van Wijngaarden I & Ijzerman AP (2004). Allosteric modulation of G protein-coupled receptors: perspectives and recent developments. *Drug Discov Today* 9**:** 752-758.

Srivastava A, Yano J, Hirozane Y, Kefala G, Gruswitz F, Snell G*, et al.* (2014). High-resolution structure of the human GPR40 receptor bound to allosteric agonist TAK-875. *Nature* 513**:** 124-127.

Stahl E, Elmslie G & Ellis J (2011). Allosteric modulation of the M_3 muscarinic receptor by amiodarone and N-ethylamiodarone: application of the four-ligand allosteric two-state model. *Mol Pharmacol* 80**:** 378-388.

Steinfeld T, Hughes AD, Klein U, Smith JAM & Mammen M (2011). THRX-198321 is a bifunctional muscarinic receptor antagonist and β_2-adrenoceptor agonist (MABA) that binds in a bimodal and multivalent manner. *Mol Pharmacol* 79**:** 389-399.

Strachan AJ, Shiels IA, Reid RC, Fairlie DP & Taylor SM (2001). Inhibition of immune-complex mediated dermal inflammation in rats following either oral or

topical administration of a small molecule C5a receptor antagonist. *Br J Pharmacol* 134**:** 1778-1786.

Strader CD, Candelore MR, Hill WS, Dixon RA & Sigal IS (1989a). A single amino acid substitution in the β-adrenergic receptor promotes partial agonist activity from antagonists. *J Biol Chem* 264**:** 16470-16477.

Strader CD, Candelore MR, Hill WS, Sigal IS & Dixon RA (1989b). Identification of two serine residues involved in agonist activation of the β-adrenergic receptor. *J Biol Chem* 264**:** 13572-13578.

Strader CD, Sigal IS & Dixon RA (1989c). Structural basis of β-adrenergic receptor function. *FASEB J* 3**:** 1825-1832.

Strader CD, Sigal IS, Register RB, Candelore MR, Rands E & Dixon RA (1987). Identification of residues required for ligand binding to the β-adrenergic receptor. *Proc Natl Acad Sci USA* 84**:** 4384-4388.

Strulovici B, Cerione RA, Kilpatrick BF, Caron MG & Lefkowitz RJ (1984). Direct demonstration of impaired functionality of a purified desensitized β-adrenergic receptor in a reconstituted system. *Science* 225**:** 837-840.

Sumichika H, Sakata K, Sato N, Takeshita S, Ishibuchi S, Nakamura M*, et al.* (2002). Identification of a potent and orally active non-peptide C5a receptor antagonist. *J Biol Chem* 277**:** 49403-49407.

Sun J, Ember JA, Chao TH, Fukuoka Y, Ye RD & Hugli TE (1999). Identification of ligand effector binding sites in transmembrane regions of the human G protein-coupled C3a receptor. *Prot Sci* 8**:** 2304-2311.

Suratman S, Leach K, Sexton PM, Felder CC, Loiacono RE & Christopoulos A (2011). Impact of species variability and 'probe-dependence' on the detection and in vivo validation of allosteric modulation at the M_4 muscarinic acetylcholine receptor. *Br J Pharmacol* 162**:** 1659-1670.

Swaminath G, Lee TW & Kobilka B (2003). Identification of an allosteric binding site for Zn^{2+} on the β_2 adrenergic receptor. *J Biol Chem* 278**:** 352-356.

Swaminath G, Steenhuis J, Kobilka B & Lee TW (2002). Allosteric modulation of β_2-adrenergic receptor by Zn^{2+}. *Mol Pharmacol* 61**:** 65-72.

Sykes DA, Dowling MR & Charlton SJ (2009). Exploring the mechanism of agonist efficacy: a relationship between efficacy and agonist dissociation rate at the muscarinic M_3 receptor. *Mol Pharmacol* 76**:** 543-551.

Talbodec A, Berkane N, Blandin V, Breittmayer JP, Ferrari E, Frelin C*, et al.* (2000). Aspirin and sodium salicylate inhibit endothelin ETA receptors by an allosteric type of mechanism. *Mol Pharmacol* 57**:** 797-804.

Tamamis P, Kieslich C, Nikiforovich G, Woodruff T, Morikis D & Archontis G (2014). Insights into the mechanism of C5aR inhibition by PMX53 via implicit solvent molecular dynamics simulations and docking. *BMC Biophys* 7**:** 5.

Tan Q, Zhu Y, Li J, Chen Z, Han GW, Kufareva I*, et al.* (2013). Structure of the CCR5 chemokine receptor-HIV entry inhibitor maraviroc complex. *Science* 341**:** 1387-1390.

Tashkin DP, Littner M, Andrews CP, Tomlinson L, Rinehart M & Denis-Mize K (2008). Concomitant treatment with nebulized formoterol and tiotropium in subjects with COPD: a placebo-controlled trial. *Respir Med* 102**:** 479-487.

Ternowitz T, Bjerring P, Andersen PH, Schröder J-M & Kragballe K (1987). Methotrexate inhibits the human C5a-induced skin response in patients with psoriasis. *J Invest Dermatol* 89**:** 192-196.

Thal DM, Sun B, Feng D, Nawaratne V, Leach K, Felder CC*, et al.* (2016). Crystal structures of the M_1 and M_4 muscarinic acetylcholine receptors. *Nature* 531**:** 335-340.

Thomas T, Fang Y, Yuriev E & Chalmers DK (2016). Ligand binding pathways of clozapine and haloperidol in the dopamine D_2 and D_3 receptors. *J Chem Inf Model* 56**:** 308-321.

Thompson A, Liu W, Chun E, Katritch V, Wu H, Vardy E*, et al.* (2012). Structure of the nociceptin/orphanin FQ receptor in complex with a peptide mimetic. *Nature* 485**:** 395 - 401.

Tison F, Keywood C, Wakefield M, Durif F, Corvol JC, Eggert K*, et al.* (2016). A phase 2A trial of the novel $mGluR_5$-negative allosteric modulator dipraglurant for levodopa-induced dyskinesia in Parkinson's disease. *Mov Disord*.

Torres M & Forman HJ (1999). Activation of several MAP kinases upon stimulation of rat alveolar macrophages: role of the NADPH oxidase. *Arch Biochem Biophys* 366**:** 231-239.

Toth MJ, Huwyler L, Boyar WC, Braunwalder AF, Yarwood D, Hadala J*, et al.* (1994). The pharmacophore of the human C5a anaphylatoxin. *Prot Sci* 3**:** 1159-1168.

Trankle C, Dittmann A, Schulz U, Weyand O, Buller S, Johren K*, et al.* (2005). Atypical muscarinic allosteric modulation: cooperativity between modulators and their atypical binding topology in muscarinic M_2 and M_2/M_5 chimeric receptors. *Mol Pharmacol* 68**:** 1597-1610.

Trankle C, Weyand O, Voigtlander U, Mynett A, Lazareno S, Birdsall NJ*, et al.* (2003). Interactions of orthosteric and allosteric ligands with [^{3}H]dimethyl-W84 at the common allosteric site of muscarinic M_2 receptors. *Mol Pharmacol* 64**:** 180-190.

Tummino PJ & Copeland RA (2008). Residence time of receptor−ligand complexes and its effect on biological function. *Biochemistry* 47**:** 5481-5492.

Ulrich JT, Cieplak W, Paczkowski NJ, Taylor SM & Sanderson SD (2000). Induction of an antigen-specific CTL response by a conformationally biased agonist of human C5a anaphylatoxin as a molecular adjuvant. *J Immunol* 164**:** 5492-5498.

Unett DJ, Gatlin J, Anthony TL, Buzard DJ, Chang S, Chen C*, et al.* (2013). Kinetics of 5-HT_{2B} receptor signaling: profound agonist-dependent effects on signaling onset and duration. *J Pharmacol Exp Ther* 347**:** 645-659.

Valant C, Gregory KJ, Hall NE, Scammells PJ, Lew MJ, Sexton PM*, et al.* (2008). A novel mechanism of G protein-coupled receptor functional selectivity: muscarinic partial agonist McN-A-343 as a bitopic orthosteric/allosteric ligand. *J Biol Chem* 283**:** 29312-29321.

Valentin-Hansen L, Groenen M, Nygaard R, Frimurer TM, Holliday ND & Schwartz TW (2012). The arginine of the DRY motif in transmembrane segment III functions as a balancing micro-switch in the activation of the β_2-adrenergic receptor. *J Biol Chem* 287**:** 31973-31982.

van der Westhuizen ET, Valant C, Sexton PM & Christopoulos A (2015). Endogenous allosteric modulators of G protein–coupled receptors. *J Pharmacol Exp Ther* 353**:** 246-260.

van Noord JA, Aumann J-L, Janssens E, Smeets JJ, Verhaert J, Disse B*, et al.* (2005). Comparison of tiotropium once daily, formoterol twice daily and both combined once daily in patients with COPD. *Eur Respir J* 26**:** 214-222.

Vanek M, Hawkins LD & Gusovsky F (1994). Coupling of the C5a receptor to G_i in U-937 cells and in cells transfected with C5a receptor cDNA. *Mol Pharmacol* 46**:** 832-839.

Venter JC, Adams MD, Myers EW, Li PW, Mural RJ, Sutton GG*, et al.* (2001). The sequence of the human genome. *Science* 291**:** 1304-1351.

Vergunst CE, Gerlag DM, Dinant H, Schulz L, Vinkenoog M, Smeets TJ*, et al.* (2007). Blocking the receptor for C5a in patients with rheumatoid arthritis does not reduce synovial inflammation. *Rheumatology* 46**:** 1773-1778.

Vilums M, Zweemer AJM, Dilanchian A, van Veldhoven JPD, de Vries H, Brussee J*, et al.* (2015). Evaluation of (4-Arylpiperidin-1-yl)cyclopentanecarboxamides As High-Affinity and Long-Residence-Time Antagonists for the CCR2 Receptor. *Chemmedchem* 10**:** 1249-1258.

Vogen SM, Finch AM, Wadi SK, Thatcher J, Monk PN, Taylor SM*, et al.* (1999). The influence of Lys68 in decepeptide agonists of C5a on C5a receptor binding, activation and selectivity. *J Pept Res* 53**:** 8-17.

Voigtländer U, Jöhren K, Mohr M, Raasch A, Tränkle C, Buller S*, et al.* (2003). Allosteric site on muscarinic acetylcholine receptors: identification of two amino acids in the muscarinic M_2 receptor that account entirely for the M_2/M_5 subtype selectivities of some structurally diverse allosteric ligands in N-methylscopolamine-occupied receptors. *Mol Pharmacol* 64**:** 21-31.

Wacker D, Fenalti G, Brown MA, Katritch V, Abagyan R, Cherezov V*, et al.* (2010). Conserved binding mode of human β_2 adrenergic receptor inverse agonists and antagonist revealed by X-ray crystallography. *J Am Chem Soc* 132**:** 11443-11445.

Wacker D, Wang C, Katritch V, Han GW, Huang XP, Vardy E*, et al.* (2013). Structural features for functional selectivity at serotonin receptors. *Science* 340**:** 615-619.

Wang C, Jiang Y, Ma J, Wu H, Wacker D, Katritch V*, et al.* (2013a). Structural basis for molecular recognition at serotonin receptors. *Science* 340**:** 610-614.

Wang C, Wu H, Katritch V, Han GW, Huang XP, Liu W*, et al.* (2013b). Structure of the human smoothened receptor bound to an antitumour agent. *Nature* 497**:** 338-343.

Wang T & Duan Y (2009). Ligand entry and exit pathways in the β_2-adrenergic receptor. *J Mol Biol* 392**:** 1102-1115.

Ward PA (2004). The dark side of C5a in sepsis. *Nat Rev Immunol* 4**:** 133-142.

Warne T, Moukhametzianov R, Baker JG, Nehme R, Edwards PC, Leslie AGW*, et al.* (2011). The structural basis for agonist and partial agonist action on a β_1-adrenergic receptor. *Nature* 469**:** 241-244.

Warne T, Serrano-Vega MJ, Baker JG, Moukhametzianov R, Edwards PC, Henderson R*, et al.* (2008). Structure of a β_1-adrenergic G-protein-coupled receptor. *Nature* 454**:** 486-491.

White JF, Noinaj N, Shibata Y, Love J, Kloss B, Xu F*, et al.* (2012). Structure of the agonist-bound neurotensin receptor. *Nature* 490**:** 508-513.

Whorton MR, Bokoch MP, Rasmussen SGF, Huang B, Zare RN, Kobilka B*, et al.* (2007). A monomeric G protein-coupled receptor isolated in a high-density lipoprotein particle efficiently activates its G protein. *Proc Natl Acad Sci USA* 104**:** 7682-7687.

Wieland K, Zuurmond HM, Krasel C, Ijzerman AP & Lohse MJ (1996). Involvement of Asn-293 in stereospecific agonist recognition and in activation of the β_2-adrenergic receptor. *Proc Natl Acad Sci USA* 93**:** 9276-9281.

Willars GB, Heding A, Vrecl M, Sellar R, Blomenröhr M, Nahorski SR*, et al.* (1999). Lack of a C-terminal tail in the mammalian gonadotropin-releasing hormone receptor confers resistance to agonist-dependent phosphorylation and rapid desensitization. *J Biol Chem* 274**:** 30146-30153.

Williams LT, Mullikin D & Lefkowitz RJ (1978). Magnesium dependence of agonist binding to adenylate cyclase-coupled hormone receptors. *J Biol Chem* 253**:** 2984-2989.

Woo AY, Jozwiak K, Toll L, Tanga MJ, Kozocas JA, Jimenez L*, et al.* (2014). Tyrosine 308 is necessary for ligand-directed G_s protein-biased signaling of β_2-adrenoceptor. *J Biol Chem* 289**:** 19351-19363.

Woodruff T, Strachan A, Sanderson S, Monk P, Wong A, Fairlie D*, et al.* (2001). Species dependence for binding of small molecule agonist and antagonists to the C5a receptor on polymorphonuclear leukocytes. *Inflammation* 25**:** 171 - 177.

Woodruff TM, Arumugam TV, Shiels IA, Reid RC, Fairlie DP & Taylor SM (2003). A potent human C5a receptor antagonist protects against disease pathology in a rat model of inflammatory bowel disease. *J Immunol* 171**:** 5514-5520.

Woodruff TM, Crane JW, Proctor LM, Buller KM, Shek AB, de Vos K*, et al.* (2006). Therapeutic activity of C5a receptor antagonists in a rat model of neurodegeneration. *FASEB J* 20**:** 1407-1417.

Woodruff TM, Nandakumar KS & Tedesco F (2011). Inhibiting the C5-C5a receptor axis. *Mol Immunol* 48**:** 1631-1642.

Woodruff TM, Strachan AJ, Dryburgh N, Shiels IA, Reid RC, Fairlie DP*, et al.* (2002). Antiarthritic activity of an orally active C5a receptor antagonist against antigen-induced monarticular arthritis in the rat. *Arthritis Rheum* 46**:** 2476-2485.

Wootten D, Christopoulos A & Sexton PM (2013). Emerging paradigms in GPCR allostery: implications for drug discovery. *Nat Rev Drug Discov* 12**:** 630-644.

Wu B, Chien EYT, Mol CD, Fenalti G, Liu W, Katritch V*, et al.* (2010). Structures of the CXCR4 chemokine GPCR with small-molecule and cyclic peptide antagonists. *Science* 330**:** 1066-1071.

Wu H, Wacker D, Mileni M, Katritch V, Han G, Vardy E*, et al.* (2012). Structure of the human κ-opioid receptor in complex with JDTic. *Nature* 485**:** 327-333.

Wu H, Wang C, Gregory KJ, Han GW, Cho HP, Xia Y*, et al.* (2014). Structure of a class C GPCR metabotropic glutamate receptor 1 bound to an allosteric modulator. *Science* 344**:** 58-64.

Yao XJ, Velez Ruiz G, Whorton MR, Rasmussen SG, DeVree BT, Deupi X*, et al.* (2009). The effect of ligand efficacy on the formation and stability of a GPCR-G protein complex. *Proc Natl Acad Sci USA* 106**:** 9501-9506.

Yokoyama T, Hara R, Fukumoto K, Fujii T, Jo Y, Miyaji Y*, et al.* (2011). Effects of three types of α_1 adrenoceptor blocker on lower urinary tract symptoms and sexual function in males with benign prostatic hyperplasia. *Int J Urol* 18**:** 225-230.

Yoshikawa Y, Oishi S, Kubo T, Tanahara N, Fujii N & Furuya T (2013). Optimized method of G-protein-coupled receptor homology modeling: its application to the discovery of novel CXCR7 ligands. *J Med Chem* 56**:** 4236-4251.

Zhang C, Srinivasan Y, Arlow DH, Fung JJ, Palmer D, Zheng Y*, et al.* (2012a). High-resolution crystal structure of human protease-activated receptor 1. *Nature* 492**:** 387-392.

Zhang D, Gao ZG, Zhang K, Kiselev E, Crane S, Wang J*, et al.* (2015). Two disparate ligand-binding sites in the human $P2Y_1$ receptor. *Nature* 520**:** 317-321.

Zhang J, Zhang K, Gao ZG, Paoletta S, Zhang D, Han GW*, et al.* (2014). Agonist-bound structure of the human $P2Y_{12}$ receptor. *Nature* 509**:** 119-122.

Zhang W-J, Gao X-J, Liu Y-L, Shao X-X & Guo Z-Y (2012b). Design, recombinant preparation and europium-labeling of a fully active easily-labeled INSL3 analog for receptor-binding assays. *Process Biochem* 47**:** 1856-1860.

Zhang X, Boyar W, Toth MJ, Wennogle L & Gonnella NC (1997). Structural definition of the C5a C terminus by two-dimensional nuclear magnetic resonance spectroscopy. *Proteins* 28**:** 261-267.